Alma Mater Studiorum – Università di Bologna

DOTTORATO DI RICERCA IN

Ingegneria Civile, Chimica, Ambientale e dei Materiali

Ciclo XXXII

Settore Concorsuale: 09/D3

Settore Scientifico Disciplinare: ING-IND/25

WASTEWATER VALORISATION THROUGH ADSORPTION PROCESSES AND ANAEROBIC DIGESTION

Presentata da: **Giorgia Rubertelli**

Supervisore
Dario Frascari

Co-Supervisore
Davide Pinelli

Coordinatore Dottorato
Luca Vittuari

Esame finale anno 2020

CONTENTS

PART I

PART II

Removal and recovery of phosphorus from municipal wastewater with a hybrid ion exchange resin 77

AIM AND STRUCTURE OF THE WORK

When contaminants are characterized by an intrinsic economic value, their removal from the waste and their recovery as a marketable product, does not only reduce the environmental footprint of the waste disposal, but also provides a revenue-generating opportunity; thus creating the possibility to economically sustain the process. This is the case of the two wastewaters investigated in the current study: olive-mill wastewater containing high content of phenolic compounds and municipal wastewater which is today considered the most potential new source of phosphorus. In terms of wastewater valorisation adsorption-based technologies result an extremely attractive solution since the pollutant values can be recovered along with their removal from the effluents. As a matter of fact, among the possible techniques available, adsorption processes by solid adsorbents have shown potential as one of the most efficient method for the treatment and removal of organic contaminants in water and wastewater treatments. Moreover, adsorption has advantages over the other methods because of simple design and can involve low investment in term of both initial cost and land required. For simplicity, the current work is divided into two main parts, both focused on the development of adsorption-based treatment processes for the valorisation of two different wastewater streams.

The first part of this study focused on the valorisation of olive-mill wastewater (OMW), which represents a major environmental concern of the olive-oil industrial production, specially for the Mediterranean area where 98% of the total olive-oil world production is concentrated. The study was part of the MADFORWATER project funded by the European Union’s Horizon 2020 programme and coordinated by the University of Bologna. The ultimate objective of MADFORWATER was to develop an integrated set of technological and management instruments for the enhancement of wastewater treatment, treated wastewater reuse for irrigation and water efficiency in agriculture, with the final aim to reduce water vulnerability in selected basins in Egypt, Morocco and Tunisia. Within this wide project the valorisation of OMWW was investigated by means of the development of an integrated and cost-effective treatment process which combined adsorption-based treatments with anaerobic digestion processes. The main objectives of the current work and its contribution to the development of the abovementioned OMW biorefinery process included the investigation of a reliable method for the selection of a cost-effective sorbent and the application/validation of the procedure to different commercially available media. Moreover, anaerobic digestion tests were performed to drive the development of the integrated process between different configurations.

The second part of my PhD thesis was focused on the removal and recovery of phosphorus from municipal wastewater. The study started at Cranfield University, under the supervision of Prof. Ana Soares and within the wider EU project SMART-Plant (Scale-up of low-carbon footprint MAterial Recovery Techniques in existing wastewater treatment PLANTs). The research project consisted in the long-term investigation of a pilot-scale adsorption plant placed within the Cranfield University’s sewage works and treating actual secondary effluent wastewater. During the time spent at Cranfield University the main objectives were the evaluation of the process performances and the validation of the novel conduction method proposed by the research group. However, once come back to Italy the study continued with the performance investigation of the resin which had undertaken almost 70 adsorption/desorption cycles in the demonstration plant. The primary scope of this laboratory-scale investigation was the evaluation of the actual impact undergone by the resin and the identification of consequent preventing operations aimed at reducing detrimental effects on the adsorbent and its performances.

ABSTRACT

1. PART I – Olive-mill wastewater valorisation through polyphenols adsorption and anaerobic digestion

A procedure for the selection of the optimal adsorbent for phenolic compounds (PC) recovery from PC-rich wastewaters was proposed and applied to compare 4 neutral resins (Amberlite XAD16N, Optipore SD-2, Amberlite FPX66, Amberlite XAD761) and one ion-exchange resin (Amberlite IRA958 Cl) for PC recovery from a Tunisian olive mill wastewater (OMW). In the initial batch isotherm tests a neutral resin (XAD16N) performed best thanks to its high PC sorption capacity (81 $mg_{PC}/g_{dry\ resin}$) and PC content in the sorbed product (0.19 $g_{PC}/g_{volatile\ solids}$). Also ion-exchange resin IRA958, used in OH form in this work, resulted interesting thanks to its satisfactory performances and very low cost (8 €/L). These two pre-selected resins were further compared by means of continuous-flow adsorption/desorption tests conducted in a 1-m packed column. The results indicate that if a low (20%) breakpoint is selected, XAD16N leads to a PC-richer sorbed product (0.14 $g_{PC}/g_{volatile\ solids}$) and a higher operating capacity (0.30) than IRA958. Conversely, if a very high (90%) breakpoint is selected, the two resins produce similar desorbed products in terms of both PC content (0.19-0.21 $g_{PC}/g_{volatile\ solids}$) and antioxidant capacity (4.6-4.9 $g_{ascorbic\ acid\ equivalent}/g_{PC}$). However, they resulted quite different in terms of bacteriostatic power. Resin-specific dynamic desorption procedures led to very high PC desorption yields (87-95%). The identification of the actual PCs present in the final desorbed product indicated for XAD16N a higher capacity to preserve the integrity of the PC mixture of the studied OMW. OMW microfiltration (0.2 μm pore-size) led to a 99.8% suspended solid removal - thus protecting the packed column from potential clogging - with a very low PC loss. Moreover AD tests conducted on the dephenolized OMW produced through the continuous adsorption breakthrough tests confirmed the importance to reduce the OMW PC content to enhance the biomethanation process (an 80% OMW dephenolization led to

an important improvement in the methane production yield, from 360 NmL_{CH4}/g_{VS} with the micro-filtered OMW to 570 and 600 NmL_{CH4}/g_{VS} with the OMW dephenolized with XAD16N and IRA958 OH, respectively). BOD reduction was further quantified to evaluate the possible direct treated-OMW reusability as irrigation-quality water.

2. PART II – Removal and recovery of phosphorus from municipal wastewater by means of a hybrid ion exchange resin

The study represents one of the really first attempt to place an adsorption-based process within an existing sewage works to remove and recover phosphorus (P) from secondary effluent municipal wastewater (MWW). The pilot-scale plant, which included a P removing column with 35 L of the commercially available hybrid ion exchange resin HAIX Layne^{RT}, went successfully to 66 adsorption/desorption cycles treating $10m^3d^{-1}$ of actual MWW (average inlet PO_4-P concentration of 5.3±0.3 $mg_{PO4\text{-}P}/L$). The proposed process was characterized by 4 important novelties: i) the employment of a new commercially available hybrid ion-exchange resin characterized by the presence of ferric nanoparticles; ii) the selective desorption of the media by a w/v 2% NaOH solution; iii) the multiple usage of the regenerant solution through consecutive adsorption/desorption cycles to enrich the P content and enhance the recovery of P by precipitation and; iv) the recycling of the treated regenerant solution once P was recovered as calcium-phosphate (Ca-P) salts. An enrichment factor ($C_{PO4\text{-}P,\ regenerant}/C_{PO4\text{-}P,MWW}$) of approximately 100 was achieved through 10 subsequent employments of the same regenerant solution. The process performances through consecutive cycles were investigated and the recycling of the regenerant solution after Ca-P precipitation allowed to perform consistent and extremely reproducible adsorption/desorption cycles. Therefore, the proposed technology resulted potentially able to fully control the effluent quality. Moreover, laboratory-scale tests (both batch and continuous) and the comparison of the resin performances with the virgin one confirmed the high hydraulic, chemical and mechanical resistance of the investigated resin. Indeed, the resin of the Cranfield pilot-plant performed similarly to the virgin resin, proving that the 66 cycles performed in the demo-plant in accordance with the novel conduction method proposed did not damage its performances, and, hence, that its operating-life can be significantly extended.

PART I

Olive-mill wastewater valorisation through polyphenols adsorption and anaerobic digestion

1.1 INTRODUCTION

Olive oil is the primary source of fat in the diet of the Mediterranean area, where 98% of the total world production is concentrated. Generally, the quantity of olive mill wastewater OMW produced throughout the oil extraction process is 1.2–1.8 m^3 for every ton of olives, resulting over 30 million m^3 of OMW annually generated in the Mediterranean basin alone (Haddad et al., 2017). The conventional olive oil production yields the 20% olive oil, 30% solid residue and the remaining as OMW (Rodríguez-Gutiérrez et al., 2012). Despite the production of OMW appears smaller than other wastes, it must be considered that in terms of pollution effect, 1 m^3 of OMW is reported to be equivalent to 200 m^3 of domestic sewage (El-Abbassi et al., 2012). The composition of OMW by weight is 83%–96% water, 3.5%–15% organic constituents and 0.5%–2% mineral compounds (Kıpçak and Akgün, 2013); but it also contains sources of polyalcohol, polyphenols, volatile acids, nitrogen compounds, pectin, oil and tannin that makes OMW in dark colour (Erkonak et al., 2008). If, on one hand the high phenolic compound (PC) and organic matter contents are the primary responsible for the environmental toxicity of OMW, on the other hand, other researchers found that the phenolic compounds are potential to be recovered as they are highly valuable for their antioxidants, anti-allergic, anti-inflammatory, anticancer and antihypertensive effects. Their removal from the OMW and their recovery as a marketable product, does not only provide a revenue-generating opportunity but also reduce the environmental footprint of OMW (Caporaso et al., 2017). OMWs have traditionally been used to irrigate the olive tree fields, until their negative environmental impacts on the ecosystem became worldwide spread and well-known. Recently several countries have forbidden this practice, as well as their direct discharge in the Mediterranean aquatic body, thus imposing OMW treatment before disposal/discharge to avoid severe adversities on the biotic and aquatic systems (Erkonak et al., 2008; Rahmanian et al., 2014; Jeguirim et al., 2017).

In this way, the main goal of this work was to develop an integrated OMW biorefinery process consisting in the combination of an adsorption-based process for the removal and recovery of a high-valuable PC-rich product with anaerobic digestion. The ultimate aim of the treatment process was to produce an irrigation-quality treated OMW reusable in agriculture.

The main objectives of this study are:

i) the development and application to an actual OMW, produced by a Tunisian olive mill, of a sorbent selection procedure based on a combination of batch and continuous flow adsorption/desorption tests, whereas most studies base the selection of the sorbent only on batch tests that often neglect the desorption step;

ii) the assessment of the final desorbed products in terms of total PC content, antioxidant activity, bacteriostatic potential and presence of compounds of high economic value;

iii) the application of a rotary microfiltration process as a pre-treatment step before PC adsorption, to avoid the gradual clogging of the adsorption column.

Moreover preliminary anaerobic digestion (AD) tests were performed in order to address the development of the integrated OMW treatment process which combined adsorption and AD. Hence, first it was demonstrated that AD was significantly inhibited by PC compounds, with the consequent forced placement of the biomethanation step after the polyphenols adsorption step. Secondly, an investigation of the biomethanation process of the dephenolized effluents produced by continuous adsorption breakthrough tests was performed. Furthermore, the final effluent of the AD process was investigated in terms of BOD and COD to evaluate its potential reusability as irrigation-quality water.

1.2 STATE OF ART

1.2.1 Olive-mill wastewater (OMW)

Olive oil is the primary source of fat in the Mediterranean diet where it is concentrated the 98% of the total olive-oil industrial production. Generally, the quantity of olive-oil produced for ton of olives is extremely variable and inconsistent through years, since it strictly depends on several factors which comprises all that parameters affecting fruit maturation, such as the seasonal climate temperature and weather; spatial conditions (altitudes and latitudes of the olive-oil trees) and many other factors related to the environment and biotic interactions surrounding the crop. Notwithstanding seasonal changing, the volume of OMW produced throughout oil extraction is a little more consistent, since it mostly depend on the process and on the volume of water that is added to enhance the multi-phase liquid. It can be estimated approximately around 1.2–1.8 m^3 for every ton of olives, resulting over 30 mil m3 of OMW generated in only the Mediterranean basin alone annually (Haddad et al., 2017).

The conventional olive oil production through multi-phase centrifuges yields an average 20% olive oil, 30% solid residue and the remaining, approximately the 50%, as the OMW (Rodríguez-Gutiérrez et al., 2012). Despite the smaller amounts of wastes that olive oil production appears to create respect to other well-known wastes of worldwide distributed production processes, it represents a major concern due to its concentration into a limited area and to its cyclical production which is on the basis of an entire continental area which includes Europe and the north African countries. Therefore, the environmental impact caused by OMW cannot be neglected, specially if we consider its pollution potential. The latter was estimated by El-Abbassi et al. (2012) 200 times higher than that of raw domestic sewage, in other words, they concluded that pollution by 1 m^3 of OMW was reported to be equivalent to 200 m^3 of domestic sewage.

The high pollution potential related to OMW is related to its composition, which also is extremely variable from case to case. However, it can be generally reported as the following by weight composition ranges: 83%–96% water, 3.5%–15% organic compounds and 0.5%–2% mineral compounds (Kıpçak and Akgün, 2013). Among these sources of volatile acids, polyphenols, pectin, polyalcohol, nitrogen compounds, oil and tannin (that gives the typical dark color OMW in dark color) have been detected and reported (Rahmanian et al., 2014). Of the latter cited compounds what makes OMW special concerns are due to the high organic matter content (COD around 20-200 g/L and possible source of eutrophication) and the high concentration of phenolic compounds (PCs) which can vary in the wide range of 0.1-18 g/L. PCs need to be extensively explained since they high characterized by highly toxic and ecologically noxious properties that can poise plants and aquatic organisms and bacterial activity, leading to significant detrimental effects on the ecosystem where OMW are disposed (Abu-Lafi et al., 2017; Mekki et al., 2013). Therefore, although untreated OMWs have traditionally been used to irrigate the olive tree fields, several countries have recently forbidden this practice, thus imposing OMW treatment process before disposal (Rahmanian et al., 2014).

From an OMW production process point of view the two-phase system seems more ecological in terms of volumes of effluents generation. It has substituted the three-phase system in Spain in the last two decades, and it is now becoming implemented successively in Portugal, Greece and Italy as well. However, the three-phase system is still surviving in countries where financial scarcity has not yet permitted the switch of the technology equipment. Due to the fact that PC are much soluble in aqueous solutions, OMW contains generally about 95% of the PC content of the original olives (Rodis et al., 2002).

The main PC of OMW classes are phenolic acids, secoiridoids and flavonoids, among which hydroxytyrosol, oleuropein and verbascoside are the most abundant and the most studied compounds (Daassi et al., 2014; Cardinali et al., 2012; Aranda et al., 2007). However, as for the olive-oil extraction yield also the OMW PC composition varies both qualitatively and quantitatively according to the olive variety, climate conditions, cultivation practices, the olive storage time and the olive oil extraction process (Fiorentino et al., 2003). On the other hand, researchers found that the phenolic compounds are potential to be recovered as it is valuable for their antioxidants, anti-allergic, anti-inflammatory, anticancer and antihypertensive effects (Demerche et al., 2013; El-Abbassi et al., 2012). In particular hydroxytyrosol is one of the most valuable and expensive PCs, with a high demand in the pharmaceutical, food and cosmetic fields. Hence, the removal of PCs from OMW does not only reduce the environmental footprint of OMW disposal but also provides a revenue-generating opportunity (Caporaso et al., 2017).

Table 1.2.1 General parameters and constituents' composition of OMW reported by Rahmanian et al. (2014).

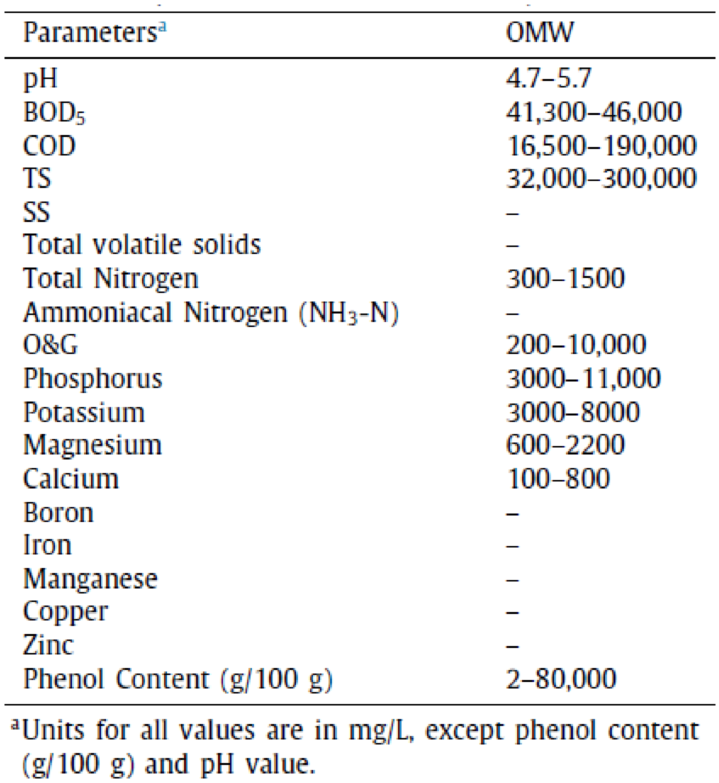

Parameters[a]	OMW
pH	4.7–5.7
BOD_5	41,300–46,000
COD	16,500–190,000
TS	32,000–300,000
SS	–
Total volatile solids	–
Total Nitrogen	300–1500
Ammoniacal Nitrogen (NH_3-N)	–
O&G	200–10,000
Phosphorus	3000–11,000
Potassium	3000–8000
Magnesium	600–2200
Calcium	100–800
Boron	–
Iron	–
Manganese	–
Copper	–
Zinc	–
Phenol Content (g/100 g)	2–80,000

[a] Units for all values are in mg/L, except phenol content (g/100 g) and pH value.

1.2.2 OMW treatment processes

Legal actions have been undertaken in the last decades in the producing countries, i.e. the straight disposal of untreated OMW to the ground fields and superficial waters bodies is prohibited in Spain currently, and also in Italy, Portugal and other European countries it is just allowed the partial discharge onto certain terrains. Moreover, the direct discharge of these wastewaters to the municipal sewage collectors is prohibited too, given the high concentrations of organic refractory pollutants. Legal limits are established in order to prevent inhibition of the biological treatment processes that take place in wastewater treatment plants.

The commonly used treatment technologies in treating OMW can be chemical, physical, biological or an integration of them. A briefly introduction the most common techniques is here hinted. Membrane filtration and biological treatment were recommended for larger scale production while oxidation technologies such as photo-Fenton was suitable for the industry with lower annual production capacity (Ioannou et al., 2017). The combination of different physicochemical techniques can recover a significant amount of phenol, while biological process are aimed at removing PCs rather than recovery them. For this reason they commonly employed as a pre-treatment method (Rahmanian et al., 2014). Moreover, biological treatment study is less favorable in OMW treatment, probably due to the consequent inhibitory effect on microorganisms depending on the appreciable content of phenolic compounds in OMW. Concerning physical treatment processes, the main limitation of membrane processes is the low efficiency in removing phytotoxicity. Necessary pre-treatments before the OMW actual treatment process play a fundamental role in the cost-effective applicability of the technology. For example, the inevitable pre-filtration is the weakness for oxidation technologies and continuous adsorption techniques. Furthermore, supercritical hydrothermal gasification was proven to be efficient in converting OMW into useful gaseous output (Casademont et al., 2018). In this way, hydrothermal treatment could be a novel agricultural effluent treatment strategy due to its common reaction medium and circumvented the pre-drying process. However, further researches are required to improve the treatment system in meeting the discharge requirement.

Since the complexity of the OMW matrix due to the presence of several and different background compounds the effect of combined treatment was investigated. Sole OMW treatment of using anaerobic digestion was insufficient due to the wastewater toxicity and biodegradability. Hence, catalytic oxidation using Fenton's reagent was suggested in degrading complex organic acids and recalcitrant components in the wastewater. Consequently, higher methane yield was achieved (306 mL of CH_4/g of COD degraded) and the COD removal increased respect to single AD (288 mL of CH_4/g of COD degraded). Nevertheless, high capital and operational costs associated with the chemical reactor and the reactants were identified by the authors as the major concern and restriction for scaling up the process to industrial size. A study was performed on utilising combined chemical–biological treatment in solving OMW problem (Karahan et al., 2016). The issue of organic complexity that led to ineffective biodegradation of OMW was highlighted. The experiment result showed that filtration and chemical pre-treatment with Fenton and iron electrode were ineffective in COD removal. However, the chemical treatment attempt was still capable in minimising the fine particulate matters which eventually improved the biodegradability characteristics of OMW. It can be further deduced that the wastewater with high organic content is difficult to be biologically treated, thus complementary methods are essential for a better treatment result. Below an more in-depth illustration of the techniques is proposed.

1.2.2.1 Thermochemical treatment

Hydrothermal process can be further categorised into carbonisation, liquefaction and gasification, where the main product is hydrochar, bio-oil and syngas respectively. Recently, hydrothermal treatments have been extensively investigated to tackle the biomass waste issue that is today considred an interesting and potential source of energy.

Attempts to convert OMW into biochar material (hydrochar) by hydrothermal carbonisation (HTC) has been undertaken (Poerschmann et al., 2013a,b). However, experiment led to the attainment of very low yield of hydrochar, probably due to the low carbohydrate content in the OMW. Hence, the former study concluded that the employment of HTC in OMW treatment was not recommend. To overcome the problem of low carbon content some attempts to impregnate OMW on the sawdust for the production of green biofuels and biochar under pyrolysis were conducted (Haddad et al., 2017). In comparison to the solely OMW biomass treatment, the combination of OMW with sawdust resulted in a biochar rather richer in K, N and P elements. Moreover, an overall mass yield in plant growth was registered after application of biochar to crops, confirming the potential of the abovementioned biochar nutrients in improving soil fertility. Moreover, it was also reported that the evaporated water could be recovered for irrigation purpose.

Wet air oxidation and wet hydrogen peroxide oxidation, some of which aided by various catalysts such as platinum, ruthenium, montmorillonite or zeolites, have been applied so far for the treatment of OMW, whether alone or very often coupled with biological anaerobic digestion post-treatments in different configurations (Ochando-Pulido et al.,. 2017). In the former papers' review the authors reported the nearly complete removal of the phenolic content and the elimination of up to 97% of the total organic carbon (TOC) upon catalytic wet air oxidation (CWAO) of OMW performed at 190 °C and 70-bar air pressure. Moreover, a decrease in the phytotoxicity of the OMW effluent was observed. However, experiments were conducted on diluted OMW (2 times).

Subcritical and supercritical water oxidation using H_2O_2 as the oxygen source in a tube reactor was studied (Erkonak et al., 2008). In this case, OMW was only filtered before the thermal treatment, without undergoing any dilution. Temperature effect was recognized, among the other investigated operating parameters (i.e. pressure, residence time and oxygen concentration) as the most significant parameter in reducing the TOC. The experimental results showed that the supercritical water oxidation process managed to reduce the total organic content (TOC) up to 99.96% at very short residence times of 5 s to 30 s. An increase in TOC conversion and in the overall treatment efficiency was also registered for higher oxygen concentration and longer reaction time, as well as for a reduction in the system pressure (respectively from 300 to 100 bar). Nevertheless, problems related to the low-pressure system and the increased rate of carbonization were detected. The authors claimed the possible blockage in continuous flow tubing reactor caused by the formation of smut that would eventually deposit at the reactor inner wall and cause blockage.

Hydrothermal gasification is worth an investigation to resolve the waste problem, meanwhile, to produce useful energy and promote materials recovery from biodegradable organic compounds and biomass wastes (Kıpçak et al., 2011).

The H_2 production was gauged from the hydrothermal treatment of OMW under supercritical water condition (803 K and 250 bar) in a sand bath preheated reactor. The commercially-ready homogenous catalysts, namely KOH, K_2CO_3, NaOH and Na_2CO_3 were employed. COD removal recorded 75%–89% in all the catalysts, especially carbonate salt. An optimum result, 76.73 mol H2/kg of OMW dry, was achieved in the hydrothermal treatment at 803 K and 230 bar for 20 min, using 58 wt% KOH catalyst and COD value of 23 ± 2.56 g O2/L OMW. A higher concentration of hydroxide catalyst resulted in a greater reduction of CO which subsequently producing more H2. This treatment method was proven to be economically and energetically efficient (Casademont et al., 2018).

The hydrogen production from the hydrothermal process of OMW was measured at different parameters (Casademont et al., 2016). The best result was reported at 603 K and 150 bar with the reaction time of 30 min that gave the highest yield of gaseous and liquid products with the lowest solid residue output. A significant rise of hydrogen production was recorded with the utilisation of Au–Pd catalyst in treating OMW under supercritical water condition (803 K, 250 bar, less than 3 min), in comparison to the other catalysts namely TiO2, V2O5 and KOH. It is worth noting that about 90% COD removal achieved for all the experimental runs with and without catalysts. This indicates that both homogenous and heterogeneous catalysts did not aid much in reducing the COD in OMW.

1.2.2.2 Physicochemical treatment

The most investigated physicochemical methods are related to membrane filtration and adsorption processes. Between these, membrane ultrafiltration process could be an adequate method in purifying OMW. Unfortunately, by treating OMW severe fouling problems occurred and more studies focused on overcoming that problem are necessary. Fouling can be reduced by setting the operating condition below the boundary flux, however it will make the process economically not feasible. Photocatalysis is suggested to act as pre-treatment to increase the boundary flux, however high costs limited its utilization (Stoller et al., 2017, 2015). Speltini et al. (2015) highlighted that OMW is a low-cost and rewarding sacrificial agent to be used in the photocatalytic hydrogen gas evolution. The study reported that 280 μmol H_2 can be produced by 30 mL of OMW. The environmental impact of the investigated process is extremely lower than the process producing H_2 from natural gas. For example, differently from the latter, the photocatalytic hydrogen of OMW generates zero

CO_2 emission. However, the overall efficiency of the photocatalytic system needs to be increased via photoreactor features upgrade.

Among the scarce attempts overtaken to investigate natural adsorbents for OMW treatment, a significant one was the employment of local natural Jordanian clay (Azzam et al., 2015). Batch experiments were performed with raw and undiluted OMW and results showed that the overall pollutant content (e.g. phenolic compounds) was reduced. A total reduction of 10%–20% COD was recorded. Following batch experiments some continuous-flow packed bed experiments were performed. As typically occurred, continuous-flow trials led to better adsorption performances: a 50% reduction in COD was reported. However, the primary concern remains the possibility of discharging the treated OMW with respect of legal discharge levels. Indeed, by now it is rather well-known that due to the complexity of the OMW matrix and to its highly concentrated presence of different compounds, many authors claimed that a single treatment methodology is insufficient and proposed to integrate different treatment techniques or including multiple treatment stages to treat the effluent effectively. In this way, an example was represented by the work of Aly et al. (2014) who coupled different filtration/adsorption step with the final aim to produce a cost-effective process with low cost adsorbents. They set up three consecutive columns of gravel, fine sand and a mixture of acidified cotton and clinoptilolite (a natural zeolite) prior to the polishing steps using activated charcoal (AC) and lime. Results suggested that most of the contaminants were removed in all the three columns, while organic particles were removed using AC and the pH was raised from 2.9 to 5.1 using lime. The conclusion of the study reported that the proposed physiochemical treatment was able to produce clean water for the agricultural water source.

1.2.2.3 Biological treatment

Most of the biological treatment studies of OMW focused on anaerobic digestion (Anastasiou et al., 2011). However, prior to that, sufficient polyphenols removal or substantial multiple dilutions is required for a more effective degradation in biological treatment (Speltini et al., 2015). multiple dilutions (70–100 times in common practices) are recommended to reduce the feed COD level to 1 g/L before subjected to biological treatment and to achieve a better treatment result. However, this would probably induce higher cost implication. El Hajjouji (2014) evaluated the performance of aerobic treatment in removing phytotoxic contents in OMW and proved its effectiveness, suggesting advantages of having this treatment before AD to improve treatment efficiency. On the contrary, Mantzavinos and Kalogerakis (2005) claimed that the aerobic processes are incapable in dealing with organic-rich OMW.

Hydrophilic phenol degradation was decreased to 72% by co-composting of OMW with sesame bark (Hachicha et al., 2009). The total organic matter was also decreased to 52.72% after co-composting. The former work found out that all the polyphenolic compounds were removed after 7 months (210 days) of processing. However, despite the proven ability in PC removal, the co-composting technique has two main disadvantages: the loss of potential energy recovery and more time-consumption than AD.

Moreover, the bio-processed OMW was found to have a great potentiality to inhibit the germination of the main fungal phytopathogens, bacterial, and weed species without adversely affect the crop growth. Despite the dose and timing in using OMW biopesticide should be carefully measured and could resulted difficult to define, the possibility of using OMW as biopesticide was found favorable (El-Abbassi et al., 2017). Further investigation is needed, however the work of El-Abbassi showed that the PC content of OMW together with other natural occurring chemicals (not precisely identified) were capable to act as a biopesticide and contributed to crop protection against plant diseases. This finding resulted of extraordinary interest, since it could represent the first step towards the abandon of synthetic insecticides, minimizing the environmental problems.

1.2.2.4 Adsorption

The abovementioned biological, physicochemical and thermochemical processes are just some of those that have been proposed by wastewater companies for the treatment of OMW, which included evaporation, ultrafiltration, reverse osmosis, flocculation, chemical oxidation, anaerobic digestion and lagooning. However, these processes generally do not include a specific treatment step aimed at the recovery of the OMW PC content. On the other hand, the inclusion in the OMW treatment train of a step leading to PC recovery could lead to a relevant decrease of the OMW treatment cost. Indeed, the recovery of a marketable high valuable PC-rich product would led to favorable revenues, helping the economic sustainment of the process. To recover PCs from OMW, several processes can be applied, such as solvent extraction, adsorption and cloud point extraction (Kalogerakis, 2013; Galanakis, 2010; Zagklis et al., 2015; Conidi et al., 2014; Bertin et al., 2015; Soto et al., 2015; El Idrissi, 2017; Frascari et al., 2016; El-Abbassi et al., 2014).

Among these, adsorption has a relatively simple design, operation and scale up. Moreover, physical adsorption method is generally considered to be the best, effective, low-cost and most frequently used method for the removal of phenolic compounds (Achak et al., 2009). For instance, 95% removal of phenolic compounds was achieved using sand filtration and subsequent treatment with powdered activated carbon in a batch system (Sabbah et al., 2004). On the other hand, the recovery yield was lower (60 %) using a solid phase extraction, by employing Amberlite XAD16 resin as the adsorbent and ethanol as the biocompatible desorbing phase (Scoma et al., 2011). Bertin et al. (2011) suggested that Amberlite XAD7, XAD16, IRA96 and Isolute ENV+ are the four most promising adsorption resins. Considering the integrated adsorption–desorption processes, ENV+ achieved the highest recovery of total phenols from OMW when elution was performed with acidified ethanol. Indeed, the highest recovery of hydroxytyrosol (77%) was achieved when nonacidified ethanol was used as the desorbing phase. Nevertheless, when the recovery of phenols is carried out with ENV+, the protocol has to be adjusted from time to time. Considering the study conducted by Ferri et al. (2011), the highest phenol adsorption (76%) was achieved using IRA96 polar resin. Conversely, non-polar adsorbents allowed higher desorption ratios. A purified olive extract rich in phenolic and oleosidic compounds was prepared from OMW by adsorption onto an amphoteric polymer resin. The corresponding yield was 2.2 % (w/v).

Ena et al. (2012) stated that granular activated carbon can be more efficient than Azolla (vegetable matrices) in terms of phenols adsorption and desorption. The recaptured powder contained hydroxytyrosol in concentrations 3.5-fold higher than those of Azolla (3.23/1.51 % matrix). Singh et al. (2008) investigated the adsorption of both phenol and 2,4-dichlorophenol through the acid treatment of coconut shells (ATSAC) and the results show higher monolayer adsorption capacity for both compounds. Achak et al. (2009) used banana peel as a low-cost solution biosorbent for removing phenolic compounds from OMW. According to the results, by increasing banana peel dosage from 10 to 30 g/L, phenolic compounds adsorption was significantly increased from 60 to 88 %. Desorption studies showed that a low pH value was efficient for the desorption of phenolic compounds. Zeolite, compared to other substrates (clay soil and bentonite), appeared to be a useful mineral in reducing the organic load of OMW. In addition, the regeneration of zeolite was easy after treatment either by simple settling or light centrifugation procedures. Besides, the low temperature ashing-procedure appears to be a very interesting ecofriendly technique since it is capable of reducing polyphenols and COD from OMW (Santi et al., 2008).

A significant drawback of this recovery technology is that, in the presence of a complex matrix such as OMW, PC adsorption yields can be significantly reduced by the competitive adsorption exerted by other compounds, in particular by carbohydrates and amino acids. Two main adsorption mechanisms can be applied for PC recovery: simple adsorption on neutral non-ionic resins and ion exchange on ionic resins. Both processes were successfully used in several fields (Krammerer et al., 2011).

On adsorption technique, pH has a relevant impact on PC: low pHs favour the protonated PC form and thus adsorption on neutral resins, whereas higher pHs favour the anionic PC form, and therefore adsorption on ion exchange resins. High pHs promote the ion exchange of PCs that do not contain carboxyl functional groups. On the other hand, the ion exchange of PCs that contain carboxyl groups can be operated also at neutral pH values (Krammerer, 2010).

1.3 MATERIAL AND METHODS

1.3.1 OMW, resins and chemicals

The tested OMW was produced by a 3-phase olive mill located in Mnihla, Tunisia. Its characterization is reported in chapter 1.4.2.

Five sorbent resins, kindly provided by DOW Chemicals Europe GmbH, Horgen, Switzerland, were tested: Amberlite XAD 16, Optipore SD-2, Amberlite FPX66, Amberlite XAD761, IRA958 Cl. The main characteristics of the 5 resins are reported in Table 1.3.1. Among these five media, three (XAD 16, FPX 66, XAD 761) are purely neutral adsorbents, one (IRA958 Cl) is a strong ion exchange resin, whereas Optipore SD-2 is a neutral adsorbent with a minor ion exchange component. IRA958 Cl was pre-treated in different ways depending on the resin form to be tested in the different assays: to test the Cl form, the resin was just rinsed in DI water. To test the OH form, the resin was rinsed in DI water, fluxed with NaOH 1M and finally washed in DI water to elute the excess ions. Differently, the neutral adsorbents XAD16, FPX 66, XAD 761 and Optipore SD-2 were activated by means of the following procedure: 1) double washing with de-ionized (DI) water to remove salts added by the poducer to preserve the resin: each step consists of a 10-minute washing under agitation at 140 rpm and subsequent liquid removal through a Whatman Phenomenex system connected to a vacuum pump; 2) double resin soaking with 0.5% HCl 0.1N ethanol in order to remove any organics that could have remained by the manufacturing process: each step consists of a 30 minute washing under agitation at 140 rpm and subsequent solvent removal; 3) and finally the resulting slurry was re-washed with DI water as described in 1) to wash out the ethanol and maintain the resin ready for the packing. All reagents and standards were purchased from Sigma Aldrich (Milan, Italy). The COD Test Tubes were acquired from Aqualytic (Dortmund, Germany).

Table 1.3.1 Technical characteristics of the tested resins

Resin	Adsorption mechanism	Matrix	Surface Area *(m^2/g)*	Pore size *(A)*	Harmonic mean particle size (mm)	Approximate industrial cost (€/L)
XAD761	Neutral adsorption	Crosslinked phenol-formaldehyde polycondensate	200	600	0.56 – 0.76	28
XAD16N	Neutral adsorption	Macroporous styrene-divinylbenzene copolymer	800	150	0.56 – 0.71	31
FPX66	Neutral adsorption		700	150	0.60 – 0.75	26
OPTIPORE SD-2	Neutral adsorption + minor ion exchange component		800	50	[a]	18
IRA958 Cl	Strong ion exchange	Crosslinked acrylic polymer with quaternary ammonium group	400	[a]	0.63-0.85	8

[a] Data not available

1.3.2 Analytical methods

Total PCs were analysed by means of an HPLC method based on the use of an Agilent Infinity 1260 HPLC, equipped with a quaternary pump, an autosampler, a thermostatted column compartment, a Jasco 875-UV Intelligent UV/vis diode-array detector and a Phenomenex Kinetex® 2.6 µm Biphenyl 100 Å column (50 x 2.1 mm). Two mobile phases were applied (solvent A: HPLC-grade water with 0.1% orthophosphoric acid; solvent B: acetonitrile). The flow was set at 1.0 mL/min and the mobile phase gradient (0-4 minutes, 100% phase A; 4-6 minutes, 70% phase A and 30% phase B; 6-15 minutes 70% phase A and 30% phase B) was designed to merge all the phenolic peaks into a single broad peak. The wave length was set a 264 nm and gallic acid was used as external standard (50 mg/L). For comparison purposes, the total PC content of the raw OMW and of the final desorbed products was measured also according to the conventional colorimetric test developed by Folin and Ciocalteu (1927). In the Foulin-Ciocalteu (FC) method, 25 mL flasks, carefully cleaned with sulfuric acid 25% and washed with de-ionized (DI) water, were filled with 12.5 mL of DI water, 125 µL of sample (diluted as required, to avoid absorbance signal saturation) and 1.25 mL of FC reagent. After 2 minutes, the reaction was quenched by adding 3.75 mL of sodium carbonate (20% w/v). Finally, the flasks were diluted to the volume mark, and left at 75°C for two hours. Then, the absorbance was read at 765 nm with a Cary 100Scan UV spectrophotometer (Agilent, Santa Clara, California), using as reference a dephenolized OMW obtained by repeated adsorptions with the Amberlite XAD16 resin until the attainment of a final PC content < 1% of the original PC level in the OMW, and then treated with FC reactants. The method was calibrated with acid gallic as external standard.

Single PCs: These analyses were performed by Letizia Bresciani of the University of Parma, applying the following procedure. The samples were previously diluted 1:10 with acidified water (0.1% formic acid, v/v); An Accela UHPLC 1250 equipped with a linear ion trap-mass spectrometer (LTQ XL, Thermo Fisher Scientific Inc., San Jose, CA, USA) fitted with a heated-electrospray ionization probe (H-ESI-II; Thermo Fisher Scientific Inc., San Jose, CA, USA) was used. Separation was carried out by means of a Restek C18 (100x2.1 mm) column, 3 µm particle size (Restek Corporation, Bellefonte, PA, U.S.). The injection volume was 5 µL, and the column temperature 40 °C. PCs were detected in negative ionization mode, with mobile phase pumped at a flow-rate of 0.3 mL/min, consisting of a mixture of acidified acetonitrile (0.1% formic acid) (solvent A) and 0.1% aqueous formic acid (solvent B). Following 0.5 min of 5% solvent A in B, the proportion of A was increased linearly to 51% over a period of 8.5 min. Solvent A was increased to 80 in 0.5 min, maintained for 2 min and then the start condition were re-established in 0.5 min and maintained for 5 min to re-equilibrate the column (total run: 17 min). The H-ESI-II interface was set to a capillary temperature of 275 °C and the source heater temperature was 200 °C. The sheath gas (N2) flow rate was set at 40 (arbitrary units) and the auxiliary gas (N2) flow rate at 5. During PC analysis, the source voltage was 4.5 kV, and the capillary voltage and tube lens voltage were -42 V and -118 V, respectively. A preliminary analysis of the single PCs was carried out by applying a negative ionization using a full-scan, data-dependent mode, scanning from a mass to charge (m/z) of 100-1500 using a collision induced dissociation (CID) equal to 35 (arbitrary units) to obtain fragmentation. Finally, further specific MS^2 analyses were carried out to identify the compounds revealed in the first step, by monitoring specific m/z transitions. PCs were identified based on available scientific data (Bertin et al., 2011; Rahmanian et al., 2014; Daassi et al., 2014).

Antioxidant capacity was measured by 2,2'-azino-bis(3-ethylbenzothiazoline-6-sulphonic acid; ABTS) decolorization assay using a Shimazu UV-VIS spectrophotometer (UV-1601). The ABTS stock solution was prepared by dissolving the ABTS reagent to a final concentration of 7 mM using a $K_2S_2O_7$ 2.5 mM solution and allowing the mixture to stand in the dark at room temperature overnight before use. The same day of the test an ABTS working solution (ABTS WS) was prepared using the stock solution by dilution with de-ionized water to an absorbance of 0.70 at 734 nm. 10-100 μL of sample were then added to 1 mL of the ABTS WS and incubated at 30°C for 30 minutes, and the absorbance value was read at 734 nm. The calibration line was obtained using ascorbic acid as standard. To calculate the antioxidant activity of the sample as $\mu g_{\text{ascorbic acid equivalent}}/\mu L_{\text{sample}}$, the following expression was applied:

$$\text{Antioxidant Activity}\left(\mu\text{g ascorbic acid eq.}/_{\mu\text{L sample}}\right) = \frac{\text{Value calulated from calibration line }(\mu\text{g ascorbic acid eq.}) \times \text{sample dilution factor}}{\text{Sample volume reacted with 1mL ABTS WS }(\mu\text{L sample})}$$

Total solids were measured by drying the sample overnight at 105°C and weighing. Volatile solids were measured by exposing the 105 °C-dried sample at 550°C overnight and re-weighing. Suspended Solids were determined by filtration with a 0.45 μm ALBET cellulose nitrate membrane filter and weighing.

COD was measured spectrophotometrically using the Aqualytic COD Vario Tubes (range: 0-1500 mg_{O2}/L).

Proteins were spectrophotometrically analyzed following the Bradford method (Bradford, 1976) by mixing 67 μL of sample with 2 mL of Bradford reagent (VWR International S.r.l). After an incubation of 10 minutes at 4°C in a dark environment, absorbance was read at 595 nm. The calibration line was obtained using Bovin Serum Albumin (BSA) as standard. *Reducing sugars* were spectrophotometrically analyzed following the dinitrosalicylic acid (DNS) assay (Miller, 1959) by mixing 100 μL of sample, 100 μL of demineralized water and 100 μL of DNS reagent. The mixtures were heated in boiling water for 15 minutes, cooled in ice to ambient temperature and after the addition of 900 µL the absorbance value was read at 540 nm. The calibration line was obtained using glucose as standard. The DNS reagent was prepared mixing 20 mL of a 96 mM DNS water solution with 8 mL of a 5.3 M Sodium potassium tartrate tetrahydrate basic solution (NaOH 2M), bringing the solution to a final volume of 40 mL.

OMW density was measured by means of a 100 mL ITI Tooling pycnometer. *pH* was measured with an EUTECH Instruments pH 2700 Series pH-meter (Thermoscientific, Walthman, Massachusetts). More details on the analytical procedures are reported in Galanakis, (2014). In the frontal analysis tests aimed at studying the fluid dynamic behavior of the adsorption bed, *electrical conductivity* (EC) was measured at the column outlet with an EUTECH Instruments 2700 series conductimeter (Thermoscientific, Walthman, Massachusetts)

1.3.3 OMW microfiltration

OMW microfiltration resulted necessary to avoid the adsorption bed clogging. The microfiltration plant, supplied by Juclas srl (Verona, Italy) and shown in Fig. 1.3.2, was composed by: a 50 L feed reservoir, a membrane pump with a 1-4 bar operating pressure, a ceramic circular filter (40 cm diameter, 0.2 µm average pore-size), a manual valve to regulate the flowrate of the recirculated retentate and the filtration pressure, a pressure sensor in the retentate line to monitor and control the process, and two outlet streams: one for the permeated filtered OMW and one for the retentate, recirculated into the feed reservoir. The plant applies a cross flow filtration, in which the suspension passes tangentially along the surface of the filter.

Figure 1.3.2 Microfiltration plant provided by JUCLAS srt (Verona, Italy): a) real image of the plant; b) flow-sheet of the plant; c) schematic illustration of the cross-flow filtration applied by the plant.

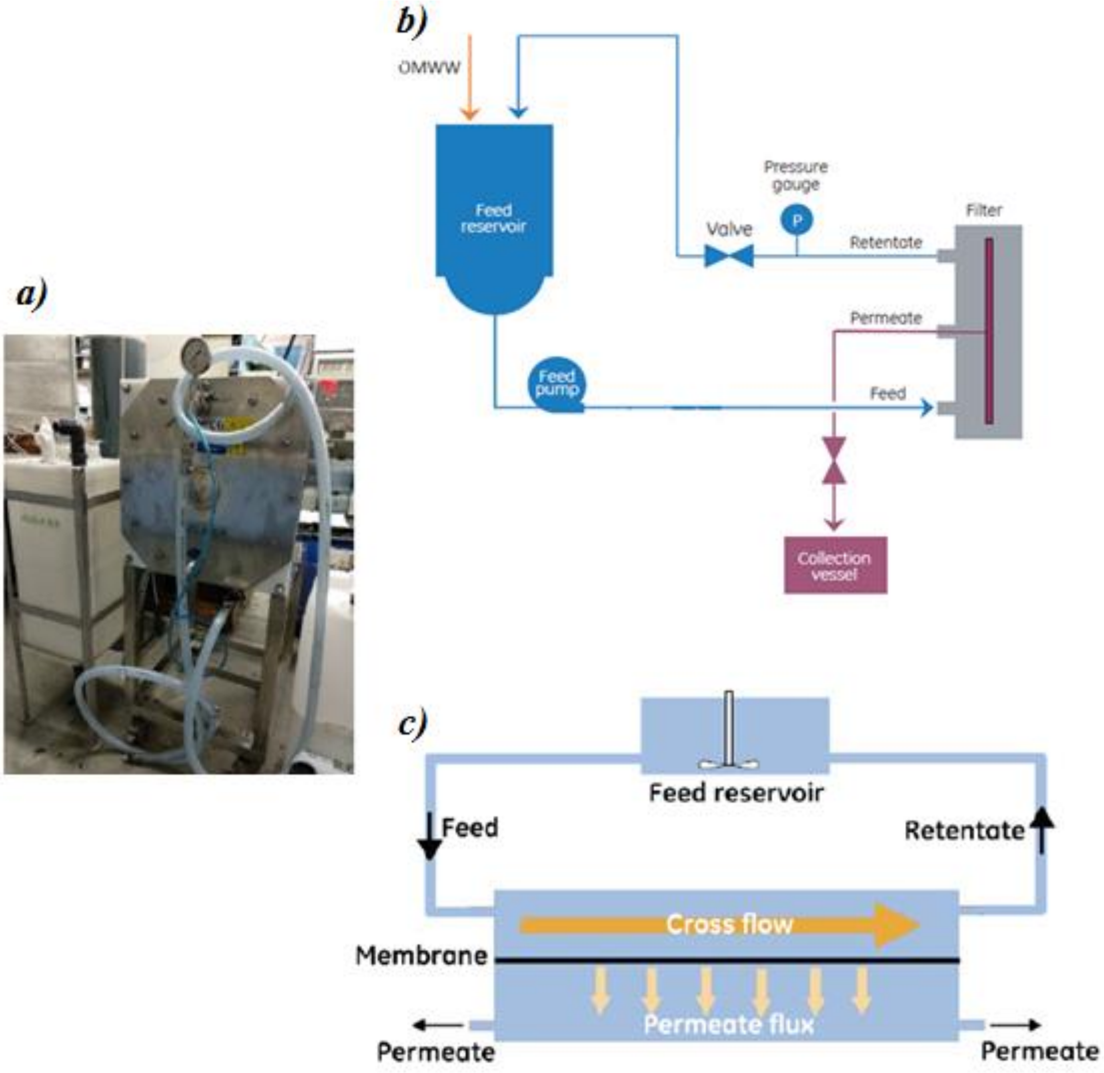

1.3.4. Phenolic compounds and COD adsorption isotherms

The PC and COD adsorption isotherms relative to the 5 tested resins were studied by mixing different amounts of dry resin with 30 mL of microfiltered OMW in 120 mL glass vials, so as to test dry resin / OMW ratios in the 2-450 $g_{\text{dry resin}}/L$ range. The vials were placed in a rotatory shaker (120 rpm, 22 °C) for 2 hours, to reach the equilibrium condition. A graphical representation of the procedure for resin activation and for the operation of the batch adsorption tests is provided in Fig. 1.3.3. For the investigated resins the optimal pH was preliminary tested and selected by means of single point batch tests performed with a media concentration of 10 $g_{\text{dry resin}}/L_{\text{OMW}}$.

Figure 1.3.3 Schematic illustration of the resin activation and batch adsorption isotherm operation.

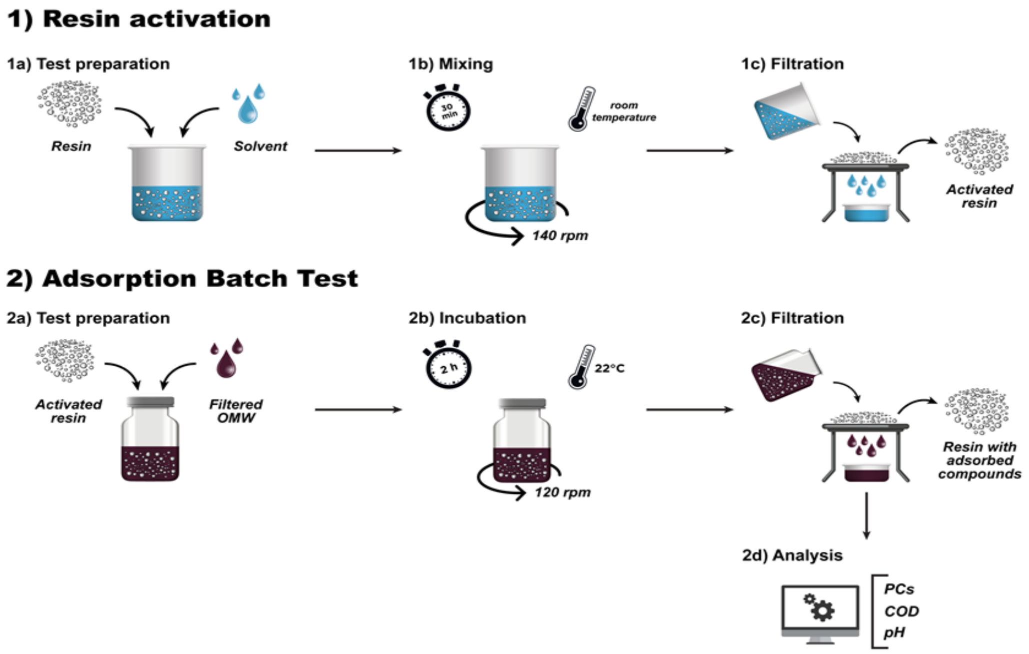

Moreover, in order to gain more insight on the type of adsorption mechanisms and to be sure that the equilibrium condition had been reached after the 2 hour equilibration time, a preliminary adsorption kinetic test was conducted for each tested resin at the higher resin concentration tested in the isotherm (450 $g_{\text{dry resin}}/L$). During these tests, the PC liquid-phase concentrations were frequently measured every 30 minutes for the first 180. The corresponding dimensionless sorbed-phase PC concentrations $C^*_{S,t,PC}$:

$$C^*_{S,t,PC} = C_{S,t,PC} / C_{S,eq,PC} \qquad \text{(Eq. 1.1)}$$

where $C_{S,eq,PC}$ indicates the average sorbed-phase concentration during the last 30 minutes of each test, were plotted versus time and interpreted with both the first-order or Lagergren model:

$$dC^*_{S,t,PC}/dt = k_1 \cdot \left(C^*_{S,eq,PC} - C^*_{S,t,PC}\right) \qquad \text{(Eq. 1.2)}$$

and the pseudo-second-order model (Ho and McKay, 1999):

$$dC^*_{S,t,PC}/dt = k_2 \cdot \left(C^*_{S,eq,PC} - C^*_{S,t,PC}\right)^2 \qquad \text{(Eq. 1.3)}$$

The PC concentration in the liquid was evaluated by HPLC. For both PC and COD, the equilibrium concentration in the solid phase, $C_{S,i,eq}$ was determined as:

$$C_{S,,eq,i} = (C_{L,0,i} \cdot V_{OMW,0} - C_{L,eq,i} \cdot V_{L,final})/m_S \qquad \text{(Eq. 1.4)}$$

where: m_S indicates the dry resin mass, $C_{L,0,i}$ and $C_{L,eq,i}$ the initial and final PC or COD concentrations in the liquid phase, $V_{OMW,0}$ and $V_{L,final}$ the OMW volume initially added and the final liquid volume resulting from the sum of the added OMW and the water initially contained in the activated resin. 95% confidence intervals associated to $C_{S,eq,i}$ were calculated by means of standard error propagation rules.

For each resin, the performance parameters obtained from the isotherms were the PC sorbed concentration ($C_{S,PC,eq,OMW}$) and the purity in PCs of the sorbed product (PC/volatile solids) in equilibrium with the PC and COD average concentration in the microfiltered OMW. Indeed, in a continuous flow adsorption process characterized by a high resin operating capacity, in most of the adsorbing bed the solid phase is in equilibrium with the PC and COD concentrations of the treated OMW. The correct evaluation of these parameters requires a model-based extrapolation of the isotherm experimental data until the PC and COD concentrations of the treated OMW ($C_{L,PC,OMW}$, $C_{L,COD,OMW}$), since all the experimental data at equilibrium are necessarily characterized by liquid phase PC and COD levels lower than the corresponding ones in the treated OMW. To this purpose, the PC and COD experimental isotherms were interpolated by means of the Langmuir (Eq. 1.5) and Freundlich (Eq. 1.6) models:

Langmuir

$$C_{S,eq,i} = \frac{C^{\infty}_{S,i} \cdot C_{L,eq,i}}{\frac{1}{K_{eq,i}} + C_{L,eq,i}} \qquad \text{(Eq. 1.5)}$$

Freundlich $$C_{S,eq,i} = K_{F,i} \cdot C_{L,eq,i}^{1/n_i} \qquad \text{(Eq. 1.6)}$$

where: $C_{S,eq,i}$ ($g_i/g_{dry\ resin}$) and $C_{L,eq,i}$ (g_i/L) indicate respectively the amount of sorbed PCs or COD per unit mass of adsorbent and the PCs or COD concentration in the liquid phase at equilibrium; $C_{S,i}^{\infty}$ ($g_i/g_{dry\ resin}$) the maximum amount sorbed per unit mass of adsorbent, corresponding to a complete monolayer on the adsorbent surface; $K_{eq,i}$ (L/g_i) the constant related to the affinity between the binding sites and PCs or COD; $K_{F,i}$ (L/$g_{dry\ resin}$) the sorption capacity in the Freundlich model; $1/n_i$ (-) the sorption intensity in the Freundlich model. The simulation of the isotherm experimental data was limited to the Langmuir and Freundlich models as the vast majority of the studies on the application of adsorption to liquid streams limited the simulation activities to these two models and obtained very high correlation coefficients with either the Langmuir or the Freundlich model (e.g. Ziati et al., 2017; Foo and Hameed, 2010; Abdelkreem, 2013).

Furthermore, the goal of the isotherm modeling activity was not to identify the most suitable model among the numerous ones available in the literature, but rather to perform a model-based evaluation of the two above-listed performance parameters, which requires the extrapolation of the PC and COD sorbed concentrations up to the values obtained in equilibrium with the corresponding levels in the treated OMW.

The model parameters were estimated by non-linear least squares regression of the calculated COD or PC solid phase concentrations ($C_{S,eq,calc,i}$) to the corresponding experimental values ($C_{S,eq,i}$). For each tested resin and parameter (PC or COD) the best-fitting model was selected on the basis of the correlation coefficient R^2, defined so as to take into account the number of model parameters (Frascari et al., 2013):

$$R^2 = 1 - \left(\frac{\sum_{i=1}^{N} \left(C_{S,eq,i} - C_{S,eq,calc,i} \right)^2}{N - P - 1} \right) \Bigg/ \left(\frac{\sum_{i=1}^{N} \left(C_{S,eq,i} - C_{S,eq,m} \right)^2}{N - 1} \right) \qquad \text{(Eq. 1.7)}$$

where N indicates the number of experimental tests in the studied isotherm, and P the number of model parameters. For each isotherm, the Langmuir and Freundlich isotherms were compared by means of F tests. The best-fitting model was considered statistically different from the other one if the test outcome – indicating the probability that the two models are not statistically different - resulted < 0.05.

For each resin, the performance parameters obtained from the isotherms were: i) the isotherm shape (favorable / unfavorable); ii) the purity in PCs of the sorbed product (PC/volatile solids); iii) the PC sorbed concentration in equilibrium with the PC average concentration in the microfiltered OMW ($C_{S,PC,eq,OMW}$); indeed, in a continuous flow adsorption process characterized by a high resin operating capacity, this parameter represents the PC sorbed concentration that will be achieved in most of the adsorbing bed.

For the resins that led to the best adsorption performances, the adsorption tests were followed by batch desorption tests. To this purpose, the OMW in equilibrium with the tested resin was removed by means of a syringe, and 30 mL of each tested desorption solvent (Fig. 1.3.4) were added. The vials were placed again in a rotatory shaker (120 rpm, 22 °C) for 2 hours, to reach the equilibrium condition. Total PCs were then measured in the liquid phase. The desorption performances of each resin / solvent combination were quantified by means of the PC desorption yield ($Y_{des,PC,}$), evaluated as $m_{PC,\ desorbed} / m_{PC,sorbed}$. The results were utilized to select for each resin the best desorption solvent(s) and the corresponding optimal pH.

Figure 1.3.4 . Schematic representation of the procedure for the operation of the desorption isotherm tests.

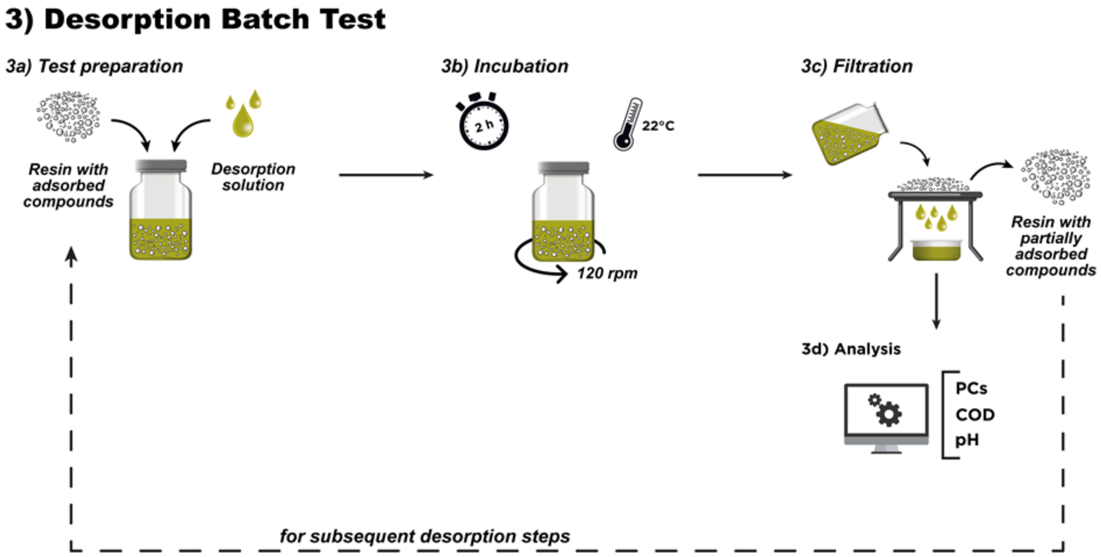

.

1.3.5 Adsorption column packing and fluid-dynamic characterization

The adsorption/desorption breakthrough tests, performed only for the resins that provided satisfactory performances in the batch isotherm tests, were conducted at 22°C in the 1.00-m column. The breakthrough tests were conducted in a plant composed of 2 glass columns (height 0.61 m, inner diameter 0.027 m) connected in series. The column temperature was controlled at 22°C by means of a jacket connected to a temperature-controlled bath. After placing a 55 mm layer of quartz sand at the bottom, each column was filled with the chosen resin using the dynamic axial compression (DAC) technique. The procedure consists in filling the column step by step by adding small amount of slurry (water and resin) and compact the bed through an axial compression provided by fluxing down-flow. After pouring each aliquot, the column was filled with water, which was extracted and recirculated downwards with a Masterflex L/S 0.1HP 1-100 RPM pump (Cole-Parmer, Vernon Hill, Illinois) until the stable settling of the resin. Then, a further aliquot was fed and the procedure was repeated. Finally, a further 55 mm quartz sand layer was placed at the top of the resin. The total resin bed length was thus 1.00 m.

For each resin tested in the semi-continuous assays, the fluid dynamic behavior of the adsorption bed was studied before each adsorption/desorption experiment by means of conventional frontal analysis tests conducted with a 0.05 M NaCl solution in the case of neutral resins. In the case of the IE resin IRA958 OH, given the very high affinity of Cl^- for the resin functional group, a different approach based on the use of Cl^- free solutions was selected: a first test was conducted with a NaOH 0.05 M solution, after fluxing the packed resin with de-ionized water, whereas a second test was conducted with de-ionized water, after fluxing the packed resin with NaOH 0.05 M. The electrical conductivity (EC) was measured at the column outlet with an EUTECH Instruments 2700 series conductimeter. These tests were used in the first place to estimate the effective porosity (ε), a parameter required to evaluate the interstitial velocity and the hydraulic retention time on the basis of the measured OMW flow rate. The effective porosity was evaluated from the retention time distribution curve according to the procedure proposed by Levenspiel (1999). The frontal analysis tests were also used to evaluate two indicators of packing quality: the reduced plate height, evaluated as ratio of the height equivalent to a theoretical plate (HETP) to the mean particle diameter of the tested resin, and the asymmetry factor, defined as the ratio between the leading and tailing semi-width of the peak at 10% of the peak height. These parameters were evaluated as described by Frascari et al. (2016).

1.3.6 Adsorption/desorption breakthrough tests

The adsorption/desorption breakthrough tests, performed only for the resins that provided satisfactory performances in the batch isotherm tests, were conducted at 22°C in the 1.00-m column (Fig. 1.3.5). During the adsorption step, the microfiltered OMW was fed with a Masterflex L/S 0.1 HP 1-100 RPM peristaltic pump. Both pressure drop and flowrate were measured hourly. The total PC and COD concentrations were measured in OMW samples taken every hour from the column exit and every 3 hours from the inlet. The average PC and COD levels at the inlet were used to normalize the corresponding outlet values. The adsorption tests were continued up to the attainment of a 0.92-0.95 outlet normalized PC concentration. The adsorption performances of each tested resin were quantified by means of the following indicators, referred to a 0.20 PC dimensionless outlet concentration used as breakpoint value: i) PC and VS adsorption yield ($Y_{ads,i,}$), evaluated as $m_{i,\ sorbed} / m_{i,fed}$; ii) resin selectivity for PCs, or PC/VS enrichment factor, defined as the PC/VS ratio of the adsorbed matter over that in the microfiltered OMW; the latter parameter corresponds to the ($Y_{ads,PC,}/Y_{ads,VS}$) ratio; iii) resin operating capacity (η_{PC}), defined as (PC mass sorbed at the breakthrough point) / (total PC mass that could be sorbed if all the resin was saturated). The VS adsorption yield was evaluated on the basis of the COD values measured during each breakthrough test, given the impossibility to accurately measured VS in the 2 mL samples periodically taken during each test. The detailed procedure relative to the evaluation of these performance indicators is reported in Table 1.3.2.

Different desorption solvents and procedures were used for each resin, on the basis of the results of the batch desorption tests and of previous works. The desorption solvent was fed with a Masterflex L/S 0.1 HP -1-100 RPM pump in counter-current flow with respect to adsorption step. The solvent flowrate was initially equal to the OMW flow rate in the corresponding adsorption test. A regular decrease in solvent flowrate was then applied to maintain the total pressure at the column inlet < 2 bars, as solvent viscosity increased due to the increase in PC dissolved concentration. Desorption was stopped when a PC concentration

< 1% of the average inlet concentration during the adsorption step was attained. The desorption performances of each tested resin were quantified by means of the PC and VS desorption yield ($Y_{des,i,}$), evaluated as $m_{i,\ desorbed} / m_{i,sorbed}$. In addition, the final desorbed product was characterized by means of the following parameters: i) specific antioxidant capacity; ii) purity in PCs, defined as PC/(volatile solids) and PC(total solids) mass fractions; iii) presence in the extract of high-value specific compounds, that could justify a further purification of the desorbed product.

Figure 1.3.5 . Flow sheet and picture of the adsorption / desorption plant. 1, tank for raw OMW or desorption solvent; 2, centrifugal pump; 3, sampling point for raw OMW or desorption solvent; 4, microfiltration unit; 5, sampling point for microfiltered OMW; 6, first column; 7, second column; 8, sampling point for effluent of the adsorption / desorption process; 9, tank for dephenolized OMW or PC-rich desorption solvent. The microfiltration unit – not shown in the picture - was bypassed during the desorption process. Of the four columns visible in the picture, two were dedicated to the breakthrough tests conducted with 1 of the 2 best-performing resins identified by means of the isotherm batch tests, whereas the other 2 were dedicated to the tests conducted with the other best-performing resin.

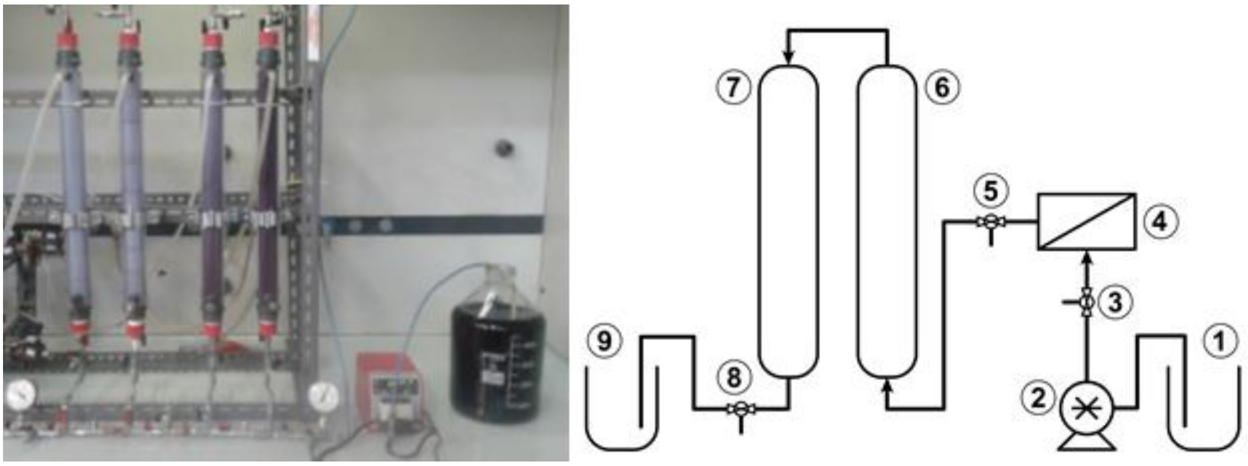

Table 1.3.2 Procedure for the evaluation of the performance indicators obtained from the breakthrough tests.

1) PC and VS adsorption yield ($Y_{ads,i,}$)

$Y_{ads,i,}$ was evaluated at a 0.20 PC breakpoint as $m_{i,sorbed,20\%}$ / $m_{i,fed,20\%}$, where $m_{i,sorbed,20\%}$ indicates the PC or VS mass adsorbed until the attainment of a 20% outlet normalized PC concentration, and $m_{i,fed,20\%}$ indicates the corresponding PC or COD mass fed to the adsorption column. $m_{i,sorbed,20\%}$ was estimated as:

$$m_{i,sorbed_{,20}\%} = m_{i,fed,20\%} - m_{i,out,20\%} \qquad \text{(Eq. 1.8)}$$

where $m_{i,out,20\%}$ is the mass lost in the outlet up to the 20% breakpoint. Eq. (S1) does not take into consideration the liquid phase PC content at the 20% breakthrough point, which is generally negligible. $m_{i,out,20\%}$ was calculated by numerical integration of the experimental breakthrough curve up to the selected 20% PC breakpoint:

$$m_{i,out,20\%} = Q \cdot \int_0^{t_{20\%}} C_{L,i,OUT} \cdot dt \qquad \text{(Eq. 1.9)}$$

where Q indicates the OMW flow rate fed to the column.

2) Resin operating capacity (η_{resin})

η_{resin} was evaluated at a 0.20 PC breakpoint as $m_{PC,sorbed,20\%}$ / $m_{PC,sorbed,saturation}$. $m_{PC,sorbed,saturation}$ indicates the PC mass theoretically adsorbed by the resin upon saturation of the sorption capacity. Since all the breakthrough tests conducted in this work were continued until the attainment of an outlet PC concentration close to the inlet PC concentration (condition of resin saturation), $m_{PC,sorbed,saturation}$ was calculated by numerical integration of the experimental breakthrough curve until the last experimental point:

$$m_{PC,sorbed,saturation} = Q \cdot \int_0^{t_{final}} \left(C_{L,PC,IN} - C_{L,PC,OUT}\right) \cdot dt \qquad \text{(Eq. 1.10)}$$

where Q indicates the OMW flow rate fed to the column.

3) PC and VS desorption yield ($Y_{des,i,}$)

$Y_{des,i,}$ was evaluated as $m_{i,\ desorbed}$ / $m_{i,sorbed}$. $m_{i,\ desorbed}$ was calculated by numerical integration of the experimental curve of PC or VS concentration obtained at the column outlet during the desorption procedure:

$$m_{i,\ desorbed} = Q_{des} \cdot \int_0^{t_{final}} C_{L,i,OUT} \cdot dt \qquad \text{(Eq. 1.11)}$$

where Q_{des} indicates the desorption solvent flow rate fed to the column.

1.3.7 OMW anaerobic digestion

The goals of the OMW anaerobic digestion (AD) tests conducted were: i) to evaluate the OMW biomethanation potential, and ii) to evaluate the possible biodegradation of PCs during the AD process. Indeed, AD could be placed before or after the PC removal step. According to the first configuration (AD before PC adsorption) the main concerns were, on one hand, the possible biodegradation and loss of phenolic compounds and, on the other hand, the inhibitory effects of the biomethanation process due to their presence. However, the main advantage related to the AD process before the PC process was the substantial reduction of organic matter, known to be competing with PCs during the adsorption step. Therefore the drastic reduction and methabolization of organic compounds would have enhanced the attainment of a purer final product. Whilst, according to the second configuration of the biorefinery OMWW process, to place the AD after the PC adsorption step would have avoided any inhibition effect by these family of compounds. Therefore, it was necessary to evaluate the possible biodegradation of the phenolic compounds and quantify the effective inhibitory effect of PCs on the AD process, with the final aim to identify the best configuration of the integrated process. Hence, two different groups of tests were set up and operated.

1.3.7.1 OMW biomethanation potential test

The biomethanation potential (BMP) of a micro-filtered OMW was compared to that of a micro-filtered and dephenolized OMW (with 95% PC removal). The inoculum was taken from an anaerobic digester fed with chicken manure. 60 mL of digestate were added to 120 mL-vials. Vials were agitated in an orbital mixer at 140 rpm and incubated at the constant temperature of 40°C. pH was periodically corrected to 8 by addition of a 0.5 M NaOH solution. The time evolutions of CH_4, PCs, COD and VFA were monitored. The tests were conducted according to a standard procedure for the determination of the biomethanation potential, i.e. with a very high ratio of inoculum to OMW (equal to 4 $g_{\text{inoculum volatile solids}}$ / $g_{\text{OMWW volatile solids}}$, corresponding to 61% v/v of inoculum and 39% v/v of OMW). This approach allowed a rapid onset of the AD process and the attainment of complete biomethanation within 3-4 weeks. However, in this specific context this approach has presented some drawbacks. Indeed, as the inoculum is rich in polyphenols, the high inoculum / OMW volumetric ratio leads to a relevant PC concentration also in the “dephenolized” tests, even if the type of PCs present is likely to be different. As a result, the “dephenolized” tests had a PC total concentration (0.75 g/L) equal to 63% of the PC concentration in the non-dephenolized tests (1.2 g/L). In addition, as most of the BOD initially present in these tests derived from the inoculum, this type of tests is not useful in order to evaluate the attainment of the thresholds for water reuse in agriculture indicated for BOD by the ISO 16075 standard. Moreover, as PC removal by adsorption is associated to a not negligible removal of other organic compounds (carbohydrates and proteins), in the dephenolized OMW, the COD was corrected to have the same value of of the micro-filtered OMW. The COD “reconstruction” of the original OMW was obtained by adding carbohydrates and proteins on the basis of an accurate OMW characterization. To verify the proper “reconstruction” of the matrix and, hence, the negligible difference between the actual micro-filtered OMW matrix effect and that of the synthetic OMW reconstructed, an additional group of tests was set up. To tap water were added respectively the main compounds characterizing the micro-filtered OMW background matrix (i.e. proteins and carbohydrates) and the PC compounds of the same OMW previously obtained. To evaluate the matrix effect the rate of biomethanation of the actual OMW COD and the “reconstructed” one (together with the same mixture and concentration of PCs) were investigated.

1.3.7.2 AD of the OMW dephenolized through the 1-m adsorption breakthrough tests performed with XAD16N and IRA958 OH.

The goals of the second set of OMW anaerobic digestion (AD) tests were: i) to evaluate the biomethanation potentials of two dephenolized OMWW obtained with two breakthrough tests with the two selected resins (XAD16N and IRA958 OH), and ii) to evaluate the reduction of the BOD5 value of the OMWW after the anaerobic process and verify the possibility to produce liquid stream with a BOD lower than the ISO 16075 threshold for WW reuse in agriculture. A single group of batch test were set up and operated. The AD of a micro-filtered and dephenolized OMW, obtained by means of a 1-m column breakthrough test with XAD16N resin was compared to that of a micro-filtered and dephenolized OMW obtained likewise using IRA958 resin in the OH form. All tests were carried out in 1080 mL bottles, filled with 500 mL of solution (Fig. 1.3.6). The inoculum was taken from an anaerobic digester fed with chicken manure and pre-treated by means of two successive washes with physiological solution (0.9% NaCl) and collection of the solid phase after a centrifuge step (5000rpm, 40minutes). This treatment was required in order to reduce the concentration of the PCs of the inoculum (different from those present in the OMW, but interfering with the analytical procedure and to allow the use of a high inoculum/OMW ratio without the drawbacks concerning the previously described AD test. The tests were set up in order to have the same inoculum concentration (20 $g_{\text{inoculum volatile solids}}$ /L) inside the two reactors. Due to the very different chemical composition of the two dephenolized OMW, the inoculum/OMW volatile solid ratio were not the same: in the case of the AD test with XAD16N dephenolized OMW, the inoculum/OMW ratio was equal to 2 $g_{\text{inoculum volatile solids}}$ / $g_{\text{OMWW volatile solids}}$, whereas 5 $g_{\text{inoculum volatile solids}}$ / $g_{\text{OMWW volatile solids}}$ were used in the case of IRA958 OH dephenolized OMW (in both cases corresponding to 37% v/v of inoculum and 63% v/v of dephenolized OMW). As a result of the pre-treatment of the inoculum, the PC total concentration in both tests resulted equal to 0.19 $g_{\text{gallic acid}}$/L for XAD16N and 0.13 $g_{\text{gallic acid}}$/L for IRA958 OH.). In addition, the contribution of the inoculum to the total BOD is relatively low (4-15%). Therefore, this test is suitable for evaluating both the dephenolized OMW biomethanation potential potential and the capacity of the AD process to produce a liquid stream with a BOD lower than the ISO 16075 threshold for WW reuse in agriculture.

Figure 1.3.6 Picture of the 1-L digesters utilized for the anaerobic digestion tests. The caps are equipped so as to allow the sampling of both liquid and gas tests.

1.3.8. Bacteriostatic test on the PC extracts obtained from the desorption stream of the breakthrough tests performed with XAD16N and IRA958 OH

The objective of the test was to quantify and compare the bacteriostatic effect of the two polyphenols extracts, obtained by breakthrough tests with XAD16N and IRA958 resins, together with the well-established cosmetic and pharmaceutical preservative (Preservative A15 – Imidazolidinyl Urea). The comparison was performed by the determination of the minimal inhibitory concentration (MIC) on *E.coli DH10B* (*Gram negative*) and *S.epidermidis ATCC14990* (*Gram positive*) bacterial strains. Prior the assay, the ethanol present in the desorbed product was removed by means of a rotavapor. The concentrated PCs mixtures were characterized in terms of PCs concentration (Table 1.3.3) after the neutralization of the pH value to 7 using a NaOH solution

Table 1.3.3 PCs concentration in XAD16N and IRA958 OH desorbed products after ethanol removal.

Concentrated PCs Extract	**HPLC PCs conc. (g $_{\text{gallic acid}}$ /L)**	**FOLIN PCs conc. (g $_{\text{gallic acid}}$ /L)**
XAD16	5.43 ± 0.31	10.44 ± 0.43
IRA958	1.73 ± 0.01	3.65 ± 0.29

Following the procedure described by Wiegand et al. (2008) regarding the agar dilution method, the three tested substances were sterilized by filtration at 0.22 µm and several dilutions were used and mixed with a nutrient-rich standard agar-medium (MHB – Mueller Hinton Broth) in order to prepare solid agar-medium plates containing a known concentration of the tested substances. Due to the low volume and concentration of polyphenols compounds available in the concentrated desorbed products each plates were made up with a 40% of PCs desorbed products and 60% of standard agar-medium (MHB), while for the preservative A15 a 400g/L stock solution was used and it was possible to prepare an agar-medium with less than a 1% of tested substance on the final medium volume. Therefore, each plates contained the following substances and concentration:

a) MHB = 21 g/L

b) Agar = 17 g/L (1.7%)

c) Antibacterial substance:

   I. XAD16N desorbed product from 4.2 to 0.5 $g_{PC\text{-}Folin}/L$

   II. IRA958 OH desorbed product from 1.46 to 0.1 $g_{PC\text{-}Folin}/L$

   III. Preservative A15 from 1 to 2.5 g/L

The two bacterial suspensions used in the tests were prepared starting from 3-4 isolated colonies grown onto a nutrient-rich medium (MHB) agar plates and transferred into a sterile flask with 20mL of MHB medium. After 8 hours of incubation at 37°C and 150rpm the turbidity was checked at 625nm and adjusted to that of a McFarland Standard 0.5 by adding sterile broth in order to prepare a bacterial suspension with a concentration of $1*10^8$ CFU/mL. A 100-fold dilution of the two suspensions was used to deliver a spot of 10µL onto each plate (in triplicate) so as a cell density around 10^4 CFU was available in each spot. As suggested by Wiegand et al., to confirm that the size of the bacterial inoculum was appropriate ($1*10^8$ CFU/mL) the determination of the viable count was performed.

All the plates so set up were incubated at 37°C for 24-48h (24h for on *E.coli DH10B* and 48h for *S.epidermidis ATCC14990*).

1.4 RESULTS AND DISCUSSION

1.4.1 Procedure for the identification of the most suitable resin(s), desorption solvent and operational conditions

The proposed procedure for the selection of a suitable resin and desorption solvent for the recovery of PCs from liquid agro-industrial wastes, and for the identification of the corresponding operational conditions, is articulated in the following 5 steps:

1. single point batch tests to identify the optimal pH for each resin
2. batch adsorption isotherms to evaluate the resin capacity for PCs and the sorbed product purity
3. batch desorption isotherms to select the desorption solvent for each resin
4. breakthrough adsorption tests to evaluate the resin selectivity for PCs and operating capacity
5. breakthrough desorption tests to evaluate the PC desorption yield and characterize the final product.

This procedure allows to estimate several performance parameters that can guide towards the selection of the most appropriate resin: resin capacity for PCs, purity in PCs of the sorbed and desorbed products, resin selectivity for PCs, resin operating capacity, PC adsorption / desorption yield, antioxidant capacity and composition of the final product. A schematic representation of the procedure is reported in Table 1.4.1, together with some additional details. A relevant drawback of the application of adsorption for the selective recovery of high added value compounds from complex mixtures is the fact that competitive adsorption exerted by other compounds could lead to a final product with a high concentration of undesired compounds (Kammerer et al., 2010). For this reason, a relevant fraction of the above-listed performance parameters are aimed at quantifying the capacity of the resin to selectively adsorb PCs, thus leading to a final desorbed product with a high PC content and a high antioxidant capacity.

The first three steps of the procedure consist in batch tests that can be conducted even at a very small scale (down to 2 mL), so as to minimize the amount of resin, liquid waste and desorption solvent required. Conversely, the last two steps consist in continuous flow breakthrough tests that typically require an adsorption column with a minimum 70-80 cm height and a large amount of liquid waste (to saturate the entire column) and desorption solvent. Therefore, the approach applied in this work to minimize the investigation cost and the amount of liquid waste required for the application of the proposed procedure, consists in using the small-scale batch tests (steps 1-3) for a pre-screening of the 2 most effective resins, which were further compared by means of breakthrough adsorption/desorption tests (steps 4-5).

Table 1.4.1 Schematic representation of the proposed procedure for the identification of the most suitable resin(s), desorption solvent(s) and operational conditions for the recovery of PCs from liquid agro-industrial wastes.

Step	Type of test	Short test description	Output: performance parameters (PP) and operational conditions (OC)
1	Single point batch tests	Batch tests aimed at identifying the best pH for the tested resins	OC: Optimal pH for the tested resins
2	Isotherms	Batch tests; 10-15 resin/liquid ratios for each tested resin	PP: Isotherm shape (favorable / unfavorable) PP: Purity of the sorbed product (g_{PC}/g_{VS}) PP: PC sorbed concentration in equilibrium with the PC average concentration in the liquid waste
3	Batch desorption tests	Preliminary tests aimed at identifying a suitable desorption solvent and desorption conditions	OC: optimal desorption solvent(s) OC: optimal pH for the desorption process
4	Breakthrough adsorption tests	Continuous flow adsorption tests; column height and residence time ≥ minimum values reported in the resin datasheet	PP: PC and VS adsorption yield PP: Resin selectivity for PCs ($Y_{ads,PC}/Y_{ads,VS}$) PP: Resin PC operating capacity
5	Breakthrough desorption tests	Continuous flow desorption tests	PP: PC and VS desorption yield PP: Specific antioxidant capacity of the desorbed product; PP: Purity of the desorbed product (g_{PC}/g_{VS}) PP: Presence in the desorbed product of high-value specific compounds

1.4.2 Characterization of the raw and microfiltered OMW

OMW microfiltration at 0.2 μm determined a 99.8 % suspended solids removal and a 9 % PC removal, associated to the PC content of the removed suspended particles. The average permeate flowrate was equal to 3 L/h, and each filtration process produced a final volume of concentrated sludge equal to 6% of the treated OMW volume. On the basis of these results, the proposed microfiltration was considered an effective process for OMW pre-treatment before its adsorption in packed columns. The main characteristics of the raw and microfiltered OMW are reported in Table 1.4.2. The studied OMW was characterized by a rather high COD (70 g/L). Moreover Letizia Bresciani from the University of Parma identified in the raw OMW 18 PCs: 9 phenolic acids and 9 phenylethanoids and secoiridoids, including compounds of high scientific and commercial interest, such as hydroxytyrosol, oleuropein and verbascoside Table 1.4.3.

Table 1.4.2 Average characteristics of the raw and microfiltered OMW (Average values ± 95% confidence intervals).

Parameter	Raw OMW	Microfiltered OMW
Total phenolic compounds ($g_{AG\ eq.}$/L; HPLC method)	1.41 ± 0.08	1.28 ± 0.07
Total phenolic compounds ($g_{AG\ eq.}$/L; Folin method)	4.4 ± 0.5	4.0 ± 0.3
Total solids (g/L)	41 ± 1	37 ± 1
Volatile solids (g/L)	25 ± 0.5	22 ± 0.5
Suspended solids (g/L)	3.5 ± 0.1	0.005 ± 0.001
Dissolved solids (g/L)	38 ± 1	38 ± 1
COD (g/L)	70 ± 5	65 ± 4
Reducing sugars (g/L)	3.5 ± 0.3	5.1 ± 0.1
Proteins (g_{BSA}/L)	0.15 ± 0.02	0.21 ± 0.02
pH	4.24 ± 0.08	4.21 ± 0.09
Antioxidant capacity (mM_{AAeq})	15 ± 1	13 ± 1

Table 1.4.3 Qualitative identification of PCs in the raw OMW, with spectrometric characteristics – performed by Letizia Bresciani (University of Parma).

Compound	Retention time	Mass / charge ratio (m/z)	MS2 Fragmentation[a]	Raw OMW[b]
Phenolic acids				
Gallic acid	2.22	169	125	n
3,4-Dihydroxyphenylacetic acid	3.23	167	123	y
3,4-Dihydroxybenzoic acid	3.68	153	123, 109	y
Dihydroxybenzoic acid [c]	3.89	153	123, 121, 109	y
Dihydroxybenzoic acid [c]	4.49	153	123, 125, 109	y
Homovanillic acid	4.60	181	137	y
Hydroxybenzoic acid	4.60	137	93	y
p-Coumaric acid	4.82	163	119	n
Caffeic acid	5.14	179	135	y
Vanillic acid	5.25	167	152, 123	n
o-Coumaric acid [c]	5.82	163	119	n
cis-Ferulic acid	5.99	193	149, 178, 134	n
Trimethoxybenzoic acid	6.15	211	167	y
Syringic acid	6.25	197	na[d]	y
trans-Ferulic acid	6.49	193	149, 178, 134	n
Phenylethanoids and Secoiridoids				
Hydroxytyrosol hexoside	3.38	315	153	n
Hydroxytyrosol	3.45	153	123	y
Tyrosol	3.80	137	109	n
Oleoside	4.47	389	345	n
Hydroxyelanolic acid	4.54	257	239	y
Hydroxyverbascoside	5.32	639	621, 529, 459	y
Elanolic acid	5.32	241	165, 183, 197, 223	y
Hydroxyverbascoside	5.69	639	621, 529	n
Elanolic acid	5.86	241	165, 197, 213	y
Verbascoside [c]	5.96	623	461	y
Verbascoside [c]	6.36	623	461	n
Hydroxytyrosol acetate [c]	6.57	195	na[d]	n
Hydroxytyrosol acetate [c]	6.86	195	na[d]	n
Elanolic acid	6.88	241	209, 165, 139	n
Oleuropein [c]	7.00	539	377, 307, 275	y
Oleuropein [c]	7.31	539	377, 307, 275	y
Oleuropein aglycone	8.25	377	241	y
Flavonoids				
Rutin	6.08	609	301, 300	n
Apigenin	7.88	269	225, 209, 251	n
Lignans				
Pinoresinol	8.92	357	311	n

[a] MS2 fragmentation indicates the fragmentation of the parent ion. [b] y, detected; n, not detected.
[c] Tentative identification. The same name reported for some compounds indicates different isomers, characterized by different retention time and which probably differ for the position of the substituent groups.
[d] na: not available. The parent ion has not been fragmented.

1.4.3 Batch isotherm tests

The batch isotherm tests described in this section correspond to points 1-3 of the resin selection procedure illustrated Table 1.4.1.

1.4.3.1 Selection of the optimal form for resin IRA958 and of the optimal pH for the isotherm tests

Since IRA958 is an anion exchange resin with a quaternary ammonium functional group, it can be used with different counter ions attached to the ion exchange site. Indeed, IRA958 can be used both in Cl form (the form supplied by the resin provider) and in OH form- The latter has lower affinity towards the quaternary ammonium functional group but would require a further preliminary step to exchange the Cl^- counter ion before performing the adsorption. Therefore, preliminary tests were aimed at selecting the optimal form to be used in this work. The affinity of Cl^- for a strong anion exchange resin (as IRA958) is 22 times higher than that of OH^- (DOW, 2016). Therefore, the OH^-/PC^- ion exchange is expected to be significantly more favorable than the Cl^-/PC^- ion exchange. Preliminary batch tests confirmed that the PC sorption capacity of the OH form was significantly higher than that of the Cl form, especially for those pH values at which the OMW needs to be increase in order to allow the huge family of phenolic compounds to be in their ionized form (pH around 9) (Figure 1.4.1). All the subsequent tests were therefore conducted with the OH form (indicated as IRA958 OH), attained by fluxing the resin with NaOH 1 mol/L.

Figure 1.4.1 Results of the ion exchange resin IRA958 in its OH- and Cl- form.

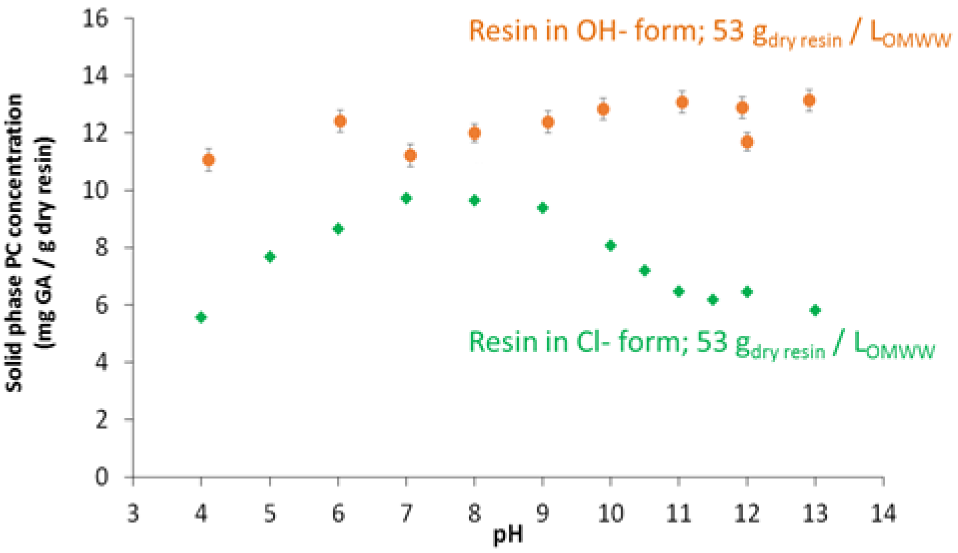

The first step in the application of the resin selection procedure consists in the identification of the optimal pH for the tested resins. Indeed, PCs are a mixture of compounds exhibiting different acidic behaviors: some of them are carboxylic acids with an acid dissociation constant K_a around 10^{-5}, while others have a very low acidity due to the phenolic hydroxyl group (K_a around 10^{-10}). Therefore, at pH 5, about half of the carboxylic acids are dissociated and thus potentially sorbed on anionic IE resins. Conversely at pH 5 the phenols are almost completely protonated, and thus poorly sorbed on IE resins. At a pH = 13, 99.9 % of a phenolic compound with acidity similar to phenol is dissociated. At the same time, in case of IE resins, at very high pHs a strong competition is expected to be exerted by OH^- ions on the dissociated PCs. Conversely, for a neutral resin a better adsorption performance is expected when the PCs are not dissociated (neutral form), therefore at pH < 4-4.5.

For the 4 tested neutral resins (XAD16N, FPX 66, XAD 761 and Optipore SD-2), preliminary, single-point batch tests conducted in the 4.2-9.3 pH range indicated that, as expected, the equilibrium sorbed concentration decreases with increasing pH. As a representative example, the data relative to XAD16N are reported in Fig. 1.4.2. All the isotherms conducted with neutral resins were therefore operated at the OMW natural pH (equal to 4.2).

As for the IE resin (IRA958 OH), several batch adsorption tests were conducted in the 4.2-13 pH range. Starting from the natural pH of the filtered OMW (4.2), the desired pH values were attained by gradual additions of NaOH. Before adding the resin (10 $g_{dry\ resin}/L_{OMW}$), the samples were re-filtered at 0.2 µm, as some precipitate was observed at pH > 8. Furthermore, the antioxidant capacity of the pH-corrected OMW was measured at 6 pH values in the 4.2-13 range, in order to evaluate whether the possible changes in the OMW chemical composition had any effect on the antioxidant activity. As shown in Fig. 1.4.3, no significant effect of pH on the OMW antioxidant capacity was detected.

As illustrated in Fig. 1.4.2, the PC solid phase concentration increased in the 4.2-9 pH range thanks to the increased PC dissociation, whereas a small decrease was observed at pH > 9, possibly due to competition exerted by OH^-. The subsequent tests relative to IRA958 were therefore conducted at pH 9. The increase in PC adsorption capacity observed with resin IRA958 OH in the 4.2-9 pH range is in agreement with the results of a previous study of PC recovery from OMW conducted with IRA958 Cl, XAD16N and IRA67 (a weak IE resin) (Pinelli et al., 2016). Indeed, a pH increase from 4.9 to 7.2 determined a 20 % increase of the PC adsorption yield with IRA958 Cl, no relevant effect with the neutral resin XAD16N, and a 50 % decrease of the PC adsorption yield with the weak resin (IRA67), due to the shift of the resin functional group from the protonated active form to the unprotonated form.

Figure 1.4.2 Resins IRA958 OH and XAD16N: PC solid phase concentration versus pH in single-point batch tests conducted at 10 $g_{dry\ resin}/L_{OMW}$.

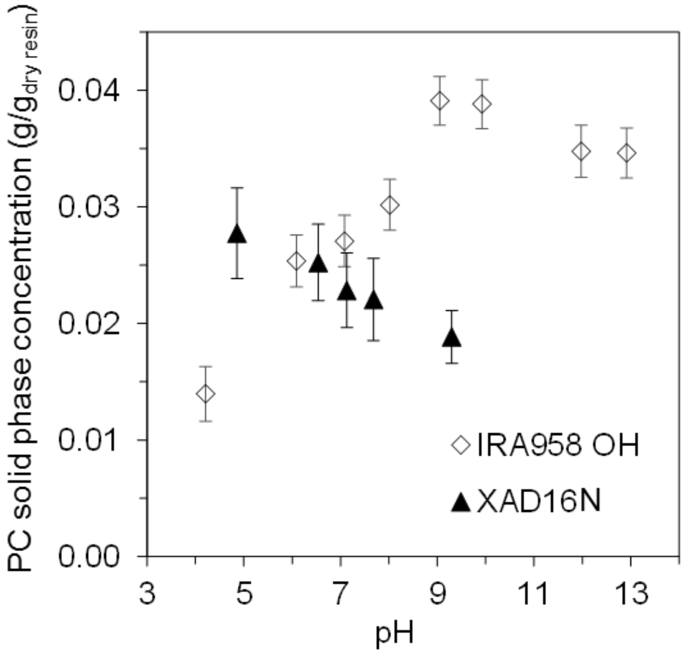

Figure 1.4.3 Specific antioxidant activity of the microfiltered OMW at different pH values

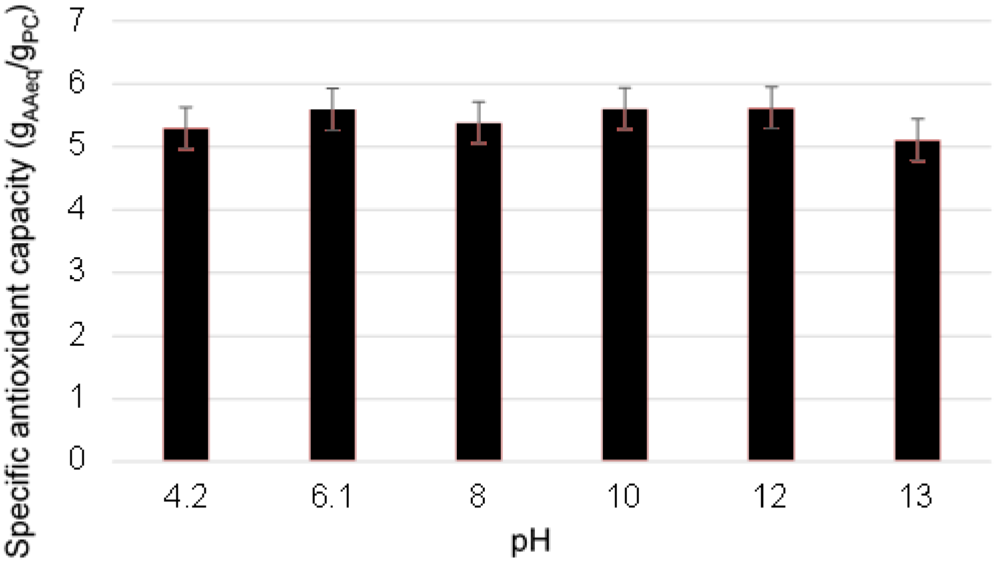

1.4.3.2 Adsorption isotherms

The second step of the proposed resin selection procedure consists in the study of the PC and COD complete adsorption isotherms (T=22 °C) relative to the 5 tested sorbents at the previously selected pH values. The preliminary 3-hour kinetic adsorption tests, performed for each resin at the higher resin concentration tested in the isotherms (450 $g_{dry\ resin}$/L), indicated that the sorbed phase PC concentrations attained after 2 hour of shaking at 120 rpm were equal to 99-101 % of the final sorbed concentrations, calculated for each resin as the average of the sorbed-phase concentrations measured during the last 30 minutes of each 3-h test. On the basis of this result, the equilibration time was set to 2 hours for all the adsorption and desorption isotherm tests.

The interpolation of the trends of dimensionless sorbed phase concentration versus time with both the first-order or Lagergren model and the pseudo-second-order model (Ho & McKay, 1999) resulted in R^2 values varying in the 0.94-0.99 range. For all the tested resins, the difference between the R^2 values obtained with the two models did not result statistically significant (significance level = 0.05). As an example, the experimental data and the corresponding best-fitting simulations relative to resin XAD16N are shown in Fig. 1.4.4.

The isotherm results are shown in Fig. 1.4.5 in terms of solid and liquid phase equilibrium concentrations and best-fitting interpolation curves, whereas Table 1.4.4 reports the best-fitting parameters and the R^2 values obtained with both the Langmuir and Freundlich models for PCs, and only with the Freundlich model for COD. Indeed, all the COD isotherms present a strong upward curvature that excludes the possibility of successfully interpolating them with the Langmuir model. For each PC isotherm, the model (Langmuir or Freundlich) characterized by the highest R^2 was selected, and the statistical significance of the difference between the two interpolations was evaluated through an F test.

The simulation of the isotherm experimental data was limited to the Langmuir and Freundlich models as the vast majority of the studies on the application of adsorption to liquid streams limited the simulation activities to these two models and obtained very high correlation coefficients with either the Langmuir or the Freundlich model (Ziati et al, 2018; Foo & Hameed, 2010; Abdelkreem, 2013). Furthermore, the goal of the isotherm modeling activity was not to identify the most suitable model among the numerous ones available in the literature, but rather to perform a model-based evaluation of the two selected performance parameters (i.e. the PC sorbed concentration ($C_{S,PC,eq,OMW}$) and the purity in PCs of the sorbed product – PC/volatile solids – in equilibrium with the PC and COD average concentration in the microfiltered OMW), which requires the extrapolation of the PC and COD sorbed concentrations up to the values obtained in equilibrium with the corresponding levels in the treated OMW.

Figure 1.4.4: Dimensionless sorbed-phase concentration ($C^*_{S,,t} = C_{S,PC,t} / C_{S,PC,eq}$, where $C_{S,PC,eq}$ indicates the average sorbed-phase concentration during the last 30 minutes of each test) versus time in the kinetic adsorption test conducted with resin XAD16N: experimental data and best-fitting interpolations obtained with the first-order or Lagergren model (Ho & McKay, 1999)
($dC^*_{S,,t} / dt = k_1 \cdot (C^*_{S,PC,eq} - C^*_{S,PC,t})$)
and the pseudo-second-order model (Ho & McKay, 1999)
($dC^*_{S,,t} / dt = k_2 \cdot (C^*_{S,PC,eq} - C^*_{S,PC,t})^2$)
Best fitting values of the model parameters:
- first order model: $k1$ = 0.127 1/min
- second order model: $k2$ = 0.00615 $g_{\text{dry resin}}$ / (mg_{PC} min).

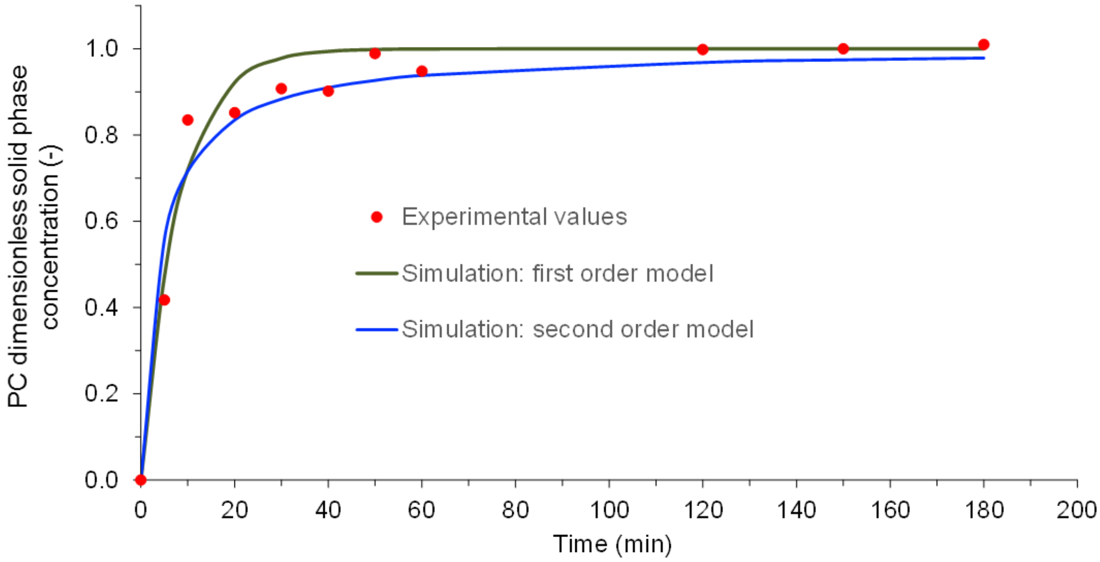

In the PC isotherms, the four non-ionic resins showed a favorable behavior (downward curvature) throughout the entire PC concentration range of interest (up to the PC concentration in the microfiltered OMW), whereas the PC isotherm of the IE resin IRA958 OH was basically linear. For resins XAD16N and FPX66 the Langmuir model resulted the best-fitting one, whereas for Optipore SD-2 the highest R^2 values were obtained with the Freundlich model. Conversely, for XAD761 and IRA958 OH the difference between the two models did not result statistically significant (p > 5 %). For these two resins, the model characterized by the highest R^2 was utilized for the subsequent data elaboration and displayed in Fig. 1.4.5. The quality of the best-fitting interpolations resulted very high for the 4 neutral resins (R^2 = 0.98-0.99), and high for IRA958 OH (R^2 = 0.90). Overall, XAD16N resulted in the higher PC sorbed concentration almost over the entire tested concentration range (0.07-1.2 g_{PC}/L in the liquid phase), whereas Optipore SD-2 performed slightly better in the very low range (< 0.07 g_{PC}/L).

A relevant resin performance parameter is $C_{S,PC,eqOMW}$, the sorbed PC concentration in equilibrium with the PC concentration in the microfiltered OMW, since it represents the sorbed concentration that will be achieved in most of the adsorbing bed in a continuous process characterized by a high operating capacity. Therefore, the higher $C_{S,PC,eqOMW}$, the lower the mass of resin needed to recover a given PC amount. $C_{S,PC,eqOMW}$ was calculated for each resin by extrapolating the selected isotherm up to the PC concentration in microfiltered OMW (1.28 g_{PC}/L). As shown in Table 3, with XAD16N $C_{S,PC,eqOMW}$ resulted equal to 81 $mg_{PC}/g_{dry\ resin}$, whereas for the other resins this parameter varied in the 47-67 $mg_{PC}/g_{dry\ resin}$ range. On the basis of the average conversion factor between Folin–Ciocalteu and HPLC method for the determination of total PCs obtained for the Tunisian OMW object of this work (2.6 $g_{PC\text{-}Folin}$ / $g_{PC\text{-}HPLC}$), the above-reported PC adsorption capacities correspond to 120-175 $mg_{PC\text{-}Folin}/g_{dry\ resin}$ if total PCs are expressed according to the Folin–Ciocalteu method. The significant difference obtained, for this specific OMW, between the PC content evaluated by HPLC and by Folin–Ciocalteu method can be ascribed primarily to the fact that both methods, when applied to the quantification of total PCs, apply one single response factor (that relative to gallic acid, by convention) to a wide list of compounds (Table 1.4.3) characterized by significantly different response factors. Therefore, both methods provide an indicator, but not an exact quantification, of the total PC concentration. In addition, Folin-Ciocalteu method has been reported to be responsive to other antioxidant molecules (Perez-Jimenez et al., 2010), being the reagent nonspecific to phenolic compounds (Huang et al, 2005; Magalhaes et al, 2006), since it can be reduced by nonphenolic compounds (Magalhaes et al, 2008), thus leading to a possible overestimation of the estimated total PC concentration.

In order to compare the PC adsorption capacities obtained in this work with the corresponding ones reported in other studies of PC adsorption from OMW conducted with different types of sorbents, the sorbed-phase PC concentrations obtained in other studies in correspondence with the same PC concentration of the microfiltered OMW object of this study (4.0 $g_{PC\text{-}Folin}$/L) were evaluated on the basis of the best-fitting adsorption isotherms reported in each study examined. This analysis led to the evaluation of a PC sorption capacity of 40-160 $mg_{PC\text{-}Folin}/g_{dry\ resin}$ in batch tests conducted with resins XAD16N, XAD7, ENV+ and IRA96 (Bertin et al., 2011), 190 $mg_{PC\text{-}Folin}/g_{dry\ resin}$ in batch tests conducted with activated carbon (Aliakbarian et al., 2015), and 450 $mg_{PC\text{-}Folin}/g_{dry\ resin}$ in batch tests conducted with peach-stone-derived activated carbon (Ziati et al, 2017). The PC sorption capacities obtained with the 5 resins tested in this work (120-175 $mg_{PC\text{-}Folin}/g_{dry\ resin}$) are therefore comparable to those reported in studies of PC recovery from OMW that focused on other adsorbent types.

Another relevant performance parameter that can be obtained by combining the PC and COD isotherms is the PC purity, or PC mass fraction, of the sorbed product. Indeed, a higher PC mass fraction determines a higher specific antioxidant capacity, and therefore a higher market value of the desorbed product. This parameter, expressed as g_{PC}/g_{COD}, was calculated as the ratio (indicated as $C_{S,PC,eqOMW} / C_{S,COD,eqOMW}$) of the PC to COD sorbed concentrations evaluated – by extrapolation of the best fitting isotherm for each resin – in correspondence of the PC or COD concentration in the microfiltered OMW used for the isotherms. This ratio corresponds to the purity of the sorbed product obtained, in a continuous-flow process, in the column fraction in equilibrium with both the PC and COD concentrations in the microfiltered OMW fed to the adsorption process. The product purity was then converted to g_{PC}/g_{VS}, by applying an average COD-VS conversion factor (2.9 g_{O2}/g_{VS}) obtained, in the second part of the work, by measuring COD and VS in different desorbed products. Volatile solids were not directly measured after each batch isotherm test, as such measurement requires a higher amount of OMW and resin than those used in these tests. As shown in Table 1.4.4, XAD16N and XAD761 resulted in the highest estimated PC purities (0.19-0.20 g_{PC}/g_{VS}), whereas for FPX66, OPTIPORE SD-2 and IRA958 OH the purities varied in the 0.07-0.12 g_{PC}/g_{VS} range. It should be noted that these values, obtained from the batch isotherm tests, refer to the estimated PC content of the *sorbed* product, whereas the experimental measurement of the PC content of the *desorbed* product – the true final product of the process - was performed only for the breakthrough adsorption / desorption tests object of the second part of the work.

The overall evaluation of the isotherm tests led to the identification of XAD16N as the best-performing resin for PC recovery from the tested OMW, thanks to its highest PC sorption capacity and second-highest PC purity of the sorbed product. On the other hand, also IRA958 OH appeared to be an interesting resin, thanks to its very low cost (4 times lower than that of XAD16N) and to the attainment of (i) a PC sorption capacity in equilibrium with the OMW PC concentration equal to 80 % of that obtained with XAD16N, and (ii) a sorbed product PC purity equal to 2/3 of that obtained with XAD16N. Therefore, in the last part of the study XAD16N and IRA958 OH were further compared by means of continuous flow breakthrough tests of PC adsorption and desorption, corresponding to points 4 and 5 of the resin selection procedure illustrated Table 1.4.1.

Figure 1.4.5 Batch isotherms conducted with the 5 tested resins: PCs (a) and COD (b) solid phase versus liquid phase concentrations and best-fitting interpolations obtained with the Langmuir or Freundlich model. For the PC isotherms, the best-fitting model is specified in Table 3, whereas all the COD isotherms were interpolated with the Freundlich model.

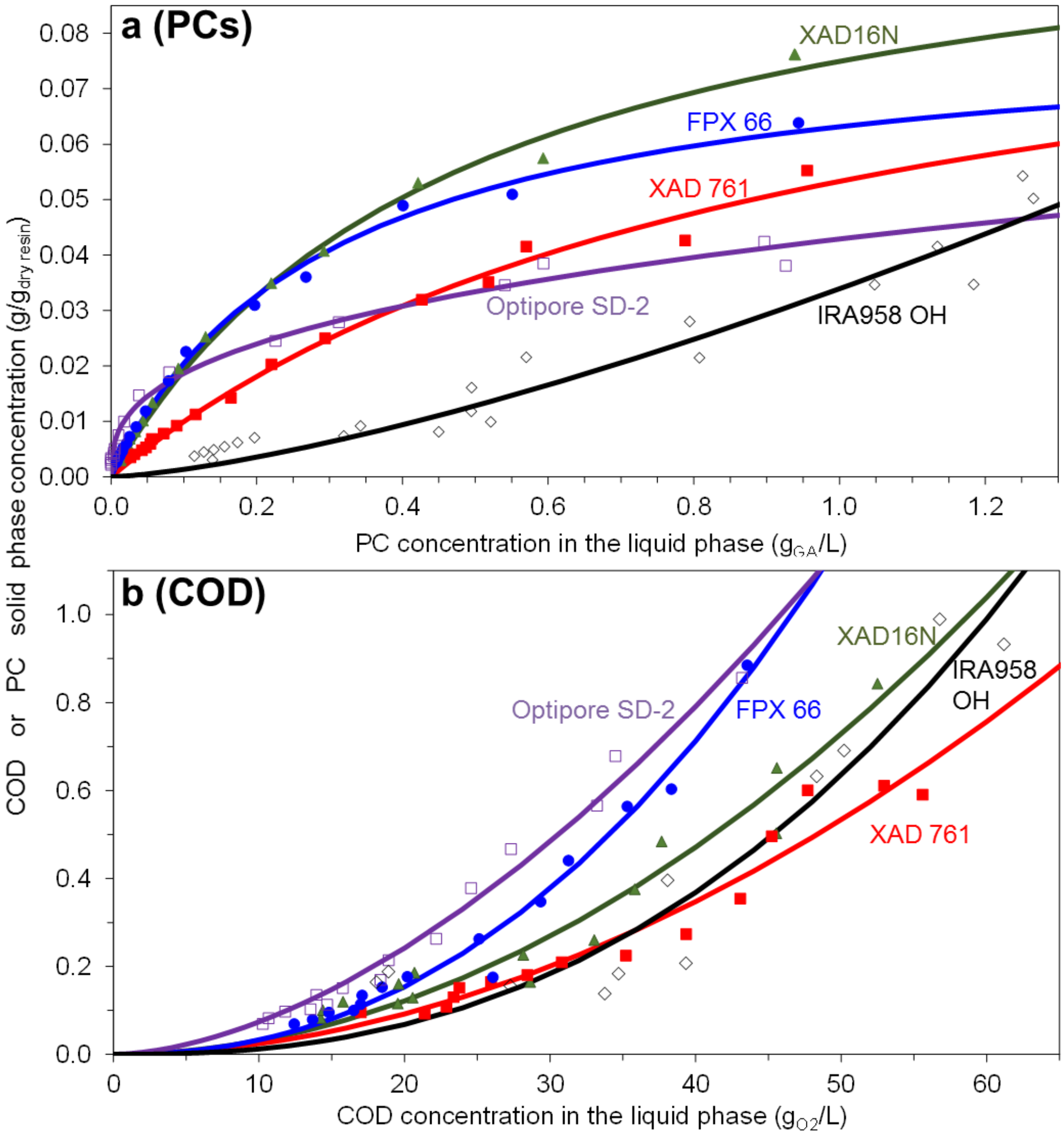

Table 1.4.4

Simulations of the isotherms conducted with the 5 tested resins: best-fitting parameters ± 95% confidence intervals and R^2 values obtained with both the Langmuir and Freundlich models for PCs and only with the Freundlich model for COD; estimate of the sorbed PC and COD concentrations in equilibrium with the corresponding concentrations in the microfiltered OMW; estimate of the purity of the sorbed product.

Resin	PC: Langmuir parameters			PC: Freundlich parameters			Best fitting model for PCs	F test		COD: Freundlich parameters			Sorbed concentrations in equilibrium with OMW		Sorbed product purity	
	$C^{\infty}_{S,PC}$ (mg_{PC} / $g_{dry\ resin}$)	$K_{eq,PC}$ (L/g_{PC})	R^2	$K_{F,PC}$ (L/$g_{dry\ resin}$)	n_{PC} (-)	R^2		p^a	Statistical difference	$K_{F,COD}$ (L/$g_{dry\ resin}$)	n_{COD} (-)	R^2	$C_{s,PC,eqOMW}{}^b$ (mg_{PC} / $g_{dry\ resin}$)	$C_{s,COD,eqOMW}{}^b$ (g_{O2} / $g_{dry\ resin}$)	PC/COD (g_{PC} /g_{COD})	PC/VS (g_{PC} /g_{VS})
XAD761	104±18	(1.1±0.3)·10^{-3}	0.988	0.38±0.02	1.38±0.02	0.986	Langmuir	36%	No	(2.9±4.3)·10^{-4}	0.52±0.13	0.933	60±13	0.9±1.3	0.07	0.20
XAD16N	111±8	(2.1±0.3)·10^{-3}	0.996	1.14±0.33	1.62±0.14	0.990	Langmuir	4.5%	Yes	(3.5±4.2)·10^{-4}	0.51±0.12	0.940	81±7	1.2±1.7	0.07	0.19
FPX66	82±5	(3.3±0.5)·10^{-3}	0.995	1.48±0.52	1.79±0.21	0.978	Langmuir	0.4%	Yes	(2.0±1.9)·10^{-4}	0.45±0.07	0.976	67±5	2.1±1.0	0.03	0.09
Optipore SD-2	41±5	(1.2±0.5)·10^{-2}	0.950	3.54±0.96	2.77±0.37	0.981	Freundlich	3.6%	Yes	(1.4±0.8)·10^{-3}	0.58±0.07	0.980	47±13	1.8±1.1	0.03	0.07
IRA958 OH	725±140	(4.9 ±1.0)·10^{-5}	0.846	(2.1±0.6)·10^{-3}	0.71±0.26	0.902	Freundlich	19%	No	(4.6±1.6)·10^{-5}	0.41±0.19	0.908	48±15	1.2±0.4	0.04	0.12

[a] Probability that the best fits obtained with the Langmuir and Freundlich models are not statistically different. Significance level = 5%.

[b] Sorbed PC and COD concentrations in equilibrium with the corresponding concentrations in the microfiltered OMW.

1.4.3.3 Desorption isotherms

Before proceeding with the breakthrough tests, resins XAD16N and IRA958 OH were further investigated by means of batch desorption tests, aimed at performing a preliminary identification of the optimal desorption solvents and pH. These tests correspond to step 3 of the proposed resin selection procedure (Table 1.4.1). In previous tests of desorption of OMW-derived PCs from resin XAD16N, ethanol acidified with 0.5 % v/v HCl 0.1 mol/L (pH 3.3) had been identified as the optimal desorption solvent (Bertin et al., 2011; Frascari et al., 2016; Ferri et al, 2011). Thus, in this work the first batch desorption tests for XAD16N were operated with pH 3.3 acidified ethanol. The results indicate that, while 1-step desorption led to quite low PC desorption yields (0.40-0.50), the operation of 5 consecutive batch desorptions with this solvent led to an overall PC desorption yield in the 0.50-0.65 range. In further attempts to increase the PC desorption yield from XAD16N, the best results were attained by operating – after 5 consecutive desorptions with acidified ethanol – 5 further desorption steps with a 50 % v/v mixture of de-ionized water and ethanol, acidified to pH 3.3 with HCl. This approach led for XAD16N to an overall PC desorption yield in the 0.75-0.80 range.

In order to desorb ionic compounds from an anionic IE resin, an anion characterized by a strong affinity for the tested resin must be supplied. The total moles of the selected desorption anion must be at least equal to the total moles of anions sorbed to the resin. As some physical adsorption can occur on the matrix of IE resins in addition to the actual IE process, the best desorption results are expected to be achieved if the selected anion is dissolved in a solvent effective in the desorption of physically-sorbed compounds. In this work, OH^- and Cl^- were compared as desorption anions for the adsorption tests conducted with IRA958 OH. In particular 4 types of desorption solutions were tested: NaOH in ethanol; NaCl in ethanol; HCl in ethanol; HCl in a 50 % v/v mixture of de-ionized water and ethanol. The best PC desorption yields (0.70 – 0.80) were obtained after 5 consecutive desorption steps conducted with a 50 % v/v mixture of de-ionized water and ethanol, acidified with HCl to a final concentration of 2 mol/L (pH -0.3).

1.4.4 Phenolic compounds and COD adsorption breakthrough tests

The goal of the breakthrough tests performed with resins XAD16N and IRA958 OH (step 4 of the proposed procedure) was to evaluate crucial performance parameters that cannot be reliably estimated from the batch isotherm tests: the resin operating capacity for PCs (η_{PC}) and the PC and VS (or COD) adsorption yields ($Y_{ads,PC}$ and $Y_{ads,VS}$). Furthermore, the $Y_{ads,PC}$ / $Y_{ads,VS}$ ratio represents an indicator of the resin selectivity for PC, another key parameter in the resin selection process.

1.4.4.1 Fluid-dynamic analysis of the column packings

As a preliminary step, a fluid-dynamic analysis of the column packings made with both resins was performed. For XAD16N, the effective porosity resulted equal to 69.8 %, and the packing quality was rather good. Indeed, the asymmetry factor of the retention time distribution curve was very close to 1 (0.98) and the reduced plate height (47), even if quite high, fell in the range typical of columns packed with adsorption resins. As for the column packing made with IRA958 OH, in both type of tests performed with NaOH solutions (see section 2.5 for details) the retention time distribution curve resulted less symmetric (asymmetry factor in the 1.2-1.7 range). The effective porosity estimated from 4 tests conducted according to the two test types illustrated in section 2.5 resulted in an average value equal to 49.0 %. The reduced plate height (40-50) resulted similar to that obtained with XAD16N.

1.4.4.2 Adsorption breakthrough tests

One adsorption breakthrough test, fed with micro-filtered OMW, was performed for each tested resin (XAD16N and IRA958 OH). The operational conditions relative to these tests, reported in the upper part of Table 4, were selected on the basis of the following criteria:

- For resin XAD16N, in previous works of PC recovery from OMW (Frascari et al., 2016; Pinelli et al., 2016) the increase in resin bed height from 0.5 to 1.8 m and in *HRT* from 0.30 to 0.52 h, with a corresponding decrease in bed volumes / h (BV/h) from 2.8 to 1.7 BV/h, determined a 3.6-fold increase in resin operating capacity. In this work, in the attempt to find an intermediate solution characterized by design values close to the ones recommended in the resin datasheet (resin bed height > 0.75 m, BV/h > 2), the resin bed height was set to 1 m and the *HRT* to 0.30 h; consequently, considering the 0.70 packed resin porosity, the BV/h (equal to ε / HRT) resulted equal to 2.3.

- For IRA958 OH, in the same previous works of PC recovery (Frascari et al., 2016; Pinelli et al., 2016), in tests conducted with a constant resin bed height of 1.8 m, the increase in *HRT* from 0.34 to 0.76 h, with a corresponding decrease in BV/h from 1.6 to 0.7, determined a 3.3-fold increase in resin operating capacity. In this work, the resin bed height and *HRT* were set to roughly the same values selected for resin XAD16N; consequently, considering the 0.49 packed resin porosity, the BV/h resulted equal to 1.47. These design values comply with the ones recommended in the resin datasheet in terms of bed height (> 0.60 m) but not in terms of BV/h (> 8), as previous studies showed that, in the specific case of PC adsorption from OMW, the high values of BV/h typically recommended for ion exchange resins lead to very low operating capacities (Pinelli et al, 2016). The reason for this outcome could be that a physical adsorption of PCs on the resin acrylic matrix is likely to occur in parallel to the PC ion exchange on the resin functional group (quaternary ammonium).

The normalized PC and COD concentrations obtained at the column outlet during the two breakthrough tests are plotted with full symbols in Fig. 1.4.6a (XAD16N) and 4b (IRA958 OH) versus dimensionless time, defined as (actual time) / *HRT* in the resin bed. The tests were continued until the attainment of an outlet PC concentration equal to 87-91 % of the inlet concentration. The PC and COD experimental points were connected by interpolating lines drawn to make Fig. 1.4.6 more readable; these lines do not represent any process simulation. The same Figures includes for comparison purposes the PC and COD time plots obtained – under similar experimental conditions - in previous studies conducted with another OMW, significantly different than the Tunisian one object of this work. The results of this comparison will be discussed in the last part of this section.

The observation of Fig. 1.4.6 indicates in the first place that XAD16N, thanks to its high PC adsorption capacity and favourable isotherm, led to a rather slow PC release, with the 20 % PC breakpoint attained after 13 HRTs. Conversely IRA958 OH, due to its lower PC adsorption capacity, features a more rapid PC release, with the 20 % breakpoint after just 4

HRTs. Also for COD the breakthrough obtained with XAD16N is less rapid than that obtained with IRA958 OH, even if in this case the difference is less marked.

The main performance parameters relative to these tests are reported in the lower part of Table 1.4.5. The PC adsorption yields evaluated at the 20 % breakthrough point were similar and very high (0.93-0.96), whereas IRA958 OH resulted in a significantly higher COD or VS adsorption yield than XAD16N (Table 1.4.5). As a result, for XAD16N the $Y_{ads,PC}$ / $Y_{ads,VS}$ ratio, that represents an indicator of resin selectivity for PCs, resulted quite high (3.6), in agreement with the favourable PC isotherm and unfavourable COD isotherm. Conversely, for IRA 958 OH the $Y_{ads,PC}$ / $Y_{ads,VS}$ ratio resulted 2.5 times lower.

For XAD16N, the PC operating capacity at the 20 % breakpoint resulted 3 times higher than that relative to IRA958 OH (Table 1.4.5). A low operating capacity plays unfavourably in the determination of the cost for the initial resin purchase and periodic resin replacement. The low operating capacity evaluated for IRA958 OH (about 0.10) suggests that this resin, as a result of its wide mass transfer zone, requires a higher bed length – and therefore a higher *HRT* - in order to operate under optimal conditions.

The elaboration of the PC and COD breakthrough curves allows to estimate the PC purity (or PC mass fraction) in the *sorbed* product at any point of the curve of normalized PC outlet concentration. Indeed, by dividing the PC and COD sorbed masses at any point of the curve by the mass of dry resin in the column experimentally measured during the packing procedure, one obtains the corresponding PC and COD sorbed concentration ($C_{S,PC}$ and $C_{S,COD}$). The detailed procedure for this calculation is reported in Material & Methods, section 1.3.6. The $C_{S,PC} / C_{S,COD}$ ratio, an indicator of purity of the sorbed product, can then be converted to a $C_{S,PC}$ / $C_{S,VS}$ ratio by applying the average COD-VS conversion factor obtained by measuring COD and VS in different desorbed products (2.9 g_{O2}/g_{VS}). The sorbed product purity at the selected 20 % breakpoint resulted equal to 0.14 g_{PC}/g_{VS} for XAD16N and 0.03 g_{PC}/g_{VS} for IRA958 OH. For both resins, the sorbed product purity increased with time. At the end of the breakthrough test (a condition close to resin saturation) the estimated purities resulted significantly higher (0.22-0.39 g_{PC}/g_{VS}; Table 1.4.5). The choice of the actual breakthrough point at which the adsorption process should be stopped depends on the goal of the process: if the technology is aimed at removing PCs from OMW for environmental reasons, the maximum PC concentration in the column outlet is set by a regulatory standard or law; conversely, if the goal is to produce a product characterized by a high PC content and therefore a high antioxidant capacity, no matter how much PC mass is released with the effluent, then a high breakpoint is likely to be the best option.

The breakthrough tests conducted with both resins were characterized by a roughly constant pressure drop equal to 0.2 bar for XAD16N and 0.30-0.35 bar for IRA058 OH. This result indicates that the 99.8 % suspended solid removal attained by the OMW microfiltration with a 0.2 μm average pore-size was effective in protecting the packed columns from potential clogging.

Table 1.4.5 Adsorption and desorption performances relative to the breakthrough tests conducted with resins XAD16N and IRA958 OH in the 1-m packed column

Parameter	XAD16N	IRA958 OH
Resin effective porosity (ε, -)	0.698	0.490
HRT (h)	0.34	0.36
Superficial velocity (m/h)	2.30	1.47
Bed volumes / h (BV/h, 1/h)	2.30	1.47
PC adsorption yield at 20% PC breakpoint ($Y_{ads,PC}$, -)	0.93	0.96
VS adsorption yield at 20% PC breakpoint ($Y_{ads,VS}$, -)	0.26	0.69
Resin selectivity for PCs at 20% PC breakpoint ($Y_{ads,PC}$ / $Y_{ads,VS}$)	3.6	1.4
PC operating capacity at 20% PC breakpoint (η_{PC}, -)	0.30	0.10
Sorbed product purity at 20% PC breakpoint (g_{PC}/g_{VS})	0.14	0.03
Sorbed product purity at end of test (g_{PC}/g_{VS})	0.39	0.22
PC desorption yield ($Y_{des,PC}$, -)	0.87	0.95
VS desorption yield ($Y_{des,PC}$, -)	0.99	0.99

Figure 1.4.6 Normalized PC and COD concentrations at the column outlet versus dimensionless time (actual time / HRT) during continuous-flow breakthrough tests conducted with resins XAD16N (a) and IRA958 OH (b). Full symbols refer to the tests conducted in the framework of this work with Tunisian OMW and described in detail in section 3.5 and Table 4. In these tests, the PC and COD experimental points are connected by interpolating lines drawn to make the figure more readable. For comparison purposes, empty symbols refer to the PC and COD time plots obtained with the same HRT in previous studies conducted with an Italian OMW, significantly different than the Tunisian one object of this work.

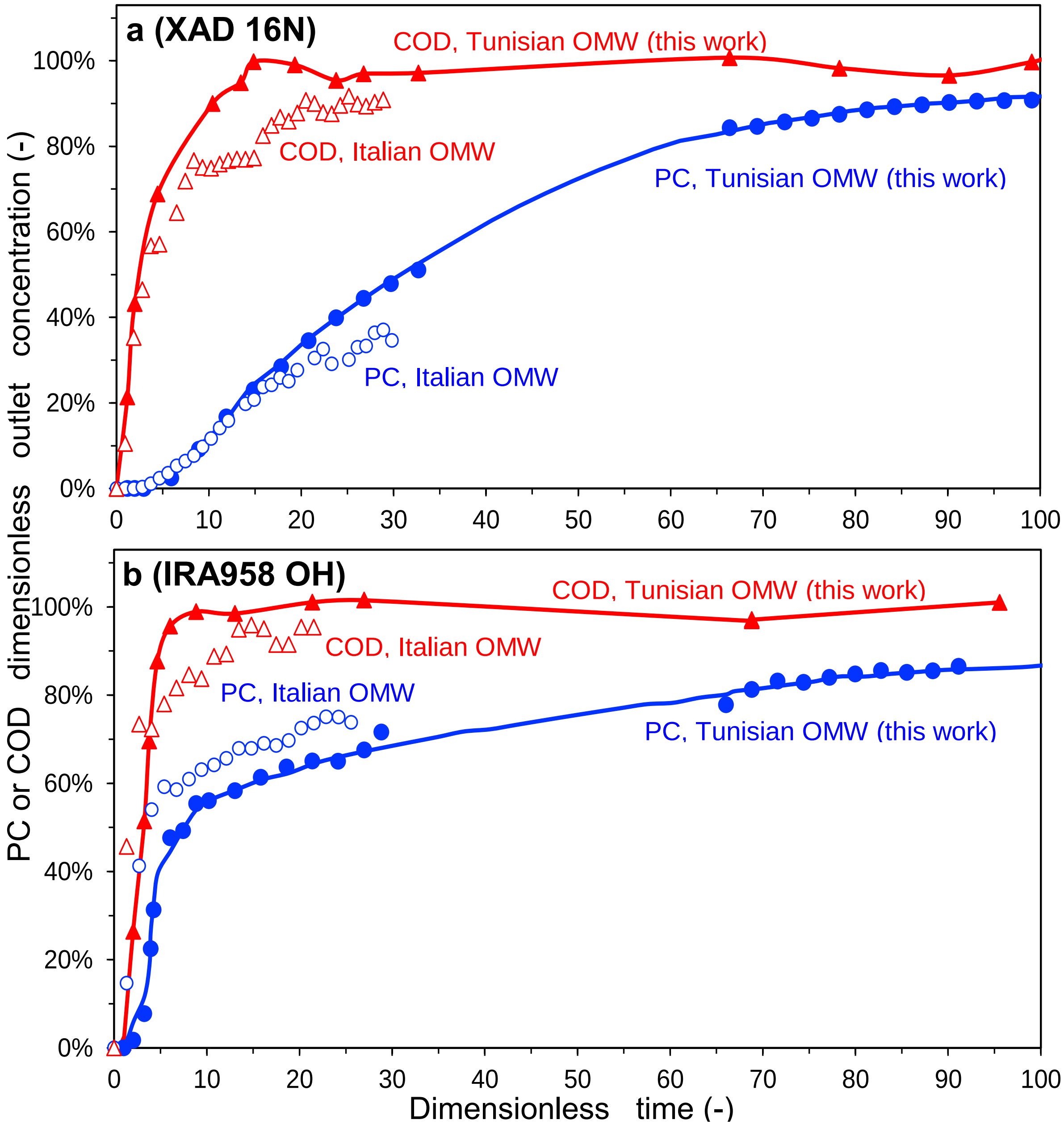

1.4.4.3 Adsorption performances obtained with a different OMW

For comparison purposes, Figs. 1.4.6 a) and b) also show with empty symbols the PC and COD time plots obtained by the same research group, with the same two resins and with very similar HRTs (0.36-037 h), in previous tests conducted with an Italian OMW characterized, with respect to the Tunisian one object of this work, by a significantly lower COD (31 versus 70 g/L) and PC (0.6 versus 1.4 g_{GA}/L) concentration. The observation of Figs. 1.4.6 a) and b) indicates that, for both resins, the use of a significantly different OMW led to very similar breakthrough dimensionless curves for both PCs and COD. More precisely, the OMW change determined a 3-5 % variation in PC adsorption yield and a 3-14 % variation in column operating efficiency (values estimated at a 20 % PC breakthrough). This important result indicates that the approach, methodology and main conclusions of this work can be applied also to OMWs with different characteristics.

1.4.5 Desorption / regeneration tests and desorbed product characterization

On the basis of the results of the batch desorption tests illustrated in section 1.4.3.3, the breakthrough test performed with resin XAD16N was followed by the application of a 2-step desorption procedure: the initial supply of 5 bed volumes of ethanol acidified with 0.5 % v/v HCl 0.1 mol/L (pH 3.3) was followed by 10 further bed volumes of a 50 % v/v mixture of de-ionized water and pH 3.3 acidified ethanol. Conversely, the breakthrough test conducted with IRA958 OH was desorbed by supplying 7 bed volumes of a 50 % v/v mixture of de-ionized water and ethanol, acidified with HCl to a final concentration of 2 mol/L (pH -0.3).

These procedures led to the attainment of very high PC desorption yields (87-95 %) and to nearly complete VS desorption yields (Table 1.4.5). The list of the specific PCs qualitatively identified in the two products is reported in the last two columns of Table 1.4.6, so as it can be compared with the raw OMW. Whereas the characterization of the two desorbed products is reported in Table 1.4.7. Coherently with the very high desorption yields, the final product purity attained with IRA958 OH (0.19 g_{PC}/g_{VS}) resulted very close to that estimated for the sorbed product (0.22 g_{PC}/g_{VS}; Table 1.4.5) whereas for XAD16N the final product purity (0.21 g_{PC}/g_{VS}) resulted equal to 55 % of the corresponding value estimated for the sorbed product. The product purity evaluated in terms of PC/total solids ratio (0.18-0.20 g_{PC}/g_{TS}) is 5-6 times higher than the corresponding value measured in the microfiltered OMW fed to the process, indicating that both the selected resins have a high selectivity for PCs. In addition, the measurement of the product purity based on the Folin–Ciocalteu method for PCs leads to estimate a significantly higher PC content in the desorbed product (0.34-0.41 $g_{PC\text{-}Folin}/g_{VS}$).

As shown in Table 1.4.6, the desorbed product obtained with XAD16N presented a complex variety of 28 PCs: 13 phenolic acids, principally represented by hydroxycinnamic and benzoic acid derivatives, 12 phenylethanoids and secoiridoids, as tyrosol, elanolic acid, verbascoside and oleuropein, 2 flavonoids and 1 lignan. With the exception of hydroxyelanolic acid, all the PCs detected in the raw OMW were identified also in the XAD16N product. Conversely, 11 PCs detected in the XAD16N extract were not found in the raw OMW, most likely because their initial concentration was below the method's detection limit. These findings confirm the high affinity of XAD16N for PCs. The desorbed product obtained with IRA958 OH presented a mixture of 20 PCs, including 9 phenolic acids and 11 phenylethanoids and secoiridoids. The adsorption/desorption process conducted with IRA958 OH led to the loss of 4 PCs initially detected in the raw OMW, whereas 8 PCs detected in the IRA958 OH extract were not found in the raw OMW due to their low initial concentration.

The detected PCs are generally recognized as potent antioxidants (Navarro & Morales, 2017), antibacterials (gram positive and gram negative) and antifungals. They also demonstrated activities against yeast (Abu-Lafi et al., 2017). Their industrial application for these properties are increasing, both in the food industry, as reported for hydroxytyrosol and verbascoside in meat preparation (Navarro & Morales, 2017; Martinez et al., 2018), or olive leaf phenolics in dairy preparation (Tavakoli et al., 2018) and OMW extract for olive oil preservation (Abu-Lafi et al., 2017), as well as in the cosmetic industries, as reported for oleuropein used as antiaging ingredient in cosmetic formulations (Aissa et al., 2017). In order to evaluate the antibacterial activity of the two PCs desorbed products, a bacteriostatic test was performed as illustrated in section 1.3.8 allowing the determination of the minimal inhibitory concentration (MIC) value for both a Gram+ bacterial strain and a Gram-. The MIC is defined as the lowest concentration of the antibacterial substance tested at which the bacterial strain does not produce a visible growth. The XAD16N desorbed product showed a MIC of 1 $g_{PC\text{-}Folin}$/L for both E.coli DH10B and S.epidermidis ATCC14990 strains. On the contrary, IRA958 OH desorbed product was only capable of inhibit the growth of E.coli DH10B with a MIC of 0.5 $g_{PC\text{-}Folin}$/L allowing instead the growth of the Gram+ bacterium

(S.epidermidis ATCC14990) at all the tested concentrations, making the determination of the MIC value not possible. These findings, compared to the results obtained with the cosmetic and pharmaceutical preservative tested (MIC value of 1.75 g/L for E.coli and 1.5 g/L for S.epidermidis), confirms the high antibacterial properties of the OMWW PCs mixtures and leaves open to a possible industrial application of this kind of products.

Notwithstanding the modest differences in composition of the final PC mixture, the specific antioxidant activities of the products obtained with the two resins resulted quite close (4.6-4.9 g_{AAeq}/g_{PC}; Table 5), in agreement with the similar PC purities (0.19 g_{PC}/g_{VS}). The specific antioxidant activities of the two final products resulted comparable to that of the microfiltered OMW fed to the process (5.3 g_{AAeq}/g_{PC}). This finding indicates that the proposed adsorption/desorption process led to a satisfactory extraction and enrichment in PCs of the treated OMW, while maintaining roughly the same specific antioxidant activity. In order to assess the antioxidant capacity of the final products of this work, the same parameter was measured in single-compound solutions of two PCs well known for their high antioxidant activity and detected in both desorbed products, namely caffeic acid and hydroxytyrosol. The result obtained for the former (1.7 g_{AAeq}/g_{PC}) was lower than the values attained for the final desorbed products, whereas the antioxidant activity of hydroxytyrosol resulted about 2 times higher (9.1 g_{AAeq}/g_{PC}). This analysis indicates that both XAD16 and IRA958 OH led to the production of a PC-rich product characterized by a relatively high antioxidant activity.

Table 1.4.6 Identified PCs in the raw OMW and in the desorbed products obtained with resins XAD16N and IRA958 OH, with spectrometric characteristics.

Compound	Retention time	Mass / charge ratio (m/z)	MS2 Fragmentation[a]	Raw OMW[b]	XAD16N desorbed product[b]	IRA958 OH desorbed product[b]
Phenolic acids						
Gallic acid	2.22	169	125	n	n	y
3,4-Dihydroxyphenylacetic acid	3.23	167	123	y	y	y
3,4-Dihydroxybenzoic acid	3.68	153	123, 109	y	y	y
Dihydroxybenzoic acid [c]	3.89	153	123, 121, 109	y	y	n
Dihydroxybenzoic acid [c]	4.49	153	123, 125, 109	y	y	y
Homovanillic acid	4.60	181	137	y	y	y
Hydroxybenzoic acid	4.60	137	93	y	y	y
p-Coumaric acid	4.82	163	119	n	y	y
Caffeic acid	5.14	179	135	y	y	y
Vanillic acid	5.25	167	152, 123	n	y	n
o-Coumaric acid [c]	5.82	163	119	n	n	y
cis-Ferulic acid	5.99	193	149, 178, 134	n	y	n
Trimethoxybenzoic acid	6.15	211	167	y	y	n
Syringic acid	6.25	197	na[d]	y	y	n
trans-Ferulic acid	6.49	193	149, 178, 134	n	y	n
Phenylethanoids and Secoiridoids						
Hydroxytyrosol hexoside	3.38	315	153	n	y	y
Hydroxytyrosol	3.45	153	123	y	y	y
Tyrosol	3.80	137	109	n	n	y
Oleoside	4.47	389	345	n	y	n
Hydroxyelanolic acid	4.54	257	239	y	n	n
Hydroxyverbascoside	5.32	639	621, 529, 459	y	y	y
Elanolic acid	5.32	241	165, 183, 197, 223	y	y	n
Hydroxyverbascoside	5.69	639	621, 529	n	n	y
Elanolic acid	5.86	241	165, 197, 213	y	y	n
Verbascoside [c]	5.96	623	461	y	y	y
Verbascoside [c]	6.36	623	461	n	n	y
Hydroxytyrosol acetate [c]	6.57	195	na[d]	n	y	n
Hydroxytyrosol acetate [c]	6.86	195	na[d]	n	n	y
Elanolic acid	6.88	241	209, 165, 139	n	y	n
Oleuropein [c]	7.00	539	377, 307, 275	y	y	y
Oleuropein [c]	7.31	539	377, 307, 275	y	y	y
Oleuropein aglycone	8.25	377	241	y	y	y
Flavonoids						
Rutin	6.08	609	301, 300	n	y	n
Apigenin	7.88	269	225, 209, 251	n	y	n
Lignans						
Pinoresinol	8.92	357	311	n	y	n

[a] MS2 fragmentation indicates the fragmentation of the parent ion. [b] y, detected; n, not detected.

[c] Tentative identification. The same name reported for some compounds indicates different isomers, characterized by different retention time and which probably differ for the position of the substituent groups.

[d] na: not available. The parent ion has not been fragmented.

Table 1.4.7 Relative composition of the desorbed products obtained from resins XAD16 and IRA958 OH and of the microfiltered OMW fed to the adsorption process.

Parameter	Microfiltered OMW	XAD16N desorbed product	IRA958 OH desorbed product
Product purity (g_{PC}/g_{VS}; HPLC method for PCs)	0.06	0.21	0.19
Product purity (g_{PC}/g_{VS}; Folin method for PCs)	0.18	0.34	0.41
Specific antioxidant capacity (g_{AAeq}/g_{PC})	5.3[a]	4.9[a]	4.6[a]
Reducing sugars (g_{sugars}/g_{VS})	0.23	0.30	0.56
Protein content (g_{BSA}/g_{VS})	0.01	0.04	0.09
Volatile solid content (g_{VS}/g_{TS})	0.59	0.99	0.92

[a] The (ascorbic acid)/(PC) ratio refers to the total PC content quantified by HPLC.

1.4.6 Anaerobic digestion of the dephenolized OMW

1.4.6.1 OMW biomethanation potential test

The main results of the first group of BMP tests, conducted with an inoculum / OMW ratio equal to 4 g_{VS}/g_{VS}, are shown in Fig. 1.4.7 in terms of cumulative methane production and total PC concentration versus time, and in Fig. 1.4.8 in terms of methane production yield and average methane production rate. For reasons of brevity the comparison between the actual micro-filtered OMW and the synthetic dephenolized OMW matrixes is not reported, since results proved the same matrix effect in terms of biomethanation rate and, hence, confirmed the reliable COD "reconstruction" of the dephenolized OMW matrix. BMP-test results of the microfiltered-OMW and of the partially dephenolized OMW clearly show that a partial (38%) OMW dephenolization led to a significant improvement of the OMW AD process, with a 33% increase in methane production yield and a 40% increase in methane production rate. These changes imply a proportional increase of the revenues from electricity production and (not proportional) decrease in capital cost, in consideration of the smaller digester required. These results indicate the importance of evaluating the increase in methane/VS yield and in methane production rate associated to a stronger dephenolization.

The plot of total PC concentration versus time (Fig. 1.4.7 b) shows that no PC biodegradation occurred during the AD process. This outcome indicates that the AD step could be placed also before the PC removal step, without any decrease in the PC recovery yield. However, the improved AD performances observed with partially dephenolized OMW indicate that a significant improvement of the overall economic evaluation of the process is expected if the AD step is placed after the PC recovery step.

Figure 1.4.7 First group of AD batch tests, conducted with an inoculum / OMWW ratio equal to 4 g_{VS}/g_{VS}: cumulative methane production (a) and total PC concentration (b) versus time**.**

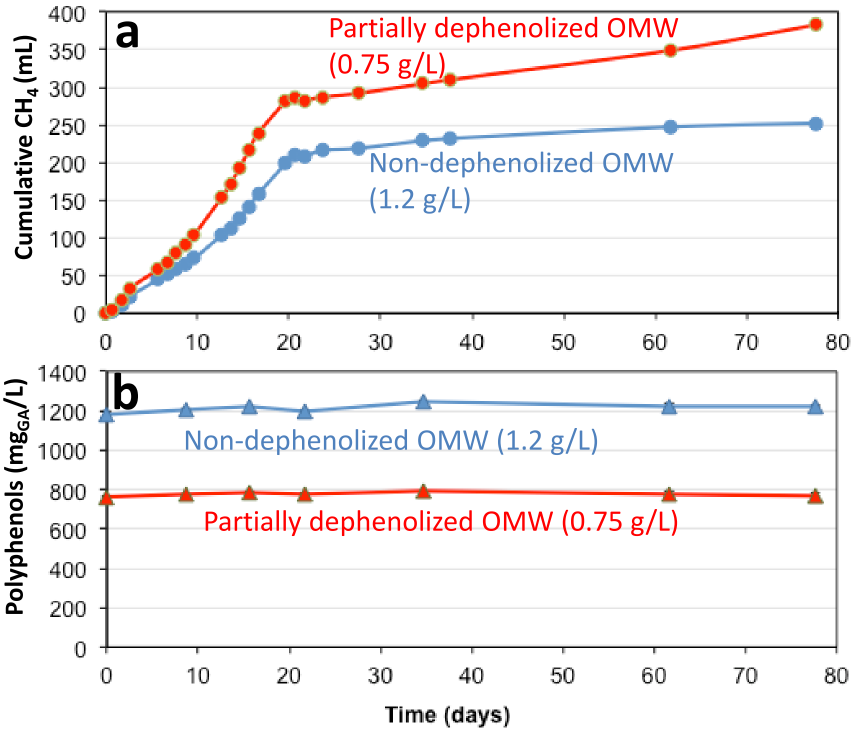

Figure 1.4.8 First group of AD batch tests, conducted with an inoculum / OMW ratio equal to 4 g_{VS}/g_{VS}: methane production yield and average methane production rate**.**

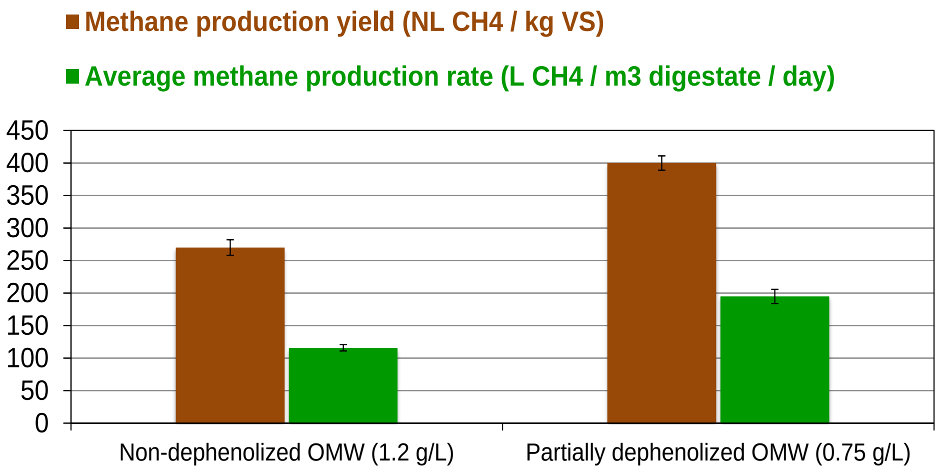

1.4.6.2 AD of the OMW dephenolized through the 1-m adsorption bt tests performed with XAD16N and IRA958 OH

The performances of the AD tests of the two micro-filtered OMW dephenolized with either XAD16N or IRA938OH resins were compared to previous data obtained by anaerobic digestion of the micro-filtered OMW using the same inoculum. For comparison sake, the main results are shown in terms of: i) methane production yield (NmL$_{CH4}$/g$_{VS}$) versus time in Fig. 14.9, ii) methane production rate (NmL$_{CH4}$/ mL$_{digestate}$/day) versus time in Fig. 1.4.10, and iii) total PCs concentration (mg $_{Gallic\ acid}$/L) versus time in Fig. 1.4.11. The results of the characterization of the two micro-filtered dephenolized OMW (in terms of TS, VS, PCs, COD and BOD5) before and after the AD process are summarised in Table 1.4.8.

These results clearly show that a strong (80%) OMW dephenolization led to an important improvement in the methane production yield, from 360 NmL$_{CH4}$/g$_{VS}$ with the micro-filtered OMWW to 570 and 600 NmL$_{CH4}$/g$_{VS}$ with the OMWW dephenolized with XAD16N and IRA958 OH respectively. Likewise, the methane production rates of both the dephenolized OMW are significantly higher than that of the raw OMW: the maximum methane production yield is reached in 60-90 days, almost half of the time needed for the AD of micro-filtered OMW. Confirming the previous results, these improvements imply a proportional increase of the revenues from electricity production and a (not proportional) decrease in capital cost, in consideration of the smaller digester required.

Regarding the BOD5 evaluation before and after the AD, in both cases the biological process certainly managed to reduce the values of COD and BOD5 with an excellent methane production, however the residual values at the end of the AD are still too high compared to the 10 mg O_2/L required by the ISO 16075 for WW reuse in agriculture. Trying to find an explanation to this negative result, the concentration of ammoniacal nitrogen at the end of the process was measured and a low value equal to 0.34 ± 0.01 g/L was found for the OMW dephenolized with XAD16 and 0.39 ± 0.02 g/L for the OMWW dephenolized with IRA958 OH. It is therefore probable that the C/N (carbon/nitrogen) ratio was too low from the beginning of the AD, consequently, the anaerobic degradation did not reach the end due to lack of nitrogen-ammoniacal nutrients. Further tests conducted with dephenolized OMWW enriched in nitrogen compounds or as co-digestion with other nitrogen-rich substances are needed to support this assumption. Alternatively, a tertiary treatment of aerobic biodegradation with activated sludge could be proposed in order to achieve the standard required by ISO 16075 for WW reuse.

Figure 1.4.9 Methane production yield expressed as NmL $_{CH4}$/g$_{VS}$ of AD batch tests with the untreated micro-filtered OMW, the OMW dephenolized with XAD16N and the OMW dephenolized with IRA958 OH.

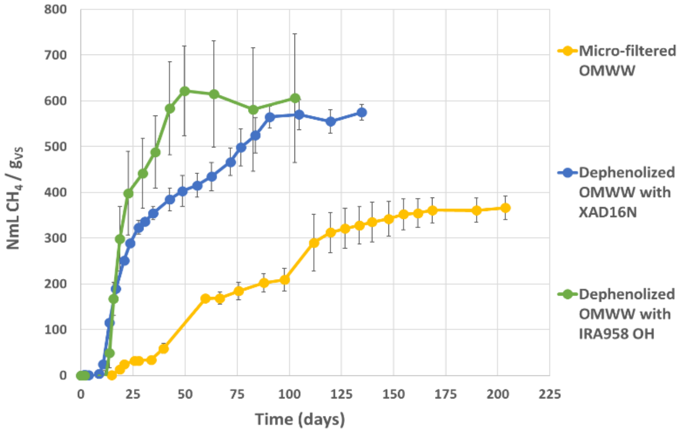

Figure 1.4.10 Methane production rate expressed as NmL$_{CH4}$/mL$_{digestate}$/day of AD batch tests with the untreated micro-filtered OMW, the OMW dephenolized with XAD16N and the OMW dephenolized with IRA958 OH**.**

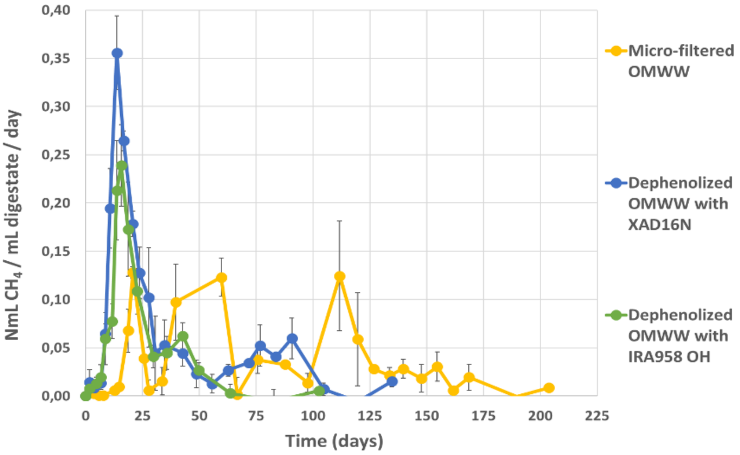

Figure 1.4.11 Total PCs concentration expressed as mg$_{GA}$/L measured with HPLC of AD batch tests with the untreated micro-filtered OMW, the OMW dephenolized with XAD16N and the OMW dephenolized with IRA958 OH**.**

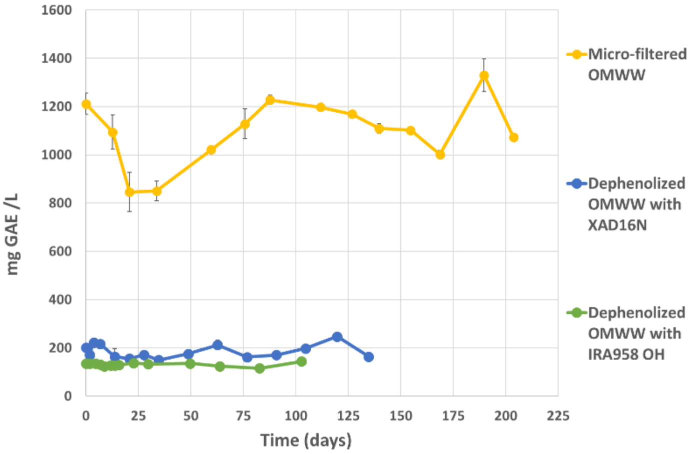

Table 1.4.8 Micro-filtered and dephenolized OMW before and after the AD**.**

	Dephenolized OMW with XAD16N		**Dephenolized OMW with IRA958 OH**	
Parameter	before the AD process	after the AD process	before the AD process	after the AD process
Total solids (g/L)	30 ± 0.1	29 ± 0.7	23 ± 0.2	25 ± 1.0
Volatile solids (g/L)	16 ± 0.1	6.8 ± 0.2	6.0 ± 0.1	4.4 ± 0.3
PCs ($g_{\text{Gallic acid}}$/L; HPLC method for PCs)	0.103 ± 0.011	0.166 ± 0.005	0.074 ± 0.007	0.144 ± 0.010
PCs ($g_{\text{Gallic acid}}$/L; Folin method for PCs)	1.57 ± 0.15	0.66 ± 0.11	0.11 ± 0.09	0.22 ± 0.01
COD (g_{O2}/L)	45 ± 1.2	12.21 ± 0.3	45 ± 1.5	8.7 ± 0.5
BOD5 (g_{O2}/L)	12	1.05	2.3	0.53

1.5 CONCLUSIONS

- A procedure was proposed and validated for the testing and selection of resins for PC recovery from PC-rich wastewaters and – after a solvent extraction step – solid wastes. The application of the procedure to a process of PC recovery from OMW confirmed that batch isotherm tests – typically used in the literature to compare resins for adsorption processes – need to be integrated by continuous-flow adsorption / desorption tests. Indeed the latter allow to take into consideration several aspects and parameters not assessable by means of batch tests, such as the resin operating capacity and the effect of the selected breakpoint on the quality of the desorbed product.

- The proposed resin selection procedure was successful in the identification of two resins (Amberlite XAD16N and Amberlite IRA958 OH) capable to produce a final mixture characterized by a high PC content and antioxidant capacity. The procedure thus contributes to the overcoming of a potential drawback of the application of adsorption to the recovery of high added value molecules from complex matrices, i.e. the risk that competitive adsorption leads to a relevant presence of undesired compounds in the final product. In particular, the batch isotherm tests allowed to make a preliminary identification of XAD16N and IRA958 OH as the most promising resins for PC recovery from the targeted Tunisian OMW. The subsequent continuous flow tests – limited to XAD16N and IRA958 OH – indicated that the final resin selection depends on the desired breakpoint, and therefore on the goal of the process. Indeed, if an environmental standard imposes in the column outlet a relatively low PC concentration, and therefore a low breakpoint, XAD16N led to a PC-richer product and a higher operating capacity than IRA958 OH, thanks to its higher PC selectivity and sorption capacity. Conversely, if the goal of the process is to produce a pure product characterized by a high PC purity and antioxidant capacity, no matter how much PC mass is released with the effluent, it is advisable to continue the adsorption step until the attainment of a very high breakpoint. In this case, the quality of the final products obtained with the two resins is similar, and IRA958 OH appears to be the most promising one thanks to its significantly lower industrial cost, despite its lower PC sorption capacity.

- OMW microfiltration with a 0.2 μm average pore-size proved to be an effective technology to attain a very high suspended solid removal - thus protecting the packed column from potential clogging - with a very low PC loss.

- The qualitatively identification of the actual PCs present in the final desorbed product – an aspect generally neglected in the literature – represents a useful integration of the product assessment. Moreover the investigation of the final product in terms of antioxidant capacity confirmed that the proposed process led to an enrichment in PC content without any irreversible detrimental effects on their properties.

- Lastly, AD has been proposed to obtain a close-loop process, given that it allows to supply energy for the phenols extraction process as well as to reduce and stabilize the organic matter content to avoid environmental risks. The AD batch tests set up using the micro-filtered and dephenolized OMW coming from the breakthrough tests with both XAD16N and IRA958 OH resins showed a very high biomethane potential and a significant improvement in both methane production yield and rate in comparison with the untreated micro-filtered OMW. These results are in agreement with previous works (Serrano et al., 2017; Frascari et al., 2019) which showed that the integration between the dephenolization step and the anaerobic digestion of the dephenolised WW contributes to significantly improve the economic and environmental performances of the proposed process. However, the anaerobic biological treatment was not able to produce a liquid stream with a BOD lower than the ISO 16075 limit for WW reuse in agriculture and this result implies that a further tertiary treatment is needed, such as for example a biological aerobic biodegradation treatment.

List of abbreviations

BMP	Bio-methanation potential
BV/h	Bed Volumes / h
CI	Confidence interval
COD	Chemical oxygen demand
HRT	Hydraulic residence time
IE	Ion exchange
OMW	Olive mill wastewater
PC	Phenolic compound
TS	Total solids
VS	Volatile solids

Nomenclature

A_s	Asymmetry factor, defined as ratio between the leading and tailing semi-width of the peak at 10 % of the peak height (-)
$C_{L,i}$	Liquid phase concentration of compound *i* ($g_{\text{PC or COD}}$/L)
$C_{L,0,i}$, $C_{L,eq,i}$	Initial and final (equilibrium) PC or COD concentration in the liquid phase (OMW) during the isotherm tests ($g_{\text{PC or COD}}$/L)
$C_{S,eq,calc,i}$	COD or PC solid phase concentration calculated according to the Langmuir or Freundlich model, for the evaluation of the R^2 value associated to each isotherm ($g_{\text{PC or COD}}/g_{\text{dry resin}}$)
$C_{S,eq,i}$	Final (equilibrium) PC or COD concentration in the solid phase (resin) during the isotherm tests ($g_{\text{PC or COD}}/g_{\text{dry resin}}$)
$C_{S,eq,m}$	Average experimental solid phase concentration of compound *i* in an isotherm test, for the evaluation of the R^2 value associated to each isotherm ($g_{\text{PC or COD}}/g_{\text{dry resin}}$)
$C^*_{S,eq,PC}$	Dimensionless sorbed-phase PC concentration measured at equilibrium at the end of the kinetic adsorption batch tests, calculated for each resin as the average of the sorbed-phase concentrations measured during the last 30 minutes of each 3-h test (-)

$C_{S,i}$	Solid phase (resin) concentration of compound *i* ($g_{PC\ or\ COD}/g_{dry\ resin}$)
$C_{S,i}^{\infty}$	maximum amount sorbed per unit mass of adsorbent, in the Langmuir model ($g_{PC\ or\ COD}/g_{dry\ resin}$)
$C_{S,i,eqOMW}$	PC or COD solid phase (resin) concentration in equilibrium with the microfiltered OMW used for the batch and breakthrough tests ($g_{PC}/g_{dry\ resin}$)
$C^{*}_{S,t,PC}$	Dimensionless sorbed-phase PC concentration measured at time *t* during the kinetic adsorption batch tests (-)
HETP	Height equivalent to a theoretical plate, in the packed column (m)
$K_{eq,i}$	Constant related to the affinity between the binding sites and PCs or COD, in the Langmuir isotherm ($L_{pore\ volume}/g_{PC\ or\ COD}$)
$K_{F,i}$	the sorption capacity in the Freundlich model ($L/g_{dry\ resin}$)
$m_{i,fed}$	Mass of PC or VS fed to the column until a certain breakpoint (mg)
$m_{i,desorbed}$	Total mass of PC or VS desorbed by the resin during the entire desorption procedure (mg)
$m_{i,sorbed}$	Mass of PC or VS adsorbed by the resin in correspondence of a certain breakpoint (mg)
m_S	Mass of dry resin in the isotherm studies ($g_{dry\ resin}$)
n_i	Inverse of the sorption intensity in the Freundlich model (-)
N	Number of experimental points in each isotherm (-)
P	Number of parameters to be estimated in each isotherm (-)
$V_{OMW,0}$, $V_{L,final}$	OMW volume initially added and final liquid volume resulting from the sum of the added OMW and the water initially contained in the activated resin, in the isotherm tests (L)
$Y_{ads,i}$	PC or VS adsorption yield, calculated as $m_{PC\ or\ VS,sorbed} / m_{PC\ or\ VS,initial}$ in the batch tests, and as $m_{PC\ or\ VS,sorbed,20\ \%} / m_{PC\ or\ VS,fed,20\ \%}$ in the breakthrough tests (-)
$Y_{des,i}$	PC or VS desorption yield in a batch or breakthrough test, defined as $m_{PC\ or\ VS,desorbed} / m_{PC\ or\ VS,sorbed}$ (-)
ε	Effective porosity (-)
η_{resin}	Resin operating capacity, defined as $m_{PC,sorbed,20\ \%} / m_{PC,sorbed,saturation}$ (-)

References

Abdelkreem M., (2013). Adsorption of Phenol from Industrial Wastewater Using Olive Mill Waste, APCBEE Procedia 5 349-357.

Abu-Lafi S., Al-Natsheh M.S., Yaghmoor R., Al-Rimawi F., (2017). Enrichment of Phenolic Compounds from Olive Mill Wastewater and In Vitro Evaluation of Their Antimicrobial Activities, Evid. Based Complement Alternat. Med. 2017 3706915.

Achak M, Hafidi A, Ouazzani N, Sayadi S, Mandi L, (2009). Low cost biosorbent ''banana peel'' for the removal of phenolic compounds from olive mill wastewater: kinetic and equilibrium studies. J Hazard Mater 166:117–125.

Aissa I., Kharrat N., Aloui F., Sellami M., Bouaziz M., Gargouri Y., (2017). Valorization of antioxidants extracted from olive mill wastewater, Biotechnol. Appl. Biochem. 64 579-589

Aliakbarian B., Casazza A.A., Perego P., (2015). Kinetic and Isotherm Modelling of the Adsorption of Phenolic Compounds from Olive Mill Wastewater onto Activated Carbon, Food Technol. Biotechnol. 53 207-214.

Aly, A.A., Hasan, Y.N.Y., Al-Farraj, A.S., (2014). Olive mill wastewater treatment using a simple zeolite-based low-cost method. J. Environ. Manag. 145, 341–348.

Anastasiou, C.C., et al., (2011). Approaches to olive mill wastewater treatment and disposal in Cyprus. Environ. Res. J. 5 (2), 49–58.

Aranda E., Garcia-Romera I., Ocampo J.A., Carbone V., Mari A., Malorni A., Sannino F., De Martino A., Capasso R., (2007). Chemical characterization and effects on Lepidium sativum of the native and bioremediated components of dry olive mill residue, Chemosphere 69 (2007) 229-239.

Azzam, M.O.J., Al-Gharabli, S.I., Al-Harahsheh, M.S., (2015). Olive mills wastewater treatment using local natural Jordanian clay. Desalin. Water Treat. 53 (3), 627–636.

Bertin L., Ferri F., Scoma A., Marchetti L., Fava F., (2011). Recovery of high added value natural polyphenols from actual olive mill wastewater through solid phase extraction, Chem. Eng. J. 171 1287-1293.

Bertin L., Frascari D., Domínguez H., Falqué E., Riera Rodriguez F.A., and Alvarez Blanco S., (2015). Conventional purification and isolation. In: C.M. Galanakis (Ed.), Food Waste Recovery: Processing Technologies and Techniques, Elsevier - Academic Press, London, 2015, pp 149-172

Bradford M.M., (1976). A rapid and sensitive method for the quantitation of microgram quantities of protein utilizing the principle of protein-dye binding, Anal. Biochem. 72 248–254.

Caporaso, N., Formisano, D., Genovese, A., (2017). Use of phenolic compounds from olive mill wastewater as valuable ingredients for functional foods Crit. Rev. Food Sci. Nutr. 1–13.

Cardinali A., Pati S., Minervini F., D'Antuono I., Linsalata V., Lattanzio V., (2012). Verbascoside, isoverbascoside, and their derivatives recovered from olive mill wastewater as possible food antioxidants, J. Agric. Food Chem. 60 (2012) 1822-1829.

Casademont, P., et al., (2016). Energy production by hydrothermal treatment of liquid and solid waste from industrial olive oil production. J. Appl. Solut. Chem. Model. 5, 103–116.

Casademont, P., et al., (2018). Hydrogen production by catalytic conversion of olive mill wastewater in supercritical water. J. Supercrit. Fluids 141, 224–229.

Conidi C., Mazzei R., Cassano A., and Giorno L., (2014). Integrated membrane system for the production of phytotherapics from olive mill wastewaters, J. Membr. Sci., vol. 454, pp. 322–329, 2014

Daassi D., Lozano-Sanchez J., Borras-Linares I., Belbahri L., Woodward S., Zouari-Mechichi H., Mechichi T., Nasri M., Segura-Carretero A., (2014). Olive oil mill wastewaters: phenolic content characterization during degradation by Coriolopsis gallica, Chemosphere 113 (2014) 62-70.

Dermeche S., Nadour M., Larroche C., Moulti-Mati F., and Michaud P., (2013). “Olive mill wastes: biochemical characterizations and valorization strategies”, Process Biochem., vol. 48, pp. 1532–1552

DOW (Trademark of The Dow Chemical Company), Tech Fact - Ion Exchange Resins Selectivity, 2016.

El Hajjouji, H., et al., (2014). Evaluation of an aerobic treatment for olive mill wastewater detoxification. Environ. Technol. 35 (24), 3052–3059.

El-Abbassi, A., Kiai, H., Hafidi, A., (2012). Phenolic profile and antioxidant activities of olive mill wastewater. Food Chem. 132 (1), 406–412.

El-Abbassi A., Kiai H., Raiti J., and Hafidi A., (2014). Cloud point extraction of phenolic compounds from pretreated olive mill wastewater. J. Environ. Chem. Eng., vol. 2, pp. 1480-1486, 2014].

El-Abbassi, A., et al., (2017). Potential applications of olive mill wastewater as biopesticide for crops protection. Sci. Total Environ. 576, 10–21.

Ena A, Pintucci C, Carlozzi P (2012) The recovery of polyphenols from olive mill waste using two adsorbing vegetable matrices. J Biotechnol 157:573–577.

Erkonak, H., Söğüt, O.Ö., Akgün, M., (2008). Treatment of olive mill wastewater by supercritical water oxidation. J. Supercrit. Fluids 46 (2), 142–148.

Ferri F., Bertin L., Scoma A., Marchetti L., Fava F., (2011). Recovery of low molecular weight phenols through solid-phase extraction, Chem. Eng. J. 166 994-1001.

Fiorentino A., Gentili A., Isidori M., Monaco P., Nardelli A., Parrella A., Temussi F., Environmental effects caused by olive mill wastewaters: toxicity comparison of low-molecular-weight phenol components, J. Agric. Food Chem. 51 (2003) 1005-1009.

Folin O., Ciocalteu V., (1927). On tyrosine and tryptofan determinations in protein, J. Biol. Chem. 73 (1927) 627–650.

Foo K.Y., Hameed B.H., (2010). Insights into the modeling of adsorption isotherm systems, Chem. Eng. J. 156 2-10.

Frascari D., (2013). “Trichloroethylene aerobic cometabolism by suspended and immobilized butane-growing microbial consortia: a kinetic study”, Biores. Technol., vol. 1244, pp. 529-538.

Frascari D., Bacca A.E.M., Wardenaar T., Oertléc E., Pinelli D., (2019). Continuous flow adsorption of phenolic compounds fromolive mill wastewater with resin XAD16N: life cycle assessment, cost–benefit analysis and process optimization. Wiley Online Library.

Frascari D., Bacca A.E.M., Zama F., Bertin L., F. Fava, D. Pinelli, (2016). Olive mill wastewater valorisation through phenolic compounds adsorption in a continuous flow column, Chem. Eng. J. 283 293-303.

Galanakis C.M., (2010). Recovery and preservation of phenols from olive waste in ethanolic extracts, J. Chem. Technol. Biotechnol., vol. 85, pp. 1148-1155, 2010,

Galanakis C.M., Schieber A., (2014). Editorial, Food Res. Int. 65 299–300.

Hachicha, S., et al., (2009). Elimination of polyphenols toxicity from olive mill wastewater sludge by its co-composting with sesame bark. J. Hazard. Mater. 161 (2), 1131–1139.

Haddad, K., et al., (2017). Olive Mill Wastewater: From a Pollutant to Green Fuels, Agricultural Water Source and Biofertilizer. Vol. 5.

Ho Y.S., McKay G., (1999). Pseudo-second order model for sorption processes, Process Biochem. 34 451-465.

Huang D., Ou B., Prior R.L., (2005). The chemistry behind antioxidant capacity assays, J. Agric. Food Chem. 53 1841-1856.

Idrissi El, (2017). Cyclodextrin-based polymeric materials for the specific recovery of polyphenolic compounds through supramolecular host–guest interactions. Journal of Inclusion Phenomena and Macrocyclic Chemistry, 88:35-42

Ioannou, L., et al., (2017). Treatment Efficiency and Economic Feasibility of Biological Oxidation, Membrane Filtration and Separation Processes, and Advanced Oxidation for the Purification and Valorization of Olive Mill Wastewater. Vol. 114.

Jeguirim, M., et al., (2017). Olive mill wastewater: From a pollutant to green fuels, agricultural water source and bio-fertilizer—Part 1. The drying kinetics. Energies 10 (9), 1423.

Kalogerakis N., (2013). Recovery of antioxidants from olive mill wastewaters: a viable solution that promotes their overall sustainable management”, J. Environ. Manage., vol. 128, pp. 749-758, 2013, Kammerer J., Kammerer D.R., Carle R., (2010). Impact of saccharides and amino acids on the interaction of apple polyphenols with ion exchange and adsorbent resins, J. Food Eng. 98 230-239

Kammerer J., Carle R., and Kammerer D.R. (2011). Adsorption and Ion Exchange: Basic Principles and Their Application in Food Processing. J. Agric. Food Chem. vol. 59, pp. 22–42, 2011.

Karahan, Ö.Ö., et al., (2016). Characteristics and biodegradability of olive mill wastewaters. Environ. Technol. 37 (10), 1240–1248.

Kıpçak, E., Söğüt, O.Ö., Akgün, M., (2011). Hydrothermal gasification of olive mill wastewater as a biomass source in supercritical water. J. Supercrit. Fluids 57 (1), 50–57.

Kıpçak, E., Akgün, M., (2013). Catalytic gasification of olive mill wastewater as a biomass source under supercritical conditions. Int. J. Chem. Mater. Sci. Eng. 7 (9).

Levenspiel O., Chemical Reaction Engineering, third ed., Wiley, New York, 1999.

Magalhaes L.M., Segundo M.A., Reis S., Lima J.L., Rangel A.O., (2006). Automatic method for the determination of Folin-Ciocalteu reducing capacity in food products, J. Agric. Food Chem. 54 5241-5246.

Magalhaes L.M., Segundo M.A., Reis S., Lima J.L., (2008). Methodological aspects about in vitro evaluation of antioxidant properties, Anal. Chim. Acta 613 1-19.

Mantzavinos, D., Kalogerakis, N., (2005). Treatment of olive mill effluents: Part I. Organic matter degradation by chemical and biological processes—an overview. Environ. Int. 31 (2), 289–295.

Martinez L., Ros G., Nieto G., (2018). Hydroxytyrosol: Health Benefits and Use as Functional Ingredient in Meat, Medicines (Basel) 5

Mekki, A., Dhouib, A., Sayadi, S., (2013). Review: effects of olive mill wastewater application on soil properties and plants growth. Int. J. Recycl. Org. Waste Agric. 2 (1), 15.

Miller G. L. (1959). “Use of dinitrosalicylic acid reagent for determination of reducing sugar”, Anal.Chem.31(3), 426-428.

Navarro M., Morales F.J., (2017). Effect of hydroxytyrosol and olive leaf extract on 1,2-dicarbonyl compounds, hydroxymethylfurfural and advanced glycation endproducts in a biscuit model, Food Chem. 217 602-609.

Ochando-Pulido J.M., Pimentel-Moral S., Verardo V., Martinez-Ferez A.; (2017). A focus on advanced physico-chemical processes for olive mill wastewater treatment. Separation and Purification Technology 179 (2017) 161–174.

Perez-Jimenez J., Neveu V., Vos F., Scalbert A., (2010). Identification of the 100 richest dietary sources of polyphenols: an application of the Phenol-Explorer database, Eur. J. Clin. Nutr. 64 Suppl 3 S112-120.

Pinelli D., Molina Bacca A.E., Kaushik A., Basu S., Nocentini M., Bertin L., Frascari D., (2016). Batch and Continuous Flow Adsorption of Phenolic Compounds from Olive Mill

Wastewater: A Comparison between Nonionic and Ion Exchange Resins, Int. J. Chem. Eng. 2016 13.

Poerschmann, J., Weiner, B., Baskyr, I., (2013a). Organic compounds in olive mill wastewater and in solutions resulting from hydrothermal carbonization of the wastewater. Chemosphere 92 (11), 1472–1482.

Poerschmann, J., et al., (2013b). Hydrothermal carbonization of olive mill wastewater. Bioresour. Technol. 133, 581–588.

Rahmanian N., Jafari S.M., Galanakis C.M., (2014). Recovery and Removal of Phenolic Compounds from Olive Mill Wastewater, J. Am. Oil Chem. Soc. 91 1-18.

Rodis P.S., Karathanos V.T., and Mantzavinou A., (2002). “Partitioning of olive oil antioxidants between oil and water phases”, J. Agric. Food Chem., vol. 50, pp. 596–601, 2002.

Rodríguez-Gutiérrez, G., et al.,(2012). New Olive-Pomace Oil Improved by Hydrothermal Pre-Treatments. INTECH Open Access Publisher.

Sabbah I, Marsook T, Basheer S (2004) The effect of pretreatment on anaerobic activity of olive mill wastewater using batch and continuous systems. Process Biochem 39:1947–1951.

Santi CA, Cortes S, D’Acqui LP, Sparvoli E, Pushparaj B (2008) Reduction of organic pollutants in olive mill wastewater by using different mineral substrates as adsorbents. Bioresour. Technol 99:1945–1951.

Scoma A, Bertin L, Zanaroli G, Fraraccio S, Fava F (2011) A physicochemical–biotechnological approach for an integrated valorization of olive mill wastewater. Bioresour Technol 102:10273–10279.

Serrano A., Fermoso F.G., Rodríguez-Gutierrez G., Fernandez-Bolaños J., Borja R., (2017). Biomethanization of olive mill solid waste after phenols recovery through low-temperature thermal pre-treatment. Waste Management 61 (2017) 229–235.

Singh KP, Malik A, Sinha S, Ojha P (2008) Liquid-phase adsorption of phenols using activated carbons derived from agricultural waste material. J Hazard Mater 150:626–641.

Soto M.L., Moure A., Domínguez H., and Parajó J.C., (2015). Recovery, concentration and purification of phenolic compounds by adsorption: a review”, J. Food Eng. vol. 105, pp. 1–27, 2011

Speltini, A., et al., (2015). Evaluation of UV-A and solar light photocatalytic hydrogen gas evolution from olive mill wastewater. Int. J. Hydrogen Energy 40 (12), 4303–4310.

Stoller, M., et al., (2015). Membrane process enhancement of 2-phase and 3-phase olive mill wastewater treatment plants by photocatalysis with magnetic-core titanium dioxide nanoparticles. J. Ind. Eng. Chem. 30, 147–152.

Stoller, M., et al., (2017). Technical and economic impact of photocatalysis as a pretreatment process step in olive mill wastewater treatment by membranes. Chem. Eng. 57.

Tavakoli H., Hosseini O., Jafari S.M., Katouzian I., (2018). Evaluation of Physicochemical and Antioxidant Properties of Yogurt Enriched by Olive Leaf Phenolics within Nanoliposomes, J Agric Food Chem. 66 9231-9240.

Wiegand I., Kai Hilpert K., R.E.W. Hancock; (2008). Agar and broth dilution methods to determine the minimal inhibitory concentration (MIC) of antimicrobial substances; Nature Protocols.

Zagklis D.P., Vavouraki A.I., Kornaros M.E., and Paraskeva C.A. (2015). Purification of olive mill wastewater phenols through membrane filtration and resin adsorption/desorption, J. Hazard. Mater., vol. 285, pp. 69–76, 2015

Ziati M., Khemmari F., Cherifi O., Didouche F.Y., (2017). Removal of polyphenols from olive mill wastewater by adsorption on activated carbon prepared from peach stones, Rev. Roum. Chim 62, 865-874.

PART II

Removal and recovery of phosphorus from municipal wastewater with a hybrid ion exchange resin

2.1 INTRODUCTION

Phosphorus (P) is non-renewable resource primary obtained from phosphate rock. Phosphate rock was listed as a critical raw material by the EU in May 2014 (European Commission, 2014) on the basis of two indicators: high supply risk and equally high economic importance. As a matter of fact, P is essential for life since it represents one of the main nutrients for plants. On the other hand, its large and uncontrolled usage as fertilizer by industries and the incomplete treatment of domestic and industrial wastewater led to a dramatic affection of the aquatic ecosystems' biodiversity. Indeed, the excessive presence of phosphorus in water bodies (result of untreated sewage effluent and agricultural run-off) has been identified as the primary cause of the eutrophication problem in river, lakes and seas. Euthrophication induces overgrowth of phytoplankton, thus deteriorating water quality, depopulating aquatic species and accelerating water scarcity (Sellner et al., 2003). Hence, legislative regulations regarding the maximum allowable concentration of phosphate in treated effluents of wastewater treatment plant (WWTP) is expected to be continuously stricter (Chamoglou et al., 2014). Meantime, municipal WW (MWW) are today considered one of the most potential new source of P for fertilizer production, since it is widely distributed and continuously available (Schoumans et al., 2015). Phosphate removal and recovery in municipal WWTPs attracted considerable research interest in last few decades and several technologies have been developed (Egle et al., 2015 & 2016). Adsorption has been considered one of the most promising methods to remove P from aqueous solutions, especially coupled with secondary treatments such as activated sludges and membrane bioreactors (Bunce et al., 2018). In secondary wastewater effluent phosphate is present as trace element and different technologies struggle to further reduce its content in a cost-effective way. Adsorption would guarantee full control of the effluent quality and the recovery of a final product instead of the solely P removal from wastewater obtainable with the traditional techniques such as the enhanced biological phosphorus removal (EBPR) and chemical precipitation (SenGupta and Pandit, 2011). Moreover adsorption has attractive advantages, such as continuous-flow operation, compact facilities, high removal efficiency and fast operation rate, easy handling of the process-operation, possible lack of high-instructed operators and feasible reduced operational costs in case of durable resins with a long operating life.

In this way, this work represents one of the first attempts to introduce an adsorption process within an existing municipal wastewater treatment plant (MWWTP) (population equivalent < 10,000), investigating the process performances through time. Many works are focusing on the developing of new engineered materials to selectively remove phosphate from the complex background matrix of MWW. However, it should be spotlighted that all adsorbents used for arsenate (As(V)) could be effectively implemented also for the phosphate uptake, due to similar structure of these elements and their oxyanions. Therefore, while in literature can be found a tremendous number of laboratory attempts coupling mono-, di- or tri-metal atoms with a likewise enormous number materials that can function as a scaffold for the metal (hydr)oxide nanoparticles, the works focused on the long-term testing of the process with actual WWTP effluents are extremely limited in the number, especially at pilot-scale dimension (Kalaitzidou et al., 2016; Drenkova-Tuhtan et al., 2017; Petruzzelli et al., 2004; Mateus et al., 2010; Choi et al., 2014).

The current study investigated for a time of approximately 1 year and a half the commercially available resin HAIX Layne^{RT} (characterized by the presence of hydrated ferric nanoparticles within a strong base anion exchanger with quaternary ammonium functional groups) within a demonstration plant treating 10 m^3d^{-1} of actual secondary effluent wastewater. During the 6 months I spent at Cranfield University under the supervision of Prof. Ana Soares, I performed approximately 30 adsorption-desorption cycles up to a total number of 66 cycles. The main objective of my study were:

i) Investigating the novel operating method proposed by Cranfield University for the pilot plant conduction. To first main question I was asked to answer was to quantify the impact of reusing the same regenerant solution multiple times for consecutive desorption steps. The double advantage of such operation was to increase the P-content of the solution enhancing the following P recovery and to reduce the usage of chemicals necessary. To do this several groups of adsorption/desorption cycle with the same regenerant were performed (*Results & Discussion* – Chapter 2.4.2).

ii) Investigating the possibility of reusing the same regenerant solution after the recovery of calcium phosphate by precipitation. The "spent" regenerant solution which had reached the limit P concentration was treated to recover the final product and then recirculated to the process. The same regenerant solution was recovered and recirculated twice to investigate and compared the process performances to that obtained at point i) (*Results & Discussion* – Chapter 2.4.4).

iii) Moreover, although the investigation and optimization of the precipitation step were beyond the scope of this study, a quantitatively estimation of the obtainable final product and analysis concerning the possible presence of hazardous contaminants was performed. The main objective of this part was to prove the effectiveness of the consecutive selective processes in obtaining a valuable product with the compulsory characteristics to enter the fertilizer-market (*Results & Discussion* – Chapter 2.4.3).

iv) Finally, collecting complete and reliable data for the development of a Life Cycle Assessment and of a costs/benefits economic evaluation of the process and its proposed conduction method. Primary way to effectively compared the current technology with others available.

Subsequently, once the plant was stopped, an investigation of the resin was considered necessary to fully characterized the process performances and their evolution through time. Indeed, no preliminary adsorption breakthrough curves had been taken at the earliest plant operation. Hence, no comparison between the first and the latter cycles was possible. The main objective of this second part was therefore aimed at fully characterizing the HAIX Layne^{RT} resin that had worked for almost 70 cycles in a pilot plant treating actual wastewater and comparing its performances with that of the same abovementioned resin brought new from the same supplier. Moreover, it was considered of high interest to investigate the resin coming from the Cranfield pilot plant after a regeneration of the ion-exchange media to evaluate a possible restoring of the total capacity. Hence, it was expected that the novel operating method proposed by Cranfield University (i.e. the continuous desorption of the only ferric nanoparticle sites) could have led to detrimental effects (e.g. steric obstruction, disabled Donnan effect) on the resin's P-removal potential. Therefore, the virgin resin (resin bought new) and the used resin coming from the Cranfield pilot plant (pre-treated in two different ways) were tested by means of batch adsorption/desorption tests and continuous flow laboratory-scale tests. The work covered the following points:

i) Complete literature review on the new type of hybrid adsorbent objective of the study (*State of Art* – Chapter 2.2.4);

ii) Comparison of the virgin resin performances with that of the pilot-plant resin to fully quantified the real impact of the operating method proposed and applied at demonstration scale. The complete characterization is based on the evaluation of the media total capacity, the media regenerability and the selectivity exerted towards phosphate (*Results & Discussion* – Chapter 2.4.5).

iii) Evaluation of the possible introduction into the proposed method of a desorption step including the elution of organic and inorganic compounds accumulated on the ion-exchange media, with the ultimate aim of restoring a disable fraction of the resin capacity. Hence, lower capacity translates into inefficient process (i.e. small amount of treated WW during the adsorption step, short breakthrough time and frequent regenerations) and therefore into higher yearly cost associated to the periodic resin replacement. The latter represents one of the heaviest items of cost for the process, specially for this type of resin characterized by a relatively high market price (22€/kg) (*Results & Discussion* – Chapter 2.4.5).

2.2 STATE OF ART

2.2.1 The broken cycle of phosphorus

Phosphate rock was listed as a critical raw material by the EU in May 2014 (European Commission, 2014) on the basis of two indicators: high supply risk and equally high economic importance. Around three and a half centuries has passed from the discovery of the phosphorus' elemental form by the German alchemist Hennig Brandt. From that initial discovery to present, phosphorus continued increasing in importance together with human understanding of its essential role to all life (plants, animals and bacteria). Currently, the production of fertilizer from mined P rock focusses on three hot spots: China, Morocco and USA. Yet, today's phosphorus use patterns in the global food production and consumption system have resulted in a global environmental epidemic of fresh-water eutrophication and marine "dead zone" (World Resources Institute, 2008) and simultaneously led to a situation where the future availability of the world's main sources of phosphorus are uncertain (Cordell et al., 2009). Indeed, although phosphorus is highly abundant in nature, it is one of the least biologically available nutrients. That is, the forms in which it exists in the biosphere are often 'unavailable' for plants which can only absorb the soluble inorganic form of phosphorus (known as orthophosphates) dissolved in soil solution. This fundamental understanding was on the basis of the Green Revolution (1840) which had the most profound impact on the phosphorus cycle. However, before the Green Revolution the human civilization history had already significantly interfered with the global phosphorus cycle (Ashley et al. 2011). The Industrial and the Sanitation Revolutions were key periods for the development of our society and for the consequent impacts on the global phosphorus cycle.

The Industrial Revolution started with the replacement of animal energy with fossil fuels (initially with coal, then cheap hydrocarbons and hydroelectricity) and the migrations of workers to cities which started a world-wide transition to an industrialized manufacturing economy. As cities grew, they developed their own internal threats, which led to the Sanitation Revolution. An important milestone in the Sanitary Revolution was represented by the outbreak of cholera occurred in London on August 1854. Where an infection, started from a cesspool containing contaminated wastewater, killed 616 people. Indeed, most houses just let sewage accumulate in backyard cesspool, or house basements, because as city became bigger the tonnages and distances became too large to return sewage to the land. Public health concerns and safe disposal fundamentally changed the 19th and 20th century civilization from land-based disposal of human wastes to massive systems of sewer interceptions from a phosphorus recycling society to a phosphorus through-put society. Slow sand filtration for water supplies expanded, massive systems of sewer interceptions were built, the science of bacteriology originated soon afterwards from 1862 to 1870s, continuous chlorination of potable water supplies started in England in 1904 as the principles of public health and sanitation became firmly established in western countries.

Following the Industrial and Sanitation Revolutions, the Green Revolution led to a largely abandon of organic fertilizers in agriculture so far used, such as manure, guano, human excreta. It was in the 1840 that Justus von Liebig's confirmed the fertilizing effect of humus on plant growth was due to inorganics salts of phosphorus and nitrogen, and not organic matter (Liebig, 1840). Despite its radical nature, that theory was widely adopted in Western agriculture. However, it was not until the post-World War II period that use of mineral phosphorus sources grew exponentially (Fig. 2.2.1). Phosphate rock was seen as a cheap and plentiful source of phosphorus and it became widely used in favour of organic sources (Brink J., 1977). In the mid-20th century, period known as the Green Revolution, several high-yielding crop varieties were developed in order to keep up with rapid population growth, increasing food shortages and urbanization. This was supported by the invention of the Haber–Bosch process, which allowed the production of high volumes of artificial nitrogenous fertilizers, with external inputs of irrigation water, nutrients, pesticides, herbicides and hydrocarbon energy, rather than manual labour (Brink J., 1977; Fresco L., 2009). Phosphate rock was now mined to keep up with nitrogen fertilizer demand. Fertilizer use sextupled between 1950 and 2000 (IFA, 2006). So, whilst the industrialized agriculture established a dependence on the mined phosphate rock, with the Industrial Revolution gaining momentum, the public health concerns mandated disposal of excreta, rather than reuse. Hence, phosphorus was mined, processed into fertilizers, spread on the fields, metabolized by plants and, then, harvested as crops to be processed and sold as commercial food. With the compulsory disposal of excreta, phosphorus was discharged in oceans, lakes and rivers instead of land, and thus permanently lost from the human food system. Cultural eutrophication of freshwater mirrored the expansion and development of modern industrial societies through Europe and North America. The resulting problems of receiving water pollution soon intensified and more sophisticated wastewater treatment processes were developed: this included secondary treatment to further reduce biochemical oxygen demand. The rapidly expanding economies and populations in the post WW II western world, plus the introduction of detergent phosphates, lead to increasingly widespread eutrophication and subsequent scientific investigations to resolve the "Great Phosphorus Debate" (Vallentyne, 1974). Phosphorus was identified as the key element in eutrophication and this led to bans of detergent phosphates, as well as implementation of tertiary wastewater treatment to remove nutrients from point source streams (Schindler and Vallentyne, 2008). Tertiary treatment was initially achieved by chemical precipitation, which permanently removed phosphorus from the human food system and created significantly waste sludge disposal problems. Later, phosphorus was removed by the more sustainable Biological Nutrient Removal process.

Figure 2.2.1 Historical sources of phosphorus fertilizers used in agriculture globally (1800-2010). Source: updated from Cordell et al. (2009).

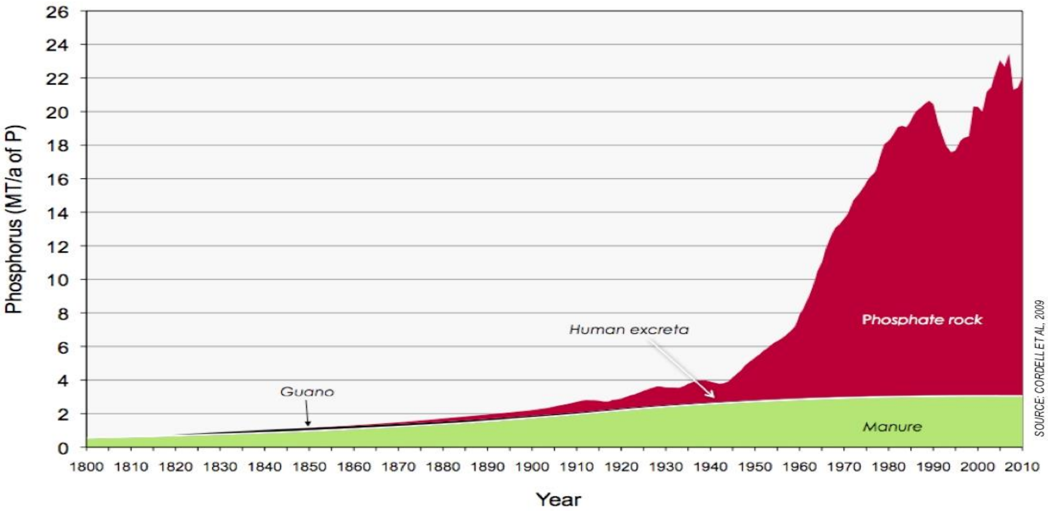

Anyway, these dated technologies were aimed at reducing the phosphorus concentration before disposal, without any idea of recovering a final product containing phosphorus. The need of discovering and developing new technologies to combine the removal and the recovery of phosphorus from waste stream came out as the awareness of the 'phosphorus issue' became more widespread and phosphate rock was classified as a limited and non-renewable resource. Nowadays, whilst there is a vigorous debate around the lifetime of the phosphate rock reserves, it is clear is that the remaining rock is lower in phosphorus concentration (%P_2O_5), higher in contaminants, more difficult to access (i.e. in environmentally and culturally sensitive areas) and, hence, that requires more energy and costs to be extracted, produced, and refined (Cordell et al., 2009). An ultimate goal of sustainable phosphorus use is ensuring that all the world's farmer have sufficient access to phosphorus to grow enough food to feed the global population, whilst minimizing adverse environmental and social impacts (Cordell, 2009). However, already today, many poor farmers (particularly in sub-Saharan Africa) have phosphorus-deficient soils and cannot access fertilizer markets due to poor purchasing power. This has led not only to low crop yields, but also increasing losses due to soil erosion, poor farmer incomes and increased hunger. Indeed, many of the world's 1.02 billion undernourished people are smallholder farmers (IAASTD, 2008). Further complicating the picture is that only five countries control 85% of the world remaining reserves – Marocco, China, US, Jordan and South Africa (Ashley et al., 2011).

According to Ashely et al. (2011) averting a major phosphorus crisis is possible; however, it will require considerable political will and substantial change to our current physical infrastructure and institutional arrangements. Sustaining global and local phosphorus cycles can only be achieved through recycling close to 100% of the phosphorus temporarily lost from the food production and consumption of food, including human excreta, manure, food and organic waste. Investing in renewable phosphorus sources (through local phosphorus recovery from wastes) can simultaneously reduce dependence on a finite resource, reduce water pollution and increase communities' phosphorus security, which is particularly important highly dependent on imports (from Europe to sub-Saharan Africa). There is no single solution to replace the massive consumption of phosphate rock. Sustainable measures aimed at recovering and reusing phosphorus in the food system can range from low-tech, small-scale solutions like direct urine reuse, through to large scale, high –tech solutions such as struvite recovery from wastewater treatment plant (Britton et al., 2009; Cordell et al., 2011). Solution will need to be region-specific, to ensure they are appropriate for the local environmental, political, economic, demographic and cultural conditions; they must also be harmonious with the region's sanitation and food security situation.

2.2.2 Technologies for P recovery

Wastewater treatment plants (WWTPs) provide one of the biggest opportunities for P recovery given the relatively high and constant P load in sewage (Schoumans et al., 2015). The recovery of P from wastewaters can provide an array of benefits: (1) meeting the effluent P limits required by legislation; (2) reducing eutrophication problems; and (3) providing a potential source of fertiliser, hence of a high valuable product that reduces the reliance on inorganic (rock-P derived) fertilisers in agriculture. P concentrations reported for municipal wastewaters are generally below 10 mg P/L (Petzet and Cornel, 2013). However, in addition to P-forms and many other innocuous compounds, municipal wastewaters contain many contaminants, both organic and inorganic, such as heavy metals and metalloids, pesticides, pharmaceuticals, personal care products, nanomaterials, perfluorinated compounds (PFCs), hormones, recreational drugs and pathogens. Therefore, the application of untreated effluent to agricultural land poses associated risks to human food consumption (Schoumans et al., 2015). Wastewaters require recovery processes with a certain degree of selectivity to remove P into a solid form that can be safely and effectively used as fertiliser. At different WWTP process steps, P exists within wastewater in a variety of forms: P in particulate forms are more easily and completely removed through clarification steps, whereas dissolved P species (both organic and inorganic) require more targeted processes for their removal. Fig. 2.2.2 illustrates the possible hot spots for P removal technologies: i) the green hot spots are accesses for aqueous phase P-recovery treatment; ii) the blu hot spots are accesses for the sewage sludge P-recovery treatment and iii) the red hot spot is the accesses for the sewage sludge ash P-recovery treatment.

Figure 2.2.2 Various possible access points for P recovery approaches during wastewater and sewage sludge treatment or before/after inceneration. (Egle et al., 2015).

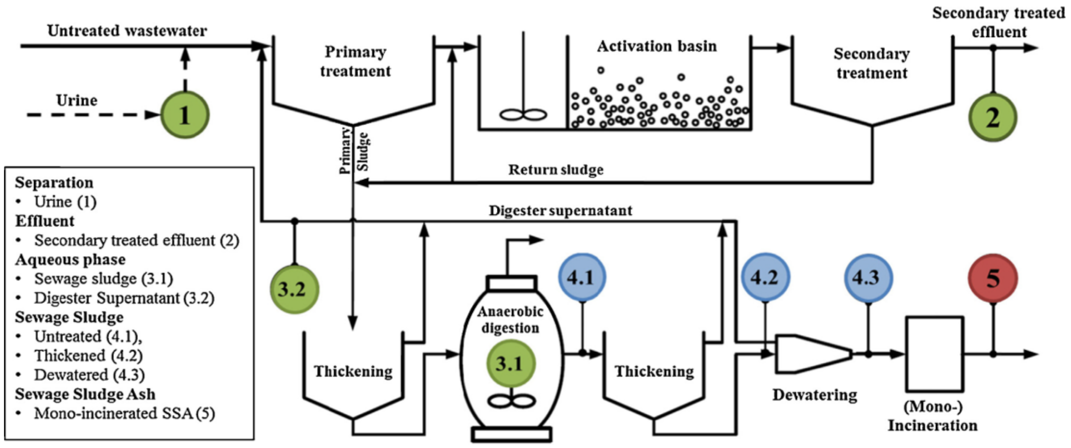

Generally, in a typical WWTP a preliminary screening and a primary treatment step are applied to remove larger particles. The latter involves the settlement and removal of organic fractions and suspended solids, which can be achieved by filtration or chemical addition. Then, a secondary treatment is applied, especially in lager WWTP and those discharging to sensitive environments. This can involve the use of microbes to break down soluble organic compounds that remain after the preliminary and primary treatment steps (through trickling filter beds or other treatments), and/or the addition of chemicals to promote the coagulation and flocculation of solids. Other than particulate P removed here through secondary clarification, specific P removal techniques can be integrated into the treatment process to target dissolved forms of P: for example chemical precipitation or enhanced biological phosphorus removal (EBPR). Moreover, tertiary and advanced treatments can be applied for the further removal or degradation of dissolved contaminants, especially when the treated water will be reused. Standard primary and secondary treatments often do not remove sufficient P to meet the required discharge concentration. Under normal secondary treatment (the activated sludge process) around 31-48% of influent P can be transferred into sludge (Petzet and Cornel, 2013). With the particulate P removed through primary settlement, that is reported to be around 17-26% of an incoming total P load, the total sludge (coming from both the primary and the secondary treatment) can leave up the removal of P to approximately 50% of the total influent P load before discharge into a receiving water body (Petzet and Cornel, 2013). Sewage sludge is the second organic waste containing the greatest amount of P. The only waste richer than sewage sludge is bone meal, but on a global scale it is produced in much smaller quantities than sludge. Nowadays, since sludge itself is considered to be a very promising source of P (Cordell et al., 2011), new technologies of processing sludge are developing faster and faster and are implemented in a growing number of sewage treatment plants. Moreover, due to the introduction of new laws in European Union, landfilling of sludge which can’t be applied in agriculture has already been prohibited in most of the member countries. However, it is important to realize that it is still often directly used as fertilizer, especially in poor countries, mainly because of a lack of access and funds to implement sewage sludge incineration and phosphorus recovery technologies (Cordell et al., 2011). On the basis of the nature of the treatment, techniques specially used to remove P from wastewaters can be operationally categorised as chemical, biological and physical.

Currently, the most widely used technology of biological treatment is conducting alternating aerobic and anaerobic processes, called enhanced biological phosphorus removal (EBPR). EBPR allows to remove and accumulate P into sludge that can be treated to recover a P-rich product. EBPR relies on polyphosphate accumulating organisms (PAOs) or denitrifying PAOs to accumulate P intracellularly as polyphosphate granules, thus avoiding any requirement for chemical precipitants (Oehmen et al., 2007). The process is enabled by alternating anaerobic and aerobic conditions: during the anaerobic process PAOs take up volatile fatty acids, which are stored as polyhydroxyalkanoates and subsequently metabolised in the aerobic phase to supply the energy needed by the PAO to accumulate P. The use of the above-described alternating anaerobic and aerobic process allows a high degree of concentration of phosphorus in the sludge (from 1% to 5%, and in extreme cases up to 15% of phosphorus in the dry matter of the residue) (Tao and Xia, 2007). Actually, most full-scale P recovery technologies currently applied, required the pre-accumulation of P (as bio P-sludge) using EBPR processes. The accumulation of P within bio-P sludge and its settlement can facilitate the recovery of P and, in the absence of contaminants, allow for direct utilisation as fertiliser. Alternatively, further treatment can facilitate the solubilisation and recovery of P in a form such as struvite ($MgNH_4PO_4 \cdot 6H_2O$) (Baur, 2009). In full scale WWTPs, EBPR processes can typically remove over 85% of P in municipal wastewater influent, often to concentrations <0.1 mg P/L (Gautam et al., 2014). Although EBPR has resulted efficient in many cases, there are however questions over the stability of its performance (Zheng et al., 2014). One of the largest causes of deterioration and failure in EBPR systems arises from the occurrence of glycogen accumulating organisms (GAOs), which compete with PAOs for carbon substrate (Oehmen et al., 2007). Operating parameters can inhibit P removal favouring GAOs' growth, such as the presence of toxic substances to PAOs in the influent (as Cr(VI) at 0.5 mg/L), the pH, high temperature (close to 30°C), aeration and the type of carbon substrate fed. Without carbon addition to ensure high and constant concentrations, the EBPR system can be very susceptible to changes in the influent composition. Consequently, climates with a tendency for sporadic heavy rainfall, which can drastically perturb nutrient concentrations, can affect biological P removal (Manyumba et al., 2009). However, the addition of organic carbon to the process implicates additional cost to the EBPR process and increases the overall carbon footprint (Guerrero et al., 2015). All these variables may impact on the final P concentrations in the treated effluents and discharges may exceed those permitted by legislation. Therefore, EPBR is reputed as not being wholly reliable due to fluctuating performance and high dependence on skilled operators resulting in difficulty in process control. Anyway, with all their limitations, EBPR processes are considered to be a cost-effective and environmentally suitable alternative to chemical processes. As a matter of fact, they require less or no chemical addition and has the potential for the full-scale recovery of P offering significant economic advantages in larger WWTPs (Manyumba et al., 2009). However, where process inefficiencies are frequent and/or legislation requires consistently low P concentrations in effluent discharge, it is also common for larger WWTPs to deploy chemical precipitation in conjunction with EBPR to ensure requirements are consistently met (Kim and Chung, 2014). This reduces the amount of P that can be solubilised and recovered through bio-P sludge digestion or direct application as fertiliser. Other limitations include the complexity of operations and a large energy and space requirement. To date, much work has been done on optimizing configurations for continuous flow systems for biological P-removal: recent applications of EBPR include incorporation in membrane bioreactors (MBR), granular sludge reactors, and sequencing batch biofilm bioreactors (SBRs). Algae-based systems for the treatment of wastewater is also now well established; however, its full scale-application for nutrient removal is more limited, especially at higher latitudes. Some example of the newer P-removal technologies are reported in Table 2.2.1:

Table 2.2.1 Examples of novel biological P-removal technologies and relative performances at different scales. (Bunce et al., 2018).

Technology	***Description***	***TP-removal rates***	***Phase of development***
EBPR SYSTEMS			
MBR-UCT	Membrane bioreactor integrated into a continuous-flow EBPR	Up to 88%	Full scale
SBBR	Sequencing batch biofilm reactor (with fixed biofilm)	70-90%	Pilot scale
Granular sludge	Advanced activated sludge process operated as Sequencing Batch Reactor (SBR)	87%	Full scale
AnoxAn	Vertical flow anaerobic-anoxic reactor	89%	Bench scale
ALGAL SYSTEMS			
Algal biofilm reactors	Fixed growth algal bioreactors	Not reported	Full scale
Suspended growth photo-bioreactors	Suspended growth algal bioreactors	61%	Pilot scale
Osmotic MPBR	Osmotic membrane photo-bioreactor	90-100%	Bench scale
Membrane photo biofilm reactor	Membrane bioreactors with algae see; operating promote phototrophic growth	66-97%	Bench scale

At the moment, the most widely used technologies of phosphate recovery are those based on precipitation of phosphoric minerals from sludge or leachates. This worldwide P-removal treatment is a chemical option that involves dosing di- or trivalent metal salts of Fe, Al or Ca to either pre-treated influent, conventional activated sludge (CAS) reactor, or to the outlet from the secondary clarifier. Chemical precipitation is more efficient at earlier stages in the wastewater treatment process when the concentration of P in solution is highest. P in forms of phosphate ions, as well as organic P and particulate P fractions are coagulated to form a metal phosphate sludge and subsequently removed after flocculation and settlement. Further, P removal rates are typically proportional to the mass of chemical added, which impacts the amount of extra solids produced; therefore, there are intrinsic cost-benefits to the amount of salt used and the method of solids separation used. Within secondary effluent (1.46 mg total P/L), ferrate was able to remove more than 80% of P in the dosage range of 5-25 mg Fe/L. The two most obvious disadvantages of chemical precipitation are the requirement and cost of chemical additions, and the generation of large volumes of sludge that are often unsuitable for reuse due to the low recoverability of P and possible incorporation of contaminants in the P-rich precipitate (as arsenic, fluoride, organic compounds, pathogens, virus). In order to develop a more environmentally sustainable precipitation process, numerous by-products and wastes have also been investigated as precipitants: red mud, fly ash hydrated oil ashes and calcined waste paper sludge are just some examples. After conventional precipitation with the most common metal salts, P effluent concentrations of 1 mg/L can be achieved by conventional gravity settling (Burton et al., 2014). However, stricter effluent standards will generally demand more sophisticated separation techniques.

The biological and chemical process described above were mainly developed to remove P from the mainstream, however to date several technologies have been tested with the specific aim to recover P, instead of only removing it. Processes for the aqueous phase, the sewage sludge or the sewage sludge ash have been investigated (Fig. 2.2.2). Recovery from the liquid phase is based mostly on precipitation or crystallization processes. Sometimes precipitation/crystallization processes are combined with a prior concentration by adsorption or ion exchange processes (Sengupta and Pandit, 2011). Recovery from sludge or ash requires a prior hydrolysis, disintegration and dissolution generally obtained through anaerobic digestion or acid/alkaline treatment to enhanced leaching of P that must be dissolved in the aqueous phase. A lot of different techniques use precipitation of P with metals to recover it from aqueous solutions. The recovery can start directly in the aqueous phase (using sludge liquor or urine from source separated toilets) with a P recovery rate of up to 50%, or via P-leaching of sludges and ashes with up to 90% recovery rate. Anaerobic digestion (AD) is the most commonly used process for the stabilization of sludge: it is noteworthy that AD of bio-P sludges (sludges obtained by the EBPR process) can generate a liquor of approximately 10-50 times higher P concentration than the WWTP influent. Indeed, AD of bio-P sludge as a solubilisation technique is a primary step in facilitating the precipitation of struvite in many commercial P recovery processes such as AirPrex®, Crystalactor®, NuReSys®, Pearl®, Phosnix® and PHOSPAQ™. Anyway, in this type of processes, assimilation into the final product (e.g. struvite) of solubilized contaminants that have been found in several AD supernatants remains the biggest concern and would warrant further investigation. The technical maturity of the processes varies, with most of them being still on a pilot scale. In addition to the naturally occurring anaerobic release from sludge, the leaching of P out of both sludge and ash can be obtained via acids (e.g. Seaborne®). Differently, some processes use thermal treatment to facilitate P solubilization before precipitation. Once P is solubilized and the pH adjusted to at least slightly alkaline conditions, it can be precipitated with metal salts (Al, Fe, Ca, Mg). In the case of Mg addition and the presence of ammonia, struvite is formed. Precipitates can then be harvested by sedimentation, filters, dried and treated to be sellable as fertilizers (e.g. ChrystalGreen). Two commercial processes in the literature, AshDec® and Mephrec®, offer recovered products in the form of mineral-P in the form thermochemical SSA treatment. Metallurgical processes like Mephrec produce P-rich slags, with low concentrations of heavy metals, where P is bound in the form of calcium silicon phosphates.

Recent description and comparison of commercial approaches for P recovery from municipal wastewater is provided in detail elsewhere (Egle et al., 2015 & 2016). Amann et al. (2018), completed the works of Egle by defining the environmental impacts of the P recovery techniques through the methodology of life cycle analysis and linking these indicators with other selected environmental criteria such as recovery potential, heavy metal and organic micropollutant decontamination potential, and fertilizer efficiency. The authors could find out some general trends, with no absolute distinction in results regarding the point of implementation (liquid phase, SS, SSA) as the studied environmental impacts were found to also highly depend on specific technology paramenters, e.g. the usage of chemicals. However, the study concluded that recovery from the liquid phase has mostly or comparably little impacts in emission and energy demand, but the low recovery potential contradicts the demand for efficient recycling rates. Technologies for the recovery from sewage sludge are associated with comparatively high emission and energy demand. Recovery from sewage sludge ash shows varying results, partly revealing trade-offs between heavy metal decontamination, emissions and energy demand. Nevertheless, recovery from ash is correlated with the highest potential for an efficient recycling of phosphorus. Further research should include implications of local infrastructures and legal frameworks to determine economically and environmentally optimized P recovery and recycling concepts.

In recent years, much work has been done to improve P removal in filter systems using active media. Reactive media filters differ from traditional filtration systems since they rely on specific P-sorption properties of the material. In contrast, conventional filtration uses the media solely as a support for attachment of biomass. Absorptive can be manufactured from either natural products, industrial waste products or man-made products. Between the several commercially available product, Polonite is the most widely studied product. Polonite has been used by Renman and Renman (2010) to treat municipal wastewater. The study covered one year of operating time and performed a phosphorus removal of 91% with a P-sorption capacity of 120g/kg. However, Shilton et al. (2006) tested Polonite for an extended period of almost 10 years and reported a significant reduction in the performance of the system during the last period of the investigation. Thus, requires more investigation over longer periods to surely assess their durability and regeneration.

P can be removed by filter media by direct precipitation or sorption mechanisms. In the case of precipitation P react with some reactive components contained into the media (e.g. calcium or iron) and accumulates on the surface of into the body where it has reacted. Generally, the use of adsorptive media has been investigated within constructed wetlands. Wetlands constructed with sorptive filter media can provide performances comparable to EBPR systems, with the removal of multiple contaminants by a combination of precipitation, microbial activity and plant uptake. However, in spite of the potential that filter media represent for effective P removal, there are some substantial limitation to the technology. The influence of pH is considered the primary concern, because its correction is related to high associated costs.

The potential for the removal of a wide range of contaminants from dilute wastewater effluents by sorption techniques has been extensively demonstrated. The scientific community as well as the manufacturing industry are focusing on developing new engineered materials and on testing directly affordable natural and waste materials to overcome the problems connected with the applicability of this technology. Indeed, the use of easily obtainable or synthesisable materials as well as waste material may reduce the need for more expensive chemical additives or modifications to existing WWTP infrastructures. As well as encouraging the precipitation of P by seeding, sorbent-based processes can include other coexisting mechanisms such as ion exchange, ligand exchange and electrostatic interactions to directly sorb P from the waste stream. Such process can potentially fit into existing WWTP infrastructures and provide enhanced P removal and recovery. Till today, however, sorbents have not been widely employed in WWTPs as stand-alone P recovery processes. Similarly, the potential of recovered sorbed-P fertiliser or soil amendment has not been widely considered or assessed. Much investigation is needed to clearly assess the potential of different combinations of biological, chemical or physical treatment with sorption process and the synergy than can be obtained by the several possible options. Regarding the wide variety of materials evaluated for the sorption of P, an extensive review of agricultural by-products and wastes for sorptive recently concluded that organic materials require some form of pre-treatment before use, due to the lack of anion binding sites (Nguyen et al., 2013).

Using sorbent materials for the removal and recovery of P for subsequent direct use as a fertilizer or soil amendment is attractive, provided that the sorbent material is economic and has adequate P affinity without retention of contaminants. If modifications are required to provide these, the cost and complexity of additional processing have to be considered. Rather few materials shown to be effective as sorbents for P are also suitable for direct application to agricultural land. Differently, in the case of engineered materials with relatively high costs, the durability and reusability of the media must be fully assessed and demonstrated through long-term investigation at pilot scale. In this case, studies must assure that the media can be easily regenerated with the minimal amount of chemicals, and that its performances can be maintained stable through several adsorption-desorption cycles. During desorption the P removed by the media is eluted and concentrated in a liquid stream that can be treated in a second time to recover products comparable to fertilizers. Other issues regarding the sorption process focus on the co-sorption of toxic compounds containing heavy metal/metalloids together with the sorption of P: selective recovery of P from wastewaters should be a key goal of any recovery process.

Sorption processes based on ion exchange technologies maybe particular suitable for use at decentralized locations (Zhao and SenGupta, 1998). It is important to take in consideration that ion exchange technologies are well established and used in many contexts, including desalination and deionization of water, making the technologies and components already widespread. Ion exchange systems have been developed with to last several operating cycles and are characterized by the advantage of delivering P recovery through post-treatment of the sorption media (Martin et al., 2009). Whilst high P removal rates have been achieved at laboratory scale, implementation at the full-scale has been limited due to the requirement for expensive chemical addition for the recovery of P and the sensitivity of some media to pH conditions (Zhao and SenGupta, 1998). Much work is required for this technology to be proved at full-scale, especially under variable flow regimes. Furthermore, chemical requirements and cost may make this technology unfeasible for use for small-scale and-or rural treatment works because chemical reinstatement is probably impractical in such scenarios. Physico-chemical processes offer the confidence of reliable P removal and simplicity of operation, however, the long-term sustainability of current technologies has not been well demonstrated, especially related to the operation and maintenance of small-scale systems. This means they may not be viable for small-scale WWTPs unless they are coupled with other processes. As a matter of facts, physico-chemical P removal systems can generally be considered effluent “polishing” treatment solutions, offering little or no additional contaminant removal but allowing the recovery of phosphate from aqueous solutions with the double effect of ensuring the outlet concentrations below the legal threshold and allowing an environmentally sustainable recovery of P that otherwise would be lost. Moreover is a technology easy to implement and conduct (hence it does not require high instructed operators), affordable, flexible, cost efficiency and selective for trace elements.

2.2.3 Hybrid material containing metal oxides/hydroxides for P recovery

As discussed above adsorption process is considered to be one of the most promising technique for the recovery of phosphorus from industrial and municipal wastewater containing trace content of phosphate ions. To date there have been a tremendous numbers of materials that have been developed for the efficient and economical removal of phosphate, included engineered man-made materials and modified natural or waste materials. However between all those attempts the category of hybrid material where metal (hydr)oxide are dispersed into a supporting material have been gaining more and more attention for their unique characteristics.

Oxides and hydroxides of metals such as La, Zr, Fe, Al, Mn, Ti, Nb and Ce have been applied to remove phosphate from aqueous system due to strong specific affinity between phosphorus-based ions and metal sites. The dominant mechanism of phosphate anions adsorption by metal (hydr)oxides is accepted as ligand exchange (Xu et al., 2017; Li et al., 2014). However, in addition to adsorption, surface precipitation reactions may be also involved, leading to the formation of a new mineral phase, multilayer adsorption of phosphate and charge compensating cations, or formation of a solid solution. The capacity of ligand exchange depends on the specific surface properties of sorbents, especially the surface charge. Indeed, oxide and hydroxide minerals are amphoteric and exhibit a pH-dependent charge: it is below the point of zero net proton charge (pH_{pzc}) that the surface of the matel (hydr)oxide is positively charged and, hence, able to adsorb anions. The pH_{pzc} for oxide and oxyhydroxide minerals varies somewhat based on the degree of mineral crystallinity, and mineral purity. For example it generally ranges between 7 and 9 for Fe oxides, and between 8 and 10 for Al oxides. If in waters the materials exhibit negative surface charge, it is unfavourable to capture anionic pollutants because of electrostatic repulsion. For example, the pH_{pzc} of manganese oxides and hydrated manganese oxides are generally in the range of 2–3 and 4–6, respectively, rendering manganese oxides inefficient sorbents to attract phosphate ions in near neutral pH environment (Pan et al., 2014). In order to improve the adsorbing capacity of metal oxide, different metals have been composited to compensate for the deficiencies of a single metal.

2.2.4 The hybrid ion exchange resin HAIX: a ferric nanoparticle adsorbent

To encapsulate the metal oxide nanoparticles in host material is necessary from the point of view of application: ferric oxides lack the mechanical strength and attrition resistance properties needed for prolonged operation in fixed-bed units; consequently, the fines formed lead to increased head loss in the system (Blaney et al, 2007). Doping particulate ferric oxides within traditional adsorbents of larger particle size combines the excellent handling, flow and mechanical characteristics of adsorbent supports with the specific affinity of ferric oxides toward the targeted anion pollutant. Moreover, the functionality of the host material may play an important role in the overall sorption behaviour of the resin (Blaney et al, 2007; Pan et al., 2009). Recently, Sengupta and his group have focused on the surface chemistry of the support materials on performance of the resulting hybrid adsorbents and have implemented the Donnan membrane principle to fabricate a novel hybrid adsorbent HAIX by doping hydrated ferric oxides (HFO) within a polymeric anion exchanger by a propriety technique (Cumbal and SenGupta, 2005; Blaney et al, 2007). This new hybrid ion exchanger comprises a strong base macroporous anion exchange resin as the “parent media” which acts as a scaffold to support a dispersion of ferric oxide nanoparticles (Cumbal et al., 2003). Among the variety of hydrated metal oxides, hydrated ferric oxide (HFO) was selected and implemented as it is readily available, innocuous, inexpensive, chemical stable over a wide pH range, and provides a sizes of freshly precipitated amorphous HFO particles between 10 and 100nm (DeMarco et al., 2003). This allows to the internal pores’ surface to be impregnated but not coated with the HFO nanoparticles, optimizing the pores’ volume and the uptake. This new type of adsorbent became rapidly a very suitable alternative to other traditional media, because they combine high mechanical and hydraulic properties with the selectivity of hydrated metal oxides toward oxyanions like phosphate. Originally, Zhao and SenGupta (1998) demonstrated the higher performance of macroporous granular polymeric anionic exchangers (e.g. Purolite IRA410) over cationic exchangers (e.g. Purolite C-145; C-100) as supports for HFO nanoparticles in As(V) removal (De Marco et al., 2003; Greenleaf et al., 2003). Moreover, minimal backwash requirements and low HFO fines formation were demonstrated; in addition, the hybrid sorbent is regeneratable in comparison with standard granular iron oxide. Since its potential viability was demostrated, different materials using ion exchange resins have been commercialised by ion-exchange producers, as in the case of HAIX sorbent (previously branded as ArsenX^{np} or PhosX^{np} and, later, as LayneRT^{TM}) by SolmeteX Co., Massachusetts; or in the case of Lanxess with the FO36 hybrid sorbent for the removal of As(V) from drinking water. Lewait FO36 can also be used for removal of HPO_4^{2-} due to its high selectivity for sorption of oxyanions by the Donnan membrane effect. In the case of HAIX LayneRT the parent media is a strong base anion exchanger with a quaternary ammonium as a functional group, meanwhile, the commercially available resin Lewait FO36 is based on a macroporous weakly basic anion exchange resin containing tertiary amine functional groups ($P\text{-}CH_2\text{-}N(CH_3)_2$). It is evident that in the case of HAIX LayneRT the quaternary ammonium group is positively charged independently from the pH, on the contrary, the tertiary amine group is able to contribute to the total anion uptake only when protonated ($pH < pKa$).

2.2.4.1 Synthesis

Fe^{3+}, the precursor of HFO, cannot be directly exchanged onto an anion exchanger due to the electrostatic repulsion. Till now there are two patented techniques developed by Sengupta and Cumbal (2005) and Pan et al. (2007), to fabricate HFO-loaded anion exchanger for arsenic removal from waters. The basic preparation procedure proposed by Sengupta and his co-workers involved a first ion exchange of anionic oxidants onto the anion exchanger (to load the anion exchanger with oxidant anions like ClO^- or MnO_4^-), a subsequent rinsing or soaping of the exchanger with a Fe(II) solution to result in an in situ precipitation of iron hydroxide particles (HFO particles), and, finally, a thermally treatment of the resulting composites. As for the technique invented by Pan et al. (2007), $FeCl_4^-$ was used as the precursor of HFO and HFO nanoparticles were immobilized within D-201, a polymeric anion exchanger, by rinsing the $FeCl_4^-$ loaded D-201 beads with NaOH–NaCl binary solution and subsequent thermal treatment.

2.2.4.2 The Donnan membrane effect

The Donnan membrane principle is essentially a specific domain of the second law of thermodynamics dealing solely with completely ionized electrolytes. The conditions leading to the Donnan membrane equilibrium arise from the inability of certain ions to diffuse out from one phase (or region) to the other in systems involving water or polar solvents. In accordance with the Donnan membrane principle, non-diffusible fixed charges in one phase in contact with water can be utilized to modulate the distribution of ions in both phases leading to efficient separation, product recovery or other applications. Scientifically, the Donnan membrane effect, or Donnan potential, is distinctly different from the effect of surface charges often present at the solid/liquid surface (Helfferich, 1962; Donnan, 1995; Sarkar et al., 2010a). It is called Donnan membrane principle because it works as a physical semipermeable membrane which restricts the movement of one particular type of ion across the phase boundary in an effort to conserve the electroneutrality. Indeed, the creation of a virtual membrane and the following semipermeability phenomenon is due to the immobility of ions (cation or anion) to diffuse out from one phase to the other. Thus, an anion exchange resin with covalently attached fixed positive charged (R^+) or a cation exchange resin with attached fixed negative charges (R^-) exhibit semipermeable behaviours towards the corresponding counter-ions which concentrate inside the exchanger phase, while groups of ions with charge similar to the functional groups (co-ions) are excluded from entering in it.

This phenomenon offers a unique opportunity to enhance the sorption properties of metal oxide nanoparticles through the wise selection of the functional groups associated with the polymeric host. In this way, due to the anionic nature of phosphate, a positively charged exchanger support is expected to result in permeation enhancement and pre-enrichment of phosphate anions within the polymeric phase and, therefore to a concentration of anions inside the anion exchanger much higher compared to that in the bulk. Hence, the iron oxide nanoparticles dispersed within the bead get exposed to much higher concentrations of anions and, being selective for ligands such as phosphate anions, ends up adsorbing more phosphate than iron oxide nanoparticles alone. Such phenomena has been proved to be greatly favourable for efficient removal of trace phosphate: Blaney et al. (2007), reported that phosphate can be efficiently removed from 200 to 260 μg/L to less than 50 μg/L. Moreover, the data reported by Sarkar et al. (2010b) from a field trial at Sahuarita, Arizona supports this fact too. There, granular ferric oxide (GFO), an iron-oxide based adsorbent, was outperformed by a hybrid anion exchanger dispersed with Fe nanoparticles (Layne^{RT}), confirming that the anion exchanger support played a critical role in enhancing the activity of the HFO nanoparticles.

Figure 2.2.2 Schematic description of Donnan membrane principle explaining the enhanced capacity of the hybrid anion exchangers.

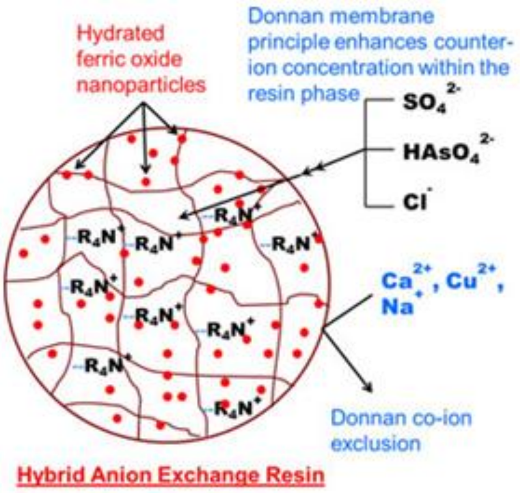

2.2.4.3 Effect of pH

pH has a fundamental role in adsorption processes, as it determines the neutral/ionic form of both the dissolved species and the resin's surface functional groups. At pH values typical of secondary wastewater effluent, in the vicinity of 7.0, the phosphate in the wastewater streams exists primarily as its divalent anion HPO_4^{2-} and its intermediate, the monovalent $H_2PO_4^-$ (Fig. 2.2.3a). Meanwhile, the surface of hydrated ferric oxide (HFO) particles is covered with hydroxyl groups (represented as ≅Fe-OH), where the Fe atom acts as a Lewis acid exchanging its structural OH with other ligands. Its acid-base properties are described by the equations below:

$$\cong Fe\text{-}OH_2^+ \leftrightarrow \cong Fe\text{-}OH + H^+ \quad \text{Log}K^S_{a1} = -7.3 \pm 0.8$$

$$\cong Fe\text{-}OH \leftrightarrow \cong Fe\text{-}O^- + H^+ \quad \text{Log}K^S_{a2} = -8.9 \pm 0.4$$

where K^S_{a1} and K^S_{a2} are the intrinsic acidity constants of the HFO groups (Stumm and Morgan, 1995; Dzombak and Morel, 1990). This means that at $pH < pK_{a1}$, where $pK_{a1}=7.3$, the hydroxyl group tends to be protonated and, hence, positively charged. Otherwise, at pH ranging between $pK_{a1}=7.3$ and $pK_{a2}=8.9$, the hydroxyl groups are present in their neutral form ≅Fe-OH; whilst at pH higher than $pK_{a2}=8.9$ hydrated ferric oxides release hydrogens and exhibit a negatively-charged surface, inverting the Donnan membrane effect and rejecting phosphate anions. In addition to the target compound's and HFO groups' ion form, generally pH determines the neutral/ionic form of the polymeric ion-exchanger support's functional groups. However, in the specific case of HAIX Layne^{RT}, the quaternary ammonium functional group is a strong base anion exchanger which exhibits a positively charge independently from the solution pH. On the contrary, in the case of weakly basic anion exchange resin containing secondary or tertiary amine groups, amines will participate in the extraction of phosphate only when protonated ($pH<pK_a$). Since for this new type of hybrid adsorbents, mechanisms of adsorption are multiple and exerted by different components (i.e. the ion exchange parent media, the HFO nanoparticles), the optimal pH must be found out by means of experimental trials. Blaney et al. (2007), quantified the influence of pH on phosphate sorption onto HAIX ArsenX^{np} (a precursor of HAIX Layne^{RT}, a resin with basically the same salient characteristics) by means of mini-column tests at varying pH: the experimental results showed that the maximum phosphate sorption occurs in the range of 6.0-8.0. Consistently, Pan et al. (2009a) tested an hybrid ion exchange resin with physical and chemical characteristics very similar to HAIX Layne^{RT} (with HFO and $R-N^+(CH_3)_3$ as active sites) and observed that the optimal pH values for phosphate removal ranged from 6.5 to 8.0 (Fig. 2.2.3 b)). The pH range between 6.0/6.5 and 8.0 determines the predominant mono- and bi-dentate forms of phosphate and, meantime, the coexistence of the neutral and the protonated form of the ferric hydroxyl groups. Moreover, the quaternary ammonium functional groups contributed to the phosphate sorption due to its irreversible positively charge nitrogen atoms. Decreasing the solution pH values, inevitably results in phosphate less negatively charged, i.e. formation of more H_3PO_4 or $H_2PO_4^-$. Consequently, an unfavourable adsorption occurs. On the other hand at high alkaline pH, HFO is deprotonated and negatively charged, so are the phosphate species. Therefore, Donnan co-ion exclusion or electrostatic repulsive forces are operative, which is favourable for desorption of the loaded phosphate (Cumbal and SenGupta, 2005).

Concluding, from an application point of view, pH-dependent adsorption and necessity of pH adjustment, represent a primary concern due to the fact that pH-correction is generally related to high associated costs that hinder the economic viability of the process. Especially for those processes investigating the recovery of a trace element characterized by concentrations considerably diluted. Since the pH of the secondary wastewater after biological treatment is usually around 7.00, and phosphate removal by HAIX has is optimum around that value (Pan et al., 2008), any pH adjustment is required.

Figure 2.2.3 **a)** effect of solution pH on the Distribution of phosphate species; **b)** Effect of solution pH on the phosphate adsorption by HFO-201 (Pan et al 2009a).

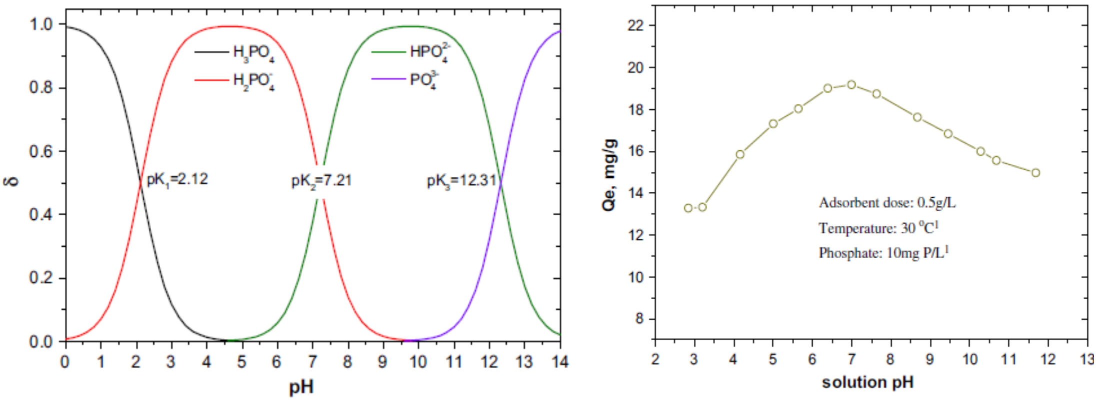

2.2.4.4 Effect of temperature

In a practical viewpoint, the effect of temperature on phosphate removal is of crucial significance since it represents one of the main drawbacks of the traditional tertiary treatments such as biological removal, which is extremely sensitive to temperature and its efficiency is considerably depressed under a low ambient temperature such as 15°C (Converti et al., 1995). Ambient temperature is usually a crucial factor concerning an adsorption process, too. Blaney et al. (2007) performed isotherms at three different temperature, namely, 7, 23 and 37 °C, under identical experimental conditions. Their results showed that the phosphate uptake is not influenced by the temperature change normally encountered due to the seasonal changes. Moreover, Pan et al. (2009a) achieved an analogous conclusion during the investigation of a resin very similar to HAIX Layne^{RT} (composed of R-N$^+$(CH$_3$)$_3$ and HFO). They found out that the dependence on the temperature was directly connected to the presence or the absence of other anions, i.e. they investigated sulphate. They found out that in the absence of sulphate, the phosphate adsorption capacities of the media (Q$_e$ – expressed as mg$_{PO4\text{-}P}$/g$_{resin}$) increased with an increase in temperature: Q$_e$ at 45°C > Q$_e$ at 30°C > Q$_e$ at 15°C. On the contrary, in the presence of sulphate, phosphate adsorption seems to be independent upon the ambient temperature. These outcomes may be explained by taking into account the different mechanisms involved in the presence or absence of sulphate. As it will be explained deeper in the next sub-chapter, the phosphate adsorption by this type of hybrid resin can be exerted by both the exchanger parent media and the HFO nanoparticles, with two different mechanisms involved: simple anion exchange processes and inner-sphere complexes formation, respectively. Because ion exchange process, driven by electrostatic or Coulombic interaction, is an endothermic process (Prevette et al., 2007), higher temperatures results in more favourable phosphate retention. Whereas, the formation of inner-sphere complexes was found to be less dependent on temperature than IEX process or outer-sphere complexes (Sabbatini et al., 1998; Manjari and Kim, 2006). In the absence of sulphate, the temperature-dependence of P-uptake may be attributed to the simultaneous activity of the two adsorption mechanisms, and supposed to be due mainly to the IEX process. Meanwhile, when the concentrations of sulphate reach high level, as in the case of actual secondary effluent municipal wastewater, most of the effective P-uptake relies on the loaded HFO nanoparticles. Thus, it is less dependent upon the temperatures.

2.2.4.5 Sorption mechanisms and effect of competing ions

The affinity of an exchange material for a particular ion is proportional to the valence and weight of the ion. Even though phosphate species have relatively high valence and weight, the phosphate concentration in wastewater is low in comparison to other anions: indeed, in typical secondary wastewater effluent phosphate concentration is about one or two orders of size smaller than sulphate, chloride, nitrate and bicarbonate concentrations. This is the reason why in conventional ion exchange processes the removal of phosphate is not efficient and does not represent a feasible treatment. The lack of selectivity towards phosphate results in quickly depletion of the all exchange sites that are occupied by competing anions. Therefore, not only resin's regeneration becomes a frequent application, but, also the P-concentrated stream obtained from the desorption has a very low grade of purity – in terms of P-content versus competing anions content. The lack of selectivity and the high operating cost of chemicals for the regenerations were sited as major shortcoming affecting the overall viability of the fixed process (Zhao and SenGupta, 1998).

According to previous works, in hybrid exchange resins as HAIX Layne^{RT}, the selectivity towards phosphate is almost completely exerted by the HFO nanoparticles, whilst the strong or weak base anion exchanger (whose main function is to supply a scaffold for the HFO nanoparticles) enhanced the P-uptake thanks to the Donnan membrane effect and does not contribute to the P-sorption. Indeed, Martin et al. (2017) conducted some experiments on HAIX Layne^{RT} to separate out the P-uptake functional components of the hybrid resin and quantifying their individual contribution to performance. Their results showed that the ferric component within the hybrid anion exchange material is responsible for removing 90% of the total phosphorus attributed to the media as a whole. Consequently, they came to the conclusion that the media can be considered a mono-component system in the main, since in the presence of counter ions they outcompete phosphate from the IEX sites. Hence, phosphate is adsorbed only onto the ferric nanoparticles. Consistent outcomes were found by SenGupta and Pandit (2011) who concluded that, at low background concentration of sulphate, P-removal by HAIX is attributed to both Coulombic interaction (CI) and Lewis acid-base (LAB) interaction, which are the two possible exchange mechanisms. While at high background concentration of sulphate (>100mg/L) P-removal is entirely attributable to LAB interaction between HPO_4^{2-}/H_2PO^- and $FeOH_2^+$. Indeed, in the case of a strong-base anion exchange resin (exactly the parent resin of HAIX Layne^{RT}) the following affinity sequence is generally obtained and has been demonstrated in previous works (Zhao and SenGupta, 1996; Blaney et al., 2007): $SO_4^{2-} > PO_4^{3-} > NO_3^- > Br^- > NO_2^- > Cl^-$. Anyway, despite the negligible direct contribution to the total P uptake, the IEX parent media creates the favourable Donnan membrane effect and provides the physical advantages to the media (i.e. high mechanical strength and hydraulic properties) necessary to develop an adsorptive process.

Figure 2.2.4 Schematic illustration of a new classification system for metal (bio)sorption mechanisms (Tan et al., 2017).

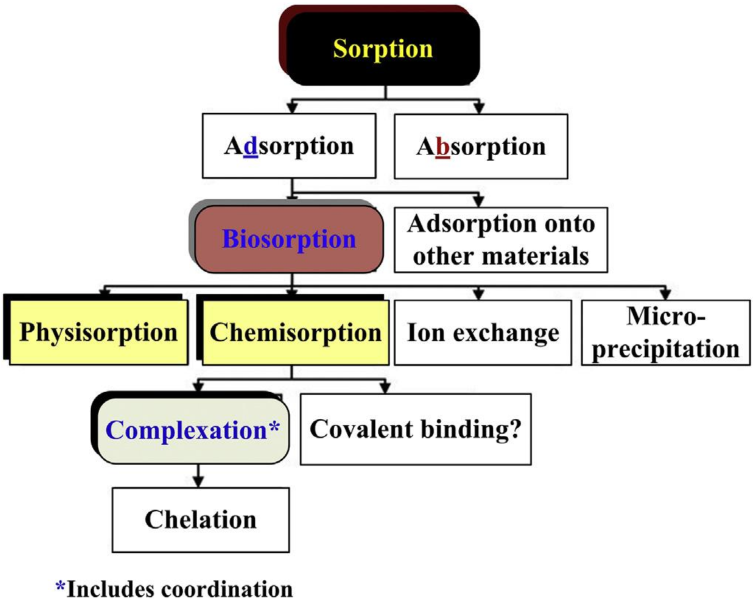

In contrast to simple ion exchanger, HFO nanoparticles are able to provide an outstanding selectivity towards the anionic P(V) species. The adsorption mechanism between the iron atom and phosphate ion is classified as a specific chemisorption called complexation. Phosphate is the molecule used as ligand, namely a molecule capable of functioning as the electron-pair donor in the electron-pair bond (a coordinate covalent bond) formed with the metal atom (in our case, iron(III)). Attachment of the ligands to the metal atom may be through only one atom, or it may be through several atoms. When only one atom is involved, the ligand is said to be monodentate; when two are involved, it is di- or bi-dentate, and so on. Coordination compounds containing polydentate ligands are called chelates and their formation is termed chelation. The simplest types of coordination compounds are those containing a single metal atom or ion (mononuclear compounds) surrounded by monodentate ligands. Coordination of such ligands to the metal virtually always occurs through an atom possessing an unshared pair of electrons, which it donates to the metal to form a coordinate bond with the latter. Whilst metal-ligand attachment in chelate complexes is through several bonds. Fig. 2.2.5 shows a schematic illustration of outer- and inner-sphere complexes involving the As(V) oxyanions $H_2AsO_4^-$ or $HAsO_4^{2-}$ (very similar to the P(V) oxyanions) and metal (hydr)oxides (for example Fe(III) hydroxide); where c) and d) involve a chelation complexation. Note that outer-sphere complexes are rather less stable than inner-sphere complexes. Indeed, outer-sphere surface complexation is a nonspecific adsorption, which involves the electrostatic attraction (Coulombic interactions) between a charged surface and an oppositely charged ion. The adsorbed ion resides at a certain distance from the mineral surface. While, specific adsorption, also called inner-sphere complexation, connects with the formation of a coordinative complex with the mineral surface through Lewis acid-base interactions. The tendency for complexes to form between a metal ion and a particular combination of ligands and the properties of the resulting complexes depend on a variety of properties of both the metal ion and the ligands. Among the pertinent properties of the metal ion are its size, charge, and electron configuration (arrangement of electrons in energy levels around an atomic nucleus). Relevant properties of the ligand include its size and charge, the number and kinds of atoms available for coordination, the sizes of the resulting chelate rings formed (if any), and a variety of other geometric (steric) and electronic factors.

For further information in Fig. 2.2.6 are shown all the possible molecular configurations of protonated P inner-sphere complexes at the FH–water interface identified and proposed by Arai and Sparks (2001) and below discussed by other authors.

Figure 2.2.5 Schematic representation of structures of arsenate molecules adsorbed on metal (oxyhydr)oxides surface: (a) outer-sphere surface complexation; (b) mononuclear monodentate inner-sphere complexation; (c) mononuclear bidentate inner-sphere complexation and (d) binuclear bidentate inner-sphere complexation (Cheng et al., 2009).

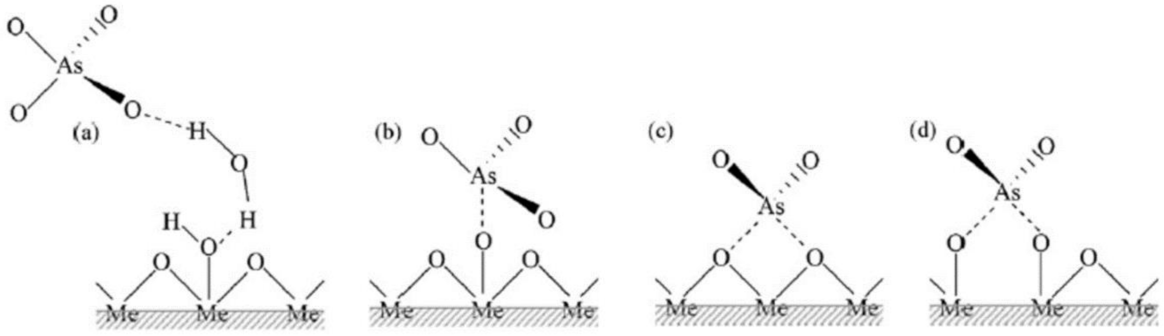

Figure 2.2.6 Possible molecular configurations of protonated P inner-sphere complexes at the FH–water interface: (a) monoprotonated bidentate mononuclear; (b) diprotonated bidentate mononuclear; (c) monoprotonated monodentate mononuclear; (d) diprotonated monodentate mononuclear; (e) nonprotonated monodentate mononuclear with hydrogen bonded with the hydroxyl group of the FH; (f) monoprotonated monodentate mononuclear with hydrogen bonded with the hydroxyl group of the FH; and (g) diprotonated monodentate mononuclear with hydrogen bonded with the hydroxyl group of the FH. (Arai & Sparks, 2001).

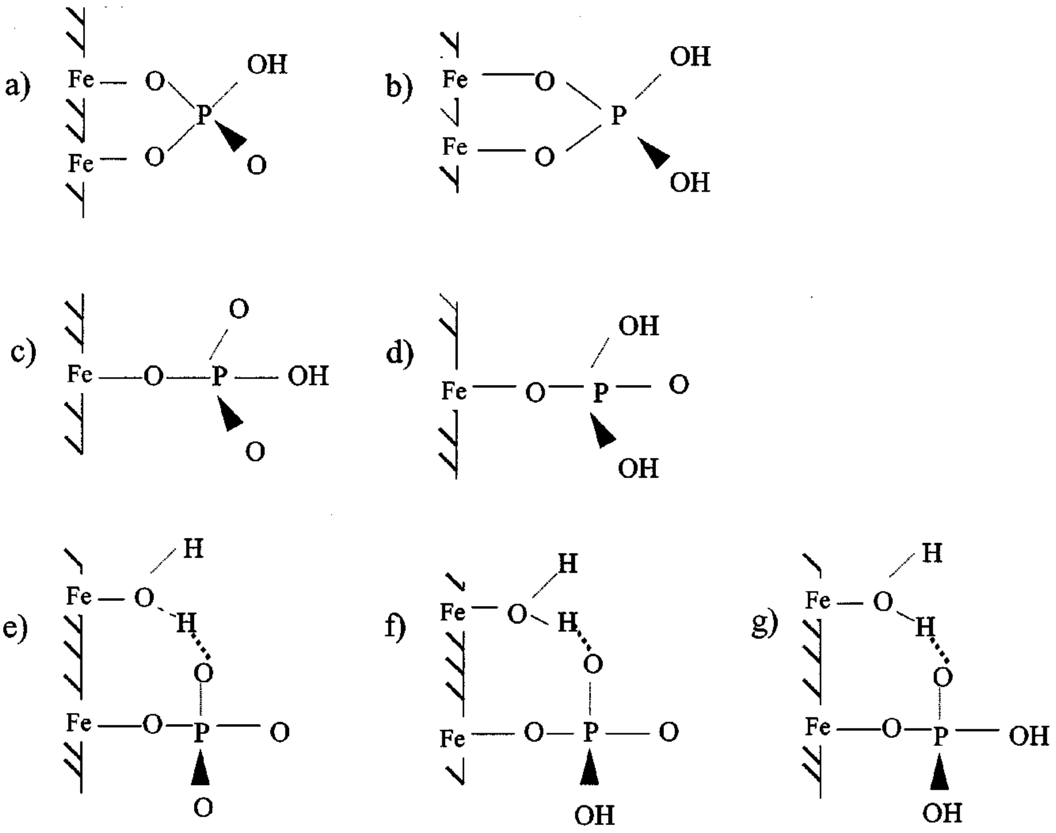

Hence, surface complexation of phosphate occurs via ligand exchange reactions in which surface hydroxyl groups (of the $\cong$Fe-OH groups of supported HFO particles) are replaced by the adsorptive phosphate ions. That of substitution is one of the most general reactions exhibited by coordination sorption, it consists in the substitution/replacement of one ligand by another: in our case OH- is outcompeted by a P(V) oxyanion. In this way, the Fe atom acts as a Lewis acid, providing coordination and exchanging its structural OH with the phosphate ligand (Lewis base). Its acid-base properties have been described in the previous chapter concerning the influence of pH. According to the intrinsic acidity constants of P(V) oxyanions and considering the expected pH values of typical municipal wastewater (pH range between 6 and 9), the dominant (>90% molar fraction) P(V) species is $H_2PO_4^-$ for pH minor than 6.2 and HPO_4^{2-} for pH>8.2 (Fig. 2.2.3 a).

To the best of the authors' knowledge a clear and defined explanation of the coordination complexes and the background conditions leading to specific bounds between phosphate anions and ferric (hydr)oxides was not found. However some conclusions common to most of the authors who have worked on this topic, are reported.

For example, according to You et al. (2015) the formation of mononuclear species could be postulated by equations:

$\cong Fe\text{-}OH_2^+ + H_2PO_4^- \leftrightarrow \cong Fe\text{-}H_2PO_4 + H_2O$ LogK $_{\cong Fe\text{-}H2PO4}$ = 43.5 ± 0.4 (Eq. S1)

$\cong Fe\text{-}OH_2^+ + HPO_4^{-2} \leftrightarrow \cong Fe\text{-}HPO_4^- + H_2O$ LogK $_{\cong Fe\text{-}HPO4^-}$ = 37.6 ± 0.2 (Eq. S2)

$\cong Fe\text{-}OH + HPO_4^{-2} \leftrightarrow \cong Fe\text{-}PO_4^{-2} + H_2O$ LogK $_{\cong Fe\text{-}PO4^{-2}}$ = 29.9 ± 0.3 (Eq. S3)

They suggested that (with excess $\cong$Fe-OH, as in the typical extraction conditions) at pH values below 6 the favoured species is $\cong Fe\text{-}H_2PO_4$ (Eq. S1). The increase of pH from 6 to 7 favours the formation of $\cong Fe\text{-}HPO_4^-$ (Eq. S2), whereas at basic pH values (between 9 and 11) the dominant complex is $\cong Fe\text{-}HPO_4$ (Eq. S3). Furthermore, the increase of the pH solution above 11 is traduced on the phosphate desorption as $\cong$Fe-OH is converted to $\cong Fe\text{-}O^-$. Increased pH affects P(V) extraction process by reducing the concentration of HPO_4^{2-} anions (Fig. 2.2.3a), which is also accompanied by an increase of the OH^- ion concentration. Thus, at pH values higher than 11 competition between HPO_4^{2-}/PO_4^{3-} and OH^- on the more negatively charged sorbent surface is enhanced, diminishing the sorption of phosphate anions. Increase the pH above 11 implies the conversion of HPO_4^{2-} to PO_4^{3-}, and then the formation of the $\cong Fe\text{-}HPO_4$ complex is not favoured. Analogous results were proposed by

Persson et al. (1996) after having studied the surface specification of orthophosphate ions on goethite as a function of pH, time, total phosphate concentration and ionic medium by means of diffuse reflectance FTIR spectroscopy. They found out that the surface specification is essentially a function of pH, and distinguished three different surface complexes with their respective symmetries. The IR data resulted in good agreement with a monodentate mononuclear coordination of phosphate to the surfaces, where the only difference between the three identified surface complexes was the degree of protonation (diprotonated, mono-protonated and non-protonated at low, intermediate and high pH values, respectively). However they also concluded that the molecular symmetries they had identified were incompatible with the bidentate, bridging structural model suggested by other authors (note that in a bridging surface complex/bidentate complex two oxygens of a phosphate ion completes the coordinate sphere of two different $\cong$Fe-OH_2 groups).

Elzinga and Sparks (2007) found that phosphate is adsorbed as different inner-sphere complexes whose nature depends on pH and initial phosphate concentration. They suggested that at pH between 3.5 and 7 two monoprotonated complexes predominate, lower pH values favour a monodentate binuclear (i.e. bridging) complex, while at pH closer to 7 a monodentate mononuclear (i.e. edge sharing) complex is favoured. At pH between 8.5 and 9 a non-protonated monodentate mononuclear complex is observed.

Lastly, differently from other authors, always You et al. (2015) reported the high affinity of P(V) for forming binuclear complexes involving two adjacent $\cong$Fe-OH groups, that can be described by the following equations:

$$2(\cong\text{Fe-OH}) + H_2PO_4^{-} \leftrightarrow \cong\text{Fe}_2\text{-HPO}_4^{-} + 2H_2O + H^{+} \quad \text{(Eq. S4)}$$

$$2(\cong\text{Fe-OH}) + HPO_4^{-} \leftrightarrow \cong\text{Fe}_2\text{-PO}_4^{-2} + H_2O + OH^{-} \quad \text{(Eq. S5)}$$

The selectivity towards phosphate of the hybrid ion exchange resin HAIX, as well as of HFO nanoparticles alone, has been largely studied. Blaney et al. (2007) demonstrated its effectiveness in removing trace phosphate levels from wastewater (0.26 mg/L), even with high concentration of competing anions (i.e. sulphate concentration of 120 and 240 mg/L). They concluded that doubling the sulphate content had practically no effect on phosphate sorption capacity of HAIX. That was the previous work suggesting that the binding mechanism of phosphate into HAIX sorption sites was different from that of sulphate. They attributed to the phosphate/sulphate separation factor ($\alpha_{P/S}$) a value of 46, where $\alpha_{P/S}$ can be expressed as below:

$$\alpha_{P/S} = \frac{\left({}^{q_P}/_{C_P} \right)}{\left({}^{q_S}/_{C_S} \right)}$$

where q and C represent the concentrations (molar or equivalent) in the polymer phase and the aqueous phase, while subscripts P and S denote phosphate and sulphate respectively. Many attention has been driven to evaluate phosphate/sulphate competition, since, of all the commonly present competing anions, sulphate is divalent and excepted to offer greater competition through enhanced electrostatic interaction. Figure 2.2.7 shows the results obtained by Pan et al. (2009) respectively with HFO-201, D-201 and ArsenX^{np} (a precursor of HAIX Layne^{RT}). Their results show that for the two ferric nanoparticles doped media, initial addition of sulphate from 0 to 100 mg/L in the phosphate-containing solution results in a great drop of P-adsorption, however, further increase in the sulphate concentration from 100 to 1500 mg/L does not pose any negative effect on P-retention. On the contrary, for the strong base anion exchanger D-201 the presence of sulphate translates itself into an immediately release of phosphate by the resin, even at very low sulphate concentrations. These results are consistent with what explained above and confirm that the selectivity towards phosphate is given exclusively by the HFO nanoparticles.

Figure 2.2.7 **a)** General characteristics of the adsorbents used in the study (Pan et al. 2009); **b)** effect of the added sulphate on the phosphate removal by HFO-201, D-201, and ArsenX^{np} (Pan et al. 2009)

a)

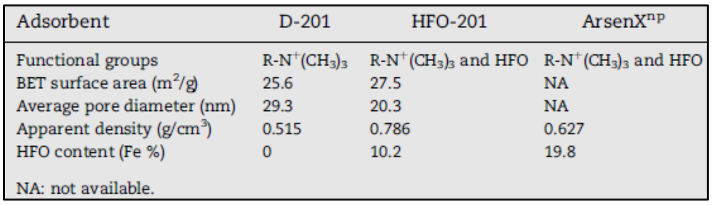

Adsorbent	D-201	HFO-201	ArsenX^{np}
Functional groups	R-N$^+$(CH$_3$)$_3$	R-N$^+$(CH$_3$)$_3$ and HFO	R-N$^+$(CH$_3$)$_3$ and HFO
BET surface area (m^2/g)	25.6	27.5	NA
Average pore diameter (nm)	29.3	20.3	NA
Apparent density (g/cm^3)	0.515	0.786	0.627
HFO content (Fe %)	0	10.2	19.8

NA: not available.

b)

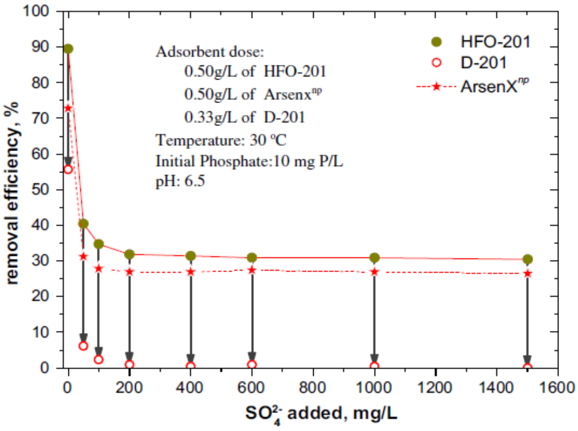

SenGupta and Pandit (2011) proposed consistent results for HAIX Layne^{RT} after having conducted several breakthrough continuous-flow trials at different background sulphate concentrations, equal to 5, 160 and 246 mg/L, and corresponding to the following [Phosphate(mg$_P$/L):Sulphate(mg/L)] ratios of 1:5, 1:40 and 1:60, respectively. They obtained almost superimposable breakthrough curves for the two highest background concentrations of sulphate, demonstrating that at high SO_4^{2-} content the ion exchange sites get exhausted rapidly with SO_4^{2-} and its breakthrough occurs almost instantaneously. This is consistent with the fact that SO_4^{2-} removal by HAIX is purely due to CI and that LAB interaction has no role to play. At those P: SO_4^{2-} ratios (1:40 and 1:60) P is present as a trace species and does not pose any competition to the anion exchange sites of the quaternary ammonium functional groups. Instead, P gets exchanged due to LAB interactions with HFO nanoparticles till exhaustion of their capacities. Moreover, extremely relevant is that any chromatographic P-elution was detected during the breakthrough curves, meaning that sulphate could not overcomes and replaces once it has been adsorbed. A noteworthy aspect is that the typical SO_4^{2-} and P concentrations in the secondary effluent of a municipal wastewater treatment plant are in this range, and, therefore, can be concluded that little or no competition is expected from the further increase in concentration of SO_4^{2-}. However, at much lower SO_4^{2-} concentration, P: SO_4^{2-} = 1:5, the breakthrough bed volumes for P almost doubled, even though there was a chromatographic elution of P. The increase in capacity of HAIX with the resulting increasing of the number of treatable bed volumes are simply due to the fact that at these P and concentrations P can compete for the CI interaction mechanism too. Consistently, the final chromatographic elution of P is caused by the replacement of SO_4^{2-} since is more preferred by the CI exchange with the quaternary ammonium functional groups.

De Kock (2015), reported a phosphate capacity for HAIX exhausted with a solution containing only phosphate (750 mg/L) of 36.1 mg/g, while for HAIX exhausted with wastewater (PO_4^{3-} 14.55 mg/L had a phosphate capacity of 13.57 mg/g. Consistently, You et al. (2016) evaluated that the presence of competing anions causes a reduction of the P(V) capacity from 12 to 10 mg$_{PO4\text{-}P}$/g.

In addition to inorganics anions, organic compounds need some considerations too. The adsorption of natural organic matter (NOM) has been reported for both ferric oxides (Genz et al., 2008; Gu et al., 2001; Hiemstra et al., 2010) and anion exchange resins (Bolto et al., 2004; Tan and Kilduff, 2007). Weng (2008) reported the interaction between humic, fulvic acid and phosphate on the surface of ferric oxide. Shaung (2013) has reported the adsorption of humic acid by hybrid ion exchange resins synthesized by mixing ferric oxide with monomer followed by suspension polymerization. From this point of view, it is important to determine the relative roles of the ferric oxide and the resin matrix in the adsorption of NOM because the two exchange sites can be selectively desorbed (Lin and SenGupta, 2009) resulting in more pure effluent that can be converted to a slow release fertilizer in the form of struvite (SenGupta and Pandit, 2009). Contamination of the regenerant stream with organic matter will be detrimental to the recovery of phosphate as a fertilizer product. Hence, as the media can be selectively regenerated with respective to the nanoparticle component the impact of long-term accumulation of other constituents requires consideration. In addition to the negative consequences of a low-quality desorption stream. It must also be considered that the role of the other constituents (i.e. organic compounds) attached to the resin's surface, is twofold: direct completion of the sorption sites and, second, retardation of mass transfer by coating the channels and reducing the Donnan membrane effect. Both the direct and the indirect effect are noteworthy, since with most sorption resin mass transfer within the structure limits the overall rate of uptake.

2.2.4.6 Regeneration

Hydrated ferric oxides show strong adsorptive affinities towards phosphates via a ligand exchange process that take place in the coordination sphere of the Fe atoms. The phosphate species are bound to the oxide surface by the formation of inner sphere complexes (Genz et al., 2004). Nevertheless the adsorptive behaviour of commercially available hybrid nanoparticulate ferric oxide embedded resin has been extensively reported (Boyer et al., 2011; Pan et al., 2009a&b; Blaney et al., 2007; Martin et al., 2009; SenGupta and Pandit, 2011) less deep motivation on the regenerant solution have been proposed and intensely investigated by the same authors. However many of these authors reported the regeneration of HAIX with a combination of sodium hydroxide and sodium chloride (Table 2.2.2).

Table 2.1.2 Regeneration of HAIX resin in different works.

Solution	Source of water	Volume	% P desorbed	No. of regeneration cycles	Reference
5% NaOH (1.25 M)* 5% NaCl	Pesticide manufacturing plant effluent	10 BV	>98%	5	Pan et al., 2009a
2% NaOH (0.5 M)* 2% NaCl	Synthetic phosphate solution; Municipal treatment plant effluent	12 BV	>95%	3	Blaney et al., 2007
2% NaOH (0.5 M)* 2.5% NaCl	Synthetic phosphate solution	10 BV	>90%	10	Sengupta & Pandit, 2011
4% NaOH (1 M)* 2% NaCl	Trickling filter plant effluent	1 BV	80%	10	Martin et al., 2009
2% NaOH (0.5 M)* 4% NaOH (1 M)*	Synthetic phosphate solution; Municipal treatment plant effluent	7 BV 7 BV	90% 97%	NA	L. Kock, 2015
2% NaOH (0.5 M)*	Trickling filter plant effluent	10 BV	80-95%	~60	This study

*Molar equivalent of % NaOH
NA: Not applicable

Since HAIX Layne^{RT} has two distinct types of adsorption sites, with two chemically different sorption mechanisms, one of the main advantage of this hybrid ion exchange resin is to treat each type of sorption site separately. Therefore, it is possible to work almost independently with the quaternary ammonium groups of the parent ion-exchange resin and the ligand exchange sites on the surface of the nanoparticle sized hydrated ferric oxide.

The relative selectivity of HFO for phosphate over sulphate has been reported 46 and the affinity sequence for strong anion exchange resin is reported as sulphate > phosphate > nitrate > bromide > nitrite > chloride > bicarbonate > hydroxide (Blaney et al. 2007; SenGupta and Pandit, 2011). Therefore, since in the case of secondary wastewater effluent the sulphate concentration can decuple phosphate's, it must be expected that phosphate adsorbed by electrostatic interaction will be easily displaced by sulphate ions. The result is the lack of interest in desorbing the ion exchange sites, except by side effects (i.e. steric hindrance and reduction of the Donnan membrane effect). Quite the opposite, HFO preferentially binds phosphate by the formation of inner-sphere complexes, and sulphate can't displace phosphate as it can only form outer-sphere complexes (Blaney et al., 2007). Work by Lin and SenGupta (2009) has shown that the two types of adsorption sites can be selectively desorbed. Sodium hydroxide regenerates the ferric oxide ligand exchange sites and sodium chloride regenerates the ion-exchange sites. As previously explain increasing the pH by using a sodium hydroxide solution has been proved to be the simplest solution to eluting the P(V) ions from the loaded HFO nanoparticles. Indeed, increase of the pH above 11 results in enhanced competition between HPO_4^{2-}/PO_4^{3-} ions and OH^- , and most importantly the HFO sorption sites on the sorbent surface are all deprotonated and negatively charged (i.e. FeO^- becomes the predominant surface functional group). Consequently, Donnan co-ion exclusion and electrostatic repulsion forces are operative, which are favourable for desorption of the loaded phosphate (Cumbal and SenGupta, 2005; Sarkar et al., 2011).

Martin et al. (2010) have looked at the uptake and desorption of competing anions (chloride, nitrate and sulphate) using model solutions. Desorption was carried out with sodium hydroxide only, and with sodium chloride followed by sodium hydroxide. By using first sodium chloride as regenerating solution, only small amount of phosphate were desorbed in the initial bed volumes together with large quantities of nitrate and sulphate. Desorption of these species by sodium chloride and not by sodium hydroxide was consistent with the outcomes exposed by Lin and SenGupta (2009) about their exchange onto the quaternary ammonium ion exchange sites and not with the ferric oxide nanoparticles.

Kock (2015) found out that HAIX exhausted with wastewater required an approximately 5 times greater concentration (0.5 M or greater) of sodium hydroxide than HAIX exhausted with synthetic phosphate solution in order to achieve appreciable phosphate desorption (95%). For both the synthetically exhausted HAIX and HAIX exhausted with wastewater the optimal flow velocity was 1 BV/h for all the sodium hydroxide concentrations studied. Faster flow velocities desorbed less phosphate and gave broader desorption profiles, meanwhile slower flow velocities (0.5 BV/h) also decreased the amount of phosphate desorbed but gave similar desorption profiles to 1 BV7h. The work also highlights that inclusion of sodium chloride in the regenerant solution is not required as very high percentages of phosphate can be desorbed from the ligand exchanges sites with only sodium hydroxide (92% with 1 M NaOH in 3 BVs). The study concluded that the addition of sodium chloride is detrimental as not only does it increase the chemical costs of regeneration, but also leads to significant TOC levels in the effluent stream which would affect negatively the precipitation of struvite or hydroxyapatite and the subsequent reuse of the recovered sodium hydroxide. Moreover, sequential regeneration (NaOH followed by NaCl) showed that the wastewater exhausted HAIX had adsorbed organic species (NOM) by ligand exchange on the surface of the hydrated ferric oxide and by ion on the quaternary ammonium ion exchange sites of the parent resin. Sodium hydroxide desorbed 96% of the total desorbed phosphate and 19% of the NOM. Sodium chloride desorbed 4% of the total phosphate and 81% of the NOM. The small percentage of NOM adsorbed by ferric oxide resulted in the need to use a higher sodium hydroxide concentration for the regeneration of the ferric oxide surface. According to the author the reason of that need is that multiple carboxyl and hydroxyl functional groups within each NOM molecule provide multiple binding sites that requires simultaneous exchange in order for desorption to occur.

2.3 MATERIAL AND METHODS

2.3.1 Analytical Methods

At the University of Cranfield the analysis of PO_4-P were carried out using the automatic spectrophotometer “*SMARTCHEM 200*”, according to the confidential methods provided by the supplier (AMS France – Alliance Instruments). COD analysis were performed with Merk Spectroquant COD Cell Test according to the manufacturer instructions (the methods corresponds to DIN ISO 15705 and is analogous to EPA 410.4, APHA 5220 D, and ASTM D1252-06 B). “Spectroquant Cell Test” for calcium, sulphate, chloride and nitrate were occasionally utilized to analyse the concentrations of the corresponding ions. The TSS were analysed following the standard method “EPA Method 160.2”.

In Bologna, the ionic composition of the samples was determined by using “HACH Cell Test” coupled with a HACH spectrophotometer.

2.3.2 Chemicals

All the chemicals: potassium nitrate, potassium phosphate, potassium sulphate, humic acid sodium salt, sodium chloride, hydrochloric acid, sodium hydroxide were acquired from Sigma-Aldrich (Dorset, United Kingdom).

2.3.3 Cranfield and Bologna WWTP wastewater effluent

At Cranfield secondary wastewater effluent, following a trickling filter process, was collected from the Universities sewage works. The works treats a population equivalent of 6500-8000 with no existing technology used for P removal. The effluent concentration range are listed in Table 2.3.1.

Table 2.3.1 Concentration range of the main compounds characterizing the secondary wastewater effluent of the Cranfield WWTP fed to the demonstration plant.

Cranfield WWTP secondary wastewater effluent				
Compound	**Symbol**	**Unit**	**Concentration**	**Relative error**
Phosphate	PO_4-P	$mg_{PO4\text{-}P}/L$	5-6	10%
Ammonia nitrogen	NH_3-N	$mg_{NH3\text{-}N}/L$	1-40	10%
Nitrate	NO_3^-	mg_{NO3}/L	32-46	10%
Sulphate	SO_4^{2-}	mg_{SO4}/L	70-80	10%
Calcium	Ca^{2+}	mg/L	30-40	10%
Chemical oxygen demand	COD	mg_{O2}/L	30-40	13%
Total suspended solids	TSS	mg/L	50-150	5%
pH		at 20 °C	6.5-7	3%

At Bologna university the experiments were conducted by using the final wastewater effluent from the WWTP “IDAR” and characterized by the parameters shown in Table 2.3.2. Since the content of phosphate was very law, it was spiked by adding mono- and di-basic phosphate salts in a relationship such that at the end the pH was the same of the original effluent.

Table 2.3.2 Average concentration of the main compounds characterizing the wastewater effluent of the Bologna “IDAR” WWTP used for the laboratory trials.

“IDAR” WWTP wastewater effluent				
Compound	**Symbol**	**Unit**	**Concentration**	**Relative error**
Ammonia nitrogen	NH_3-N	$mg_{NH3\text{-}N}/L$	5.1	10%
Sodium	Na^+	mg/L	136	10%
Ammonium	NH_4^+	mg/L	0.51	10%
Potassium	K^+	mg/L	19	10%
Magnesium	Mg^{2+}	mg/L	25	10%
Calcium	Ca^{2+}	mg/L	136	10%
Phosphate	PO_4-P	$mg_{PO4\text{-}P}/L$	1	10%
Fluoride	F^-	mg/L	0.11	10%
Chloride	Cl^-	mg/L	151	10%
Nitrite	NO_2^{2-}	mg/L	invalid	10%
Nitrate	NO_3^-	mg/L	6.74	10%
Sulphate	SO_4^{2-}	mg/L	104	10%
Biological oxygen demand	BOD_5	mg_{O2}/L	15	16%
Chemical oxygen demand	COD	mg_{O2}/L	41	13%
Total suspended solids	TSS	mg/L	8.3	5%
Total organic Carbon	TOC	mg/L	7.9	13%
pH		at 20 °C	7	3%

2.3.4 The adsorbent media HAIX Layne^{RT}

The adsorbent media, currently marketed as Layne^{RT} (and previously known as ArsenX^{np} and Phosx^{np} – SolmeteX Co., Massachusetts), is a commercially available media, principally used for arsenic removal. This type of hybrid anion exchanger (HAIX) media was developed by Blaney et al., (2007) and the adsorptive behaviour has been extensively reported (Boyer et al., 2011; Pan et al., 2009a&b; Blaney et al., 2007; Martin et al., 2009; Sengputa & Pandit, 2011). The HAIX resin comprises a strong base macroporous anion exchange resin (whose matrix is a styrene, divinylbenzene and ethylstyrene copolymer) which act as a scaffold to support a dispersion of ferric oxide nanoparticles (Cumbal et al., 2003) and has a chloromethyl trimethylamine functional group. The salient properties of the polymeric ion exchanger, known as the "parent media" are illustrated in Table 2.3.3. Approximately 26% of the internal and external surfaces of the material are covered with iron in hydrated ferric oxide form. The size of the media varied between 0.18 and 1.0 mm with a mean size of 0.69 mm (Martin et al., 2017). The media was activated with the following procedure: i) a first wash with deionized water by batch mode for 30 minutes, stirring at 250 rpm to remove any fine iron particle left over from manufacturing; ii) a batch pre-conditioning regeneration with a 2% (w/v) NaOH solution, media concentration of 10 g/L, stirring at 250 rpm for 2 hours in order to convert the resin's form from the chloride one (in which Layne^{RT} is supplied) to the hydroxyle form; iii) a double rinse in DI water as i).

Table 2.3.3 Salient properties of the hybrid polymeric ion exchanger supporting HFO nanoparticles HAIX Layne^{RT} – sold by SolmeteX Co., Massachusetts.

Characteristics	HAIX
Structure	Macroporous Polystirene-Divinilbenze
Appareance	Brown spherical beads
Functiona group	Quaternary ammonium
Iron content	75-90 mg as Fe/g resin
Bulk density	790-840 g/L
Particle size	300-1200 µm
Ion-exchange capacity	1 meq/mL

2.3.5 Cranfield pilot-scale plant

2.3.5.1 Technical specifications

The demonstration-plant located at the Cranfield University Pilot Hall was manufactured and provided by MionTec GmbH (Germany) and consisted of: a drum filter (micro-screen 60 µm) for solids removal, a compressed air diaphragm pump with float flow measurement, two ion exchange columns with different sizes (Table 2.3.4) and one storage tank for the regenerant solution. Two pressure gauges are positioned before the two columns and allow to determine the pressure drops across the columns during the operating time. The first column is filled with 69 L of synthetic zeolite (BYK Additives LTD, UK) which was originally thought for the removal and recovery of ammonia. Unfortunately, due to a design underestimation of the suspended solids into the wastewater, the TSS removal operated by the drum filter resulted insufficient to allow a proper consecutive adsorption process. The solids accumulated into the bed covering the media surface and preventing ammonium adsorption. In addition to this, the small campus' wastewater treatment plant was not able to provide a steady ammonia concentration at the inlet of the plant, which was actually characterized by significant oscillations (range 0-40 mg/L) strictly dependent on daily time and temperature. This results in an alternation of media adsorption/leaching of ammonia depending on the inlet concentration without ever letting the media to reach capacity. For these two reasons the first column was considered filled with "exhausted zeolite" and acted as a depth filter before feeding the second column. The media of the first column was never regenerated and only backwashed once a day with tap water to remove the solids – 20 BV of backwashing at a flow-rate of 800 L/h. The second column was filled up with 34.7 L of HAIX Layne^{RT} media, for a bed volume of 60% of the total column volume. The plant was in principle operated manually and the piping of the columns is designed in a way that allows for any necessary IEX operations and processes. Without opening connections and only turning valves it is possible to run down-flow/up-flow a single or serial columns.

Figure 2.3.1 Real image of the adsorption pilot-plant treating actual secondary effluent wastewater of the Cranfield University campus MWWTP.

Table 2.3.4 Technical specifications and operating adsorption/desorption conditions of the adsorption pilot-plant treating actual secondary effluent wastewater of the Cranfield University campus MWWTP.

	Parameters	**Zeolite Column**	**HAIX Column**
Technical specifications of the columns	Outer diameter	315 mm	225 mm
	Inner diameter	307 mm	217 mm
	Sectional Area	7.40 dm^2	3.70 dm^2
	Media Volume (BV)	69 L (932 mm)	34.72 L (939 mm)
	Cylindric column height	115.9 L (1566 mm)	58.3 L (1577 mm)
Adsorption operating parameters	Flow	400 (L h^{-1})	400 (L h^{-1})
	EBCT	10 min	5.2 min
	Superficial velocity (v_s)	5.8 BVs/h (5.4 m/h)	11.5 BVs/h (10.8 m/h)
Regeneration operating parameters	Flow	***	200 (L h^{-1})
	EBCT	***	10.4 min
	Superficial velocity (v_s)	***	5.76 BVs/h (5.4 m/h)

2.3.5.2 Operating conditions of adsorption

The plant was fed with secondary wastewater effluent from a trickling filter works of the campus' municipal wastewater treatment plant (population equivalent of 6500-8000) - Cranfield, UK). During the adsorption step the wastewater was fed down-flow (Fig. 2.3.2) at a flow of 10 m^3/day (approximately 400L/h). The empty bed contact time (EBCT) corresponding to that flowrate was 10.4 minutes for the filtration step across the first column and 5.2 minutes for the P removal column filled with HAIX resin. The outlet concentration reached the P breakpoint once a day, unlikely, due to the compulsory manual intervention the plant needed to be stopped, desorbed and put again into service, it was impossible to run sequential breakthrough curves by stopping the process always at the same breakpoint. Indeed, it resulted in several breakpoints at different concentrations without being able to maintain the outlet concentration constantly below the law's threshold of 2 mg/L. During the adsorption cycle samples at the outlet were collected hourly by an auto-sampler, meanwhile samples at the inlet, at the drum filter outlet and at the filtering column filled with exhausted zeolite outlet, samples were taken manually twice a day. COD, TSS, pH and PO_4-P contents were kept monitored. The elaboration of the adsorption breakthrough tests was undertaken by means of the following performances parameters: adsorption yield (Y_{ads}) and resin operating capacity (η_{resin}), described and detailed in Table 2.3.7.

Figure 2.3.2 Adsorption flow-sheet of the adsorption pilot-plant treating actual secondary effluent wastewater of the Cranfield University campus MWWTP.

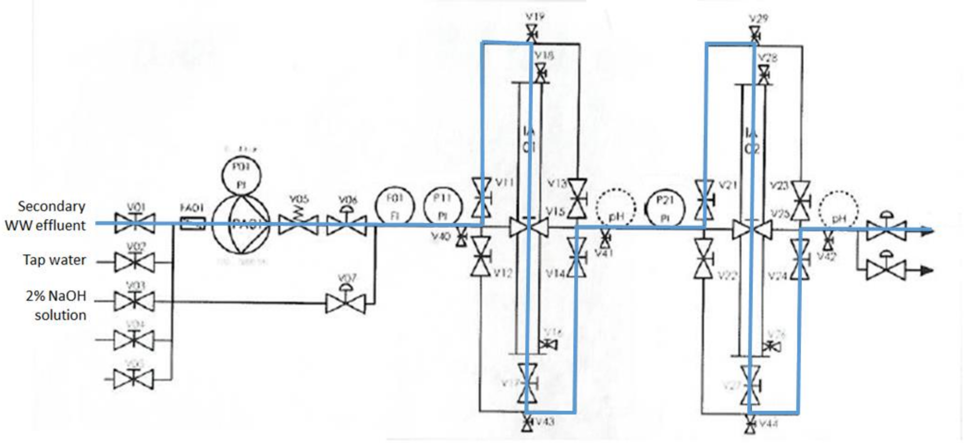

2.3.5.3 Operating conditions of desorption

After each adsorption step the P-column was empty and backwashed in DI water for 5 BV and then regenerated by fluxing 10 BV of 2% (w/v) NaOH solution with an EBCT of 10 minutes. Both the backwash and the desorption were performed in an up-flow configuration. The daily backwash of the P-column before the regeneration enabled to avoid the accumulation of solids into the solution through different cycles, and indeed to keep the final concentrated stream cleaner and purer. The storage tank contained a volume of regenerant solution of 350 L, equivalent to 10 BVs. This solution was fed from the bottom of the P-column (Fig. 2.3.3) and the outlet at the top of the column was recirculated into the same tank. For the whole duration of the desorption the solution in the storage tank was kept homogeneous by stirring with an internal impeller electrically fed. After the desorption the column was empty by gravity (to avoid any dilution of the solution by feeding a different solution) and the regenerant solution collected again into the storage tank. Finally, 5 BVs of tap water were fluxed up-flow to wash out the remaining regenerant solution and then the system was turned back into service for a new adsorption cycle. The 350 L of regenerant solution were reutilized through different cycles in order to enrich the P content. Once the solution was too concentrated to perform a further efficient desorption step, it was collected apart as ‘spent NaOH’ solution ready to be treated and a fresh solution was prepared. The elaboration of the desorption breakthrough tests was undertaken by means of the desorption yield (Y_{des}) described in Table 2.3.7.

Figure 2.3.3 Desorption flow-sheet of the adsorption pilot-plant treating actual secondary effluent wastewater of the Cranfield University campus MWWTP.

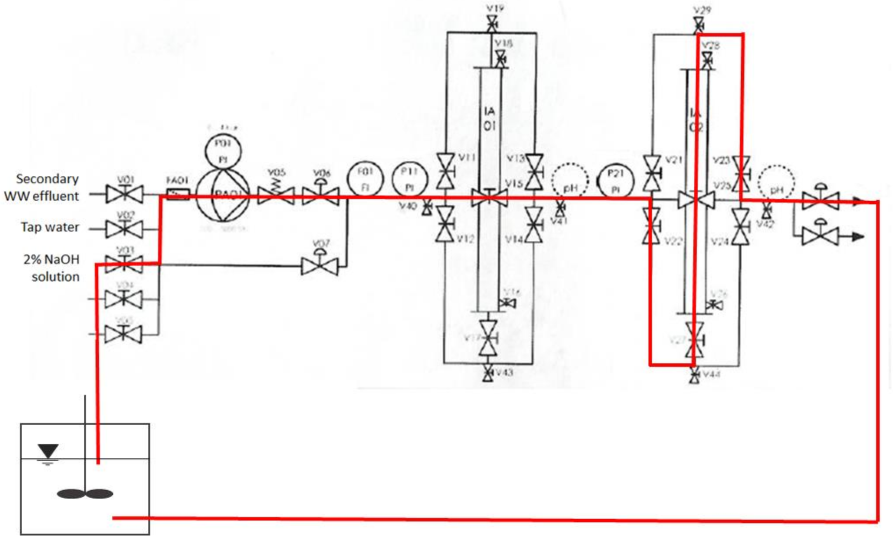

2.3.6 Batch test for the recovery of calcium-phosphate

Preliminary batch tests were conducted to evaluate the optimal Ca:P molar ratio to reduce the P content of the spent brine. Batch test were performed in triplicate in 1 L beker containing 600 mL of solution. The hydrated lime, $Ca(OH)_2$, was added as a solution in deionized water with a concentration of Ca^{2+} around 10^2 g/L. Ca:P molar ratios of 2 and 3 were selected and tested. After the addition, the solution was agitated by means of an internal impeller set at 45 rpm. The solution was let under agitation for 6 hours, and samples were regularly taken to monitor the PO_4-P and Ca^{2+} concentrations and the pH. Temperature ranged between 14 to 18 °C (room temperature). The addition of calcium hydroxide by means of a very concentrated solution made the variation of the solution negligible and volume of the liquid was therefore considered constant before and after the addition. Indeed, approximately 8.5 and 5.6 mL of $Ca(OH)_2$ solution were added to the 600 mL of regenerant solution, for a variation (expressed as Volume of solution added / Starting volume of regenerant solution) of 0.9% and 1.4% in the case of Ca:P ratio of 2 and 3, respectively. The main objective of the test was not to find the optimal dosing, concentrations, mixing and reaction time to enhance the hydroxyapatite formation (HAP), on the contrary, these parameters were not investigated because the precipitation step was not an object of the study. The experiments were conducted to identify the Ca:P molar ratio to be applied at the pilot scale with the primary aim to recover the regenerant solution, and, hence, not the possible most valuable final product. Therefore, the trials scope was to find the Ca:P ratio that allowed to signifincantly decrease the P concentration in the regenerant solution with any excess of unreacted Ca^{2+} remaining in solution. The reduction was evaluated in term of mass of the *i*-compound, by considering – as previously explained – the volume of the solution constant with the following equation:

$$Reduction\ (\%) = {}^{Mass\ precipitated_{i-compound}}\Big/_{Initial\ Mass_{i-compound}}$$

$$= {}^{(Initial\ Conc._{\ i-compound} -\ Final\ Conc._{\ i-compound})}\Big/_{Initial\ Conc._{\ i-compound}}$$

(Eq. 2.0)

2.3.7 Recovery of calcium phosphate and recycling of the regenerant solution at the pilot scale

After the regenerant 2% NaOH solution has been used multiple times for desorption so that the PO_4-P content has reached concentrations that does not allow to continue desorbing the media satisfactory, the solution is considered “spent regenerant” or “used regenerant”. This side stream is therefore treated to recover the final product and then, recirculated to the regenerant storage tank.

The total volume used for desorption (350 L) has been treated 50 L at a time by moving the solution into a second tank. A solution made by dissolving $Ca(OH)_2$ powder in deionized water (to have a concentration of about 10^2 g/L) was added to the tank containing the 50 L. The mass of $Ca(OH)_2$ powder to be added to the solution was selected from the previous batch tests. Two different Ca:P molar ratios were tested at pilot scale: 2 and 3. In order to guarantee homogenous conditions inside the reaction tank, an internal impeller was used (40 rpm). The mixing worked for 6 hours, then it was stopped to allow precipitation. The precipitated was later let settling under gravity overnight since the solution was enough clarified to be pumped out through a filter to ensure the total recovery of the product. Finally, the product was dried overnight at 55°C. During the precipitation manual samples were taken from the liquid phase every half an hour during precipitation, as well as with the same timetable both pH and temperature were monitored. A last sampling was taken after the overnight settling before separating the solid from the treated sodium hydroxide.

The treated NaOH solution was later checked to ensure a low concentration of PO_4-P and any unreacted calcium content; pH was checked to be around 13 and adjusted by the addition of NaOH salt in case of a decrease in its value during the reaction. Finally, the solution was recirculated to the regenerant 2% NaOH solution tank, ready to run further desorption steps. In Fig. 2.3.4 is shown a complete design of the process, included the recovery process.

Figure 2.3.4 Complete configuration of the pilot-plant treating actual secondary effluent wastewater of the Cranfield University campus MWWTP.

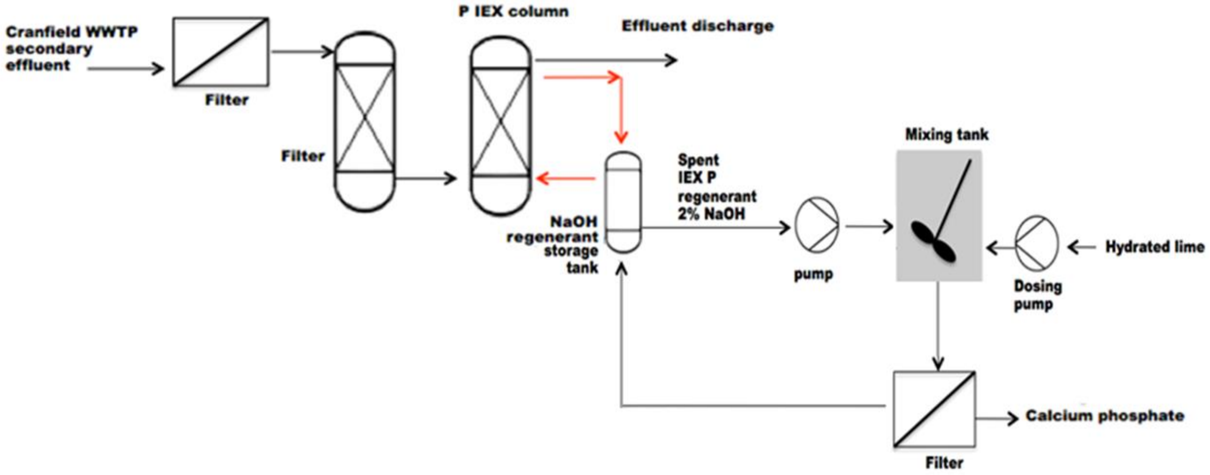

2.3.8 Desorption batch tests

Desorption batch tests were necessary to pre-treat the resin, which came from the Cranfield pilot-plant, before performing the adsorption isotherms. The aims of the laboratory tests performed at Bologna University were to: i) evaluate the resin performance after almost two years of operating time (comparison with virgin resin); ii) evaluate the possible advantages to perform a resin bed treatment after about a two years' time to elute also the several compounds attached to the parent ion exchange resin trying to restore the resin total capacity. The desorption batch tests were conducted by placing the resin with the eluting solution with a media concentration of $10g_{resin}/L_{solution}$. The desorption lasted 2 h at a constant stirring of 200 rpm. The two desorption solutions, prepared by mixing the specific salts with DI water, were respectively: the w/v 2% NaOH solution used to desorb only the ferric nanoparticles' Fe groups and the w/v 2% NaOH + 5% NaCl solution to desorb both the ferric nanoparticles and the ion exchange sites. After the desorption, a sample of the solution was analysed in terms of PO_4-P and COD content. Furthermore, the resin was rinsed in DI water 3 times with the same media concentration used for the desorption. Each wash lasted 30 minutes and was stirred at 200 rpm. Desorption were always performed at room temperature (20-25 °C).

2.3.9 Adsorption kinetic tests

Kinetic tests were performed according to the same operating conditions of the adsorption isotherms: initial concentration of P in the liquid phase, temperature of 20-22°C, pH around 6.9 and shaking at 200 rpm. The ratio between the mass of dry resin and the volume of liquid phase was set to 4g/L, on the basis of previous studies to be used for comparison (Martin et al., 2017; Zeng et al., 2004). 200mL of solution with a P concentration of 7.0 ± 0.2 mg/L for the P-synthetic solution and of 6.0 ± 0.2 mg/L for the actual ww, were placed in a 250-mL bottles with 0.8g of dry resin. Kinetic tests were conducted for both the synthetic P-solution and actual wastewater, each test was set up in triplicate. Samples were taken each 20 minutes for the first hour and then every 30 minutes up to the 6th hour. A latter point was taken after 24 h to verify that adsorption process reached true equilibrium. Experimental data were interpolated by means of the two following equations (Tran et al, 2017):

1) Pseudo-first-order (PFO) equation :

$$q_t = q_e\,(1 - e^{k_1 t}) \qquad \text{(Eq. 2.1)}$$

where q_e and q_t are the amounts of adsorbate uptake per mass of adsorbent at equilibrium and at any time t (min), respectively; and k_1 (1/min) is the rate constant of the PFO equation.

2) Pseudo-second-order (PSO) equation:

$$q_t = \frac{q_e^2 k_2 t}{1 + q_e k_2 t} \qquad \text{(Eq. 2.2)}$$

where q_e (mg/g) and q_t (mg/g) are the amount of adsorbate adsorbed at equilibrium and at any t (min), respectively; and k_2 (g/(mg min)) is the rate constant of the PSO equation.

Generally, although the PSO model can adequately describe adsorption kinetic test adsorption kinetic experimental data, this model does not reveal the adsorption mechanisms. In order to have an insight into the reaction pathways and the adsorption mechanisms the two following equations were applied (Martin et al., 2017):

3) Intra-particle diffusion equation:

$$q_t = k_{IP}\, t^{0.5} \tag{Eq. 2.3}$$

where q_t (mg/g) is the amount of adsorbate adsorbed at any t (min) and k_{IP} (mg/g min$^{-0.5}$) is the rate constant.

4) Film diffusion equation:

$$\ln(1 - F) = -k_{FD}\, t \tag{Eq. 2.4}$$

where F is the fractional attainment of equilibrium at any t (min) and k_{FD} (min^{-1}) is the rate constant.

To calculate the parameters of kinetic, application of nonlinear methods instead of the linear method were applied, in according to what recommended by many researchers (Tran et al, 2017). Furthermore, to identify the best-fit model, calculation of the chi-squared (χ^2) value was calculated in addition to the coefficient of determination (R^2) for the nonlinear method. In the chi-squared test, the squares of the differences between the experimental data and data calculated using the models are divided by the corresponding data obtained and then summed. If the data obtained using a model are similar to the experimental data, χ^2 is close to zero. High χ^2 values indicate high bias between the experiment and model (Tran et al, 2017).

Where where $q_{e,exp}$ (mg/g) is the amount of adsorbate uptake at equilibrium, $q_{e,cal}$ (mg/g) is the amount of adsorbate uptake achieved from the model using the Solver add-in (in Microsoft Office Excel), and $q_{e,mean}$ (mg/g) is the mean of the $q_{e,exp}$ values.

$$\chi^2 = \sum \frac{\left(q_{e,\exp} - q_{e,cal}\right)^2}{q_{e,cal}} \tag{Eq. 2.5}$$

$$R^2 = 1 - \frac{\sum \left(q_{e,\exp} - q_{e,cal}\right)^2}{\sum \left(q_{e,\exp} - q_{e,mean}\right)^2} \tag{Eq. 2.6}$$

2.3.10 Adsorption isotherms

The PO_4-P adsorption isotherms relative to the 3 forms of the tested resin, were studied by mixing the same amount of dry resin (0.1 g) with 100 mL of wastewater or synthetic P solution, with the final ratio between the mass of dry resin and the volume of liquid of $1 g_{media}/L$. For each point the concentration of PO_4-P was adjusted to the wanted value by adding mono- and di-basic phosphate salts in a relationship such that at the end the pH was the same of the original effluent. 120 mL glass vials were used and placed in a rotatory shaker (200 rpm, 22 °C) for 6 hours, to reach the equilibrium condition. The duration of the experiment (6h) was preliminary defined by means of a kinetic test.

The equilibrium concentration in the solid phase, $C_{S,i,eq}$ was determined as:

$$C_{S,,eq,i} = (C_{L,0} - C_{L,eq,i}) \cdot V_L / m_S \qquad \text{(Eq. 2.7)}$$

where: m_S indicates the dry resin mass, $C_{L,0}$ and $C_{L,eq}$ the initial and final PO_4-P concentration in the liquid phase and V_L the liquid volume. 95% confidence intervals associated to $C_{S,eq}$ were calculated by means of standard error propagation rules. Experimental isotherms were interpolated by means of the Langmuir (Eq. (2.8)) and Freundlich (Eq. (2.9)) models:

Langmuir

$$C_{S,eq,i} = \frac{C_{S,i}^{\infty} \cdot C_{L,eq,i}}{\frac{1}{K_{eq,i}} + C_{L,eq,i}} \qquad \text{(Eq. 2.8)}$$

Freundlich

$$C_{S,eq,i} = K_{F,i} \cdot C_{L,eq,i}^{1/n_i} \qquad \text{(Eq. 2.9)}$$

where: $C_{S,eq,i}$ ($g_i/g_{dry\ resin}$) and $C_{L,eq,i}$ (g_i/L) indicate respectively the amount of sorbed i-compound per unit mass of adsorbent and the i-compound concentration in the liquid phase at equilibrium; $C_{S,i}^{\infty}$ ($g_i/g_{dry\ resin}$) the maximum amount sorbed per unit mass of adsorbent, corresponding to a complete monolayer on the adsorbent surface; $K_{eq,i}$ (L/g_i) the constant related to the affinity between the binding sites and the i-compound; $K_{F,i}$ ($L/g_{dry\ resin}$) the sorption capacity in the Freundlich model; $1/n_i$ (-) the sorption intensity in the Freundlich model.

The model parameters were estimated by non-linear least squares regression of the calculated the i-compound solid phase concentrations ($C_{S,eq,calc,i}$) to the corresponding experimental values ($C_{S,eq,i}$). The best-fitting model was selected on the basis of the correlation coefficient R^2, defined so as to take into account the number of model parameters:

$$R^2 = 1 - \left(\frac{\sum_{i=1}^{N} \left(C_{S,eq,i} - C_{S,eq,calc,i} \right)^2}{N - P - 1} \right) \Bigg/ \left(\frac{\sum_{i=1}^{N} \left(C_{S,eq,i} - C_{S,eq,m} \right)^2}{N - 1} \right) \qquad \text{(Eq. 2.10)}$$

where N indicates the number of experimental tests in the studied isotherm, and P the number of model parameters. For each isotherm, the Langmuir and Freundlich isotherms were compared by means of F tests. The best-fitting model was considered statistically different from the other one if the test outcome – indicating the probability that the two models are not statistically different - resulted < 0.05.

2.3.11 Laboratory adsorption column packing, preliminary regeneration and fluid-dynamic characterization

The column used for the breakthrough tests were characterized by a column total height of 1 m and an inner diameter of 0.013 m. The column packing was achieved by first placing a 200 mm layer of quartz sand at the bottom, in order to help the liquid draining before the outlet. Then, the column was filled by repeatedly adding the same small amount of wet resin (20 mL bed volume) and then waiting for the settling before adding the next amount. DI water was let flow down under gravity to help resin beads to settle and compact during the packing. The same operation were repeated since the resin bed length was 0.94 m, the same bed height of the P removal column operating in the pilot-plant at Cranfield. The last 0.06 m on the top of the column were left empty (i.e. filled with water) to let space for resin swelling and avoiding any increase in pressure due to the expansion of the media. For the tests on the used resin sent from Cranfield, after the column packing the resin was pretreated by desorbing with different solutions:

- In the first case it was regenerated by means of a w/v 2% NaOH solution in DI water. 10 BVs were passed with an EBCT of 10 minutes;
- In the second case the resin was regenerated with a solution of w/v 2% NaOH and w/v 5% NaCl.

An average sample of the total volume passed through the column was collected and kept frozen to qualitatively and quantitatively analyse the compounds eluted. Meanwhile for the virgin resin the preliminary regeneration was not needed, however the resin was pretreated with w/v 2% NaOH solution to change the ion form of the ion exchange parent media into the OH- as for the other two resin beds.

Successively, the fluid dynamic behaviour of the bed was studied before each adsorption experiment by means of conventional frontal analysis tests conducted with DI water after having equilibrated the column with a 0.05 M NaOH solution. The electrical conductivity (EC) was measured at the column outlet with an EUTECH Instruments 2700 series conductimeter. These tests were used in the first place to estimate the effective porosity (ε), a parameter required to evaluate the interstitial velocity and the hydraulic retention time (HRT) on the basis of the measured fluid flow rate. The effective porosity was evaluated from the retention time distribution (RTD) curve according to the procedure proposed by Levenspiel et al. (1999) and here illustrated.

Hence, the RTD method consists in the experimentally determination of the retention time distribution curve by monitoring an inert tracer concentration at the outlet. In our case the test was conducted by a *step input* consisting in first equilibrating the column with a 0.05 M NaOH tracer solution and subsequently fluxing DI water. By monitoring the concentration at the outlet, in our case by an indirect measurement since we monitored the conductivity of the solution, it was possible to obtain the retention time distribution curve versus time. The latter gives important information about the mixing that is occurring inside a reactor or a packed bed, and it is one of the most important parameters in their characterization. The response obtained at column/reactor outlet is showed in Fig. 2.3.5.

Figure 2.3.5 Response of a step injection test by monitoring the tracer element concentration at the outlet of the column (Fogler & Gürmen, 2008).

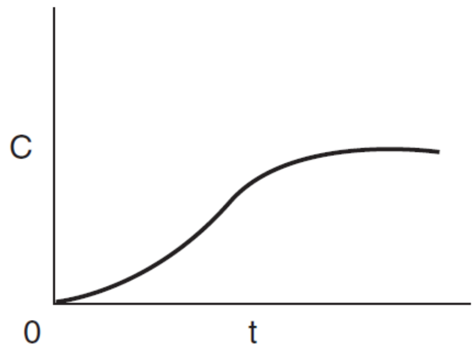

From this curve, it was possible to calculate the *Cumulative Retention Time Distribution Function* or *F curve*. The *F function* is defined as:

$$F(t) = \frac{C(t)_{out}}{C_o} \qquad \text{(Eq. 2.11)}$$

Then, from the *F curve* the *RTD Function* can be estimated as:

$$E(t) = \frac{d\,F(t)}{dt} \qquad \text{(Eq. 2.12)}$$

Once the *E function* is found, the average residence time can be calculated with the following equation:

$$\bar{t} = \tau = \int_0^\infty t \times E(t)dt \qquad \text{(Eq. 2.13)}$$

The theoretical residence time (τ) is equal to the average residence time if there are not dead zones inside the column/reactor. With this information is also possible to estimate the packed bed porosity (for a packed column or a packed bed reactor) by applying the following expressions:

$$Liquid\ Volume = Volumetric\ Flow\ \ rate\ \times\ \tau \qquad \text{(Eq. 2.14)}$$

$$\varepsilon = \frac{Liquid\ Volume}{BV_{resin}} \qquad \text{(Eq. 2.15)}$$

The *E curve* is very important to characterize a packed bed and to evaluate the packing quality and the column efficiency. τ and ε are very significant parameters, because the column/reactor performance and the reproducibility of the results obtained depend directly on them. A high quality packing has to be homogeneous and stable, with no air bubbles of air trapped, with no channels or preferential paths formation.

The frontal analysis tests and the *E curve* obtained (which should have the theoretical shape shown in Fig. 2.3.5) were also used to evaluate two indicators of packing quality by means of two approaches based on the analysis of the retention times distribution curve obtained, as explained above, by calculating point by point the derivative of the sigmoidal experimental curve of normalized EC versus time provided by the fluid-dynamic test (Levenspiel et al., 1999). The first approach is based on the Theoretical Plate Model which evaluates the number of theoretical plates N_{tp} as:

$$N_{tp} = 5.54 \cdot \left(\frac{\tau}{w_{1/2}}\right)^2 \qquad \text{(Eq. 2.16)}$$

where τ is the residence or retention time; $W_{1/2}$ is the peak width at half height (Fig. 2.3.6). With the number of plates N_{tp} the *height equivalent of a theoretical plate* or *HETP* can be estimated as:

$$HETP = \frac{L}{N_{tp}} \qquad \text{(Eq. 2.17)}$$

where L is the column length. The higher is the number of plates (N) or the smaller is the value of HETP, higher is the efficiency of the column. With these two parameters the *reduced plate height* or *h* can be calculated with the expression:

$$h = \frac{HETP}{d_p} \qquad \text{(Eq. 2.18)}$$

According of different analytical and process chromatographic column producers, application in which the packing quality and column performance are as significant as for an adsorption process, values of $h \leq 3$ are characteristic of a high efficiency column (GE Healthcare Bio-Sciences AB).

The second approach is based on the asymmetry factor (A_s), defined as the ratio between the leading and tailing semi-width of the peak at 10% of the peak height, and representing the peak deviation from a Gaussian peak:

$$A_S = \frac{b}{a} \qquad \text{(Eq. 2.19)}$$

Where b is the right half of the *E curve*, and *a* is its left half (Fig. 2.3.6). If $0.8 \leq As \leq 1.8$ the packing can be considered of good quality..

Figure 2.3.6 Theoretical E curve obtainable for step injection analysis by deriving the F curve RTD Function.

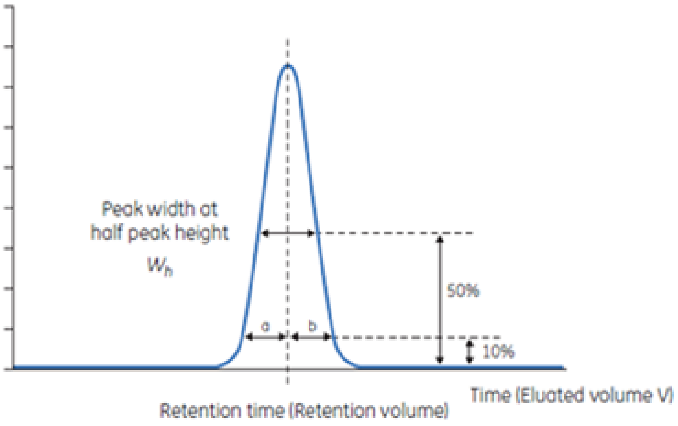

2.3.12 Continuous-flow adsorption/desorption breakthrough tests

The adsorption/desorption breakthrough tests were conducted at 24-25°C in the 0.94-m resin bed height. The column temperature was controlled through a jacket connected to a temperature-controlled bath. During the adsorption step, the wastewater was fed downstream with a Masterflex L/S 0.1 HP 1-100 RPM peristaltic pump. The flowrate was set to have an EBCT of 5.2 ± 0.1 minutes in accordance to the operational conditions of the Cranfield pilot plant. Both pressure drop and flowrate were measured hourly. Samples at the outlet were taken hourly since the curve remained flat and every 15 minutes once the curve started to rise; inlet samples were checked every 3 hours. The average PO_4-P concentration at the inlet was used to normalize the corresponding outlet values. The adsorption tests were continued up to the attainment of approximately 0.80-0.85 outlet normalized concentration. The adsorption performances of each tested resin were quantified by means of the following indicators, referred to a defined outlet concentration breakpoint value: i) adsorption yield ($Y_{ads,i,}$), evaluated as $m_{i,\ sorbed} / m_{i,fed}$; ii) resin operating capacity (η_i), defined as (mass sorbed at the breakthrough point) / (total mass that could be sorbed if all the resin was saturated). The detailed procedure relative to the evaluation of these performance indicators is reported in Table 2.3.7.

The desorption was performed with the w/v 2% NaOH solution for the three forms of the resin. The solution was fed with a Masterflex L/S 0.1 HP -1-100 RPM pump in counter-current flow with respect to adsorption step (i.e. up-flow). The flowrate was set to have an EBCT of 10 minutes and a total volume of 10 BVs of regenerant was passed through the bed. An average sample of each bed volume collected at the outlet was kept and analyzed. No pressure drops were detected, mainly because of the empty head-space left at the top of the column that let the bed expand and an incipient fluidization occur. Actually, the fluid velocity was not enough high to generate a complete fluidized bed where the suspended solids behave as though they were a fluid, swirling around much like an agitated tank. However, fluid velocity was enough high to balance the weight of the resin and let it expand and move slowly. The desorption performances of each tested resin were quantified by means of the desorption yield ($Y_{des,i,}$), evaluated as $m_{i,\ desorbed} / m_{i,sorbed}$, and reported in Table 2.3.7.

Table 2.3.7 Main parameters used to evaluate the performances of continuous flow tests.

1) PO_4-P adsorption yield ($Y_{ads,P}$)

$Y_{ads,P}$ was evaluated at different breakpoint values (indicated as X%) as:

$$Y_{ads,P,X\%} = m_{P,sorbed,X\%} \,/\, m_{P,fed,X\%} \qquad \text{(Eq. 2.20)}$$

where $m_{P,sorbed,X\%}$ indicates the P mass adsorbed until the attainment of a X% outlet normalized PC concentration, and $m_{P,fed,X\%}$ indicates the corresponding P mass fed to the adsorption column. $m_{i,sorbed,20\%}$ was estimated as:

$$m_{P,sorbed,X\%} = m_{P,fed,X\%} - m_{P,out,X\%} \qquad \text{(Eq. 2.21)}$$

where $m_{P,out,X\%}$ is the mass lost in the outlet up to the X% breakpoint. Eq. (S1) does not take into consideration the liquid phase PC content at the X% breakthrough point, which is generally negligible. $m_{P,out,X\%}$ was calculated by numerical integration of the experimental breakthrough curve up to the selected X% P breakpoint:

$$m_{P,out,X\%} = Q \cdot \int_0^{t_{X\%}} C_{L,P,OUT} \cdot dt \qquad \text{(Eq. 2.22)}$$

where Q indicates the wastewater flow rate fed to the column.

2) Resin operating capacity (η_{resin})

η_{resin} was evaluated at different P breakpoint (indicated as X%) as:

$$\eta_{resin,X\%} = m_{P,sorbed,X\%} \,/\, m_{P,sorbed,100\%} \qquad \text{(Eq. 2.23)}$$

where $m_{P,sorbed,100\%} = m_{P,sorbed,saturation}$ and indicates the P mass theoretically adsorbed by the resin upon saturation of the sorption capacity. Since all the breakthrough tests conducted in this work were continued until the attainment of an outlet P concentration close to the inlet P concentration (condition of resin saturation), $m_{P,sorbed,100\%}$ was calculated by numerical integration of the experimental breakthrough curve until the last experimental point:

$$m_{P,sorbed,100\%} = Q \cdot \int_0^{t_{final}} (C_{L,P,IN} - C_{L,P,OUT}) \cdot dt \qquad \text{(Eq. 2.24)}$$

where Q indicates the wastewater flow rate fed to the column.

3) PO_4-P desorption yield ($Y_{des,P}$)

$Y_{des,P}$ was evaluated as:

$$Y_{des,P} = m_{P,desorbed} \,/\, m_{P,sorbed} \qquad \text{(Eq. 2.25)}$$

where $m_{P,desorbed}$ was calculated by the summation:

$$m_{P,desorbed} = \sum_{i=1}^{10} V_{BV,i} \cdot \bar{C}_{BV,i} = V_{BV} \sum_{i=1}^{10} \bar{C}_{BV,i} = (Q \cdot EBCT) \sum_{i=1}^{10} \bar{C}_{BV,i} \qquad \text{(Eq. 2.26)}$$

where i are the number of bed volumes passed through the bed, $V_{BV,i}$ is the volume of the i-volume which is a constant, and $\bar{C}_{BV,i}$ is the average concentration of the i-BV collected at the outlet.

2.4 RESULTS AND DISCUSSION

2.4.1 Secondary wastewater filtration

As explained in M&M filtration was performed by a combination of a drum filter and a second fixed bed column filled with a synthetic zeolite. Originally, the bed of zeolite had been thought as an ion-exchange column, but due to an underestimation of the suspended solids (SS) in the secondary wastewater fed and a significant fluctuation of the NH_4-N inlet concentration (ranging from 1-40 mg/L) the adsorption process resulted almost difficult to control and evaluate in performances. For this reason, the column filled with synthetic zeolite was converted in a depth filter in order to reduce the SS content and allowing the subsequent P-removal column to work properly. However, the investigation of the microfiltration step was not object of this study and, therefore, the evolution through time of the depth filter was not deeply investigated. The SS content of the filtered water was analysed once a day at different time to evaluate the effectiveness of the drum-filter/depth-filter combination. Results showed that from an initial SS concentration ranging from 50 to 150 mg/L in the secondary wastewater fed to the process, the effluent of the filtration step settled around a content of 10±3 mg/L. Moreover, the phosphate concentration was monitored before and after the zeolite column to ensure that any adsorption was taking place.

2.4.2 Evaluation of the impact of reusing the same regenerant solution multiple times enriching the P concentration

The first goal of my study on the Cranfield pilot-scale plant was to evaluate the evolution of the performances through different cycles and understand if the idea on the basis of the novel approach proposed by the University and regarding the management of the regenerant solution was either promising or unsuitable to satisfy an effective and efficient process. The demonstration plant went through several adsorption breakthrough tests, followed by a regeneration concerning the only ferric nanoparticle active sites. As explained in the first chapters due to the presence of other anionic compounds with concentrations up to two order of magnitude greater than *ortho*-phosphates (i.e. sulphates 100-200 mg/L; phosphates 5-7 mg/L) a simple anion exchange site is not able to selectively adsorbed phosphate from wastewater. Indeed, the quaternary ammonium functional group, that characterized the polymeric IEX resin which works as a scaffold for the dispersed ferric nanoparticles (and called “parent media”), has been largely demonstrated to lack selectivity towards phosphates in the presence of competitors (Zhao & SenGupta, 1997; Pan et al, 2009; Blaney et al., 2007; Martin et al., 2009).

For that reason, the investigated approach proposed to desorb uniquely one of the two different type of active sites that characterized the hybrid ion exchange resin HAIX Layne^{RT}: the ferric nanoparticles active sites. High pH solutions are most commonly used for the regeneration of ferric hydroxide-based adsorption media (Sarkar et al., 2007). The desorption due to high pH values has been attributed to electrostatic repulsion between negatively charged phosphate species, and the negative surface charge that develops on ferric hydroxides at pH values above their point of zero net proton charge (pH_{pznpc}). Thus, regeneration occurs by switching pH to 13 (fluxing a w/v 2% NaOH solution) in order to deprotonate the $\cong Fe\text{-}OH_2^+$ and also to invert the Donnan membrane effect with the consequent leaching of negatively charged phosphates’ groups (Chaudhary and James Farrell, 2015). While, at the same time, –OH is not able to completely outcompete the organic matter and the counter ions attached to the ion exchange active sites, resulting in a more selective elution and a purer desorbent stream.

Here, the same regenerant solution (originally a fresh 2% NaOH solution) is used multiple times with the primary result of a rising P content with the increasing number of consecutive desorptions operated.

In Fig. 2.4.1 is shown a series of adsorption/desorption cycles performed by reusing the same regenerant solution multiple times for the consecutive desorption steps. Data are shown in terms of: i) outlet PO_4-P concentration (blue markers) and ii) PO_4-P concentration in the regenerant solution used to desorb the resin bed before the subsequent adsorption cycle (red circle), versus the number of BVs treated (or number of total cycles undertaken by the resin bed).

While in Table 2.4.1, are summarized the number of bed volumes treated during the cycle, the final outlet P concentration after the before-mentioned number of fluxed BVs and the relative adsorption and desorption yields of each cycle performed with the same regenerant. The performance indexes (i.e. Y_{ads} and Y_{des}) reported in Table 2.4.1 must be read with attention since each adsorption yield referred to a different amount of mass fed and each P-desorption yield referred to different quantities of mass adsorbed. Indeed, due to the impossibility to check the outlet concentration at real time and to monitor the system during the night-time, the breakthrough curves were always stopped at different outlet concentrations. Therefore, the number of BVs reported by Table 2.4.1 must be read as the duration of the adsorption cycle until the system was stopped for elution. However, an immediate comparison of that data is not far from describing the performances' evolution though several consecutive cycles, thanks to the fact that the durations of cycles are enough close.

Table 2.4.1 shows that both adsorption and desorption performances decreased through cycles, consequently affecting each other. The incomplete desorption of the adsorbed compounds resulted in a minor availability of active sites for phosphate uptake and, hence, in a lower mass of P adsorbed during the following adsorption cycle.

Two main aspects should be taken into account to explain the desorption yield trend: the regenerant solution's pH and P-concentration. As previously explained the elution of the adsorbed P is mainly due to the switch in pH, which allows to invert the Donnan membrane effect and deprotonate the $\cong$Fe-OH_2^+ group, with the consequent leaching of phosphate molecules by electrostatic repulsion. In this way, the major parameter to look into is precisely pH.

pH remained above 13 (i.e. around 13.1 ± 0.1) for the first 7 consecutive regenerations, even though with a light decreasing trend, confirming the possibility to reuse the regenerant solution several times since the preservation of its desorption driving force. For the last cycles, pH of the regenerant solution resulted lower than 13, and respectively: 12.96; 12.86 and 12.72. Despite the impossibility to define precisely the pH trend through cycles due to the value of variations within the measurement error of the pH-meter (±0.2), an integral pH reduction from the first to the last cycle occurred. This is likely due to that part of OH that resulted able to outcompete other compounds from the ion-exchange parent media and, hence, responsible for the elution of other organic and inorganic compounds. Instead, the P-concentration in the regenerant solution increased rapidly for the first 6 cycles and then became significantly more flatten and less steep ($\alpha_2 < \alpha_1$).

Since desorption is controlled by pH it is probable that the drop in desorption performances of the last three cycles is mainly due to the decrease in the OH concentration; however the high concentration of P reached in the regenerant solution (466 mg_P/L at cycle 52) may play a role as well.

Actually, a decrease in the process performances due to the multiple employment of the regenerant solution was expected since the proposed operating method of the plant is based on the assumption that is not necessary to completely elute all the adsorbed mass of P for cyclic column operation (Jelinek & Sorg, 1998).

Figure 2.4.1 10 consecutive cycles performed with the same regenerant solution (originally fresh w/v 2% NaOH solution). On the x-axis are represented both the total number of bed volumes fed to the process and the corresponding total number of cycles performed by the column. The primary y-axis referred to the outlet P concentration (blu indexes) while the secondary y-axis referred to the P concentration of the regenerant solution used to desorb the resin bed before the adsorption breakthrough curves (red circles). α_1 and α_2 represent the linear slopes of the increasing P concentration of the regenerant solution.

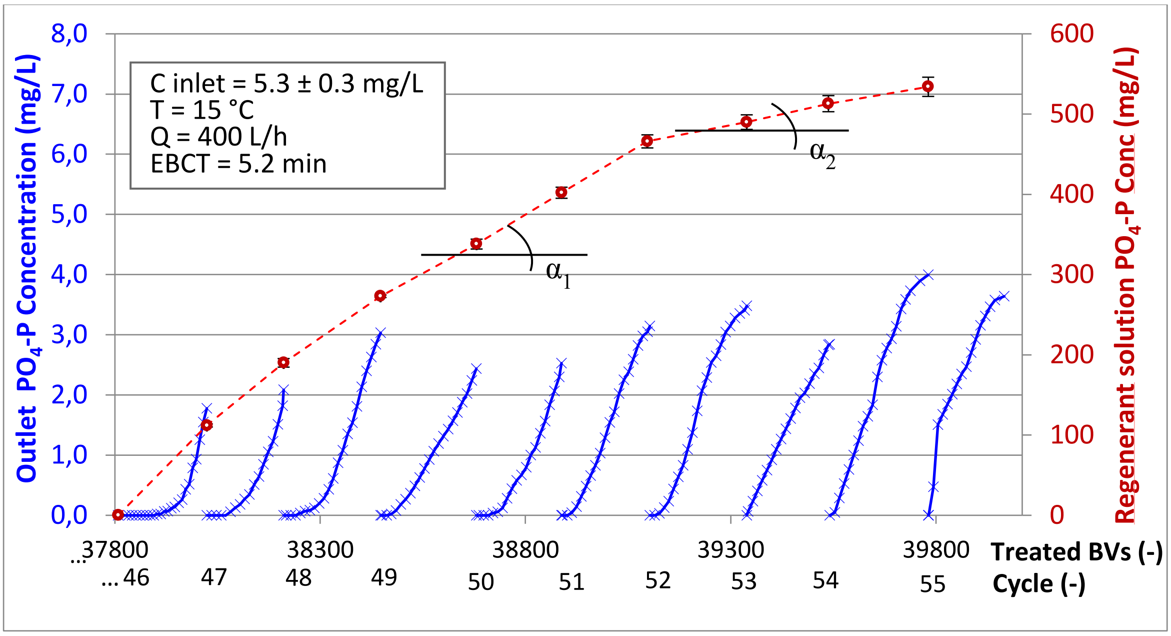

Table 2.4.1 Performances of the 10 consecutive cycles performed with the same regenerant solution showed in Fig, 2.4.1

Total Cycles (-)	Cycles with the same regenerant (-)	BV treated (-)	Final outlet conc. (mg_P/L)	Y_{ads}* (-)	Y_{des}* (-)
46	*1*	216	1.8	98%	87%
47	*2*	187	2.1	91%	85%
48	*3*	230	2.8	83%	83%
49	*4*	233	2.4	81%	71%
50	*5*	207	2.5	85%	69%
51	*6*	215	3.1	74%	76%
52	*7*	236	3.5	68%	28%
53	*8*	202	2.8	65%	30%
54	*9*	240	4.0	56%	32%
55	*10*	185	3.6	51%	

*Yads = Mass of P adsorbed / Mass of P fed to the process;
*Ydes = Mass of P desorbed / Mass of P adsorbed.

Another interesting way to look into the effect of reusing the same regenerant is given by the plot of the overlapped adsorption breakthrough curves through cycles. Evidently, the adsorption is drastically conditioned by the desorption occurred before, with a P outlet breakthrough which occurs gradually and continuously earlier (Fig 2.4.2).

Figure 2.4.2 Overlapped breakthrough curves of consecutive cycles performed with the same regenerant solution (continuous and dotted black lines), and first adsorption cycle with a new fresh 2% NaOH solution (continuous red line) after the previous 10 cycles performed with the same regenerant solution .

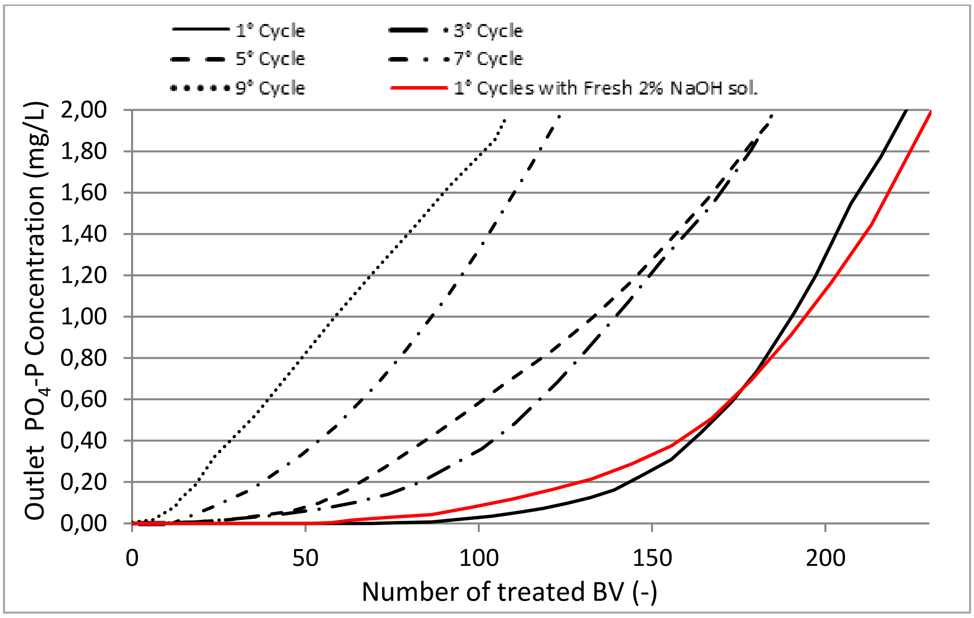

The breakthrough curves gradually move from the typical sigmoidal shape to a linear trend starting from the first bed volumes. Despite the detrimental effect on the operating time that the column can operate before leading to a defined outlet concentration, in Fig. 2.4.2 is possible to understand the potential of the proposed conduction method by looking at the overlapped breakthrough curves after having desorbed the resin bed with a new fresh 2% NaOH solution. As a matter of fact the process results completely reversible, with the possibility of maintaining the adsorption performances within defined targets by simply reducing the number of cycle performed. This finding is a key aspect of the proposed method, as it allows to refresh the media and to restore the highest performances even after years of operating time. Consistent with this finding is the fact that the first desorption with a fresh regenerant solution has always led to a desorption yield beyond the unit (in the range 130%-150%) suggesting the possibility to desorb a part of the P mass previously accumulated and not desorbed by a multiple-used regenerant solution.

According to the above-described results, the number of cycles that can be run with the same regenerant solution finds its maximum when desorption results not satisfactorily effective and, therefore, a new series of cycles with fresh NaOH solution must be started. Actually, the number of cycles is the result of an economic analysis that takes into account the evolution of several factors through cycles. Between those, two key factors are: i) the number of BVs that can be treated up to a defined breakpoint (i.e. the breakthrough time of the adsorption step) and, ii) the increasing concentration in the regenerant solution after each desorption (which is directly proportional to the mass of product that can be recovered). Indeed they are both related to the specific cost to treat the operational unit of the process (for example 1 m^3 of WW): greater are the number of WW BVs that can be treated and the mass of P that can be eluted for each cycle, then, lower is the specific cost of the process for unit of treated WW. Moreover, the purity of the final product obtained, directly proportional to its market value, is another key factor for the feasibility of the process since the quality of the final product, together with the quantity (expressed by point ii)), lead to the benefits which allow to reduce the specific cost to treat an operational unit of MWW. However, the quality of the final product mainly concerns the downstream process, which is not aim of this thesis.

To explore the evaluation of factor i), i.e. the number of treatable BVs for each adsorption run, more experimental tests should be performed by always stopping the system at a specific breakpoint. Indeed, it is well-known that the breakpoint itself has a fundamental role in the process performance. An important finding has been observed by plotting the number of BVs that have been treated up to selected breakpoints during the adsorption step versus the concentration in the regenerant solution used to desorb the resin bed before the adsorption cycle (Fig. 2.4.3). Three environmentally significant thresholds were chosen to investigate that relationship: 1 mg_P/L, 0.5 mg_P/L and 0.1 mg_P/L, respectively. Indeed, 1 mg/L is the legal environmental outlet target today applied by EU countries, while 0.5 and 0.1 mg_P/L have been selected because it is expected that future discharge level will be based upon the background level of phosphorous in rivers, which is reported to be around 0.1 mg_P/L (EA 2000).

Fig. 2.4.3 clearly shows the linear correlation between these two variables, despite the different breakpoints selected, suggesting a possible prediction of the cycle performances through cycles on the basis of the P concentration in the regenerant.

Figure 2.4.3 Number of BVs that can be treated up to a defined breakpoint versus the PO_4-P concentration in the regenerant solution used to desorb the resin bed before the adsorption cycle.

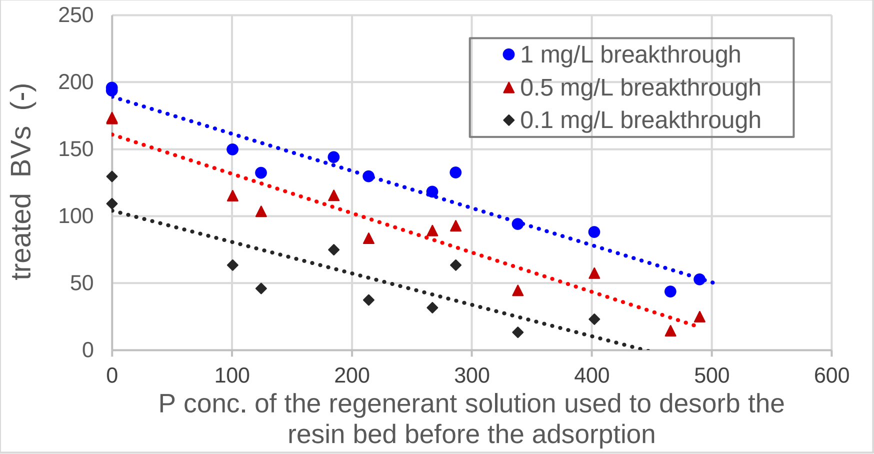

Moreover, a complete breakthrough curve was performed. The aim of the test was to evaluate the column performances after having desorbed with a fresh 2% NaOH solution, in order to have the actual adsorption potential (for an inlet P-concentration around 5 mg/L) of the resin after 55 cycles. Experimental data were elaborated in terms of resin operating capacity and adsorption yield, both at different breakpoints. Fig 2.4.4 plots the outlet P concentration versus the number of BVs fluxed trough the column. Based on the shape of the curve, favourable equilibrium was attained, with a sharp exchange front suggesting good mass transfer characteristics. Results are consistent with those previously attained by other research groups in laboratory-scale trails (Martin et al, 2009; Martin et al, 2017; Blaney et al., 2007). 0.1 mg/L breakthrough occurred at around 100 bed volumes. The experimental data were elaborated according to the M&M chapter and the main operating parameters. Results are shown in Table 2.4.2.

Figure 2.4.4 Adsorption breakthrough curve after 55 cycles performed by the resin bed of the Cranfield pilot-plant: outlet PO_4-P concentration versus the number of bed volumes fed to the process.

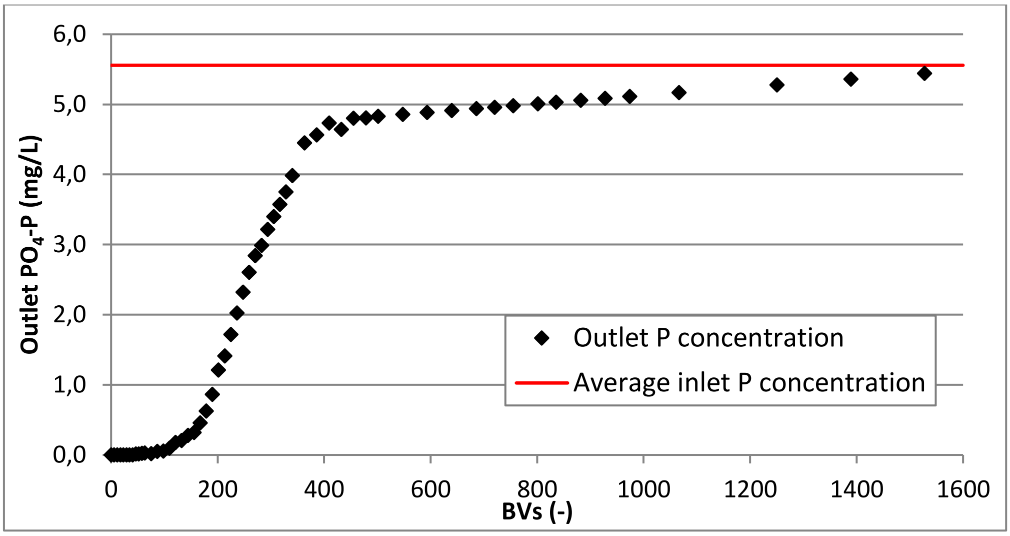

Table 2.4.2 Performances of the breakthrough curve shown in Fig. 2.4.4 after the desorption of the resin bed with a fresh 2% NaOH solution.

	Breakpoint 0.1 mg/L	Breakpoint 0.5 mg/L	Breakpoint 1 mg/L
Bed volume (BV_{resin} , L)		34.7 ± 0.5	
Empty bed contact time (EBCT, min)		5.2 ± 0.1	
Superficial velocity (v_{sup} , m/h)		10.8 ± 0.2	
Bed volumes/h (BV/h, 1/h)		11.5 ± 0.3	
Inlet PO_4-P Concentration (mg/L)		5.5 ± 0.2	
Resin total capacity ($Q_{resin, sat}$, g_{PO4-P}/L_{resin})		2.1 ± 0.2	
Resin total capacity ($Q_{resin, sat}$, $mg_{PO4-P}/g_{dry\ esin}$)		6.8 ± 0.4	
Volume of treated WW ($V_{treated\ WW}/BV_{resin}$, -)	110	173	196
P adsorption yield at i-breakpoint (Y_{ads} , -)	100 ± 4%	98% ± 4%	97% ± 4%
P operating capacity (η_{resin})	29% ± 5%	46% ± 6%	51% ± 5%

P operational capacity is a function of the permitted effluent phosphorus concentration. With compliance to the effluent threshold of 0.1 mg/L (the most likely environmentally significant target for future effluent regulations) the operating capacity resulted to be about 2.0 $mg_P/g_{dry\ resin}$, the 29% of the exhaustive capacity for an average influent P-concentration of 5.5 ± 0.2 mg/L. An increase of 57% in the number of treatable BVs and of 59% in the operating capacity were obtained for the 0.5 mg/L breakpoint respect to the 0.1 mg/L. Whilst much smaller increases of the same parameters (13% and 11%, respectively) were obtained with compliance to the 1 mg/L breakpoint, suggesting no significant advantages to reach such concentration at the outlet. The results obtained were compared with former studies, that used the same media, on the basis of column diameter, bed depth, inlet P concentration, EBCT and Reynolds number. The Reynolds (Re) number, which relates to the characteristic of the flow through the media bed, is defined as:

$$Re = \frac{\rho V D}{\mu(1-\varepsilon)}$$

Where ρ is the density of the water, V is the superficial velocity of the feed solution through the bed, D is the average diameter of the media particles (0.69 mm), ε is the void fraction (0.3, typical of the parent ion exchange media (Ping & SenGupta, 2000). and μ is the dynamic viscosity of the water (0.001 Pa·s). For the current column configuration resulted of 2.96. Martin et al. (2013) conducted experiments with different column diameters to investigate the impact of contactor scale on the efficacy of ferric nanoparticle embedded media for phosphorus removal. It is noteworthy that for a column diameter of 500 mm, 1 m bed depth, an EBTC of 4 min, an inlet P-concentration of 4.7 mg/L and a Re number of 4.11 they obtained a capacity of 6.27 mg_P/g_{media} after 1000 bed volumes had been passed. The former study does not specify the story of the resin used in the column trials (i.e. if and how many times it had been previously used and regenerated), suggesting no notable long-term previous utilization. Therefore, the very similar total capacities obtained let us assume that the proposed process did not negatively attach the resin potential to uptake phosphate and that, even after 55 cycles operated at demonstration scale with actual secondary effluent WW, the removal performances are similar to those obtained with a fresh/new HAIX $Layne^{RT}$ resin.

Petruzzelli et al. (2004) performed some field experiments of the deeply and most largely investigated ion-exchange process for the selective removal of phosphorus, known as the REM NUT® process. They concluded that the main limitation for the extensive application of the process, was the availability of specific anion exchangers for selective removal of phosphate in the typical presence of competing ion that characterized secondary WW effluents. As a matter of fact, with compliance to the 1 mg_P/L breakthrough they obtained a retention capacity averaging 1 g_P/L_{resin} for an inlet P concentration ranging around 6 mg/L. By considering the same breakthrough value, the process object of this study led to a retention capacity doubling that of the REM NUT® process, resulting about 2.1 g_P/L_{resin} and confirming the great potential of the new hybrid ion exchange adsorbent proposed.

One of the main concern regarding the proposed conduction method, namely the repetitive desorption of the only ferric nanoparticle sites by neglecting what is happening on the parent ion exchange media, consisted in the possibility of the resin deterioration through time. Indeed, the accumulation of organic matter and anions on the resin surface through cycles may generate a series of disadvantages such as steric obstruction, the neutralization by multilayer adsorption of the Donnan membrane effect exerted by the fixed positively charged given by the quaternary ammonium and a possible (bio)degradation of the resin (De Kock, 2012). Consequently, the final result would be a drastic reduction of the resin capability to uptake phosphate. For this reason it was important to evaluate the actual performance of the resin by means of a resin performance comparison with previous cycles. Unfortunately, breakthrough curves were not analyzed in the earlier usage of the resin when the demonstration plan was started, therefore two strategies were applied to have an indication of the resin performance after having operated for 50-60 cycles: i) the previous comparison of the process performances (evaluated with the complete adsorption breakthrough curve) with some case studies found in literature – such as the REM NUT process; ii) a comparison with the vergin HAIX Layne^{RT} resin by means of laboratory tests (see Chapter 2.4.5 - *Investigation of the resin performances after the long-term testing in the demonstration plant*).

The main conclusion regarding this first part can be summarized as follows.

- The pilot-scale unit, placed within an existing municipal wastewater treatment plant (population equivalent $< 10{,}000$) and treating actual secondary wastewater effluent from a trickling filter, was successfully operated from cycle 35 to cycle 55.
- The proposed operation method, consisting in the consecutive re-utilization of the desorption solution, has the potential to allow the full control on the effluent quality by defining a limit number of cycles that can be performed with the same regenerant solution on the basis of its pH and P content.
- The consecutive groups of cycles operated showed the possibility to elute the mass of P not desorbed by the multiple-used regenerant by starting a new group of cycles and introducing a new fresh 2% NaOH regenerant solution. Therefore, the total capacity of the resin is restored every time a new series of cycles is started.
- Adsorption and desorption performances were analysed through consecutive cycles. The final process performances are summarized in Table 2.4.3, considering all the 10 cycles and an hypothetic interruption at the 6th cycle:

Table 2.4.3 Final process performances considering a different number of consecutive cycles performed with the employment of the same regenerant solution.

Cycles Performances						
	Total Mass Fed	Total Mass Adsorbed	Total Mass Desorbed	$\mathbf{Y_{ads}}$	$\mathbf{Y_{des}}$	$\mathbf{Y_{proc}}$
10 cycles	396 g PO_4-P	302 g PO_4-P	187 g PO_4-P	**76%**	**62%**	**47%**
6 cycles	241 g PO_4-P	206 g PO_4-P	163 g PO_4-P	**85%**	**79%**	**67%**

*Yads = Mass of P adsorbed / Mass of P fed to the process;
*Ydes = Mass of P desorbed / Mass of P adsorbed.
*Yprocess = Mass of P desorbed / Mass of P fed to the process.

- The proposed process led to the attainment of a final enrichment factor F (defined as the ratio between the final P concentration in the regenerant solution and initial P concentration in the wastewater $F = {C_{P,\ regenerant}}/{C_{P,\ ww\,fed}}$) of 101 and 88, by stopping the process at 6 and 10 cycles, respectively, with significant advantages for the subsequent P recovery by precipitation of calcium phosphate.
- Since desorption resulted to be controlled by pH, it is probable that the decrease in its value below 13 caused the significant drop in the desorption yield occurred at cycle 52.

- A linear correlation was found between the number of BVs that can be treated up to a defined breakpoint (i.e. 1 mg_P/L) and the P concentration in the regenerant solution used to desorb the resin before the adsorption cycle.
- It is also important to consider that the overall mass balance which includes all the groups of cycles operated, remains open and suggests that 25-29% of the mass adsorbed is not desorbed. Combining this fact to the possibility to reset the resin capacity showed by the overlapped breakthrough curves obtained after having desorbed the resin bed with a fresh regenerant, the most likely hypothesis is that part of the mass is accumulating within the column, maybe as precipitate. Notwithstanding, the ferric nanoparticles active sites can be completely regenerated and no pressure drops were detected.

2.4.3 Recovery of calcium-phosphate from the P-rich brine

In addition to the proposal of reusing the same volume of regenerant solution consecutive multiple times in order to obtain a P-rich brine, the second novelty of the proposed process was based on the assumption of the possibility of recycling and reusing the recovered solution after precipitation. In order to develop a cost-effective process this step results crucial, indeed, the result of the downstream process (i.e. the solid final product) represents the revenue which should compensate the operational cost of the process related to energy and chemicals. Therefore, the investigation of the optimal condition to perform the recovery of the final product by the P-rich brine would have required long time and wide attention, especially if we are considered that the aim is a selective precipitation of a target ion dissolved in a solution characterized by the presence of other several numerous organic and inorganic compounds. Indeed, according to some authors who performed a detailed characterization of the 2% NaOH solution used to desorb a resin embedded with ferric nanoparticles, the eluate is characterized by the following compounds: PO_4^{3-}, SO_4^{2-}, Cl, NO_3^-, CO_3^{2-}, Si, Zn, K, Ca, Fe, Zr, Al, Mg and several organic compounds such as humic and fulvic acids (Kalaitzidou et al., 2016; Drenkova-Tuhtan et al., 2017).

On the contrary, for the current study, a complete characterization of the P-rich brine resulted from the process was not performed, making any prediction on precipitation complicated and rather unreliable. The choice of the research group was that of focusing on the possibility of recovered the spent regenerant and recirculated it to the regenerant storage tank for multiple groups of cycles. Therefore, the precipitation of calcium-phosphate was evaluated and investigated not to obtain the most valuable product, but to obtain a recovered NaOH solution with low P and Ca^{2+} contents.

In Fig. 2.4.5 are shown the results of the laboratory test performed to evaluate the time of the reaction and the trend of the P and Ca^{2+} concentrations through time. To illustrate, the results showed that after 1 h the P content resulted of 169 mg/L for the Ca:P molar ratio of 2 and 18 mg/L for the ratio of 3. Therefore, starting with a P concentration of 548mg/L in the regenerant solution it was possible to obtain the reduction in P content (expressed as Mass of P precipitated / Initial mass of P) of 69% with the Ca:P molar ratio of 2 and of 97% with the Ca:P molar ratio of 3, respectively. After 6 hours of reaction, pH was checked and resulted for both the two final solutions around 12.8 ± 0.1, equivalent to that of the starting untreated solution. Without considering any precipitation, the addition of $Ca(OH)_2$ to have a Ca:P ratio of 2 and 3 should have led to an increase in pH of 1.16 and 1.34 respectively. However, since no change in the pH was detected, it is presumable that the amount of OH groups added as $Ca(OH)_2$ reacted as well and precipitated by forming different salts. While calcium resulted around 20±2 mg/L for the ratio of 2 and 45±5 mg/L for the ratio of 3. Thus, suggesting that the excess of calcium fed was necessary to significantly reduce the P content, probably due to several reactions between Ca^{2+} and other compounds. No lower Ca:P ratios were tested because previous experiments conducted by other students revealed the impossibility to substantially reduce the P content without a strong excess of calcium. On the basis of these results both the two tested ratios resulted interesting and were tested at pilot scale to recover the "spent" regenerant solution. In particular, the Ca:P molar ratio of 3 resulted extremely interesting because it led to an almost complete precipitation of phosphate, restoring the total desorption potential of the solution to be recycled. While, the Ca:P molar ratio of 2 showed a lower reduction in P respect to the ratio of 2 but, on the other hand, from an economic point of view, it would allow to reduce the chemicals needed, and therefore the operating cost of the process. Data shown in Fig. 2.4.5. Also in this case the optimal solution could be identified only by an economic evaluation of the process, which, as already explained, goes beyond the scope of this study.

Figure 2.4.5 PO_4-P concentration through time during the laboratory-scale precipitation of calcium-phosphate.

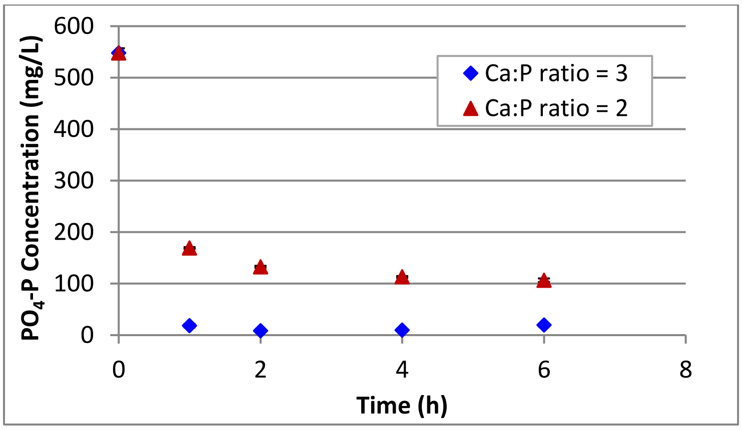

The two experiments were repeated at pilot scale. The spent solution that had been used for the ten consecutive cycles started with fresh 2% NaOH solution illustrated in section 2.4.2 and which had reached a P concentration of 538 mg/L was treated the first time with a Ca:P molar ratio of 2. As for the lab-scale experiments the reaction occurred very fast and after a time of 2 h led a total reduction in the P content of the 54%, resulting in a final concentration of 246 ± 3 mg/L. Calcium resulted of 31 ± 2 mg/L and pH around 12.5. The lower reduction compared to that obtained at lab scale was likely the result of a problem with the mixing. From the 350 L of solution it was possible to recover approximately 2.5 kg of calcium salts.

Once the recovered NaOH reached again the P content of 550 mg/L, it was treated a second time by applying a Ca:P molar ratio of 3. The reaction time was confirmed to be around 2 h and, finally, a solution with concentrations of 11 ± 2 mg/L of PO_4-P and 26 ± 2 mg/L of Ca^{2+} were obtained. In this case, a decrease in pH was observed, too. By treating the whole volume of 350 L, it was possible to recover 3.5 Kg of product. In Fig 2.4.6 are shown the recovered product after being dried and a SEM image of the salt. As expected, the SEM image shows the amorphous structure of the precipitate. Indeed, as previously explained, for this part of the study there was no interest in the identification of the optimal conditions leading to the formation of a crystalline product.

Figure 2.4.6 a) Recovered product after precipitation and filtration; b) SEM image of the recovered calcium-phosphate.

Notwithstanding the product obtained was not yet optimized, it was necessary to validate the process by assessing the possible attainment of a final product in compliance with the Fertilizer regulation (VO (EG)2003/2003). In order to assess the former compliance, a sample of the amorphous calcium phosphate obtained by the two precipitations performed at pilot scale, was sent to an external laboratory to ensure the absence of contaminants respect to its final destination as fertilizer. The organic analytes were selected in accordance as indicative of the types of impurities that could feasibly be present and that may possess an affinity for the precipitated material. Results are shown in Table 2.4.4. Only Cadmium (Cd) and Chromium (Cr) concentrations resulted higher than the limit of law reported by the Italian D. Lgs. 29/2010. While the trace organics resulted below the limit of detection of the method.

Table 2.4.4 Impurities in the recovered calcium-phosphate – analyses performed by a private laboratory.

				First pilot-scale recovery	**Second pilot-scale recovery**
Category	**Analyte**	**Method of analysis**	***Limit of Law (mg kg^{-1})**	**Response mg kg^{-1}**	
Heavy Metals					
	Cadmium (Cd)	WAS049	1.5	< 2.4	< 2.4
	Chromium (Cr)	WAS049	0.5	< 12	< 12
	Copper (Cu)	WAS049	230	< 80	< 80
	Lead (Pb)	WAS049	140	< 24	< 0.24
	Mercury (Hg)	WAS013	1.5	< 0.4	< 0.4
	Nickel (Ni)	WAS049	100	< 12	< 12
	Zinc (Zn)	WAS049	500	72	72
				Response µg kg^{-1}	
Trace Organics	Benzene	GEO56		< 400	< 400
	Nonylphenol	GEO84		< 80	< 80
	Hydrocarbons (PAHs)**	GEO19		< 40	< 40
				Response cfu kg^{-1}	
Coliforms	Total Coliforms	W10		0	0
E. coli	Escherichia coli	W10		0	0

*D. Lgs. 29/2010 (Italy)

** As total of naphthalene, acenaphthylene, fluorene, phenanthrene, anthracene, fluoranthene, pyrene, benzo[a]anthracene, chrysene, benzo[b/k]fluoranthene, benzo[a]pyrene, indeno[123-cd]pyrene, dibenzo[ah]anthracene & benzo[ghi]perylene.

2.4.4 Evaluation of the impact of reusing the regenerant solution after the precipitation of calcium-phosphate

An approach analogous to that used for the evaluation of the impact of reusing the same regenerant multiple times, was applied to evaluate the possibility of recycling and reusing the regenerant solution after the precipitation of calcium phosphate. The volume of “spent” regenerant which had reached a concentration of 538 mg/L was treated with a Ca:P molar ratio of 2 and then recirculated into the 2% NaOH solution storage tank. Before putting back into service, the once “recovered” regenerant, which was finally characterized by a P-concentration of 246 ± 3 mg/L, the dissolved calcium was checked as well. Indeed, a high Ca^{2+} concentration in the regenerant solution could have react with the phosphate adsorbed by precipitating on media surface leading to the irreversible damage of the resin and the impossibility to regenerate and reutilize it. After the precipitation, the concentration of the regenerant resulted of 31 ± 2 mg/L, close to that of the wastewater. Therefore, the solution was used without any further precaution or treatment. Moreover, pH was checked after the precipitation and resulted around 12.6. Hence, it was adjusted to the value of 13.2 ± 0.2 by the addition of 0.8 kg of solid NaOH, in order to ensure an effective desorption.

As shown in Fig. 2.4.7 the regenerant solution went through four consecutive cycles (56, 57, 58 and 59, respectively) before reaching again a concentration above 500 mg_P/L. The 350 L of solution were treated a second time by adding $Ca(OH)_2$ with a Ca:P molar ratio of 3, which allowed to obtained a solution with a PO_4-P and Ca^{2+} of 11 ± 2 and 26 ± 2 mg/L, respectively. pH needed to be adjusted due to a decrease to 12.4 during precipitation. After the NaOH salt addition of 1.2 Kg it resulted of 13.3 ± 0.1. The regenerant solution recovered twice was then used to perform seven consecutive cycles. Long breakthrough curves were performed as well to evaluate and compare key parameters as the shape of the curve and the resin utilization efficiency (= resin operating capacity) with the previous cycle performed after having desorbed with a fresh 2% NaOH solution.

Figure 2.4.7 Consecutive cycles performed with the same regenerant solution: the first 4 with regenerant recovered once and, the last 7 with the regenerant recovered twice. On the x-axis are represented both the total number of bed volumes fed to the process and the corresponding total number of cycles performed by the column. The primary y-axis referred to the outlet P concentration (blu indexes) while the secondary y-axis referred to the P concentration of the regenerant solution used to desorb the resin bed before the adsorption breakthrough curves (red and black circles).

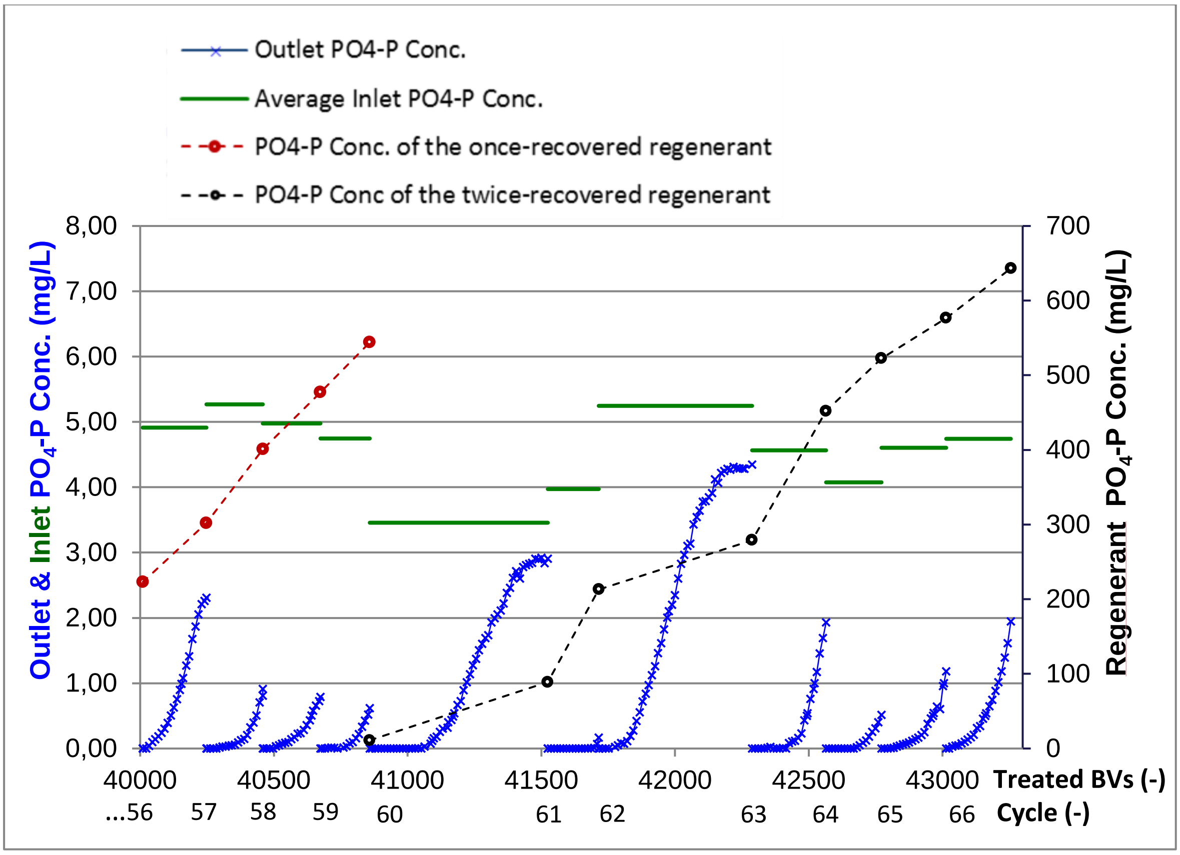

Comparison between cycles was made difficult by the variable inlet P concentration which ranged between 5.27 and 3.46 mg/L. Table 2.4.5 is therefore shown not to allow a comparison between the consecutive cycles, but to clarify the potential of the system even with oscillating operating conditions, such as a variable inlet P concentration. According to Zhao and SenGupta (1998), adsorption showed great potential especially for those wastewater treatment plant decentralized and treating a relatively low population equivalent (minor than 10,000). These sewage works, due to their small size are generally characterized by variable flow regimes and fluctuating concentrations depending on the time of day and population’s habits. Therefore, for the described situation, the technology must be able to face variations of the inlet concentration characterized by an hourly-dependent time. To illustrate, Table 2.4.5 shows that with the exception of cycle 56 (visibly different from the others) and of cycles 60 and 62 (where the low adsorption yield is due to the longer breakthrough performed) the adsorption yield resulted always higher than 90%. Moreover, it is noteworthy that, despite significant variability of the P inlet concentration during the same adsorption breakthrough curve, Fig 2.4.7 gives an important demonstration of the fact that no elution of P, due to a decrease in the inlet P concentration and, hence, of the changing equilibrium between the solid and the liquid phase concentration, occurred.

Table 2.4.5 Performances of the consecutive cycles performed with the recovered regenerant solution showed in Fig. 2.4.7.

Total Cycles	Cycles with the same regenerant	BV treated	Average Inlet P conc. (mg_P/L)	Final P conc. (mg_P/L)	Y_{ads}	Y_{des}
56	*1*	*238*	*5 ± 0.4*	*3.6*	*82%*	*92%*
57	*2*	*211*	*4.9 ± 0.3*	*2.3*	*97%*	*89%*
58	*3*	*215*	*5.3 ± 0.2*	*0.9*	*96%*	*66%*
59	*4*	*184*	*5.0 ± 0.3*	*0.8*	*97%*	*92%*
60	*1*	*665*	*4.8 ± 0.2*	*0.6*	*66%*	*82%*
61	*2*	*191*	*3.4 ± 0.8*	*2.9*	*100%*	*88%*
62	*3*	*573*	*3.9 ± 0.2*	*0.2*	*55%*	*100%*
63	*4*	*276*	*5.2 ± 0.3*	*4.3*	*92%*	*61%*
64	*5*	*207*	*4.7 ± 0.2*	*1.9*	*98%*	*66%*
65	*6*	*242*	*4.1 ± 0.9*	*0.5*	*95%*	*64%*
66	*7*	*242*	*4.7 ± 0.2*	*1.2*	*89%*	

*Yads = Mass of P adsorbed / Mass of P fed to the process;
*Ydes = Mass of P desorbed / Mass of P adsorbed.

Unfortunately, the variable inlet P concentration impeded also the comparison with the group of consecutive cycles started with a fresh 2% NaOH solution aimed at evaluating the possibility and the impact of recycling and reusing the same regenerant. However, the comparison was performed by selecting some of the performed breakthrough curves.

Therefore, in Fig. 2.4.8 were plotted only those cycles with an inlet P concentration close to the average inlet P concentration characterizing the previous series of cycles started with a fresh regenerant solution described in section 2.4.2 (5.3 ± 0.3 mg/L). Indeed, the average P content for the cycles plotted with the black circles resulted of 4.9 ± 0.2 mg/L. Fig, 2.4.8 showed the number of bed volumes that can be treated up to the 1 mg/L breakthrough versus the P concentration of the regenerant solution used to desorb the resin bed before the adsorption breakthrough curve was performed. The red dotted line represents the linear correlation previously identified in the study of the consecutive cycles started with a fresh regenerant solution.

Unexpectedly, the former trend was not confirmed, instead, the number of bed volumes treatable through cycles up to the 1 mg/L breakpoint remained rather stable despite the increasing P concentration in the regenerant solution. The average number of the treated BVs resulted of 220 ± 21, similar to the value obtained after having regenerated with a fresh regenerant solution (196 BVs). Moreover, as shown in Fig. 2.4.7 consecutive adsorption breakthrough curves did not lose the typical sigmoidal shape by becoming steeper from the first bed volumes, and allowed to treat several bed volumes until the target ion was leached at low concentration.

Figure 2.4.8 Number of BVs that can be treated up to the 1 mg/L breakpoint versus the PO_4-P concentration in the regenerant solution used to desorb the resin bed before the adsorption cycle

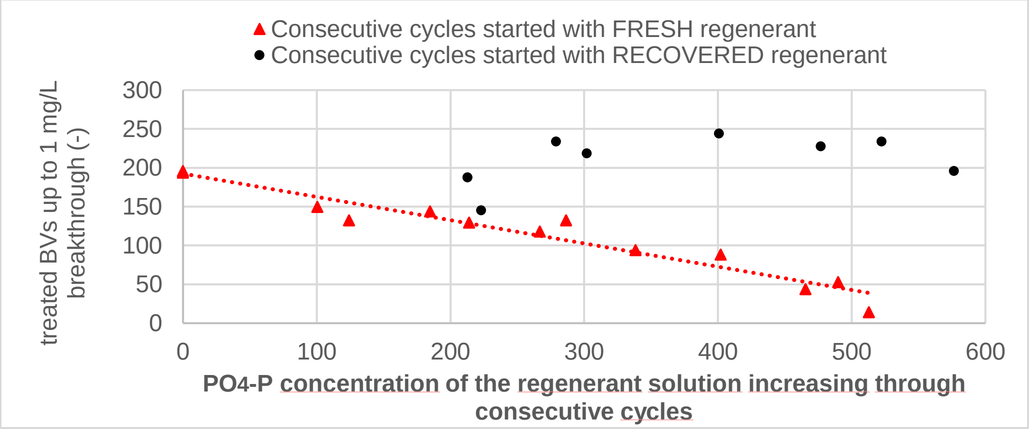

This can be understood also by overlapping the adsorption breakthrough curves versus the number of BVs fed. Hence, Fig 2.4.9 a) clarifies as the process shows an extraordinary reproducibility trough cycles despite the multiple employment of the regenerant solution. It is also important to highlight that the three adsorption breakthrough curves here represented with black indicators, and characterized by performing after a regeneration with the recovered regenerant (with P content of 302, 401, 477 mg/L, respectively), are really close to the red curve obtained after renerating with fresh NaOH solution.

In the previous chapter the main responsible for the degeneration of the process performances through cycles was identified as the impossibility to perform a successful desorption of the resin bed with the consequence reduced availability of active sites for the following adsorption step. The drop in desorption yields after 6 cycles was mainly attributed to the decrease in pH, however it was not clear if the high P content of the regenerant played any role. The results showed in Fig. 2.4.8 suggest that desorption performance does not depend on the P content of the regenerant solution and that pH is the only controlling-factor. After the 2 precipitations of calcium-phosphate, the solution pH was adjusted to 13.2 (after the first recovery) and to 13.3 (after the second recovery); however, in spite of the consecutive desorptions performed up to cycle 66, its value was never detected below 13 after each regeneration step. The fact that pH did not decrease again for other 11 cycles may be due to the fact that the concentration of other organic and inorganic compounds different form phosphate and present in the regenerant solution has increased as well through the several cycles previously performed (the 10 cycles of section 2.4.2). These compounds, that were sorbed by the ion-exchange parent media and then outcompeted by OH groups during the first desorptions, could have finally reached a liquid equilibrium concentration with the solid-phase concentration on the parent media. However, this remains still an hypothesis, since analysis to investigate this phenomenon could not be performed.

Fig. 2.4.9 b) and the relative Table 2.4.6, allows a direct comparison between the complete breakthrough curves obtained with fresh NaOH solution (elaborated in section 2.4.2) and cycle 62, characterized by analogous inlet P-concentrations. The main difference between the operating parameters of the two trials was the concentration of the regenerant solution used to desorb the resin bed before the adsorption cycle. Consistently with what illustrated before the two curves resulted in not significant different operating performances and confirmed the reproducibility of the process performances even after 10 consecutive employments of the same recovered regenerant solution.

Figure 2.4.9 a) Consecutive breakthrough curves operated after regenerating with the same regenerant solution (recycled after precipitation. b) Overlapped breakthrough curves performed after regenerating with a fresh 2% NaOH solution (red indexes) and after regenerating with a twice-recovered regenerant solution (black indexes).

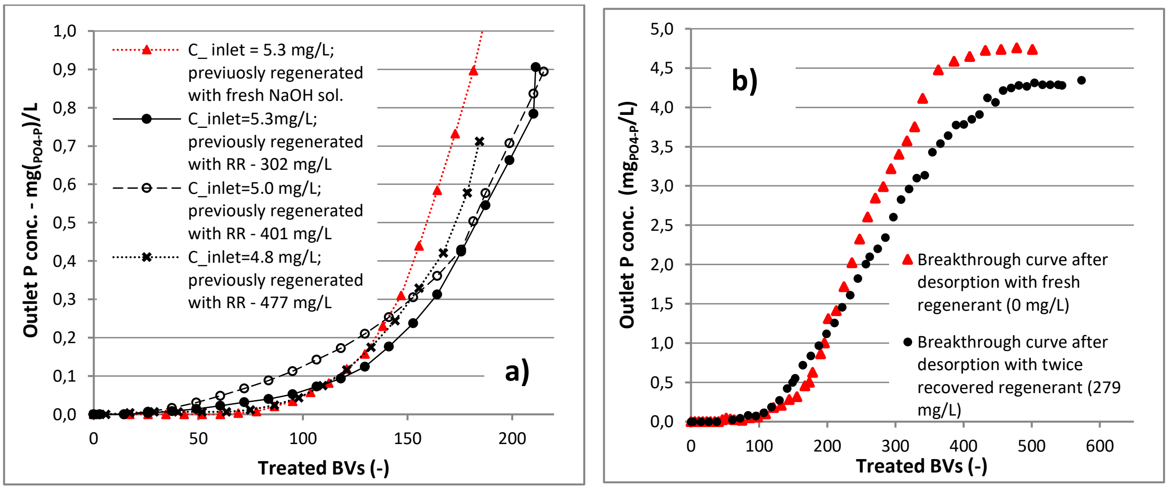

Table 2.4.6 Operating and performances parameters of the breakthrough curves shown in Fig. 2.4.10 b).

	Ads. cycle after regeneration with fresh regenerant	Ads. cycle after regeneration with recovered regenerant
Bed volume (BV_{resin} , L)	34.7 ± 0.5	
Empty bed contact time (EBCT, min)	5.2 ± 0.1	
Superficial velocity (v_{sup} , m/h)	10.8 ± 0.2	
Bed volumes/h (BV/h, 1/h)	11.5 ± 0.3	
Inlet PO_4-P Concentration (mg/L)	5.5 ± 0.2	5.3 ± 0.3
Resin total capacity ($Q_{resin, sat}$, g_{PO4-P}/L_{resin})	2.1 ± 0.2	2.3 ± 0.4
Resin total capacity ($Q_{resin, sat}$, $mg_{PO4-P}/g_{dry\ esin}$)	6.8 ± 0.4	7.5 ± 0.7
0.1 mg/L breakpoint - Volume of treated WW ($V_{treated\ WW}/BV_{resin}$, -)	110	95
0.1 mg/L breakpoint - P adsorption yield (Y_{ads}, -)	100 ± 4%	100% ± 8%
0.1 mg/L breakpoint - P operating capacity (η_{resin})	29% ± 5%	22% ± 4%
1 mg/L breakpoint - Volume of treated WW ($V_{treated\ WW}/BV_{resin}$, -)	196	187
1 mg/L breakpoint - P adsorption yield (Y_{ads}, -)	97% ± 4%	95% ± 8%
1 mg/L breakpoint - P operating capacity (η_{resin})	51% ± 5%	41% ± 6%

Concluding, the former results suggested that the regenerant solution could be recovered and recycled for other groups of consecutive cycles with any particular concern or disadvantages. On the contrary an improvement in the desorption step allowed the process to settle on reproducible runs, with the extended potential to fully predict and control the process development.

pH resulted the main controlling factor of the desorption performances; on the contrary the P content of the regenerant solution seemed not to impact significantly the desorption and the following adsorption step.

A detailed characterization of the regenerant solution before and after the precipitation of calcium phosphate, so as after each desorption step, would have probably provided important information, however due to the lack of time it could not be performed yet, and will be objective of further investigation by the research group of Cranfield University.

The current section is the first case study investigating at a pilot-scale the possibility of recovered the final product by a selective precipitation from the P-rich brine and recirculate the solution for multiple groups of consecutive cycles. Indeed, the cost of chemicals and the management of the exhausted brine disposal represent the major drawback of the ion-exchange technology (Bunce et al., 2018). This study proposed a novel approach to this problem statement and proved its applicability and reliability on a demonstration plant, placed in an existing sewage works and treating 10 m^3/d of actual secondary wastewater. Moreover the proposed process showed great potential to face the variability of inlet concentration characterizing small scale MWWTP as the Cranfield WWTP.

2.4.5 Investigation of the resin performances after the long-term testing in the demonstration plant

The positive results obtained after having performed 66 adsorption/desorption cycles at the demonstration plant encouraged a deeper investigation of the resin which had showed an extraordinary mechanical force, durability and resistance to degradation. The aim of this last part was to investigate the status and the performance of the resin, which had been working for almost one year and a half treating more than $1,02 \cdot 10^4$ bed volumes of secondary effluent wastewater, by comparing it with the same HAIX Layne resin (bought from the same supplier) at its first usages/runs. This data were essential to assess if the operating approach with whom the adsorption/desorption cycles at the pilot plant were conducted had negatively conditioned the evolution of the process performances. Indeed, no process performances of the plant at its earliest cycles, as soon as it was started, were noticed and investigated. Hence, we did not have any ideas of the process performances evolution through the years, except for the last 20 cycles.

To quantify the expected difference in performance would have provided the real impact due to the decision of performing the desorption steps with a solution of sodium hydroxide to regenerate only the ferric nanoparticles and not the ion exchange sites composed of quaternary ammonium functional groups. As a matter of fact, 66 cycles were performed by completely neglecting the ion-exchange activity that we know deeply interact with many different compounds, especially with organic matter (Tanboonchuy et al., 2012; Weng et al. 2008; Yan et al., 2016; Antelo et al., 2007; Borggaard et al., 2005). The drawbacks expected from this choice were that through several cycles inorganic anions and organic compounds would have accumulated on the surface of the resin with several disadvantages such as steric obstruction, the neutralization of the Donnan membrane effect (exerted by the fixed positively charged given by the quaternary ammonium) (Weng et al., 2008) and a possible degradation of the resin. With the final result of disabling the total resin capacity and consequently reducing the effectiveness of phosphorus removal.

Moreover, the second objective of this group of experiment was to evaluate the advantages of performing a desorption with a solution of both sodium hydroxide and sodium chloride, in order to elute also all those compounds attached to the parent media and resetting their relative negative effects. According to previous studies, to contemporary desorb the two different sorption sites a solution of 2% NaOH and 5% NaCl was used (Pan et al., 2009a; Blaney et al., 2007; Sengupta & Pandit, 201; Martin et al., 2009).

In order to answer the above research question and to have a complete overview on the resin performances, the following three forms of the resin were tested: i) new resin, ii) the resin from Cranfield pilot plant regenerated in accordance with the long-term process with only sodium hydroxide (w/v 2% NaOH), iii) the resin from Cranfield pilot plant regenerated with a solution of sodium hydroxide and sodium chloride (w/v 2% NaOH, 5% NaCl) in order to elute as much as possible and free the ion exchange sites. Hereafter these three forms will be called virgin resin, resin-1 and resin-2, respectively.

2.4.5.1 Adsorption kinetic tests

Kinetic tests were performed to evaluate the true equilibrium time to be applied in the adsorption batch isotherms. Experimental data are plotted in Fig. 2.4.10 in terms of removal efficiency versus time. Where the removal efficiency is defined as the ratio between the mass of P adsorbed at any time t and the mass of P fed at time zero ($M_{ads,t}$ / M_{fed}). Data showed that after 20 min the media had adsorbed 95% and 84% of the mass of P fed, for the trials with synthetic P solution and real wastewater, respectively. After 40 min the removal efficiencies were respectively of 99.1% and 96.7%. Indeed, the test with synthetic solution took 40 minutes until the P removal set in the vicinity of the unit (>99%); while the test with actual wastewater was a bit slower and overcame the 99% removal efficiency after 1.5 h.

Consistently with the work of Martin et al. (2017), who coupled the adsorption kinetic tests with mass spectrometry, the adsorption of phosphorus using the Layne^{RT} media was very rapid. However they found no significant difference between the model solution and the actual wastewater trials (data elaborated using an ANOVA F-test, which returned a p-value < 0.5). On the contrary, in our case, the first point at 20 minutes suggested a retardation of P adsorption for the actual WW respect the synthetic P-solution. Thus, indicating that other competing ions or solid components in wastewater may influence the overall phosphorus uptake rate.

The P adsorption kinetic data were fitted with several kinetic models (first order, second order, intra-particle and film diffusion equations) by non-linear regression, using the approach detailed in M&M. The intra-particle diffusion model was ruled out because its correlation coefficient (R^2) for the present experimental data was too small (< 0.5), resulting unable to describe the adsorption kinetic data for the entire experimental period.

This contrasts with commonly used adsorbents characterized by a macroporous structure, such as activated carbon, where intra-particle diffusion is reported to dominate as rate-controlling mechanism (Cooney, 1998). On the contrary the film-diffusion model resulted in a well-described kinetic of P uptake. Moreover, based on R^2 and χ^2, the kinetics of phosphate adsorption on the HAIX Layne media can be satisfactorily described by either of PFO and PSO equations in their nonlinear forms. The equations' constants of the three models satisfactory applied are summarized in Table 2.4.7. R^2 values resulted very close to 1 and the chi-squared (χ^2) values close to 0 (meaning that data obtained with the model are really close to experimental data). The good correlation of both the PFO and PSO equations is probably the result of the complex system under investigation, where different adsorption mechanisms are playing simultaneously, including ion-exchange and ligand-exchange processes. Moreover, data were monitored with an extended time interval to accurately describe the phosphate uptake.

As a matter of fact, Tran et al. (2017) suggested that the measurement of adsorption kinetics should be started at an initial time of less than 2 min to truly understand the process. However an accurately modelling and understanding of the rate-controlling mechanisms went beyond the scope of the trial, primary aimed at identifying the true equilibrium time and assess the duration of the adsorption batch isotherms. On the basis of the results obtained and on the work of other researchers, the equilibrium time was fixed at 6 h.

Figure 2.4.10 Kinetic test for phosphate adsorption with synthetic P-solution and actual wastewater spiked with phosphate salts maintaining the pH. Removal efficiency versus time.

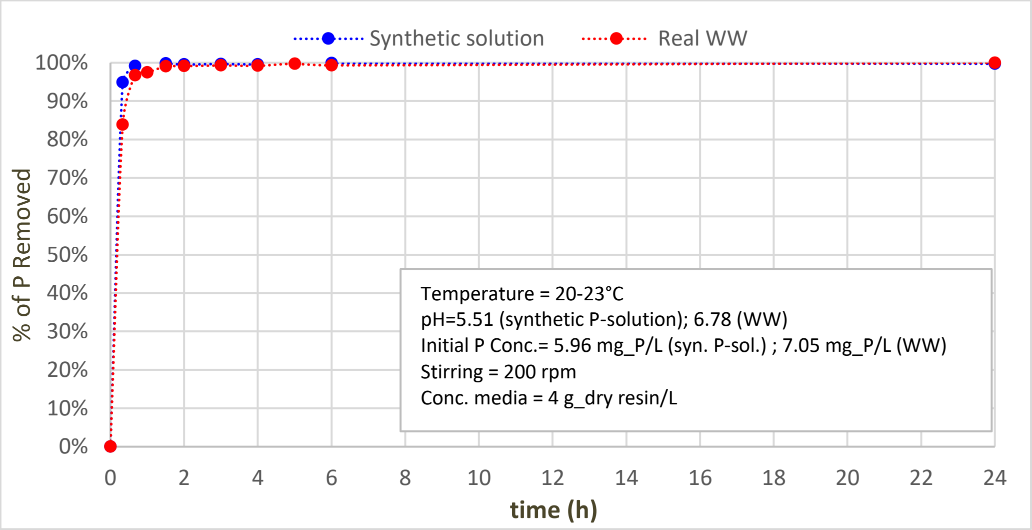

Table 2.4.7 Model and parameters used to fit the experimental data of the batch kinetic tests performed with synthetic P solution and actual wastewater.

Model	Parameters	Kinetic test with synthetic P-solution	Kinetic test with actual ww
PFO equation	k_1 (1/min)	0.1518	0.0924
	q_e ($mg_P/g_{dry\ resin}$)	1.49	1.74
	R^2	0.9999	0.9996
	χ^2	3.0 10^(-5)	6.0 10^(-4)
PSO equation	k_2 (g/mg_P min)	0.576	0.164
	q_e ($mg_P/g_{dry\ resin}$)	1.63	1.77
	R^2	0.9997	0.973
	χ^2	4.0 10^(-4)	5.0 10^(-3)
Film diffusion equation	k_{FD}	0.148	0.09
	R^2	0.9999	0.9991
	χ^2	7.0 10^(-5)	5.0 10^(-4)

2.4.5.2 Adsorption batch isotherms

Adsorption isotherms for phosphate (P) were performed both with a synthetic P-solution and with actual wastewater effluent from the municipal wastewater treatment plant (MWWTP) of Bologna. In order to obtain resin-1 and resin-2, a desorption batch test was performed before the adsorption isotherms. The 2% NaOH solution desorbed 4 ± 0.1 $mg_P/g_{dry\ resin}$ and 6 ± 1 $mg_{COD}/g_{dry\ resin}$; while the 2% NaOH + 5% NaCl solution desorbed 4.6 ± 0.2 $mg_P/g_{dry\ resin}$ and 97 ± 5 $mg_{COD}/g_{dry\ resin}$. From these results it is clear the role played by NaCl, responsible for the massive elution of organic matter that, on the contrary, the 0.5 M NaOH was not able to outcompete. However, the mass of P desorbed did not change significantly, indicating that phosphate is almost completely adsorbed by those active sites that can be regenerated by switching the pH to the alkaline value of 13. The virgin resin and the two resin obtained after the pre-treatment (resin-1 from the desorption with only NaOH and resin-2 with NaOH + NaCl) were tested together first by means of adsorption batch isotherms with a P-synthetic solution.

Results are shown in Fig. 2.4.11 in terms of solid ($C_{s,eq}$) and liquid ($C_{L,eq}$) phase equilibrium concentrations. As expected the isotherm performed with resin-1 allowed for lower concentrations in the solid phase, due to the less number of available sorption sites. However, if we consider the first point (the only one with $C_{L,eq}$ below 5 mg_P/L) it resulted quite steep and close to those of the other two resins. Moreover, if we look at virgin resin and resin-2 we can observe that the two isotherms are almost overlapped until the point around 80 mg_P/L and that the trend of the interpolating model is mostly defined by the last points around 180 mg_P/L, which, however, are characterized by a significant relative error (25-50%). This finding resulted of high interest since suggested two key elements. On one hand, the organic matter sorbed to the ion exchange resin surface was proved to clearly attach the resin performances by reducing the availability of exchange sites; specially as the concentration of the target compound in the wastewater increases and more active sites are necessary for adsorption. However, on the other hand, resin-2's performances demonstrated that it was possible to completely restore the resin potential capacity by simply performing a regeneration of the resin bed with the previously used NaOH and NaCl solution. Notwithstanding it must be considered another important aspect, indeed the investigated process has been developed to remove ortho-phosphates from secondary wastewater effluent, hence, from streams characterized by concentration of PO_4-P ranging between 1 to 15 mg/L.

By considering only the first part of the isotherms, namely the most significant from the process point of view, resin-1 adsorbed 7.7 ± 0.3 $mg_P/g_{dry\ resin}$ versus the 9.9 ± 0.3 $mg_P/g_{dry\ resin}$ adsorbed by the virgin resin (both were started with an initial concentration in the liquid phase of 10.0 ± 0.2 mg_P/L). It is therefore remarkable that, after 66 cycles performed in a demonstration plant, the resin still shows a capability to uptake phosphate only 20% lower than that exerted by the virgin resin.

In Table 2.4.8, are shown the modelling parameters of the model used to interpolate the data. The model which showed the highest R^2 for all the three isotherms was the Freundlich model, and hence is also displayed in Fig 2.4.11. The modelling of the experimental data was limited to Freundlich and Langmuir since the scope was not the identification of the best fitting model between the wide numerous equations available in literature, instead, it was the possibility to satisfactory interpolate the same equilibrium point for the six isotherms performed and to allow a comparison (Table 2.4.8). Moreover, Langmuir and Freundlich models are the most widely used in literature on adsorption by metal (hydr)oxides.

Figure 2.4.11 PO_4-P adsorption isotherms with synthetic P-solution solution: experimental data and Freundlich model. The red and black markers represent the performance of the resin which undertook 66 cycle in the Cranfield pilot-plant and which was regenerated with two different solutions; while the blu marker represent the same resin but in its virgin (unused) form.

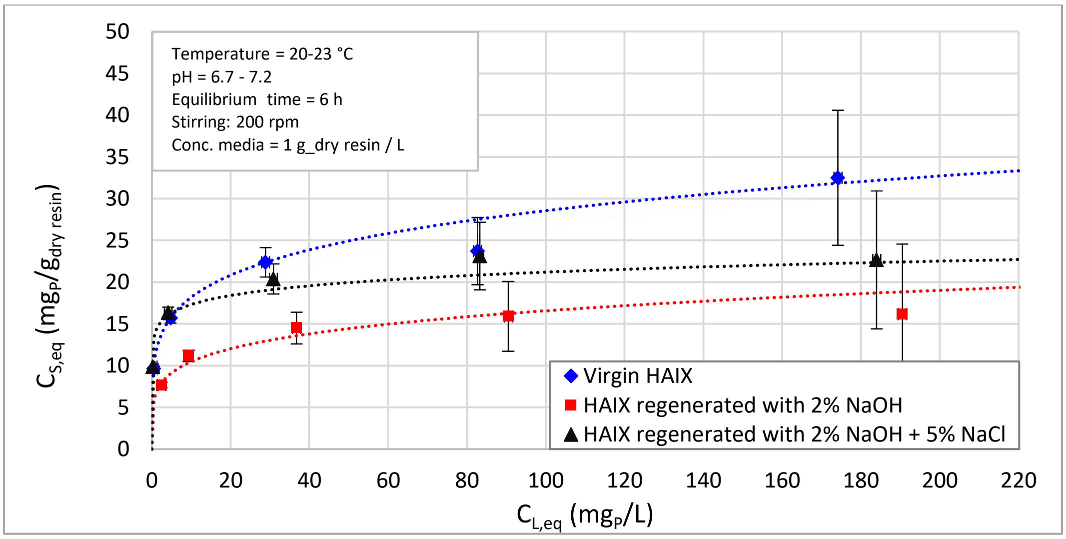

Data obtained with isotherms performed with synthetic P-solution allowed to achieve interesting outcomes, however they lack two fundamental effects played by the presence of competing ions and by the wastewater matrix, respectively. For matrix effect is meant the effect of several background species, including cations (such as Ca^{2+} and K^{+}) and different organic compounds (such as humic and fulvic acids) previously proved to significantly interact with ortho-phoshates (Tanboonchuy et al., 2012; Weng et al. 2008; Yan et al., 2016; Antelo et al., 2007; Borggaard et al., 2005; Wang et al., 2015). Adsorption isotherms with actual wastewater effluent were therefore performed for the same three resins. Results are shown in Fig. 2.4.12, always in terms of solid and liquid phase concentrations at equilibrium and with the relative best fitting models (Frendlich model).

Figure 2.4.12 PO_4-P adsorption isotherms with actual municipal wastewater effluent (from "IDAR" work) spiked with phosphate salts: experimental data and Freundlich model. The red and black markers represent the performance of the resin which undertook 66 cycle in the Cranfield pilot-plant and which was regenerated with two different solutions; while the blu marker represent the same resin but in its virgin (unused) form.

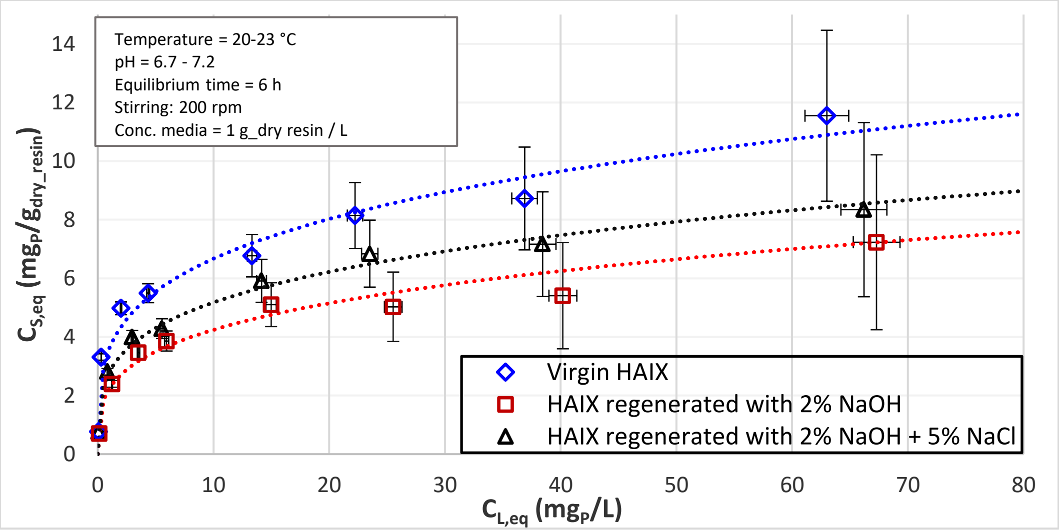

The isotherms with real wastewater covered a more limited range of liquid concentrations, due to the fact that phosphate was spiked in actual municipal wastewater. Thus, the addition of high concentration of phosphate resulted impossible since it led to the formation of precipitate. However, as explained before, from the process point of view the most interesting part of the isotherms was that close to actual concentrations of secondary effluent (<15 mg/L). Isotherms were therefore performed up to concentrations that guaranteed no modification of the solution's matrix and of its effect from one point to another.

As expected, the first fact came out with the experiment was that the solid concentrations obtained at equilibrium were lower than those resulted by using a P synthetic solution. Hence, the presence of competing ions and the effect of the complex wastewater matrix resulted to negatively affect phosphate adsorption. This finding is in strict compliance with the study of Pan et al. (2009a) on the same type of resin (ArsenX^{np}). Indeed, they proved that, for a given solution with an initial P concentration of 10mg/L, an increase in the sulphate background concentration from 0 to 100 mg/L led to a drastic drop of phosphate adsorption: approximately 58%. In our case the background concentration of sulphate encountered an analogous increase, rising from 0 mg/L of the synthetic P solution, to the 104±10 mg/L of the actual wastewater. Moreover, by looking at those points with a $C_{L,eq}$ below 10 mg/L it is interesting to note that the solid phase concentrations of resin-1 and resin-2 are really close. This translates into a conclusion highly consistent with what can be found in literature (Blaney et al., 2007; Martin et al., 2017). Namely, even though the regeneration with 5% NaCl had released the compounds attached to the parent media making the ion-exchange sites available again, in the presence of high concentration of competing ions (most of all, sulphate) that type of site is not able to selectively remove phosphate, which is outcompeted by other compounds with higher affinity for the quaternary ammonium functional group.

Table 2.4.8 Freundlich and performance parameters calculated for the two types of isotherms performed.

Resin	Isotherms with synthetic P-solution				Isotherms with actual municipal wastewater			
	Freundlich parameters			*$C_{S,eq,calc}$ with $C_{L,eq}$=5.5mg/L ($mg_P/g_{dry\ resin}$)	Freundlich parameters			*$C_{S,eq,calc}$ with $C_{L,eq}$=5.5mg/L ($mg_P/g_{dry\ resin}$)
	$K_{F,P}$ ($L/mg_{dry\ resin}$)	n_P (-)	R^2		$K_{F,P}$ ($L/mg_{dry\ resin}$)	n_P (-)	R^2	
Virgin resin	11.6±2.1	5.1±0.9	0.984	16.2	3.71±1.0	3.75±1.7	0.973	5.9
Resin reg. with 2% NaOH	7.6±1.2	6.5±1.6	0.97	9.9	2.23±0.49	3.59±0.9	0.965	3.6
Resin reg. with 2% NaOH + 5% NaOH	13.0±1.7	8.4±2.4	0.995	15.9	2.81±0.37	3.67±0.6	0.988	4.4

* $C_{S,eq}$ calculated by interpolation with the Freundlich parameters shown in the table at the average inlet concentration characterizing the Cranfield pilot-plant process.

Further considerations can be taken into account by comparing the values of $C_{S,eq}$ (shown in Table 2.4.8), calculated at the average concentration characterizing the Cranfield pilot plant process (5.5 mg/L) by interpolating the experimental data with the Freundlich parameters found. Indeed, looking at the isotherms with synthetic P-solution the solid phase concentration of resin-1 resulted 39% and 38% lower respect that of the virgin resin and resin-3, respectively. Hence, what we can concluded from these data is that the 9.9 mg/g of P adsorbed by resin-1 are only due to that part of ferric nanoparticle sites still reachable and available. Moreover, we know that the presence of the compounds attached to the parent media contributes for an average total P-uptake reduction of about 38.5%. In the case of synthetic P-solution it can not be defined if the higher solid phase concentration for the virgin resin and resin-2 is mainly due to the direct ion-exchange adsorption of phosphate by the quaternary ammonium groups available, or, differently, is due to the obstruction of the ferric nanoparticles sites' by the 97 ± 5 $mg_{COD}/g_{dry\ resin}$ present on the media surface. Indeed, as previously explained, the presence of these compounds reduce the Donnan membrane effect primary responsible for the active sites exposure to higher anions' concentrations and, therefore, leading to higher adsorption capacities.

Further information can be found in the isotherms with actual wastewater. In this case the difference between the $C_{s,eq}$ of the virgin resin and resin-1 was confirmed of 39%, in spite of a marked decrease in the total mass of P adsorbed. While $C_{s,eq}$ of resin-1 resulted of 18% minor than that of resin-2. These outcomes suggested a more complicated explanation. The 18% reduction from resin-2 to resin-1 can be only due by the presence of accumulated compounds on the surface resin with all the consequent negative impacts previously explained. Indeed, resin-1 and resin-2 are exactly the same resin (taken from the P recovery column of Cranfield pilot plant), which has gone through the same long operating time and whose only difference is the undertaken pre-treatment with different regeneration solutions. Meanwhile, the difference between resin-2 and the virgin resin ($C_{s,eq}$ of 4.4 and 5.9 mg/g, respectively) resin can only lay on a deterioration of resin-2 occurred through time. As a matter of fact, it is possible that some ferric nanoparticles are no more available due to chemical reactions, transformations during aging or that some ferric nanoparticles have been released and lost (Martin et al., 2009). This difference in performance between resin-2 and the vergin resin was not detectable with the synthetic P-solution, since the less availability of Fe groups could be easily veiled by the large amount of ion-exchange sites completely available.

Concluding, according to the data it may be assumed that in the case of equilibrium with actual wastewater, the 39% reduction of the solid concentration of resin_1 respect to the virgin resin can be attributed for a 21% to the presence of accumulated compounds on the resin surface and, for a 18%, to a resin deterioration occurred during the long operating time in the demonstration plant. It must be highlighted that the above comparison has been made for the environmentally significant concentration of 5.5 mg_P/L, but it could be performed also for a different concentration.

From this first set of experiments the resin coming from the Cranfield pilot-plant has shown performances lower compared to that of the virgin resin. The regeneration of the media with a NaOH and NaCl solution allowed to rise the resin performance of approximately 22% in terms of solid phase concentration in equilibrium with a representative P concentration of 5.5 mg/L and in the presence of typical high contents of several background organic and inorganic species characterizing a municipal wastewater effluent. However, data provided by laboratory batch tests were not sufficient to define if, the introduction of a desorption step to regenerate the ion exchange parent media too, would have enhanced phosphate adsorption in a measure necessary to justify the additional economical costs of the operation. As a matter of fact, the answer is always related to an economical analyses of the process which takes into account the benefits and cost related to the introduction into the process of a further step involving the purchase of chemicals, the treatment and the disposal of additional highly concentrated streams and the operational costs related to the operation. To try answering this question and to add a further part for a complete and deep economical evaluation scheduled in the early future, some continuous flows test were conducted to quantitatively evaluate the advantages connected to the sodium chloride regeneration of the resin bed.

2.4.5.3 Lab-scale continuous breakthrough tests

Continuous-flow breakthrough tests concluded the laboratory tests aimed at comparing the resin performances of the long-tested HAIX Layne^{RT} resin taken from the Cranfield pilot-plant with the aforementioned resin bought new from the same supplier. The following trials were performed with a column of 13 mm–internal diameter and a total length of 1 m. The disadvantages and the advantages of performing breakthrough tests with a diameter size so reduced are explained in the following parameter, aimed at clarifying why that column was chosen and used for the following experiments.

2.4.5.3.1 Fluid-dynamic analyses of the columns packing

The fluid dynamic behaviour of two beds with the same 94 cm bed height and different diameters (2.7 and 1.3 cm, respectively) was investigated to compare advantages and disadvantages of the two systems. For this scope, conventional frontal analysis tests were conducted, characterized by fluxing DI water after having equilibrated the column with a 0.5M NaOH solution.

For the first column with a 2.7 cm diameter, three tests were conducted at different superficial velocities: 3.35, 7.06 and 10.53 m/h. The latter corresponding to an EBCT of 5.4min, specifically close to that applied in the continuous adsorption breakthrough tests. The average effective porosity (ε) of the three tests resulted equal to (76 ± 3)%, with a rather good packing quality. Indeed, the average asymmetry factor of the retention time distribution curve was close to 1 (1.0 ± 0.15) and the reduced plate height (60 ± 4), even if quite high, fell in the typical range of columns packed with adsorption resins. Whereas, for the column with a diameter of 1.3 cm, all the three tests conducted at different velocities (the same used for the previous column) revealed a multi-pick signal at the outlet of the column. Thus, meaning that preferential fluid pathways and challenging were present. Indeed, the conductivity profiles detected at the outlet were consistent for the three superficial velocities tested and led to the identification of two distinct picks characterized by a first mini-pick with an average maximum height (78 ± 5)% lower than that of the main pick and with an average hydraulic retention time (HRT) (47 ± 2)% earlier than that characterizing the main flow pattern. Since the presence of two picks, for the fluid dynamic trials with the 1.3cm-column diameter the elaboration in terms of asymmetry factor and reduced plate height was meaningless and, therefore, not performed. It must be clarified that little irregularities in the flow pattern due to the lowering of the diameter from 2.7 to 1.3 cm was expected and, for this reason, a comparison with the fluid dynamic behaviour of the 2.7 cm diameter column was performed. Fig. 2.4.13 shows the overlapped cumulative retention time curves for the two columns, in terms of dimensionless conductivity (normalized by the average conductivity of the trace solution) versus dimensionless time (actual time/HRT).

It is well known that, from a scale-down point of view, to ensure partial flow pattern similarity between trials with different diameters, a practical concern related to the column diameter as a function of the media size must be considered. As a matter of fact, to minimise the impact of the wall the diameter of the column is required to be 20-40 times that of the media size, otherwise high porosity zones near the wall will exert too much influence on the overall flow patter (Tobis and Vortmeyer, 1988; Jadhav and Pangarkar, 1990).

In our case, the column diameter was reduced to 1.3 cm by ensuring a ratio of 33 (within the former range) however, data showed that column wall still exerted a detectable impact on the flow pattern, leading to the untimely leakage that translated in the first mini-pick. Despite this negative effect, the use of the column with a diameter of 1.3 cm would have allow a significant reduction in the wastewater volume to be fed to the process, in the usage of chemicals to desorb the column and, consequently, in the volume of waste stream to be treated and disposed. For all the former items, during the planning of the experiments that reduction was estimated to be equal to 78% respect to the process eventually overtaken with the bigger diameter column. Such advantage in terms of costs and environmental impact was considered extremely important, especially considering that the main aim of the tests was a direct comparison between three different resin and, hence, far away from any process scale-up purpose where, on the contrary, these aspect can not be neglected.

Therefore, despite the awareness of the wall-impact problem, on the basis of the economic and environmental advantages related to the usage of the smaller column together with the actual scope of the trials, the compromise of a not-perfect flow-pattern was accepted and the smaller column selected.

Figure 2.4.13 Comparison between the two cumulative retention time curves obtained through the fluid dynamic tests performed with the 1.3 and 2.7 cm diameter columns.

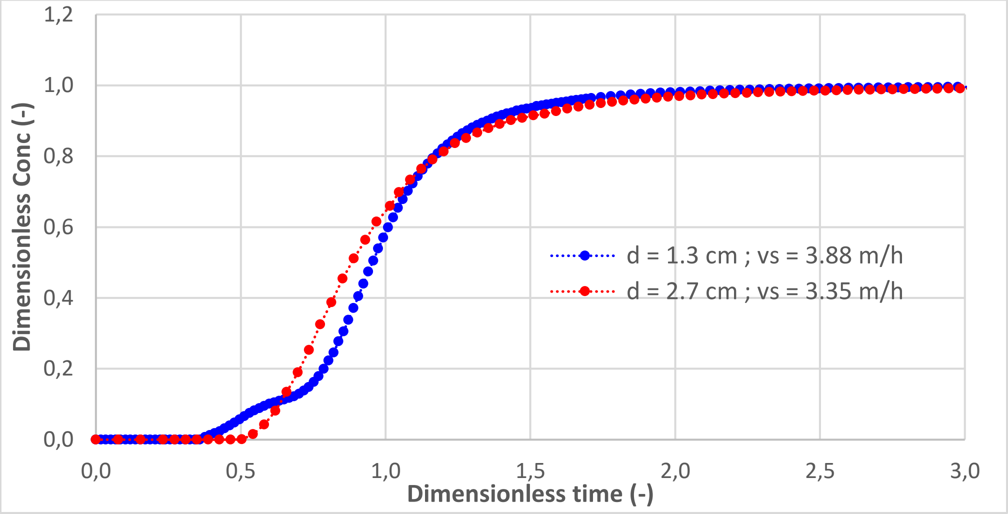

Moreover, further fluid dynamic tests were conducted on the three columns packed with the virgin resin and with Cranfield pilot plant resin, to face a further practical aspect. Hence, it is also known that irregularities in flow pattern caused by packing are more significant in smaller beds (Van Deemter and Zuiderweg, 1956), specially where the column wall exerts the previous described impact, and also that they are increased when the Reynolds number exceeded 10 (Rhodes, 2008).

To prove that possible differences between the three resin during the adsorption breakthrough tests could not be caused by different packing qualities of the resin beds, the fluid dynamic behaviour of the three packed columns was tested and compared under the same operating conditions. The results showed no significant differences between the trials, confirming the highly reproducibility of the packing method proposed. Moreover, the Reynolds number resulted always lower than 10, even for the highest superficial velocity corresponding to an EBCT of approximately 5 min (Re = 1.8).

2.4.5.3.2 Resin bed pre-treatment

Before the adsorption breakthrough curve, the two columns packed with the HAIX resin used in the Cranfield pilot plant were desorbed through a continuous flow process. Desorption was necessary since the resin sent to Bologna University was taken from the column after an adsorption cycle without any desorption. Moreover, in order to simulate as much as possible the Cranfield pilot plant operation the defined volume of the selected solution was fed to the column maintaining an EBCT of 10.4 minutes. In Table 2.4.9 are shown the main operating parameters and the mass of PO_4-P and COD desorbed:

Table 2.4.9 Desorption continuous-flow operating parameters and performances of the two columns packed with the HAIX resin used in the Cranfield pilot plant.

Pre-treatment of HAIX from Cranfield pilot plant		
	Column 1	Column 2
Bed Height (cm)	94	
BV_{resin} (mL)	125	
Mass of dry resin (g)	38 ± 2	
EBCT (min)	10.4 ± 0.5	
Superficial velocity (m/h)	7.6 ± 0.4	
Regenerant Solution (w/v %)	2% NaOH	2% NaOH + 5% NaCl
Volume of solution fluxed (BVs)	10	15
Mass of PO_4-P desorbed ($mg_P/g_{dry\ resin}$)	5.2 ± 0.1	5.3 ± 0.1
Mass of COD desorbed ($mg_{COD}/g_{dry\ resin}$)	4 ± 1	75 ± 5

Data resulted consistent with those obtained in batch desorption tests, illustrated at the beginning of section 2.4.5.1. As already noted, the mass of P desorbed (expressed as $mg_i/g_{dry\ resin}$) resulted equal for the two desorption solutions, demonstrating the negligible contribution of sodium chloride to this scope. Moreover, the desorption step was considered a reliable reproduction of the Cranfield pilot-scale process. Indeed, the mass desorbed resulted very close to the average value (4.4 ± 0.4 $mg_P/g_{dry\ resin}$) obtained by desorbing with a fresh 2% NaOH, when a new series of cycles was started. While the elution of organic compounds by the 2% NaOH and 5% NaCl solution resulted 21% lower than that obtained in batch conditions (section 2.4.5.1), but, at the same time, always 95% higher than that obtained with only NaOH 2%. The former resin bed pre-treatment was a further proof of the selective desorption operated by the process, which allowed to obtain a highly pure phosphate solution with limited concentration of foreign compounds.

2.4.5.3.3 Laboratory-scale continuous-flow adsorption breakthrough tests

Despite the impact of the wall on the overall flow pattern described in the former section by means of a fluid dynamic characterization, columns with 1.3 cm inner diameter were used for the following breakthrough trials to compare the three forms of the resin. Indeed, always at section 2.4.5.3.2 they were proved to be characterized by the same geometric similarity and kinematic behaviour and therefore to be linked to the same rate critical features of the process. Thus, confirming to be suitable for trials with comparison scope. The three different resin beds were characterized by a length of 94 cm, equal to that of the Cranfield pilot plant. Moreover, to allow the possibility of a comparison with the scaled up demonstration column, the superficial velocity (i.e. the hydraulic loading rate m^3 m^{-2} h^{-1}) was set to have the same EBCT of the pilot plant process. As a matter of fact, in the case of fixed bed adsorbers, internal diffusion in commonly considered the most important limiter because the concentration gradient is lower within the media in comparison to the surrounding liquid/solid interface. This means that the dimensionless group $D_s t/R^2$, (where $D_s t$ is the intraparticle coefficient over time, and R is the external radius of the adsorbent particle) should remain constant during scale up or scale down (Martin et al., 2013). Given that D_s and R are likely to remain fixed this means that the fluid residence time, or empty bed contact time, should also be fixed between comparisons of scale. Therefore, despite the awareness of the flow shortcut beside column walls and its influence on the process performance, in the scale down the resin bed length and the EBCT of the Cranfield pilot plant were maintained in a final attempt to compare different scales of the process.

Notwithstanding the breakthrough curves were performed up to 85% dimensionless outlet P concentration, the data here shown do not cover the entire trials. Unfortunately, due to the delay of the new instrument’s delivery that should have been used to complete the data analysis, most of the adsorption breakthrough samples taken during the experiments could not be analysed. Hence, here is shown only a part of the total data that will be ready for the PhD final review.

In Fig. 2.4.13 are shown the adsorption breakthrough curves up to 1 mg/L breakpoint. While in Table 2.4.10 are illustrated the main operating parameters and some process performances of the related trials. For the virgin HAIX trial it was possible to analyse data up to the 85% outlet concentration. This is the reason why (despite the points analysed with a rather large intervals) it was possible to perform a complete elaboration with the final determination of the adsorption yield and of the resin operating capacity (i.e. resin utilization efficiency). The latter, evaluated at the very low breakpoint of 0.1 resulted of (70.8±4)%, extremely high. First, it is interesting to note that, within the little variability of some operating parameters as the inlet P concentration and the EBCT, the three resin beds performed unexpectedly similarly.

In particular, the WW volumes that could be treated up to the breakpoint of 0.1 mg/L were 215, 203 and 233 BVs for the virgin resin, the used resin regenerated with w/v 2% NaOH and the used resin regenerated with 2% NaOH + 5% NaCl respectively. The volumes are 252, 245 and 266 BVs if a 1 mg/L breakpoint is assumed. The differences in BV between the 3 conditions do not seem to be significant. The determination of the number of treated BVs depends on the flow rate Q according to the equation: $(Q \cdot t) / BV$; where Q is the flow rate (mL/min), t is the time (min) and BV is the volume occupied by the resin bed (void fraction included – mL). The error associated to the number of BVs treated can be obtained using the error propagation method which includes the relative variations of Q (around 10%) during the tests and of the uncertainty in the resin bed volume (around 2%). The standard deviations of the BVs for 0.1 and 1 mg/L breakpoints are 7% and 4% respectively, both lower than 10% error due to the volumetric flow rate alone. In support of this it must also considered that the used resin regenerated with 2% NaOH and 5% NaCl performed even better than the virgin resin, which is hard to justify.

However it is interesting to note that in the three trials performed the number of treated BVs increased only of 17%, 21% and 14% between the 0.1 mg/L and the 1 mg/L breakpoints, synonymous of very steep breakthrough curves and of rather narrow mass transfer zones. This can also be noted by looking at the curves between the 1.6% and 15% of the normalized P outlet in Fig. 2.4.13. These process performances obtained, e.g. BVs treated, media capacity, resulted comparable to that reported by other authors (Kalaitzidou et al., 2016; SenGupta and Pandit, 2011; Martin et al., 2013).

The extraordinary performances obtained with the small column trails exceeded that obtained at pilot scale. Indeed, if we look again at Fig. 2.4.8 we find out that the average number of BVs that could be treated up to 1 mg/L breakpoint (for the consecutive cycles with recovered regenerant solution) was around 220 ± 21. The difference in performance further increased if a lower P outlet threshold is chosen, i.e. 0.1 mg/L. The number of BVs that the demonstration column of Cranfield could treat before leaching the 0.1 mg/L of P was 110 and 95, in the case of resin bed previously regenerated with fresh NaOH or recovered NaOH solution, respectively. The fact that the same resin, namely the CPP resin regenerated with 2% NaOH, performed more efficiently in a laboratory-scale column (furthermore with a flow pattern affected by column wall) than a pilot-scale column with a diameter approximately 17 times bigger is directly in contradiction with the best of authors' knowledge on adsorption process studies (Martin et al., 2013; Cooney, 1998).

Some assumptions can be taken into account to explain this outcome. On one hand, the first consideration is related to the fluid dynamic behaviour of the two resin beds (the bench-, and the pilot- scale). In the case of the small column trials, the fluid dynamic behaviour of the process was investigated before breakthrough tests and analysed in detail to validate the procedure used to obtained the three packed beds. That validation occurred on the basis of the reproducible and consistent behaviour of the flow patter through the 3 different resin beds packed according to the same procedure. Hence, despite the awareness of the wall impact which is only related to the too small inner diameter of the column, the packing method was proved to be reliable. Whilst, on the contrary, the flow pattern behaviour of the pilot-scale resin bed could not be investigated. A first explanation of the marked difference performed by the same CPP resin in an even more controlled system at laboratory-scale may lay precisely on the quality of packing, a fundamental aspect of the fixed bed adsorption processes. As explained at section 2.3.5.3 of M&M, after the desorption the pilot-scale column was empty by gravity to avoid any dilution of the regenerant solution. Subsequently, 5 BVs of tap water were fluxed up-flow to wash out the remaining regenerant solution from the resin bed. Hence, the system was turned back into service for a new adsorption cycle after a complete expansion of the media volume and the subsequent settling of the whole mass of media under the lonely force of gravity. The first hypothesis is that the packing obtained according to this procedure led to the formation of a resin bed insufficiently compact, homogeneous and uniform and characterized by the presence of several voids and preferential pathways. Thus, responsible for the flow pattern irregularities leading to premature release of the target compound. To overcome the problem, 5 to 10 further BVs of tap water could be fluxed down-flow at higher flow rate after the regeneration procedure and before the following adsorption step, in order to compress the adsorbent bed. Alternatively, a mechanical apparatus producing vibration could be used to enhance and ensure a high grade of the media compaction.

On the other hand, another possible explanation for the gap between the two different scale adsorption processes may led on the different MWW used in the experiments. Hence, in the case of the Cranfield pilot plant, experiments were conducted with secondary WW effluent from a trickling filter, while in the case of Unibo bench-scale trials the WW used was collected from the final effluent of the MWWTP of Bologna and successively spiked to increase the P content. It is well known that the background species characterizing the WW matrix play a fundamental role in the adsorption of P onto the ferric (hydr)oxides; hence, their qualitatively and quantitatively presence is extremely significant for the process. For example, sulphate is the main competitor of phosphate (Zhao and SenGupta, 1996; Blaney et al., 2007), however it can not be the responsible for the difference in the total P uptake by the CPP resin regenerated with 2% NaOH, since it was present at critical levels in both the WWs used (80 and 104 mg/L, respectively – see Table 2.3.1 and 2.3.2 in M&M). Humic acid, has also been reported to significantly reduce P uptake, due to its high tendency to be adsorbed onto the surface of iron (hydr)oxides (Genz et al., 2008; Gu et al., 2001; Hiemstra et al, 2010; Antelo et al., 2007; Fu et al., 2013). However, a direct measure of the humic acid for the two WWs was not performed, it can only be noted that its content is necessarily included into the COD measure, which again resulted really close: 35 and 40 mg/L, respectively. Moreover, it has been reported that in many cases adsorption by inner-sphere complex formation increases with increasing electrolyte concentration (Antelo et al., 2005). Hiemstra and Van Riemsdijk (1999) attributed this effect to changes in the electric potential in the interface, which decreases the electrostatic repulsion between the charged surface and the anion, and, consequently, favours adsorption. The hardness of the WW used can therefore play a fundamental role in the adsorption of P. For example the presence of Ca^{2+} was found to hardly improve the P adsorption (Tanboonchuy et al., 2012; Antelo et al., 2005) and may contribute to the best small columns trials since the 4 times higher concentration than the CPP WW (35 versus 136 mg/L).

Figure 2.4.13 Adsorption breakthrough curves shown in terms of 5-data moving average – as normalized outlet P concentration – respect to the average inlet P concentration, versus the number of actual WW BVs fed to the column. The operating parameters are those shown in Table 2.4.10.

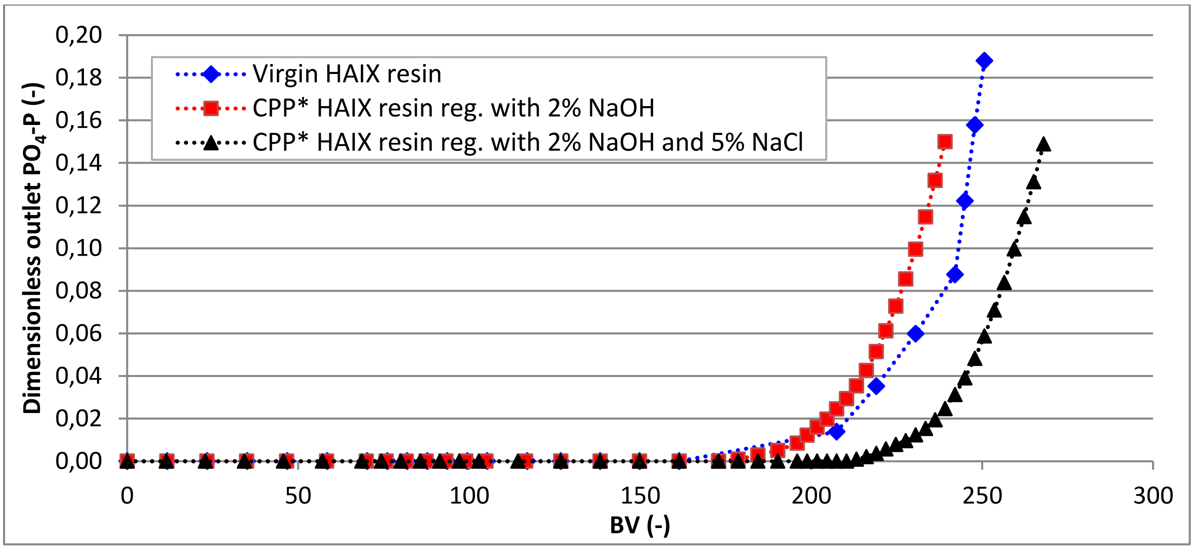

*CPP = Cranfield Pilot Plant

Table 2.4.10 Most significant operating parameters, adsorption capacities and solely for the virgin HAIX Layne^{RT} performance parameters for the adsorption breakthrough tests shown in Fig. 2.4.11.

	Virgin resin		**CPP* resin regenerated with 2% NaOH**		**CPP* resin regenerated with 2% NaOH & 5% NaCl**	
i-breakpoint value	0.1 mg/L	1 mg/L	0.1 mg/L	1 mg/L	0.1 mg/L	1 mg/L
Bed volume (BV_{resin} , mL)	125					
Mass of dry resin (W_{dry}, g)	38					
Empty bed contact time (EBCT, min)	5.13 ± 0.02		5.15 ± 0.02		5.25 ± 0.02	
Superficial velocity (v_{sup} , m/h)	11 ± 0.1		10.9 ± 0.1		10.7 ± 0.1	
Bed volumes/h (BV/h, 1/h)	11.7 ± 0.3		11.6 ± 0.3		11.4 ± 0.2	
Inlet PO_4-P Conc. (mg/L)	7.1 ± 0.2		6.6 ± 0.2		6.9 ± 0.1	
Resin total capacity ($Q_{resin,\ sat}$, $g_{PO4\text{-}P}/L_{resin}$)	7.3		n.a.*		n.a.*	
Resin total capacity ($Q_{resin,\ sat}$, $mg_{PO4\text{-}P}/g_{dry\ esin}$)	14.6		n.a.*		n.a.*	
Volume of treated WW ($V_{treated\ WW}/BV_{resin}$, -)	215	252	203	245	233	266
P adsorption yield at *i*-breakpoint (Y_{ads} , -)	99.9%	99.1%	n.a.*	n.a.*	n.a.*	n.a.*
P operating capacity (η_{resin})	(70.8±4)%	(79.5±4)%	n.a.*	n.a.*	n.a.*	n.a.*
P capacity at *i*-breakpoint ($Q_{resin,\ bp}$, $mg_{PO4\text{-}P}/g_{dry\ resin}$)	5.17	5.80	4.37	5.08	5.25	5.96

*CPP = Cranfield Pilot Plant; *n.a.= not applicable

Concluding, despite the adsorption batch isotherms highlighted the differences in performances between the three forms of the resin, especially between the CPP resin regenerated with 2% NaOH and the other two forms, the continuous-flow tests led to not significant differences between the three performances. Thus, confirming the importance to always integrate batch tests with continuous-flow trials. Indeed they allow to investigate the process at environmentally significant boundary conditions, such as the solid phase concentrations in equilibrium with typical values of P in actual wastewater and the duration of the adsorption step (breakthrough time, here evaluated as number of treated BV) at defined outlet P concentration thresholds (i.e. 0.1 and 1 mg/L).

The elution of the ion-exchange parent media with NaCl resulted unnecessary, since the CPP resin regenerated with NaOH performed not significantly different from the virgin resin. This extraordinary result suggested and confirmed the notable durability, regenerability and high resistance of the investigated resin, which performed similarly to the virgin resin even after 66 cycles operated in an adsorption demo-plant within an actual sewage works. Therefore, these trails proved the possibility to keep the resin into service for longer period and several others adsorption/desorption cycles. This finding results of fundamental interest and adds important information for the future economic and LCA analyses aimed at assessing the sustainability of the process. Indeed, the yearly cost associated to the periodic resin replacement represents one of the heaviest items of cost for the process, specially for this type of resin characterized by a relatively high market price (22 €/kg).

Moreover, the performance comparison of the CPP and the virgin resins, proves the high potential of the novel conduction method proposed by Cranfield University, which includes the regeneration with only NaOH, the multiple use of the solution and the re-cycling after the precipitation. As a matter of facts, no detrimental and irreversible effects could be detected and assigned to the proposed conduction method.

Finally, a deeper investigation regarding the pilot-scale column packing is proposed. Fluid dynamic tests or adsorption breakthrough tests are suggested in order to evaluate the advantages of introducing a further step in the plant conduction method to ensure good quality packing and sufficient compactness of the resin bed before each adsorption step.

2.5 CONCLUSIONS

The main conclusions on the Removal and Recovery of P from MWW through a hybrid ion exchange resin can be summarized as follows:

- The Cranfield pilot plant went successfully through 66 adsorption/desorption cycles working within an actual sewage works (population equivalent < 10,000) and real secondary WW effluent from a trickling filter, for an extended period of almost 1 year and a half.
- During the six-months of plant operation performed by the undersigned (between cycle 35 to cycle 66), the adsorption process did not show any variability in performances due to seasonal changes (e.g. temperature).
- The plant showed capabilities to work with variable conditions (i.e. inlet P concentration decreasing approximately from 6 to 3 mg/L) without any undesired elution and leaching of the target compound. Indeed, the proposed technology resulted potentially able to fully control the effluent quality.
- Overall, the proposed technology offers reliable P removal, simplicity of operation and long-term sustainability with little maintenance. This study, which represents one of the first attempts to place a phosphate adsorption process in an existing MWWTP, highlighted the wide potential of the technology in removing trace contaminants even for highly complex matrices with high content of competing ions. As a matter of fact, according to literature and to the results of this study, P removal by adsorption can be considered an efficient effluent "polishing" treatment solution,

thus offering the recovery of phosphate from aqueous solutions. Hence, the current adsorption process can be proposed as an integration of the MWWTP and can be coupled with several other secondary treatment technologies (e.g. activated sludge, anaerobic MBR).

- The capability of adsorption technology to work with very low concentrations allows to work with final effluents of MWWTP already characterized by the presence at earlier stages of other P removal technologies (e.g. EBPR), which actually would struggle to ensure an effluent P content constantly below 0.1 mg/L in a cost-effective way. Thus, the versatility of adsorption-based technologies enables the possibility of being employed both as primary P-recovery technology treating secondary effluent wastewater (as in the case of this study), and as a final polishing treatment integration of MWWTP already equipped with some traditional P-removal technologies. In the latter case adsorption would ensure the observance of the incoming stricter environmental thresholds.
- The proposed process conduction method, which included the consecutive multiple employment of the regenerant solution through several adsorption/desorption cycles and its recycling after having recovered the solid product by precipitation, showed a promising potential in terms of brine management, whose disposal together with the cost of chemicals represents the major drawback of adsorption technologies.
- The regenerant solution recovered by precipitation and subsequently recirculated did not lead to any detrimental effect on the process and, on the contrary, performed consecutive cycles settling on extraordinarily reproducible runs, with the extended potential to fully predict and control the process performances. Moreover this study represent the first attempt to investigate the possible multiple recirculation of the regenerant solution (it was recovered and recirculated twice) after a selective precipitation at a demonstration scale.

In addition, the last part of the study focused on the characterization of the resin used in the demonstration plant led to the following conclusions:

- The investigated HAIX Layne^{RT} resin demonstrated extraordinary selectivity towards phosphate, mechanical and chemical durability, going successfully through a long actual field-experience.
- The use of NaOH to regenerate only the ferric nanoparticle sites led to no significant and irreversible detrimental effects on the resin capacity, thus validating the proposed

procedure for the plant conduction. Indeed, despite a marked difference in the results from batch tests, in continuous-flow adsorption trials the performances of the virgin and of the regenerated resin resulted not significantly different. In other words, full resin regeneration with NaCl resulted not necessary, confirming: i) the negligible contribution of the ion-exchange sites for P-uptake in complex matrixes where competing ions are present and ii) the negligible impact (i.e. steric obstruction and neutralization of the Donnan membrane effect) of the organic and inorganic compounds accumulated on the ion-exchange parent media throughout the 66 cycles performed.

- The laboratory tests performed proved the possibility to keep the resin into service for much longer operating-times than the 66 adsorption/desorption cycles performed at Cranfield’s pilot-scale plant. This finding results of fundamental importance for the economic sustainability of the process. Indeed, the yearly cost associated to the periodic resin replacement represents one of the heaviest items of cost for the process, specially for this type of resin characterized by a relatively high market price (22 €/kg).

Overall, the investigated HAIX Layne^{RT} resin resulted a potential candidate for the full-scale development of a P-recovery process from MWW, since it is commercially and worldwide available and because its employment in the current study resulted in consistent, reliable and durable high quality performances for P removal. Moreover, the abovementioned qualities have been successfully demonstrated by other authors in other adsorption field experiences (i.e. arsenate removal) (Sarkar et al., 2007 and 2010).

Some suggestions for further investigation and optimization of the proposed process are: i) an economic costs/benefits analyses to identify the optimal number of times that the regenerant solution can be reused for consecutive desoprtions; and ii) an improvement of the precipitation step to recover a higher valuable product, such as hydroxyapatite instead of amorphous calcium-phosphate.

List of abbreviations

BV/h	Bed Volumes / h
BV	Bed volume (= volume occupied by the media, included void between beads = cross-sectional area of the column x length of the resin bed)
CI	Confidence interval
COD	Chemical oxygen demand
CPP	Cranfield pilot-plant
EBCT	Empty bed contact time
EBPR	Enhanced biological phosphorus removal
HAIX	Hybrid anion exchange
HFO	Hydrated ferric oxides
HRT	Hydraulic residence time
IE or IEX	Ion exchange
MWW	Municipal wastewater
MWWTP	Municipal wastewater treatment plant
M&M	Material and methods
NH_3-N	Ammonia nitrogen
PFO	Pseudo-first order
PO_4-P	Phosphate expressed as phosphorus
PSO	Pseudo-second order
R&D	Results and discussion
TS	Total solids
TSS	Total suspended solids
VS	Volatile solids

Nomenclature

A_s	Asymmetry factor, defined as ratio between the leading and tailing semi-width of the peak at 10 % of the peak height (-)
$C_{L,i}$	Liquid phase concentration of compound *i* (g/L)
$C_{L,0,i}$, $C_{L,eq,i}$	Initial and final (equilibrium) PO_4-P concentration in the liquid phase during the isotherm tests (g_P/L)
$C_{S,eq,calc,i}$	PO_4-P solid phase concentration calculated according to the model (e.g. Langmuir or Freundlich), for the evaluation of the R^2 and χ^2 value associated to each isotherm ($g_{PO4\text{-}P}/g_{\text{dry resin}}$)
$C_{S,eq,i}$	Final (equilibrium) PO_4-P concentration in the solid phase (resin) during the isotherm tests ($g_{PO4\text{-}P}/g_{\text{dry resin}}$)
$C_{S,eq,m}$	Average experimental solid phase concentration of compound *i* in an isotherm test, for the evaluation of the R^2 value associated to each isotherm ($g_{\text{PC or COD}}/g_{\text{dry resin}}$)
$C_{S,i}$	Solid phase (resin) concentration of compound *i* ($g_i/g_{\text{dry resin}}$)
$C_{S,i,eqOMW}$	*i*-compound solid phase (resin) concentration in equilibrium with the solution used for the batch and breakthrough tests ($g_{i\text{-compound}}/g_{\text{dry resin}}$)
HETP	Height equivalent to a theoretical plate, in the packed column (m)
k_1 ; k_2 ; k_{FD}	k_1 (min^{-1}) is the rate constant of the PFO equation; k_2 (g mg^{-1} min^{-1}) is the rate constant of the PSO equation; k_{FD} (min^{-1}) is the rate constant – used for kinetic tests
$K_{eq,i}$	Constant related to the affinity between the binding sites and *i*-compound, in the Langmuir isotherm ($L_{\text{pore volume}}$ /g_i)
$K_{F,i}$	Sorption capacity in the Freundlich model (L/$g_{\text{dry resin}}$)
$m_{i,fed}$	Mass of *i*-compound fed to the column until a certain breakpoint (mg)
$m_{i,desorbed}$	Total mass of *i*-compound desorbed by the resin during the entire desorption procedure (mg)
$m_{i,sorbed}$	Mass of *i*-compound adsorbed by the resin in correspondence of a certain breakpoint (mg)
m_S	Mass of dry resin in the isotherm studies ($g_{\text{dry resin}}$)
n_i	Inverse of the sorption intensity in the Freundlich model (-)
N	Number of experimental points in each isotherm (-)
P	Number of parameters to be estimated in each isotherm (-)

q_e ; q_t	amounts of adsorbate uptake per mass of adsorbent at equilibrium and at any time t ($mg_P/g_{dry\ resin}$) – used for kinetic tests
V_L	Liquid volume added in the isotherm tests (mL)
$Y_{ads,i}$	*i*-compound adsorption yield, calculated as $m_{i,sorbed}$ / $m_{i,initial}$ in the batch tests, and as $m_{i,sorbed,\ X\ breakpoint}$ / $m_{PC\ or\ Vi,fed,\ X\ breakpoint}$ in the breakthrough tests (-)
$Y_{des,i}$	*i*-compound desorption yield in a batch or breakthrough test, defined as $m_{i,desorbed}$ / $m_{i,sorbed}$ (-)
ε	Effective porosity (-)
η_{resin}	Resin operating capacity, defined as $m_{i,sorbed,X\ breakpoint}$ / $m_{i,sorbed,X\ breakpoint}$ (-)
w/v %	Weight/Volume Percentage Concentration (g/L)

References

Amann A., Zoboli O., Krampe J., Rechberger H., Zessner M., Egle L., (2018). Environmental impacts of phosphorus recovery from municipal wastewater. Resources, Conservation & Recycling 130 127–139.

Antelo J., Arce F., Avena M., Fiol S., López R., Macías F., (2007). Adsorption of a soil humic acid at the surface of goethite and its competitive interaction with phosphate. Geoderma 138 (2007) 12–19.

Antelo J., Avena M., Fiol S., López R., Arce F., (2005). Effects of pH and ionic strength on the adsorption of phosphate and arsenate at the goethite-water interface. Journal of Colllid and Interface Science 285 (2005) 476–486.

Arai Y. and Sparks D. L., (2001). ATR–FTIR Spectroscopic Investigation on Phosphate Adsorption Mechanisms at the Ferrihydrite–Water Interface. Journal of Colloid and Interface Science 241, 317–326.

Arnoutn S., Nagels E., (2016). Modelling thermal phosphorus recovery from sewage sludge ash, CALPHAD: Computer Coupling of Phase Diagrams and Thermochemistry 55 26–31.

Ashley K., Cordell D., Mavinic D., (2011). A brief history of phosphorus: from the philosopher’s stone to nutrient recovery and reuse. Chemosphere 2011, 84, 737–746.

Baur, R.J., (2009). Waste Activated Sludge Stripping to Remove Internal Phosphorus. US7604740 B2.

Blaney L. M., Cinar S., SenGupta A. K., (2007). Hybrid anion exchanger for trace phosphate removal from water and wastewater. Water Research 41 1603-1613.

Bolto B., Dixon D., Eldridge R., King S., Linge K., (2002). Removal of natural organic matter by ion exchange, Water Research, 36:5057-5065.

Borggaard O.K., Raben-Lange B., Gimsing A.L., Strobel B.W., (2005). Influence of humic substances on phosphate adsorption by aluminium and iron oxides. Geoderma 127 (2005) 270-279.

Boyer TH, Persaud A., Banerjee P., Palomino P., (2011). Comparison of low-engineered materials for phosphorus removal from organic-rich surface water; Water Research, 45:4803-4814.

Brink J., (1977). World resources of phosphorus. Ciba Foundation Symposium Sept 13–15, pp. 23–48.

Britton, A., Prasad, R., Balzer, B., Cubbage, L., (2009). Pilot testing and economic evaluation of struvite recovery from dewatering centrate at HRSD’s Nansemond WWTP. In: Don Mavinic, Ken Ashley, Fred Koch (Eds.), International Conference on Nutrient Recovery from Wastewater Streams Vancouver, IWA Publishing, London, UK.

Bunce J.T., Ndam E., Ofiteru I.D., Moore A., Graham D.W.; (2018). A review of phosphorus removal technologies and their applicability to small-scale domestic wastewater treatment Systems; Wastewater Management.

Burton, F. L., Tchobanoglous, G., Tsuchihashi, R., David Stensel, H., and Metcalf & Eddy, Inc. (2014). Wastewater Engineering: Treatment and Resource Recovery, 5th Edn. New York, NY: McGraw-Hill.

Chamoglou M., Papadimitriou T., Kagalou I (2014). Key-descriptors for the functioning of a Mediterranean reservoir: the case of the New Lake Karla-Greece. Environ. Process 1:127-135.

Chaudhary B. K. and Farrell J., (2015). Understanding Regeneration of Arsenate-Loaded Ferric Hydroxide-Based Adsorbents. Environmental Engineering science Volume 32, Number 4, 2015.

Cheng, H., Hu, Y., Luo, J., Xu, B., & Zhao, J. (2009). Geochemical processes controlling fate and transport of arsenic in acid mine drainage (AMD) and natural systems. Journal of Hazardous Materials, 165, 13–26.

Choi J.W., Kwon K.S., Lee S., An B., Hong S.W., Lee S.H., (2014). Pilot-scale test for a phosphate treatment using sulfate-coated zeolite at a sewage disposal facility. Water Air Soil Pollut 225:1835.

Cooney D.O., (1998). Adsorption Design for Wastewater Treatment. CRC Press, Florida, 1998.

Cordell D., Drangert J.-O., White S., (2009). The Story of phosphorus: global food security and food for thought. Global Environ. Change 19, 292–305.

Cordell, D., Rosemarin, A., Schröder, J., Smit, A., (2011). Towards global phosphorus security: a systemic framework for phosphorus recovery and reuse options. Chemosphere 84, 747–758.

Cumbal L., SenGupta A.K. (2005). Arsenic removal using polymer-supported hydrated iron(III) oxide (HFO) nanoparticles: role of Donnan membrane effect. Environ Science Technology 39 (17) : 6508–6515.

Cumbal L., Greenleaf J.E., Leun D., SenGupta A.K., (2003). Polymer supported inorganic nanoparticles: characterization and environmental applications, React. Funct. Polym. 54 (1–3) 167–180.

D. Lgs. 29/2010 https://www.gazzettaufficiale.it/eli/id/2010/05/26/010G0096/sg

De Kock L., (2015) Hybrid ion exchanger supported metal hydroxides for the removal of phosphate from wastewater, Phd Thesis, University of Johannesburg.

DeMarco M.J., SenGupta A.K. and Greenleaf J.E., (2003). Arsenic removal using a polymeric/inorganic hybrid sorbent. Water Res 37:164–176.

Donnan FG (1995) Theory of membrane equilibria and membrane potentials in the presence of non-dialysing electrolytes. A contribution to physical-chemical physiology. J Membr Sci 100:45–55.

Drenkova-Tuhtan A., Schneider M., Franzreb M., Meyer C., Gellermann C., Sextl G., Mandel K., Steinmetz H., (2017). Pilot-scale removal and recovery of dissolved phosphate from secondary wastewater effluents with reusable ZnFeZr adsorbent @ Fe3O4/SiO2 particles with magnetic harvesting. Water Research 109 77-87.

Dzombak D.A. and Morel F.M., (1990). Surface Complexation Modeling: Hydrous Ferric Oxide. John Wiley & Sons, Inc, Hoboken, New York.

EA 2000. EA Aquatic eutrophication of England and Wales: a management strategy Environment Agency Bristol; 2000.

Egle, L., Rechberger, H., Krampe, J., Zessner, M., (2016). Phosphorus recovery from municipal wastewater: an integrated comparative technological, environmental and economic assessment of P recovery technologies. Sci. Total Environ. 571, 522e542. http://dx.doi.org/10.1016/j.scitotenv.2016.07.019.

Egle, L., Rechberger, H., Zessner, M., (2015). Overview and description of technologies for recovering phosphorus from municipal wastewater. Resour. Conserv. Recycl. 105, 325e346. http://dx.doi.org/10.1007/s00506-013-0127-x.

Elzinga E.J. and Sparks D.L. (2007). An in situ ATR-FTIR investigation of the effects of pH and loading level on the mode of phosphate surface complexation. Journal of Colloid and Interface Science, 308: 58-70.

European Commission, 2014, Communication from the commission: on the review of the list of critical raw materials for the EU and the implementation of the raw materials initiative. European Commission, Brussels.

FAO, 2009 - FAO, 2009. More people than ever are victims of hunger. Food and Agriculture Organization of the United Nations, Press Release, June.

Fogler S.H & Gürmen M.N., (2008). Elements of Chemical Reaction Engineering, forth ed., Pearson, Michigan.

Frascari D., (2013). Trichloroethylene aerobic cometabolism by suspended and immobilized butane-growing microbial consortia: a kinetic study. Biores. Technol., vol. 1244, pp. 529-538,

Fresco L., (2009). Challenges for food system adaptation today and tomorrow. Environ. Sci. Policy 12, 378–385.

Fu Z., Wu F., Song K., Lin Y., Bai Y., Zhu Y., Giesy J. P., (2013). Competitive interaction between soil-derived humic acid and phosphate on goethite. Applied Geochemistry 36 (2013) 125–131.

Gautam, R.K., Banerjee, S., Gautam, P.K., Chattopadhyaya, M.C., (2014). Remediation technologies for phosphate removal from wastewater: an overview. Adv. Environ. Res. 36, 1e23.

GE Healthcare Bio-Sciences AB, Column efficiency testing – Application note28-9372-07 AA, Uppsala, Sweden.

https://www.gelifesciences.com/gehcls_images/GELS/Related%20Content/Files/1352880951136/litdoc28937207_20141127221416.pdf, 2010 (accessed 20.08.2019).

Genz A., Baumgarten B., Goernitz M., Jekel M., (2008). NOM removal by adsorption onto granular ferric hydroxide, Water Research, 42:238-248.

Genz A., Kornmuller A., Jekel M., (2004). Advanced phosphorus removal from membrane filtrates by adsorption on activated aluminium oxide and granulated ferric oxide; Water Reasearch, 38:3523-3530.

Gu B., Schmitt J., Chen Z, Llang L, McCarthy JF, (1994). Adsorption and desorption of natural organic matter on iron oxide: mechanisms and models, Environ. Sci. Technol. 1994:38-48,

Guerrero, J., Guisasola, A., Baeza, J.A., (2015). Controlled crude glycerol dosage to prevent EBPR failures in C/N/P removal WWTPs. Chem. Eng. J. 271, 114e127.

Helfferich FG (1962) Ion exchange. McGraw-Hill, New York;

Hiemstra T., Antelo J, van Potterdam AMD, van Riemsdijk WH, (2010). Nanoparticles in natural system II: the natural oxide fraction at interaction with natural organic matter and phosphate, Geochimica et Cosmochimica Acta, 74:59-69.

Hiemstra T., Van Riemsdijk W.H., (1999). Surface structural ion adsorption modeling of competitive binding of oxyanions by metal (hydr)oxides. Journal Colloid and Interface Science. 210 (1999) 182

IAASTD, (2008). International Assessment of Agricultural Knowledge, Science and Technology for Development (IAASTD). Agreed to at an intergovernmental Plenary Session in Johannesburg, South Africa in April. <www.agassessment.org>.

IFA, 2006. Production and International Trade Statistics. International Fertilizer Industry Association, Paris. <http://www.fertilizer.org/ifa/statistics/pit_public/pit_public_statistics.asp>

Jadhav S.V., Pangarkar V.G., (1990). Particle-liquid mass transfer in three-phase sparged reactors: scale-up effects, Chem. Eng. Sci. 46 (4) 919–927.

Jelinek R. T., & Sorg T. J., (1998). Operating a small-full scale ion exchange system for uranium removal. J. Am. Water Works Assoc. 80(7), 79-83.

Kalaitzidou K., Mitrakas M., Raptopoulou C., Tolkou A., Palasantza P.A., Zouboulis A., (2016). Pilot-scale phosphate recovery from secondary wastewater effluent. Environ. Process. 3 (Suppl 1): S5-S22.

Kim J.-O., Chung J., (2014). Implementing chemical precipitation as a pretreatment for phosphorus removal in membrane bioreactor-based municipal wastewater treatment plants. KSCE J. Civ. Eng. 18, 956e963.

Krüger O., Adam C., (2015). Recovery potential of German sewage sludge ash. Waste Management 45 400–406.

Levenspiel O., (1999). Chemical Reaction Engineering, third ed., Wiley, New York, 1999.

Li G., Gao S., Zhang G., Zhang X.; (2014). Enhanced adsorption of phosphate from aqueous solution by nanostructured iron(III)–copper(II) binary oxides, Chem. Eng. J. 235 124–131.

Liebig J., (1840). Die organische Chemie in ihrer Anwendung auf Agricultur und Physiologie (Organic chemistry in its applications to agriculture and physiology). Friedrich Vieweg und Sohn Publ. Co., Braunschweig, Germany).

Lin J.C. and SenGupta A.K., (2009). Hybrid anion exchange fibers with dual binding sites: Simultaneous and reversible sorption of perchlorate and arsenate, Environmental Engineering Science.

Manjari S.R., Kim, H.J., (2006). Temperature- and pressure dependence of the outer-sphere reorganization free energy for electron transfer reactions: a continuum approach. Journal of Physical Chemistry B 110 (1), 494–500.

Manyumba F., Wood, E., Horan, N., (2009). Meeting the phosphorus consent with biological nutrient removal under UK winter conditions. Water Environ. J. 23, 83e90.

Martin B.D, De Kock L., Stephenson T., Parsons S.A., Jefferson B., (2013). The impact of contactor scale on a ferric nanoparticle adsorbent process for the removal of phosphorus from municipal wastewater. Chemical Engineering Journal 215-216 209-215.

Martin B.D., De Kock L., Gallot M., Guery E., Stanowski S., MacAdam J., McAdam E.J., Parsons S.A. and Jefferson B. (2017) Quantifying the performance of a hybrid anion exchanger/adsorbent for phosphorus removal using mass spectrometry coupled with batch kinetic trials, Environmental Technology, 39:18, 2304-2314.

Martin B.D., Parsons S.A., Jefferson B. (2009). Removal and recovery of phosphate from municipal wastewater using a polymeric anion exchanger bound with hydrated ferric oxide nanoparticles. Water Science & Technology 60.10 2937-2645.

Mateus D.M.R., Pinho H.J.O., (2010). Phosphorus removal by expanded clay – six years of pilot-scale constructed wetlands experience. Water Environ. Res. 82, 128.

Nguyen T.A.H., Ngo H.H., Guo W.S., Zhang J., Liang S., Yue Q.Y., Li Q., Nguyen T.V., (2013). Applicability of agricultural waste and by-products for adsorptive removal of heavy metals from wastewater. Bioresour. Technol. 148, 574e585.

Oehmen, A., Lemos, P. C., Carvalho, G., Yuan, Z., Keller, J., Blackall, L. L., et al.; (2007). Advances in enhanced biological phosphorus removal: from micro to macro scale. Water Res. 41, 2271–2300.

Pan B., Han F., Nie G., Wu B., He K., Lu L.; (2014). New strategy to enhance phosphate removal from water by hydrous manganese oxide, Environ. Sci. Technol. 48 5101–5107.

Pan B.J., Wu J., Pan B.C., Lv L., Zhang W., Xiao L., Wang X., Tao X., Zheng S., (2009a). Development of polymer-based nanosized hydrated ferric oxides (HFOs) for enhanced phosphate removal from waste effluents, water research 43 4421–4429.

Pan B.J., Pan B.C., Zhang W., Lv L., Zhang Q., Zheng S., (2009b). Development of polymeric and polymer-based hybrid adsorbents for pollutants removal from waters. Chemical Engineering Journal 151 (2009) 19–29

Pan B.C., Chen X.Q., Zhang W.M., Pan B.J., Shen W., Zhang Q.J., Du W., Zhang Q.X., Chen J.L., Chinese patent: CN 200510095177.5 (2007)

Persson P., Nilsson N., and Sjrberg S. (1996) Structure and bonding of orthophosphate ions at the iron oxide-aqueous interface. J. Colloid Interface Sci. 177, 263-275.

Petruzzelli D., Dell'Erba A., Liberti L., Notarnicola M., Sengupta A.K.; (2004). A phosphate-selective sorbent for the REM NUT® process: field experience at Massafra Wastewater Treatment Plant. Reactive & Functional Polymers 60 195-202.

Petzet, S., Cornel, P., (2013). Phosphorus recovery from wastewater. In: Hester, R.E., Harrison, R.M. (Eds.), Waste as a Resource. The Royal Society of Chemistry, Cambridge, UK, pp. 110e143.

Ping L., SenGupta A.K., (2000). Intraparticle diffusion during selective sorption of trace contaminants: the effect of gel versus macroporous morphology. Environ. Sci. Technol. 34 5193-5200.

Prevette, L.E., Kodger, T.E., Reineke, T.M., Lynch, M.L., (2007). Deciphering the role of hydrogen bonding in enhancing pDNA–polycation interactions. Langmuir 23 (19), 9773–9784.

Puttamraju P, SenGupta AK (2006) Evidence of tunable on-off sorption behaviors of metal oxide nanoparticles: role of ion exchanger support. Ind Eng Chem Res 45(22):7737–7742).

Renman, A., and Renman, G. (2010). Long-term phosphate removal by the calcium-silicate material Polonite in wastewater filtration systems. Chemosphere 79, 659–664.

Rhodes M., Introduction to Particle Technology, second edition., John Wiley & Sons, Hoboken, USA, 2008. 153–155.

Sabbatini, N., Perathoner, S., Lattanzi, G., Dellonte, S., Balzani, V., (1988). Electron- and energy-transfer processes involving excited states of lanthanide complexes: evidence for inner-sphere and outer-sphere mechanisms. Inorganic Chemistry 27 (9), 1628–1633.

Sarkar S, Blaney L. M., Gupta A., Ghosh D., SenGupta A. K., (2007). Use of ArsenX^{np}, a hybrid anion exchanger, for arsenic removal in remote villages in the Indian subcontinent. Reactive & Functional Polymers 67 (2007) 1599–1611.

Sarkar S., Chatterjee P.K., Cumbal L.H. and SenGupta A.K., (2011). Hybrid ion exchanger supported nanocomposites: Sorption and sensing for environmental applications. Chem Eng J 166:923–931.

Sarkar S., Greenleaf J. E., Gupta A., Ghosh D., Blaney L. M., Bandyopadhyay P., Biswas R. K., Dutta A. K., SenGupta A. K., (2010b). Evolution of community-based arsenic removal systems in remote villages in West Bengal, India: Assessment of decade-long operation. Water Research 44 (2010) 5813 e 5822.

Sarkar S., Prakash P., SenGupta A.K. (2010a). Donnan membrane principle: opportunities for sustainable engineered processes and materials. Environ Sci Technol 44(4): 1161–1166.

Scheidig, K., Mallon, J. and Schaaf, M., (2009). Profitable recovery of phosphorus from sewage sludge and meat & bone meal by the Mephrec process – a new means of thermal sludge and ash treatment. In: International Conference on Nutrient Recovery from Wastewater Streams, Vancouver, Canada.

Schindler, D.W., Vallentyne, J.R., (2008). The Algal Bowl – Overfertilization of the World's Freshwater and Estuaries. University of Alberta Press, Edmonton, Alberta. ISBN: 978-0-88864-484-8.

Schoumans, O.F., Bouraoui, F., Kabbe, C., Oenema, O., van Dijk, K.C., (2015). Phosphorus management in Europe in a changing world. Ambio 44, 180e192.

Sellner K.G., Doucette G.J., Kirkpatrick G. (2003). Harmful algal blooms: causes, impacts and detection. J. Ind. Microbiol. Biotechnol. 30. 383-406.

Sendrowski A., Boyer T.H., (2013). Phosphate removal from urine using hybrid anion exchange resin, Desalination 322 104–112.

Sengupta A.K., Cumbal L.H., (2005). US patent: US 7291578.

SenGupta S. and Pandit A., (2011). Selective removal of phosphorus from wastewater combined with its recovery as a solid-phase fertilizer; Water Research 45 3318-3330.

Shilton, A. N., Elmetri, I., Drizo, A., Pratt, S., Haverkamp, R. G., and Bilby, S. C. (2006). Phosphorus removal by an "active" slag filter–a decade of full scale experience. Water Res. 40, 113–118. doi: 10.1016/j.watres.2005.11.002

Shuang C., Wang M., Zhou W., Li A., (2013). Enhanced adsorption and antifouling performance of anion-exchange resin by the effect of incorporated Fe3O4 for removing humic acid, Water Research, 47:6406 – 6414.

Stumm W. and Morgan J.J., (1995). Aquatic Chemistry: Chemical Equilibria and Rates inNaturalWaters, 3rd edn. JohnWiley & Sons, New York.

Tan Y, Kilduff J.E., (2007). Factors affecting selectivity during dissolved organic matter removal by anion-exchange resins, Water Research, 41:4211-4221.

Tanboonchuy V., Grisdanurak N., Liao C.H. (2012). Backgroud species effect on aqueous arsenic removal by nano zero-valent iron using fractional factorial design. Journal of Hazardous Materials 205-206 (2012) 40-46.

Tanboonchuy V., Grisdanurak N., Liao C.H., (2012). Background species effect on aqueous arsenic removal by nano zero-valent iron using fractional factorial design. Journal of Hazardous Materials 205-206 (2012) 40–46.

Tao, X., Xia, H., (2007). Releasing characteristics of phosphorus and other substances during thermal treatment of excess sludge. J. Environ. Sci. 19, 1153e1158. Issue.

Tobis J., Vortmeyer D., (1988). The near-wall channelling effect on isothermal constant pattern adsorption, Chem. Eng. Sci. 43 (6) 1363–1369.

Tran H.N., You S.J., Hosseini-Bandegharaei A., Chao H.P., (2017). Mistakes and inconsistencies regarding adsorption of contaminants from aqueous solutions: A critical review. Water Research 120 (2017) 88e116.

Vallentyne J.R., (1974). The Algal Bowl: Environment Canada, vol. 22. Miscellaneous Special Publication, Ottawa, Ontario.

Van Deemter J.J., Zuiderweg F.J., (1956). Longitudinal diffusion and resistance to mass transfer as causes of nonideality in chromatography, Chem. Eng. Sci. 5 271–289.

VO (EG)2003/2003 Regulation (EC) No 2003/2003 of the European Parliament and of the Council of 13 October 2003, relating to fertilizers.

Wang H., Zhu J., Fu Q.L., Xiong J.W., Can H., Hu H.Q., Violante A. (2015). Adsorption of phosphate onto ferrihydrite and ferrihydrite-humic acid complexes. Pedosphere 25(3): 405-414, 2015.

Weng L., Van Riemsdijk W.H., Hiemstra T. (2008). Humic Nanoparticles at the oxide-water interphase: interactions with phosphate ion and asorption. Environ. Sci. Technol. 2008, 42, 8747-8752.

World Resources Institute, 2008. Agriculture and ‘‘Dead Zones’’ http://www.wri.org/publication/content/7780

Xu R., Zhang M., Mortimer R.J.G., Pan G. (2017). Enhanced phosphorus locking by novel lanthanum/aluminum–hydroxide composite: implications for eutrophication control, Environ. Sci. Technol. 51 3418–3425.

Yan J., Jiang T., Yao Y., Lu S., Wang Q., Wei S.; (2016). Preliminary investigation of phosphorus adsorption onto two types of iron oxide-organic matter complexes. Journal of Environmental Sciences 42 (2016) 152-162.

You X., Farran A., Guaya D., Valderrama C., Soldatov V., Cortina J.L., (2016). Phosphate removal from aqueous solutions using a hybrid fibrous exchanger containing hydrated ferric oxide nanoparticles. J Environ Chem Eng 4:388–397.

You X., Guaya .D, Farran A., Valderrama C, Cortina J.L., (2015). Phosphate removal from aqueous solution using a hybrid impregnated polymeric sorbent containing hydrated ferric oxide (HFO); J Chem. Technol. Biotechnol.; 91: 693–704.

Zeng L., Li X., Liu J. (2004). Adsorptive removal of phosphate from aqueous solutions using iron oxide tailings. Water Research 38:1318-1326.

Zhao D. and SenGupta A. K. (1998). Ultimate removal of phosphate from wastewater using a new class of polymeric ion exchangers. Wat. Res. 32, 1613-25.

Zheng, X., Sun, P., Han, J., Song, Y., Hu, Z., Fan, H., Lv, S., (2014). Inhibitory factors affecting the process of enhanced biological phosphorus removal (EBPR) – a mini-review. Process Biochem. 49, 2207e2213.